

Cell death and inflammation in skin homeostasis and small cell lung cancer

Inaugural-Dissertation
zur
Erlangung des Doktorgrades
der Mathematisch-Naturwissenschaftlichen Fakultät
der Universität zu Köln



vorgelegt von
Lioba Katharina Körner
aus Köln

Köln, 2022

Berichterstatter:

Prof. Dr. Manolis Pasparakis

Prof. Dr. Hamid Kashkar

Prof. Dr. Wendy Wei-Lynn Wong

Tag der mündlichen Prüfung: 14.02.2023

Abstract

Z-DNA binding protein 1 (ZBP1) has evolved as a key player in viral infections and tissue homeostasis promoting necroptotic cell death. Whilst a RHIM-RHIM dependent interaction between ZBP1 and RIPK1 has been implicated to exert inhibitory functions, RHIM-mediated recruitment of RIPK3 to ZBP1 was shown to induce necroptosis.

In this work, we firstly show that TNFR1 and ZBP1 act synergistically to trigger skin inflammation upon keratinocyte-specific loss of FADD, reinforcing ZBP1 as a crucial player in skin homeostasis. We then aimed to shed light on the mechanisms of ZBP1 downstream signaling in presence of RIPK1 and FADD, as most studies thus far dissecting ZBP1 signaling *in vivo* required loss of one of these two proteins. To this aim we generated a constitutively active C-terminally truncated version of ZBP1 (ZBP1ca).

Keratinocyte-specific ZBP1ca expression was able to induce apoptosis as well as necroptosis dependent on RIPK1 and RIPK3 RHIM-RHIM interactions, respectively. Mechanistically, this RIPK1-mediated apoptosis appeared to be independent of its kinase activity, identifying a novel mechanism of ZBP1-driven cell death.

Having established ZBP1ca as a potent inducer of inflammation, we aimed to make use of this construct in a therapeutic setting. To this end, we utilized a mouse model for small cell lung cancer (SCLC), the most aggressive lung cancer subtype, which is in urgent need for novel targeted therapies. Our data suggest resistance of a subset of SCLC cell lines to the induction of immunogenic cell death by MLKL activation, further warranting the close investigation of molecular mechanisms underlying this deadly disease. Using different genetically modified mouse models investigating the role of inflammatory signaling in SCLC, we observed a strong dependency on NEMO/RelA-dependent NF- κ B signaling for SCLC development, suggesting inhibition of NF- κ B signaling as a therapeutic option for SCLC.

Taken together, our study highlights a novel mechanism for ZBP1-induced cell death in sterile conditions and gives new insights about ZBP1-mediated signaling. Furthermore, we present data which can aid in the treatment of SCLC as human patients may benefit from NF- κ B inhibition.

Table of content

Abstract	I
Abbreviations	IV
Abbreviations of units	VI
1. Introduction	1
1.1 Cell death and Inflammation.....	1
1.2 Immunogenicity of regulated cell death.....	2
1.3 TNF signaling pathway	3
1.3.1 TNFR1-mediated pro-survival signaling	3
1.3.2 TNFR1-mediated apoptosis	6
1.3.3 TNFR1-mediated necroptosis	9
1.4 ZBP1 protein function.....	10
1.4.1 ZBP1 protein structure	10
1.4.2 ZBP1 as a driver of inflammation and cell death.....	12
1.4.3 ZBP1 in skin homeostasis	13
1.4.4 ZBP1 in cancer.....	14
1.5 Cell death and inflammatory signaling in cancer.....	15
1.5.1 Immunogenic cell death in cancer.....	15
1.5.2. Inflammatory signaling in cancer.....	16
1.6 Lung cancer.....	17
1.6.1 Characteristics of small cell lung cancer	18
1.6.2 Murine model of small cell lung carcinogenesis	19
1.7 Aims of the study.....	20
2. Publications, Manuscripts and Results	21
2.1 ZBP1 causes skin inflammation by inducing RIPK3-dependent necroptosis and RIPK1-mediated apoptosis in keratinocytes	21
2.2 Small Cell Lung Cancer development is independent of necroptotic signaling.....	53
2.2.1 Expression of ZBP1ca kills murine SCLC cell lines <i>in vitro</i>	53
2.2.2 ZBP1ca expression <i>in vivo</i> does not alter SCLC development	56
2.2.3 Impairment of necroptosis does not affect SCLC progression	59
2.3 NEMO- and RelA-dependent NF- κ B Signaling Promotes Small Cell Lung Cancer.....	61
3. Discussion.....	89
3.1 ZBP1 causes skin inflammation by inducing RIPK3-dependent apoptosis and RIPK1-mediated apoptosis in keratinocytes	89
3.2 Small Cell Lung Cancer development is independent of necroptotic signaling.....	92
3.3. NEMO- and RelA-dependent NF- κ B Signaling Promotes Small Cell Lung Cancer....	93

3.4. Concluding Remarks and Future Prospects	96
4. General Material & Methods	97
4.1 Chemical and biological materials.....	97
4.2 Mouse experiments	100
4.2.1 Animal care	100
4.2.2 Adenovirus Inhalation.....	100
4.2.3 MRI scans	100
4.2.4 Tamoxifen & anti-PD1 Injections	101
4.2.5 Lung tissue preparation	101
4.3 Histological analysis	101
4.3.1 Haematoxylin & Eosin staining.....	101
4.3.2 DAB stainings.....	101
4.4 Molecular Biology	101
4.4.1 Isolation of genomic DNA from tail biopsies	101
4.4.2 Genotyping PCRs.....	102
4.4.3 3' mRNA sequencing analysis.....	104
4.4.4 Ligase-independent cloning	104
4.5 Cell culture	105
4.5.1 Generation of stable cell lines via lentiviral transduction.....	105
4.5.2 Cell death assay	105
4.6 Biochemistry.....	106
4.6.1 Preparation of protein extracts from tissue.....	106
4.6.2 Protein lysate preparation from cells	106
4.6.3 Western blot analysis	106
4.7 Statistical analysis	106
5. General References	107
6. Acknowledgements	118
7. Erklärung zur Dissertation	119

Abbreviations

A20	Tumor necrosis factor alpha induced protein 20
Ad-Cre	Adeno Cre
Ad-Flp	Adeno-Flp
ADAR1	Deaminase Acting on RNA 1
AP1	Activator protein 1
ATP	Adenosin triphosphate
BAK	Bcl-2 homologous antagonist/killer
BAX	Bcl-2-like protein 4
BCL2	B-cell lymphoma 2
Bid	BH3 interacting domain death agonist
cIAP1/2	Cellular inhibitor of apoptosis protein1/2
cFLIP	Cellular FLICE like inhibitory protein
Cre	Causes recombination
cGas	Cyclic GMP-AMP synthase
CYLD	Cylindromatosis
DAMP	Danger associated molecular pattern
DD	Death domain
ddH₂O	Double-distilled water
DED	Death effector domain
DMEM	Dulbecco's Modified Eagle Medium
DMSO	Dimethyl sulfoxide
DNA	Deoxyribonucleic acid
E-KO	Epidermis specific knock out
FADD	Fas-associated-via-death.domain protein
ERK	Extracellular signal-related kinases
GSDMD	Gasdermin D
GSDMDN	N-terminal Gasdermin D
GSDME	Gasdermin E
HMGB1	High-Mobility-Group-Protein B1
HOIL-1	Heme-Oxidized IRP2 ubiquitin ligase 1 homolog
HOIP	HOIL-1 interacting protein
HSP70	Heatshock-Protein 70
HSV	Herpes simplex virus
IAV	Influenza A virus
IHC	Immunohistochemistry

ICI	Immune checkpoint inhibition
IEC-KO	Intestinal epithelial cell specific knock out
IFN	Interferon
IKK1/2	Inhibitor of κ B kinase 1/2
iMEF	Immortalized mouse embryonic fibroblast
IL-1β	Interleukin 1 β
IL-10	Interleukin 10
IL-18	Interleukin 18
IRF3	Interferon regulatory factor 3
ISG	Interferon-stimulated gene
JNK	Jun n-terminal kinases
LEC-KO	Lung epithelial cell specific knock out
LUBAC	Linear ubiquitin chain assembly complex
MAPK	Mitogen-activated protein kinase
MCMV	Murine cytomegalovirus
MIB2	Mind Bomb 2
MLKL	Mixed lineage kinase domain-like protein
MOMP	Mitochondrial outer membrane permeabilization
NEMO	Nuclear factor κ B essential modulator
NF-κB	Nuclear factor “kappa light chain enhancer” of activated B cells
NLR	Nod like receptor
NSCLC	Non-small cell lung cancer
OTULIN	OUT deubiquitinase with linear specificity
PAMP	Pathogen-associated molecular pattern
PCR	Polymerase chain reaction
PD-1	Programmed cell death protein 1
PRR	Pattern recognition receptor
PS	Phosphatidylserine
RB1	Retinoblastoma protein 1
RHIM	Receptor interacting protein homotypic interaction domain
RIG-I	Retinoic acid inducible gene I
RIPK1/3	Receptor interacting serine/threonine kinase 1/3
RNA	Ribonucleic acid
RPMI	Roswell Park Memorial Institute Medium
SCLC	Small cell lung cancer
SDS	Sodium dodecyl sulfate
SHARPIN	SHANK associated RH domain interactor

STING	Stimulator of interferon genes
SMAC	Second mitochondria-derived activator of caspase
TAB2/3	TAK1-binding protein 2
TAK1	TGF- β -activated kinase 1
TLR	Toll like receptor
TMB	Tumor mutational burden
TNF	Tumor necrosis factor
TNFR1/2	Tumor necrosis factor receptor 1/2
TP53	Tumor protein 53
TRADD	Tumor necrosis factor receptor 1-associated via death domain
TRAF2	Tumor necrosis factor receptor associated factor 2
TRIF	TIR-domain-containing adapter-inducing interferon β
WT	Wild type
XIAP	X-linked inhibitor of apoptosis
ZBP1	Z-DNA binding protein 1

Abbreviations of units

°C	Degree Celcius
A	Ampere
bp	Base pair
g, mg, μg, ng	gram, milligram, microgram, nanogram
h, min, sec	hours, minutes, seconds
kDa	kilo Dalton
l, ml, μl	liter, milliliter, microliter
M, mM, μM, nM	molar, millimolar, micromolar, nanomolar
rpm	rounds per minute
V	Volt

1. Introduction

1.1 Cell death and Inflammation

A dynamic equilibrium between cell death, proliferation and survival is essential for the maintenance of tissue homeostasis throughout life. Whereas cell death is a crucial regulator of development and homeostasis in physiological as well as in pathological settings, elimination of harmful cells can also result in inflammation¹. Inflammation has been associated with cell death for more than 150 years, however cell death has only recently been shown to contribute as an active component to tissue inflammation instead of being a mere consequence.

Whilst inflammation is a crucial reaction mediated by the immune system to protect from injury or infection, aberrant inflammation can lead to increased tissue damage. Therefore, inflammation and cell death need to be tightly controlled to minimize pathological effects.

Inflammatory signaling can be triggered by recognition of pathogen-associated molecular patterns (PAMPs) or danger-associated molecular patterns (DAMPs) that are sensed by pattern recognition receptors (PRRs) expressed by immune cells such as macrophages and neutrophils. DAMPs are poorly characterized molecules released from cells upon plasma membrane rupture such as High-Mobility-Group-Protein B1 (HMGB1), Heat Shock Protein 70 (HSP70) or adenosine triphosphate (ATP). PAMPs are molecular motifs expressed by bacteria and viruses, such as flagellin, lipoteichoic acid, peptidoglycan or nucleic acid variants. Upon PRR stimulation, cytokines and chemokines are transcribed which can multiply the inflammatory response by activating additional pro-survival and pro-inflammatory signaling pathways by binding to their respective receptors. The transcription factor nuclear factor “kappa-light-chain-enhancer” of activated B-cells (NF- κ B) signaling pathway is one of the prime examples for induction of pro-survival and pro-inflammatory signaling^{2,3}.

While many innate immune receptors trigger a pro-survival transcriptional program, they can also cause cell death in order to clear infected cells⁴. Hence, cell death has been described as an essential regulatory process modulating the immune response⁵.

Classically, cell death has been divided into apoptosis and necrosis. Whereas apoptosis was considered a programmed type of cell death early on, necrosis was until recently thought to exclusively happen accidentally due to mechanical, chemical or physiological insults. In contrast to this, the discovery of programmed necrotic cell death pathways, such as necroptosis, or pyroptosis describe necrosis, in most situations, as a regulated form of cell death. The interplay between these cell death pathways has been implicated in the pathogenesis of diverse human conditions, amongst them several types of cancer. Thus, dissection of the

molecular mechanisms underlying these pathways will provide a better understanding for processes regulating health and disease.

1.2 Immunogenicity of regulated cell death

Apoptosis is the first type of regulated cell death which has been described and serves as an essential player in tissue homeostasis, development and regulation of immune responses^{4,6}. Apoptosis is morphologically characterized by cytoplasmic shrinkage, chromatin condensation, nuclear fragmentation and formation of apoptotic bodies while the plasma membrane stays intact⁷. These apoptotic bodies are quickly engulfed and digested by phagocytes which recognize the exposure of phosphatidylserine on the outer plasma membrane of apoptotic cells⁸⁻¹¹. Noteworthy, apoptotic cells have been shown to secrete anti-inflammatory cytokines such as interleukin-10 (IL-10), adding an additional layer of complexity to suppress the recruitment of immune cells^{8,12}. In addition, the exposure of phosphatidylserine in apoptotic cells was reported to induce the expression of anti-inflammatory mediators such as prostaglandin E2 or TGF β ¹. Therefore, apoptosis has classically been described as an immune-tolerant type of cell death. However, this widely accepted notion is currently under debate. Apoptosis is not considered to be exclusively immune-suppressive anymore, since several factors determine the immunological outcome of apoptotic cell death. Depending on the dying cell type, the cause of death, the activation status of the dying cell, its microenvironment or the quantity of dying cells, apoptosis has been suggested to also trigger an inflammatory response⁸.

Apoptosis was shown to be inflammatory due to the exposure of calreticulin and the release of pro-inflammatory cytokines in photodynamic cancer therapy, anthracycline treatment or ionizing irradiation¹³. Additionally, apoptosis can trigger tissue inflammation and thereby immunogenic cell death upon certain genetic modifications¹⁴⁻¹⁶. Whether this is solely dependent on a phenomenon called secondary necrosis remains to be investigated. In conclusion, the effect of apoptosis on the immune response likely depends on tissue surroundings as well as on communication between immune cells and dying cells. Thus, the traditional view of apoptosis as immunologically silent is currently being reinvestigated.

Contrary to apoptosis, necroptosis is morphologically characterized by cellular swelling, swelling of organelles and membrane rupture. Due to loss of plasma membrane integrity and hence release of intracellular components such as ATP, HSP70 and HMGB1, necroptosis is considered to be highly immunogenic^{4,17,18}. The massive release of these intracellular components activates PRR signaling and, consequently, initiates an immune response and triggers inflammation⁴. Induction of necroptosis has only been described upon inhibition of apoptotic pathways suggesting that it serves as a back-up mechanism⁴. Furthermore, induction of necroptosis was shown to trigger anti-tumor immunity in several adoptive transfer models

of cancer¹⁹. Thus, whereas apoptosis is essential for development, necroptosis appears to be a potent trigger of inflammation and alarms the immune system in danger situations.

In addition to necroptosis, pyroptosis has also been identified as a highly immunogenic form of necrotic cell death due to release of intracellular components and maturation of the cytokines interleukin 1 β (IL-1 β) and interleukin 18 (IL-18). While necroptosis is mainly triggered upon inhibition of apoptotic cell death, pyroptosis is usually initiated by microbial infections which ultimately lead to inflammasome activation and cell death²⁰.

To date, specific effects of different types of cell death on the immune system remain incompletely understood. The immunogenicity of differentially regulated cell death types likely depends on more than the morphological characteristics of differentially regulated cell death types, further enhancing the complexity of an interplay between distinct signaling cascades within tissues. Due to the immense therapeutic potential of regulated cell death, especially in regards to cancer therapy, investigating the exact underlying molecular mechanisms remains an important field of scientific research.

1.3 TNF signaling pathway

Tumor-necrosis factor (TNF) is a major inflammatory cytokine provoking inflammation, which was firstly described to cause destruction of the tumor vasculature by induction of necrosis in animal models of experimental cancers²¹. TNF is produced downstream of innate immune receptors by immune, endothelial and epithelial cells and binds to tumor-necrosis factor receptor 1 (TNFR1) and tumor-necrosis factor receptor 2 (TNFR2). While TNFR1 recognizes soluble TNF, TNFR2 requires membrane-bound TNF for full activation. TNFR2 expression is restricted to a certain subset of cells whereas TNFR1 is ubiquitously expressed. This contributes to the fact that TNFR1 is seen as the key player of TNF-signaling and is among the best studied receptors regarding pro-survival and cell death signaling. The outcome of TNFR1 stimulation is highly dependent on the cellular context, where TNFR1 signaling either leads to activation of a pro-inflammatory and pro-survival response or triggers cell death which can be apoptotic or necroptotic.

1.3.1 TNFR1-mediated pro-survival signaling

TNFR1 stimulation by TNF triggers formation of a membrane-bound pro-survival protein complex known as complex I (Figure 1)²². Upon ligation of TNF to TNFR1, the receptor trimerizes which leads to conformational changes in its cytosolic death domain (DD), ultimately resulting in recruitment of TNFR1-associated death domain protein (TRADD) and Receptor-Interacting Protein Kinase 1 (RIPK1) via DD-DD homotypic interactions²³⁻²⁵. TRADD then facilitates recruitment of TNF receptor associated factor 2 (TRAF2) and/or TRAF5 and

recruitment of the E3 ubiquitin ligases cellular inhibitor of apoptosis 1 and 2 (cIAP1/2)^{26,27}. Addition of K11-, K48- and K63-linked ubiquitin chains by cIAP1/2 to themselves as well as to TNFR1 and RIPK1 results in binding of transforming growth factor β activated kinase (TAK1) and TAK1 binding protein 1 and 2 (TAB1/2) as well as to the recruitment of the linear ubiquitin chain assembly complex (LUBAC), composed out of the E3 ligase HOIL-1 interacting protein (HOIP), haem-oxidized IRP2 ubiquitin ligase-1 (HOIL-1) and SHANK-Associated RH Domain Interactor (Sharpin)²⁸⁻³³. LUBAC further mediates M1-ubiquitination of TNFR1, TRADD, RIPK1 and of the NF- κ B essential modulator (NEMO). Following the recognition of M1-linked and, to a lesser extent, K11- and K63-linked ubiquitin chains by NEMO, NEMO is recruited to the complex via its ABIN and UBAN domains^{34,35}. Recruitment of NEMO results in formation of the I κ B kinase (IKK) complex which is composed out of the regulatory subunit NEMO and the catalytic subunits IKK1 and IKK2. TAK1 phosphorylates IKK2 leading to subsequent phosphorylation and K48-ubiquitination of the NF- κ B suppressor I κ B α and its proteasomal degradation^{24,36-38}. Consequently, the NF- κ B dimer p50/p65 (RelA) is released from I κ B α -mediated inhibition and translocates into the nucleus where it activates transcription of a pro-survival and pro-inflammatory genetic program²⁴.

NF- κ B signaling induced by TNFR1 is positively and negatively regulated via post-translational modifications of RIPK1 such as ubiquitination and phosphorylation. Phosphorylation of RIPK1 by IKK2, MAPK-activated protein kinase 2 (MK2) and TANK-binding kinase 1 (TBK1) together with ubiquitination by mind bomb 2 (MIB2) keep RIPK1 in the pro-survival complex I which ensures proper NF- κ B activation and prevents cell death³⁹⁻⁴¹. The kinases TBK1 and IKK ϵ are recruited to complex I via their adaptor proteins NAP1 and TANK and phosphorylation of RIPK1 by TBK1/IKK ϵ is crucial to negatively regulate cell death-inducing RIPK1 kinase activity⁴².

Deubiquinating enzymes such as A20, the deubiquitinase cylindromatosis (CYLD) and the OTU deubiquitinase with linear specificity (OTULIN) have been demonstrated to take over different roles in TNFR1 signaling⁴³⁻⁴⁹. The recruitment of A20 to complex I is mediated via its ability to bind to K63- and M1-linkages and requires the catalytic activity of LUBAC^{46,50-52}. A20 plays a dual role in the regulation of NF- κ B signaling. On the one hand it can negatively regulate NF- κ B signaling by preventing binding of the IKK complex thus restricting NEMO recruitment via M1-ubiquitin chains⁵³. Moreover, A20 can deubiquitinate RIPK1 by hydrolyzing its K63-linked ubiquitin chains, resulting in RIPK1 proteasomal degradation and destabilization of complex I. On the other hand, A20 can support pro-survival signaling by stabilizing M1-linked ubiquitin chains^{45,53}. Thus, A20 either stabilizes ubiquitin-chains to promote NF- κ B signaling or hydrolyzes ubiquitin-chains, impairing NF- κ B signaling and sensitizing to TNF-mediated cell death.

CYLD is also recruited via LUBAC to complex I, but contrary to A20 it does not depend on LUBAC catalytic activity. Whereas A20 exhibits dual functions, the sole function of CYLD is to

hydrolyze K63-linked ubiquitin chains as well as M1-linked ubiquitin chains and thereby compromise NF- κ B signaling^{44,54-56}. OTULIN has been suggested to prevent LUBAC auto-ubiquitination and thereby its degradation^{48,49}.

In addition to NF- κ B signaling, TNFR1 stimulation leads to activation of the mitogen-activated protein kinase (MAPK) pathway. Similar to NF- κ B activation, this pathway relies on phosphorylation events by TAK1. TAK1 mediated phosphorylation of the MAPKs Jun N-terminal kinases (JNK), extracellular signal-related kinases (ERK) and p38 ultimately results in transcription factor activator protein 1 (AP-1) translocation into the nucleus and transcription of genes involved in survival and inflammation^{57,58}.

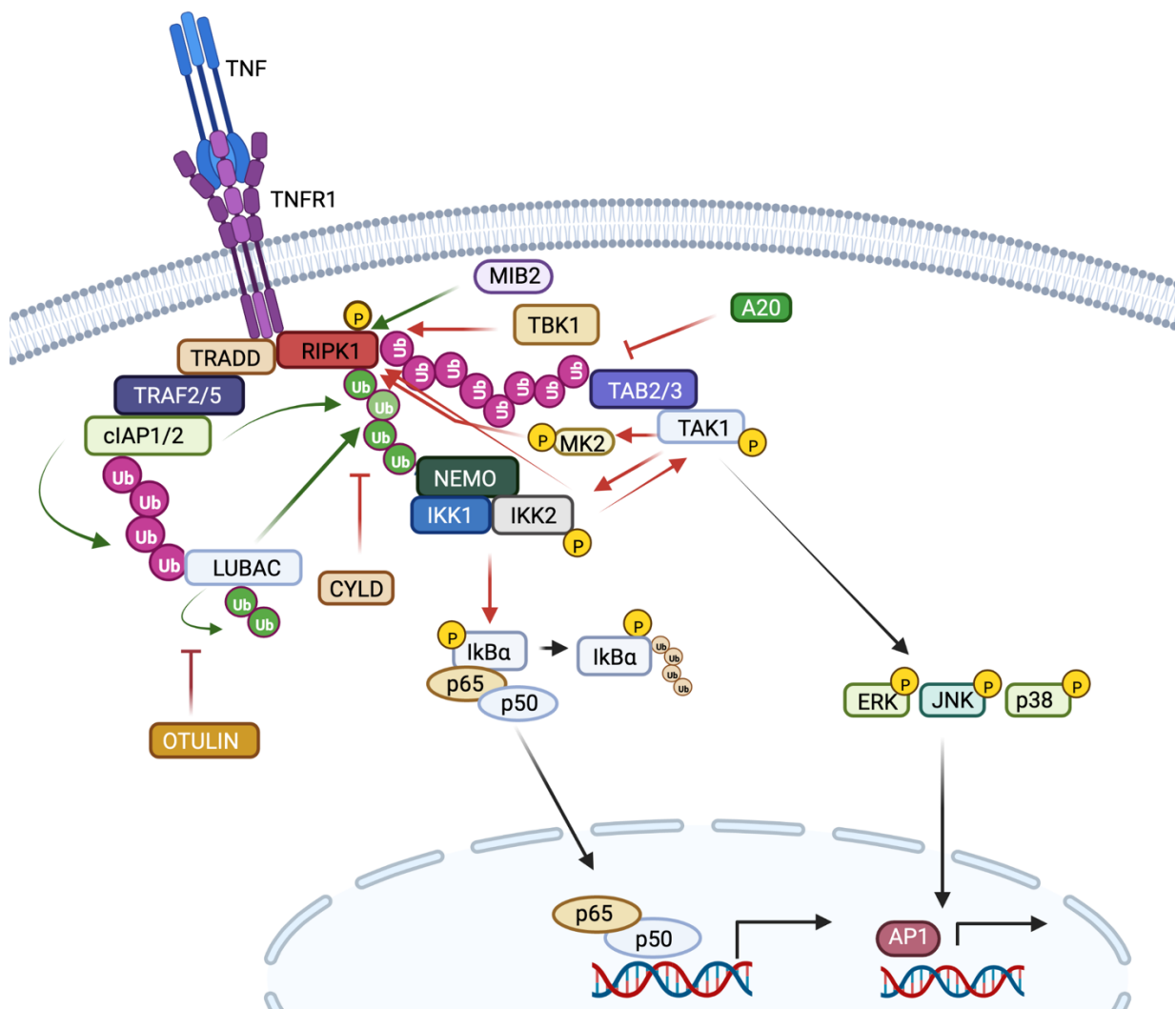


Figure 1 Scheme representing TNFR1 induced complex 1 formation by TNF ligation. Upon TNF ligation to TNFR1 several ubiquitination and phosphorylation events lead to assembly of a receptor-bound complex-I which mediates pro-survival NF- κ B and MAPK signaling. Red arrows represent phosphorylation events, green arrows represent ubiquitination events. M1 ubiquitin chains are marked in green, K63 chains are depicted in pink and K48 chains are brown. Created with BioRender.com.

Taken together, the ligation of TNF to TNFR1 results in a complex signaling network, recruiting several proteins which depend on post-translational modifications in order to ultimately induce transcriptional programs promoting pro-survival and inflammatory signaling cascades.

1.3.2 TNFR1-mediated apoptosis

Under physiological conditions, TNF stimulation of TNFR1 leads to formation of the pro-survival complex I. However, upon impaired complex I signaling, TNFR1 stimulation can also result in apoptotic cell death by formation of complex IIa or IIb (Figure 2)^{4,22,59}. Complex IIa as well as complex IIb depend on Fas-associated-via-death-domain protein (FADD) and caspase-8, however complex IIa utilizes TRADD as an adaptor for FADD whereas complex IIb relies on RIPK1 and its kinase activity^{60,61}. Formation of complex IIa after TNFR1 stimulation is induced under conditions of a disturbed NF- κ B response e.g., due to inhibition of protein synthesis or suppression of NF- κ B translocation^{59,61}. TRADD recruits FADD via homotypic DD-DD interactions and FADD serves as an adaptor protein by associating with pro-caspase-8 via its death effector domain (DED). Pro-caspase-8 is activated by autoproteolytic cleavage. Pro-caspase-8 activation has been proposed to occur via intermolecular cleavage within one caspase-8 homodimer accompanied by interdimer cleavage between two caspase-8 homodimers, ultimately leading to release of the active p18 and p10 fragments⁶²⁻⁶⁴. However, caspase-8 can additionally form heterodimers with cellular FLICE like inhibitory protein (cFLIP), a catalytically inactive homolog of caspase-8^{65,66}. This heterodimerization leads to inhibition of extrinsic apoptosis in an isoform- and concentration-dependent manner. Thus, cFLIP serves as an antagonist of caspase-8-induced cell death⁶⁷. Activated caspase-8 can engage and activate the effector caspases-3 and -7 which in turn cleave cellular substrates and thereby induce apoptosis⁶²⁻⁶⁴.

Alternatively, under conditions such as IAP depletion, TAK1 or NEMO ablation, complex IIb is formed^{61,68,69}. Complex IIb is composed out of RIPK1, which serves as an adaptor protein recruiting FADD via DD-DD interactions, followed by recruitment of the receptor interacting serine/threonine kinase 3 (RIPK3), caspase-8 and cFLIP. Although RIPK3 has been reported to be part of the complex, it is not required for its activity but contributes to RIPK1-mediated apoptosis in a kinase-independent-manner^{4,68}. Similar to complex IIa, complex IIb formation ultimately leads to caspase-3 and -7-triggered apoptotic cell death via caspase-8.

Importantly, only ablation of the core components of complex I result in complex IIb formation. While loss of NEMO leads to complex I destabilization, complete ablation of NF- κ B signaling and RIPK1-dependent apoptosis, loss of the NF- κ B subunit RelA/p65 impairs NF- κ B signaling to a large extent but exhibits NF- κ B-independent functions only to a minor extent¹⁶. Disruption of the X-linked NEMO gene results in embryonic lethality of male mice whereas heterozygous loss of NEMO leads to skin inflammation and increased keratinocyte apoptosis in female animals⁷⁰. Moreover, tissue-specific loss of NEMO has been demonstrated to result in RIPK1-kinase activity mediated apoptosis^{15,16,71,72}.

RelA/p65-deficient mice die in utero. Although epithelial-specific loss of RelA/p65 renders animals more sensitive to chemical induction of colitis, additional loss of c-Rel in the skin or

additional loss of c-Rel and RelB in the intestine is required to induce sterile inflammation, suggesting compensatory NF- κ B signaling upon RelA/p65 loss to prevent cell death in epithelial cells^{16,73,74}.

Of note, it remains unclear whether both complexes, complex IIa and complex IIb, exist independently or all proteins build a single complex II. Lastly, it is currently unknown whether TRADD or RIPK1 are recruited from a membrane-bound complex I or from the cytoplasm.

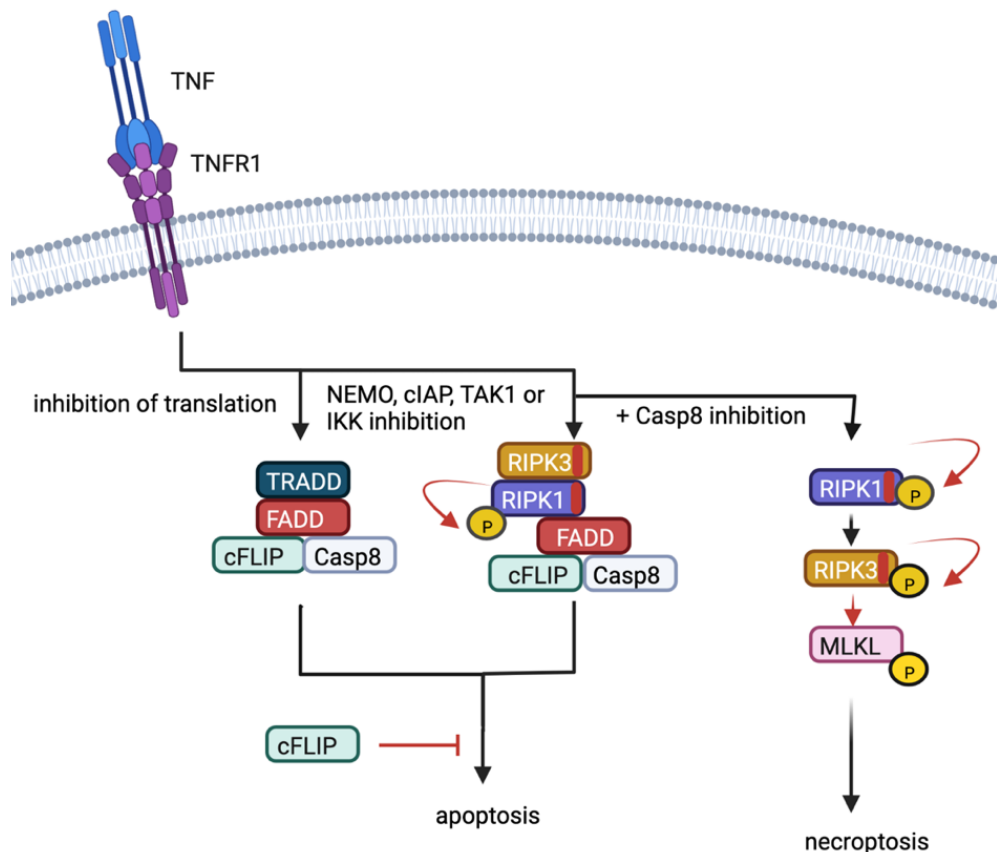


Figure 2. Schematic representation of signaling events upon ligation of TNF to TNFR1 in conditions of compromised complex I signaling. Destabilization of complex I by inhibition of protein translation results in formation of a TRADD-dependent complex IIa. Complex I destabilization by inhibition or loss of NEMO, ciAPs, TAK1 or IKK leads to RIPK1-kinase activity dependent apoptosis. Additional inhibition of caspase-8 results in formation of the necrosome. Phosphorylation events are marked by red arrows. Created with BioRender.com.

1.3.2.1 Intrinsic apoptosis

In addition to extrinsic apoptosis, TNFR1 stimulation is also linked to a signaling pathway triggering death from within the cell due to internal stimuli via caspase-8⁷⁵. Caspase-8 can, in addition to the effector caspases-3 and -7, cleave the pro-apoptotic BH3 interacting domain death agonist (Bid) into truncated Bid (tBid).

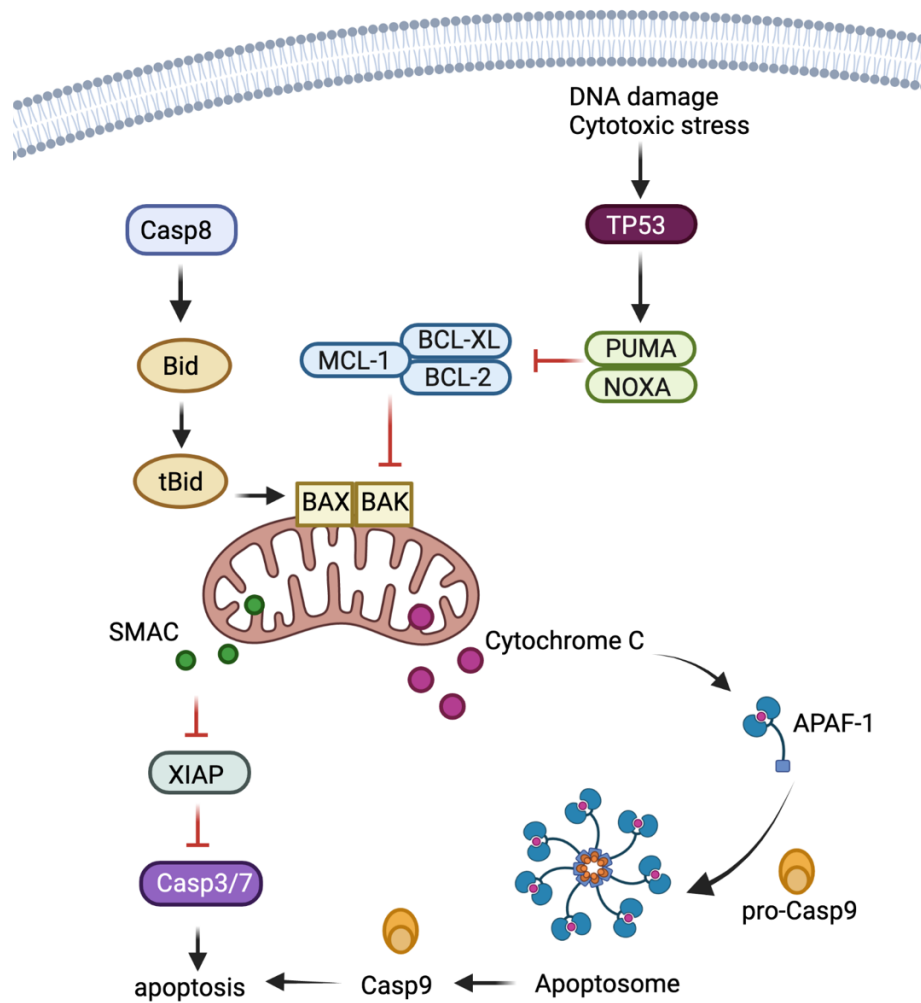


Figure 3. Scheme depicting intrinsic apoptosis. Cytotoxic stress such as DNA damage or ER stress leads to induction of intrinsic apoptosis through mitochondrial permeabilization. Created with BioRender.com.

Processing of Bid to tBid results in BCL2 homologous antagonist/killer (BAK) and BCL2 associated X (BAX) oligomerization at the mitochondrial outer membrane, inducing irreversible permeabilization of the mitochondrial outer membrane (MOMP)^{76,77}. MOMP leads to SMAC (second mitochondria-derived activator of caspase, also known as DIABLO) and cytochrome C release into the cytosol⁷⁸. Upon release, SMAC inhibits x-linked inhibitor of apoptosis (XIAP), preventing XIAP-mediated caspase inhibition. Cytosolic cytochrome C forms a complex with APAF-1 and pro-caspase-9, initiating the so-called apoptosome, leading to caspase-9 oligomerization and caspase-9 mediated cleavage of the effector caspases-3 and -7 ultimately resulting in apoptosis⁷⁹⁻⁸³ (Figure 3).

Additionally, exceeding a stimulation threshold of the pro-apoptotic BH3-only proteins in response to cytotoxic stress can activate BAX and BAK oligomerization, result in MOMP, and therefore induce apoptosis independently of caspase-8^{77,84,85}. This threshold is sensed and multiplied by diverse control mechanisms, one of the most important ones being tumor protein 53 (TP53). Upon activation due to cytotoxic stress, TP53 serves as a transcription factor and induces expression of the pro-apoptotic genes *Puma/Bbc3* and *Noxa/Pmaip1* which in turn can bind and inhibit the pro-survival BCL-2 protein family members such as BCL-2, MCL-1 or BCL-XL⁸⁶. Thus, TP53 plays a direct role in induction of this mitochondria-mediated apoptotic pathway, which results as a consequence of intracellular stress signals and is commonly annotated as intrinsic apoptosis.

1.3.3 TNFR1-mediated necroptosis

Disturbance of complex I mediated signal transmission in combination with ablation of the apoptotic proteins FADD or caspase-8 or insufficient caspase-8 activation results in TNFR1-mediated necrosome formation and thereby shifts TNFR1-mediated cell death from apoptosis to necroptosis⁴ (Figure 2).

The necrosome is composed of the receptor-interacting protein homotypic interaction domain (RHIM)-containing proteins RIPK1, RIPK3 and the pseudokinase mixed lineage kinase domain-like protein (MLKL)⁸⁷. A complex signaling cascade, dependent on the kinase activities of RIPK1 and RIPK3⁶⁰ ultimately results in MLKL-mediated plasma membrane rupture, and thereby necroptotic cell death. In detail, autophosphorylation of RIPK1 leads to a homotypic RHIM-RHIM mediated interaction between RIPK1 and RIPK3 resulting in the assembly of amyloid like filamentous structures. Consequently, RIPK3 oligomerizes leading to autophosphorylation which allows recruitment and phosphorylation of murine MLKL at Ser345, Ser347 and Thr349 (Thr357 and Ser358 in humans)^{88,89}. This RIPK3-driven phosphorylation of MLKL leads to a conformational change, exposing its brace domain and its N-terminal four helix bundle domain (4HB). Consecutive binding of MLKL to inositol phosphate-6 leads to an additional conformational change of the protein, releasing the 4HB and allowing its oligomerization and translocation to the plasma membrane where MLKL initiates membrane rupture, thus necroptosis^{88-90,91}. Despite different mechanisms of plasma membrane rupture mediated by MLKL being proposed in the literature, to date the exact process of how MLKL triggers necroptosis remains elusive^{92,93}.

Although it is tempting to describe plasma membrane rupture as a point of no return, it has been demonstrated that MLKL-dependent phosphatidylserine exposure and calcium influx can lead to activation of the ESCRT-III complex. ESCRT-III activity can sustain plasma membrane integrity following MLKL activation which can lead to either a delay in death or to survival of a cell primed to undergo necroptosis⁹⁴.

Thus, activation of MLKL can be reversed and cells can survive despite activation of the necroptotic machinery.

1.4 ZBP1 protein function

In addition to membrane-bound receptors that have been described to induce cell death, such as TNFR1, elimination of intracellular pathogens also requires a tight balance between cell death and inflammatory signaling in order to cope with infections. Amongst PRRs which localize at the endosome, such as Toll like Receptor 3 (TLR3), TLR7, TLR8 and TLR9; intracellular cytosolic sensors such as Retinoic acid inducible gene I (RIG-I)-like receptors (RLRs), Nod-like receptors (NLRs) or the cyclic GMP-AMP synthase (cGAS)-stimulator of interferon genes (STING) are essential to mediate host defense against intracellular pathogens by driving a powerful innate immune defense program⁹⁵⁻⁹⁸

The nucleic acid sensor Z-DNA binding protein 1 (ZBP1), previously called DAI or DLM-1, was firstly identified in tumor stromal macrophages upon interferon- γ treatment and has emerged as another mediator of host defense and as a key regulator of cell death and inflammatory responses upon infections as well as upon impaired or enhanced protein signaling due to diverse genetic modifications⁹⁹⁻¹⁰⁹. ZBP1 is currently characterized as a key player in cell death signaling due to its potent ability to trigger RIPK3-MLKL mediated necroptosis.

1.4.1 ZBP1 protein structure

ZBP1 has a molecular weight of 44 kilo Dalton (kDa) and contains two N-terminal nucleic acid sensing $Z\alpha$ domains. The $Z\alpha$ domains were firstly identified in Adenosine Deaminase Acting on RNA 1 (ADAR1) and were shown to stabilize left-handed Z-RNA and Z-DNA^{110,111}. Due to crystallization of Z-DNA with the second $Z\alpha$ ($Z\alpha 2$) domain of ZBP1 in complex, Z-nucleic acids have been proposed as a ligand for ZBP1¹¹². While ADAR1 and ZBP1 are the only mammalian proteins that harbor $Z\alpha$ domains, the viral proteins E3L, from vaccinia virus, and ORF112, from cyprinid herpes virus 3, also contain the highly conserved motif, suggesting that ZBP1 signaling is a target of pathogen effector molecules^{113,114}.

In addition to the N-terminal $Z\alpha$ domains, ZBP1 contains three C-terminal RHIMs. The RHIM was initially discovered in RIPK1 and RIPK3 and can potentially mediate interactions between the four RHIM-containing proteins ZBP1, RIPK1, RIPK3 or TIR-domain-containing adapter-inducing interferon- β (TRIF) (Figure 4, see section 1.3.3; section 1.4.2)^{115,116,103,104,112,116-119}.

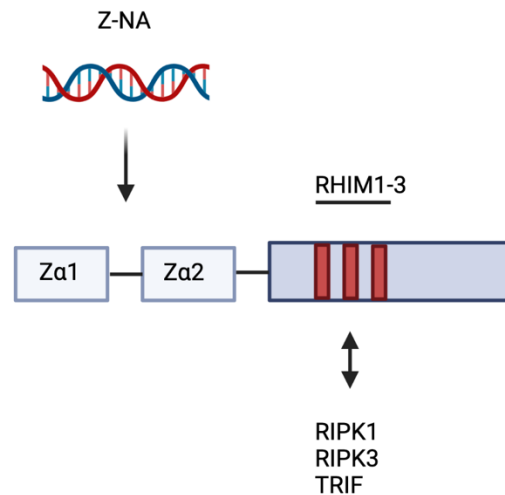


Figure 4. Scheme depicting protein structure of ZBP1. ZBP1 is composed of 2 N-terminal Z α domains sensing Z-nucleic acids and three C-terminal RIP homotypic interaction motifs (RHIM) which are depicted in red. Potential RHIM-mediated protein-protein interactions are indicated. Created with BioRender.com.

Whereas a crucial role of the first RHIM of ZBP1 for a homotypic RHIM-RHIM interaction has been elegantly demonstrated *in vitro* and *in vivo*, the function of the RHIM2 and RHIM3 require further elucidation^{119,120}.

Interactions between RIPK1, RIPK3 and ZBP1 have been shown in previous studies, but a potential RHIM-RHIM dependent interaction between ZBP1 and the fourth RHIM containing protein (TRIF) remains poorly characterized. However, a recent study suggested the formation of a so-called “TRIFosome” inducing caspase-8-mediated cell death and IL-1 β release upon TLR4 stimulation. This “TRIFosome” complex was proposed to consist of TRIF, ZBP1, RIPK1, FADD and caspase-8 and was suggested to rely on ZBP1 as an adaptor protein between TRIF and RIPK1, supporting the hypothesis for a RHIM-RHIM dependent interaction between ZBP1 and TRIF¹²¹.

The sequence conservation of the RHIM is centered around the I(V)QI(V)G sequence and mutation of one of these core residues prohibits RHIM-RHIM homotypic interactions¹²².

Alternative splicing incorporating a premature stop codon results in expression of an additional 15 kDa isoform of ZBP1, which lacks the C-terminal RHIMs. This isoform was suggested to exhibit inhibitory functions due to competitive ligand binding between the two isoforms but the absence of subsequent RHIM-mediated downstream signaling in the short isoform. Whether this is the case still remains to be investigated.

1.4.2 ZBP1 as a driver of inflammation and cell death

As described above, ZBP1 was initially identified to be induced upon interferon (IFN) signaling (section 1.4). Moreover, its expression was proposed to lead to a positive feedback loop, enhancing type I IFN production as well as different interferon-stimulated genes (ISGs). It has been suggested that ZBP1 multiplies TBK1-mediated IRF3 signaling upon binding of double-stranded DNA^{123,124}. Aside from type I IFN production, ZBP1 was also proposed to recruit RIPK3 and RIPK1 via RHIM-homotypic interactions in order to activate NF- κ B signaling^{116,119}. Therefore, ZBP1 has been implicated in pro-inflammatory and pro-survival signaling but to date this function is widely under debate and ZBP1 is mostly described as a fundamental signaling node in triggering RHIM-dependent necroptosis upon viral infections or dysfunctional upstream protein signaling. ZBP1 has been shown to play a prominent role in murine cytomegalovirus (MCMV), influenza A virus (IAV), and herpes simplex virus (HSV) due to sensing of virus derived molecular patterns. However, it can also be activated in a ligand-dependent manner in non-infected cells, implicating the presence of a virus-independent ligand^{104-106,108,109,125,126}. After $Z\alpha$ -mediated activation, ZBP1 undergoes a homotypic RHIM-dependent interaction with RIPK3 to activate MLKL and to thereby induce necroptosis (section 1.3.3, Figure 4).

Although several ligands such as single-stranded RNA, nucleoprotein polymerase subunit PB1, viral ribonucleoprotein or genomic viral DNA have been proposed to stimulate ZBP1, it was, in line with the initial hypothesis, recently demonstrated that Z-nucleic acids can trigger ZBP1-dependent necroptosis and inflammation in viral infections as well as in non-infected cells^{108,117,120,125}.

In addition to its essential function in mediating necroptosis, a vital role for ZBP1 in apoptosis has been established. IAV infection has been shown to induce ZBP1-dependent necroptosis, as well as ZBP1-triggered apoptosis, the latter mediated by the ZBP1-RIPK3-RIPK1 axis^{126,127}. Interestingly, absence of RIPK1 or mutation of its RHIM domain triggered ZBP1-mediated necroptosis, identifying RIPK1 as an essential inhibitor of ZBP1 activation^{100,101}. A recent study showed, that not only absence of RIPK1 but also absence of either caspase-8 or FADD induced ZBP1-dependent necroptosis *in vitro*, supporting the presence of a RIPK1-FADD-caspase-8 complex preventing necroptotic cell death. Additionally, this study proposed a requirement for cGAS, STING and TBK1 for ZBP1-mediated necroptosis¹²⁸. Of note, ZBP1 was shown to exhibit synergistic functions with TNFR1 to drive colitis in mice lacking FADD in intestinal epithelial cells, providing evidence for crosstalk between these two distinct signaling pathways and furthermore showing a prominent role for FADD in inhibiting necroptosis¹⁰².

As described above, ADAR1 also harbors a $Z\alpha$ domain. Interestingly, mice with impaired ADAR1 functions due to hemizygous expression of ADAR1 with mutated $Z\alpha$ domain triggered pathology which was promoted by ZBP1 induced type I IFN signaling. Surprisingly, this effect was independent of MLKL-mediated necroptosis, caspase-8 mediated apoptosis or pro-

inflammatory RIPK1-RIPK3 driven signaling, suggesting an additional so far unknown functional role for ZBP1 upon binding of dsRNAs¹²⁹⁻¹³¹.

Taken together, ZBP1 is essential for host defense against some viruses but needs to be kept under tight control in order to prevent extensive type I IFN signaling and tissue-damaging necroptosis as well as RIPK3-mediated apoptosis.

1.4.3 ZBP1 in skin homeostasis

Recent studies have highlighted keratinocyte-intrinsic inflammatory and cell death signaling as essential mechanisms regulating skin homeostasis. Extensive characterization of genetic mouse models has described keratinocyte death as a key pathway to trigger severe inflammatory skin pathologies^{71,73,14,132}. Amongst these proteins, ZBP1 has emerged as a key player in skin homeostasis.

The skin is composed of epidermis and dermis and constitutes the largest organ in humans (Figure 5). It forms a life-sustaining immunological and structural barrier establishing the first line of defense against chemical, mechanical and microbial challenges.

The epidermis is the outer layer of the skin and comprises a multilayered epithelium which is composed of basal layer, spinous layer, granular layer and stratum corneum¹³³.

Being the outer layer of the skin, the epidermis forms a physical barrier and mainly protects from environmental threats but also carries out thermoregulation and exchange of lipids. To do so, it contains associated structures such as hair follicles, sebaceous glands and sweat glands. In addition to suprabasal differentiated keratinocytes, the epidermis is composed of multiple stem cell populations which reside in the basal layer and are crucial for tissue homeostasis^{133,134}. Hence, tight regulation between suprabasal cell differentiation and basal cell proliferation is crucial to maintain skin homeostasis. Distinct cell populations within the epidermis are characterized by expression of different marker proteins as well as by their location within the epidermis. Under homeostatic conditions each stem cell compartment is specialized to provide the epidermis with a certain subset of differentiated epidermal cells, however upon skin damage most stem cells can switch to produce all epidermal lineages such as keratinocytes or melanocytes.

ZBP1 has been implicated in skin inflammation by inducing keratinocyte cell death. It has been demonstrated that lack of RIPK1 specifically in keratinocytes unleashes ZBP1, resulting in ZBP1-mediated keratinocyte death and thereby triggering inflammation. This ZBP1-dependent cell death was characterized as RIPK3-mediated necroptosis. Similar results could be obtained upon mutation of the RIPK1 RHIM domain in keratinocytes, indicating that RIPK1 inhibits keratinocyte necroptosis by RHIM-RHIM homotypic interaction with ZBP1. Hence, a model for competitive binding of RIPK1 and RIPK3 to ZBP1 has been proposed^{100,101}.

In this context, ZBP1-mediated keratinocyte necroptosis and the resulting skin inflammation was shown to depend on sensing of nucleic acids by ZBP1^{120,135}. Of note, inflammatory skin lesions triggered by keratinocyte-specific loss of FADD were not dependent on ZBP1 but fully mediated by RIPK3 and only partially mediated by TNFR1 signaling arguing against a sole role for ZBP1-induced cell death upon disruption of the RIPK1-FADD-Caspase 8 complex in the skin¹³⁶.

Taken together, ZBP1 has been identified as a key player in skin pathology by inducing keratinocyte death and inflammation and unleashing of ZBP1 signaling leads to cell death-dependent skin tissue damage.

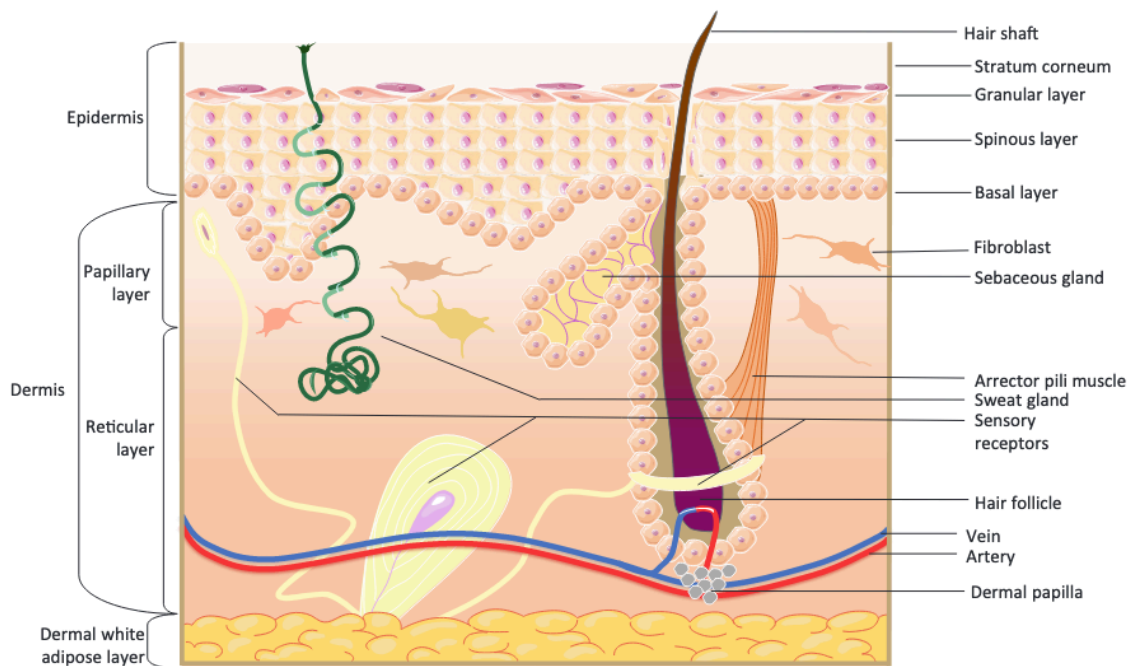


Figure 5. Structure of the skin. The skin is composed of epidermis and dermis. The epidermis is mainly composed of differentiated keratinocytes whilst the dermis contains additional fibroblasts and immune cells¹³³.

1.4.4 ZBP1 in cancer

In addition to its crucial function in skin homeostasis, ZBP1 signaling has been implicated in several tumor entities and in cancer therapy. Human ZBP1 expression has been reported to be restricted to lymphatic tissues and the small intestine, but it was shown that ZBP1 is also expressed in the human colorectal cancer cell line HT29¹³⁷⁻¹³⁹.

As ZBP1 was first thought to potently recognize DNA, it was used as an adjuvant for DNA vaccination in order to enhance anti-tumor immunity¹⁴⁰. The results *in vitro* and *in vivo*, however, showed that ZBP1 was not essential for either innate or adaptive responses to B-DNA or DNA vaccination, respectively¹⁴¹. ZBP1-MLKL-mediated necroptosis was proposed to trigger radiation-induced antitumor immunity by synergizing with the tumor-intrinsic STING pathway. Pharmacological activation of ZBP1 using a small molecule induced ZBP1-dependent necroptosis in tumor-associated fibroblasts and could thereby render mouse

models of melanoma sensitive to immune checkpoint blockade^{142,143}. Moreover, it was demonstrated that combined treatment of IFN γ and KPT-330, a molecule inhibiting nuclear export, could dramatically regress tumor growth in a mouse model of subcutaneously transplanted melanoma. This was dependent on ZBP1 expression and resulting necroptosis in stromal cells¹⁴⁴. Thus, ZBP1 was shown to exert anti-tumorigenic functions by induction of intrinsic tumor cell necroptosis, as well as by induction of necroptosis in surrounding fibroblasts and stromal cells.

On the contrary, ZBP1 was also suggested to trigger necroptosis in breast cancer development, and to thereby fuel tumor growth¹⁴⁵. Furthermore, ZBP1 is selectively expressed in late B cell development, which was proposed to be essential for the T-cell dependent humoral immune response and has been suggested to promote myeloma cell proliferation¹⁴⁶. Therefore, the role of ZBP1 in tumor development and therapy remains controversial and likely differs between distinct tumor entities requiring further elucidation.

1.5 Cell death and inflammatory signaling in cancer

1.5.1 Immunogenic cell death in cancer

As described above, necroptotic cell death triggered by ZBP1 has been suggested to exhibit pro-tumorigenic as well as anti-tumorigenic functions.

Apart from ZBP1, necroptosis has been widely described to exhibit dual functions in tumorigenesis in different settings. On the one hand, necroptosis of endothelial cells was proposed to promote tumor cell extravasation and metastasis. Furthermore, necroptosis was suggested to drive tumor development in a mouse model of pancreatic ductal adenocarcinoma and was shown to direct lineage commitment in liver cancer^{147,148}.

On the other hand, tumor cell necroptosis has been reported to potently stimulate anti-tumor immunity in syngeneic mouse models of cancer¹⁴⁹. In detail, it was proposed in two studies that RIPK3-dependent inflammatory cytokine production was the sole source for immunogenic properties of necroptotic cell death and that anti-tumor immunity induced by necroptosis due to CD 8 T cell cross priming relies on RIPK3-mediated NF- κ B signaling^{150,151}. However, a different set of experiments suggested that NF- κ B signaling was dispensable for efficient anti-tumor immunity induced by necroptotic cells¹⁵². These studies provide evidence that necroptotic cell death of tumor cells could be implicated in tumor therapy.

Similar to a substantial number of studies that documented necroptosis as being anti-tumorigenic, pyroptotic cell death was proposed to trigger potent anti-tumor immunity. Pyroptosis is a lytic form of cell death which is ultimately executed by pore-forming gasdermin proteins. These proteins are cleaved by caspases into active N-terminal fragments which cause membrane rupture and cell death. Prime examples for well-studied gasdermin proteins

are gasdermin E (GSDME) and gasdermin D (GSDMD), which are cleaved by caspase 3 or caspase 1/11, respectively.

GSDME was identified as being tumor suppressive by activating tumor-intrinsic pyroptosis and thereby enhancing anti-tumor immunity upon cleavage by granzyme B¹⁵³. Additionally, injection of gasdermin-conjugated nanoparticles could sensitize 4T1 tumors to immune checkpoint inhibition, providing further evidence of utilizing pyroptosis as a potential option for tumor therapy¹⁵⁴.

In addition to lytic cell death, apoptosis induced by anthracyclines has been described to induce effective anti-tumor immune responses, demonstrating that also apoptotic cells can also exhibit anti-tumor immunity (see section 1.2)¹⁵⁵. However, acquired resistance of cancer cells to apoptosis is a major reason for failure of therapy. Thus, bypassing the apoptotic pathway to induce death of tumor cells is a promising approach to overcome this problem. Necroptotic cell death is a prime candidate for tumor therapy, especially in light of recent studies showing that necroptosis of tumor cells strongly synergized with programmed cell death protein 1 (PD-1) blockade¹⁴⁹.

In summary, induction of lytic cell death can either create an inflammatory, pro-tumorigenic environment or result in efficient anti-tumor immunity. Thus, induction of immunogenic cell death has to be carefully investigated for each cancer entity before being used as a potential therapeutic target.

1.5.2. Inflammatory signaling in cancer

Inflammation has been recognized as one of the hallmarks of cancer and while chronic inflammation can lead to tumor growth, an adequate activation of the immune system can result in elimination of transformed cells¹⁵⁶. TNFR1 signaling regulates inflammation, cell survival and death by inducing distinct intracellular signaling cascades (section 1.3)²². Previous studies have revealed important functions for TNFR1 signaling in the development of different tumor entities. Mice deficient in TNF were described to be resistant to DMBA/TPA induced skin carcinogenesis¹⁵⁷. Increased TNF signaling led to liver inflammation and tumorigenesis in obese mice, suggesting tumor promoting functions for TNFR1 signaling¹⁵⁸. Moreover, TNFR1 has been suggested as a prognostic molecule in ovarian cancer¹⁵⁹. Stimulation of TNFR1 ultimately leads to nuclear accumulation of the nuclear factor κ B (NF- κ B), promoting transcription of genes regulating inflammation and cell survival (section 1.3)^{22,160}. In line with an important role of TNFR1 in cancer, the NF- κ B pathway has emerged as a crucial mediator of tumor growth and progression^{161,162}. It has been demonstrated that NF- κ B signaling is beneficial for tumorigenesis in several cancer entities. Ablation of NF- κ B signaling by IKK2 or p65/RelA depletion in Kras-driven mouse models of lung adenocarcinoma attenuated tumor proliferation and prolonged survival¹⁶³⁻¹⁶⁵. Genetic deletion of IKK2 in a mouse model of colitis

associated cancer led to reduction of tumor numbers, by sensitizing epithelial cells to apoptosis¹⁶⁶. Moreover, p65 mediated NF- κ B signaling was essential for DMBA/TPA-induced skin carcinogenesis *in vivo* by protecting keratinocytes from DNA-damage induced cell death¹⁶⁷. In line with these reports, inhibition of NF- κ B signaling in mammary epithelial cells reduced tumor development in diverse mouse models of mammary tumorigenesis¹⁶⁸⁻¹⁷⁰.

However, NF- κ B signaling has also been shown to exhibit tumor suppressing functions in different tissues and models of carcinogenesis. Inhibition of NF- κ B signaling in human keratinocytes promoted Ras-mediated oncogenic transformation in a xenograft model¹⁷¹ and NF- κ B inhibition via expression of I κ B α SR (SR= super repressor) in murine skin led to development of squamous cell carcinoma^{172,173}. Liver parenchymal cell-specific knockout of NEMO caused the spontaneous development of chronic hepatitis, hepatocyte apoptosis and hepatocellular carcinoma (HCC) in mice^{15,174}. Ablation of IKK2 in hepatocytes led to increased liver tumorigenesis upon diethylnitrosamine (DEN) application¹⁷⁵. Interestingly, NF- κ B activation has been proposed to induce T-cell mediated immune surveillance and therefore tumor rejection in lung adenocarcinoma¹⁷⁶. Therefore, NF- κ B signaling has been identified as a key player in various tumor entities, but the outcome strongly varies, depending on each individual malignancy.

1.6 Lung cancer

Lung cancer is the leading cause of malignant cancer-related deaths with around 1.8 million mortalities in 2020 and is the second most prevalent cancer entity worldwide¹⁷⁷⁻¹⁷⁹. The relative 5-year survival rate varies immensely, depending on individual lung cancer subtypes, but an estimation of a 5-year overall survival rate for lung cancer patients is around 21.7% (National Cancer Institute, NCI). Lung cancer occurs mainly due to extensive tobacco smoking, but up to 20% of diagnosed lung cancer cases also arise in non-smokers^{179,180}.

Lung Cancer has been divided into two major groups based on histopathological and clinical criteria: non-small cell lung cancer (NSCLC) and small cell lung cancer (SCLC). Whereas NSCLC makes up 85% of diagnosed lung cancer cases, SCLC accounts for 15%. NSCLC is a heterogenous diseases and describes three different tumor entities: adenocarcinomas, which arise from type II alveolar cells and make up 50% of NSCLC cases, squamous cell carcinomas which originate from the bronchial tubes and account for 30% of NSCLCs and the additional 20%, which comprise other less- defined subtypes^{181,182,183}. SCLC on the other hand is treated as a single disease and further classifications are lacking to a large extent. Recently, four SCLC subtypes based on the expression of transcription factors were suggested: *ASCL1*^{high} (SCLC-A) and *NEUROD1*^{high} (SCLC-N) make up the neuroendocrine subtypes, while *POUF2F3*^{high} (SCLC-P) and *YAP1*^{high} (SCLC-Y) comprise the non-neuroendocrine subtypes¹⁸⁴.

Detection of specific driver mutations such as in KRAS or EGFR in NSCLC led to development of targeted therapies, which replaced chemotherapy as a first-line treatment and tyrosine-kinase inhibitors are currently used as the standard of care therapy for NSCLC¹⁸².

Despite great improvements for NSCLC therapy, SCLC remains poorly understood and due to the lack of identification of driver mutations clear targeting approaches are missing. In spite of recent characterization of the above described four SCLC subtypes, SCLC is still treated as one single disease. Hence, it is crucial to dissect molecular signaling pathways underlying SCLC in order to identify druggable genetic driver mutations.

1.6.1 Characteristics of small cell lung cancer

SCLC is an extraordinarily aggressive lung cancer subtype which affects approximately 200,000 people worldwide per year¹⁸⁵. The most common risk factor for developing SCLC is heavy smoking, as the vast majority of SCLC patients are past or current smokers. Due to exposure to tobacco, SCLC cells have an unusually high mutational load. In fact, SCLC complies with 7.4 protein-changing mutations per million base pairs the second highest tumor mutational burden (TMB) after melanoma^{186,187}.

Although SCLC has long been assumed to exclusively originate from neuroendocrine precursor cells within the lung, it has been suggested that other lung epithelial cells might also serve as cells of origin^{188,189}.

SCLC forms primary tumors in the chest with additional mediastinal lymph node metastases and the most common sites for further metastasis are bones, bone marrow, adrenal glands, liver and soft tissues^{190,191}. It is mainly characterized by early onset of metastatic spread, neuroendocrine differentiation and small tumor cells¹⁹²⁻¹⁹⁴.

SCLC is divided into limited and extensive stage according to the Veterans Administration Lung Study Group system. Due to early metastasis and rapid growth as well as the lack of timely detection methods, the majority of patients are diagnosed at the extensive stage, resulting in a median survival of 7-13 months and an overall survival rate of only 2%^{186,195}.

Patients are often initially sensitive to platinum-based chemotherapy (cisplatin or carboplatin) combined with a topoisomerase II inhibitor (etoposide) but relapse shortly after and become resistant to cytotoxic treatment¹⁹⁶. Although SCLC is characterized by an absence of immune cell infiltration or immune response, immune checkpoint inhibition (ICI) was approved by the FDA for third-line treatment of SCLC in 2018 due to its high TMB, which is a promising characteristic for the success of ICI, raising hopes for potential clinical effects. However, this treatment strategy did not lead to significantly improved survival. In 2019, ICI in combination with chemotherapy was approved by the EMA as a first-line therapy for patients with extensive stage SCLC¹⁹⁷. This combination only improved median survival by approximately two months, thus more efficient therapies for SCLC are desperately needed.

Molecularly, SCLC is composed of homogenous small cells with scant cytoplasm, granular nuclear chromatin and absent or inconspicuous nucleoli¹⁹⁵. Comprehensive genomic profiling revealed a bi-allelic loss of *RB1* and *TP53* in all patients, demonstrating loss of these tumor suppressors is obligatory in SCLC^{187,198-201}. *TP53* provides essential functions by regulating cellular responses to different cytotoxic stresses (section 1.3.2) and Retinoblastoma protein 1 (*RB1*) is a negative regulator of cell cycle progression by preventing the switch from G1 to S phase. Both proteins are crucial for tumor suppression in diverse cancer entities^{86,202-204}.

Interestingly, the protein BCL-2 (section 1.3.2) is upregulated in a subset of SCLC patients and venetoclax, a BCL-2 inhibitor already approved for treatment of different tumor entities amongst them NSCLC, reduced tumor growth *in vivo* and *in vitro*, uplifting cell death induction as a potential clinical target²⁰⁵⁻²⁰⁷. However, different cell death pathway components such as caspase-8, caspase-10 or CD95 have been reported to be silenced in a fraction of SCLC cell lines, suggesting a strategy for immune escape by evading cell death^{208,209}. Additional genetic alterations commonly found in patients diagnosed with SCLC are loss of p107 or p130, amplification of MYC family members or alterations in PTEN, all leading to proliferation and increased survival of SCLC cells²¹⁰.

Overall little progress has been made in understanding the molecular mechanisms causing SCLC. Thus, it is of utter importance to dissect the signaling pathways underlying this severe disease in order to find new therapeutic targets or to improve the existing first line therapies.

1.6.2 Murine model of small cell lung carcinogenesis

As described under 1.6.1, loss of the tumor suppressors *RB1* and *TP53* is obligatory in SCLC. Indeed, the pathology of human SCLC is phenocopied by ablation of *Rb1* and *Tp53* in mouse lung epithelial cells. In detail, the well-established RP mouse model carries loxP flanked *Rb1* (exon 19) and loxP flanked *Tp53* (exons 2-10) alleles. Intratracheal instillation of replication-deficient Adeno-Cre results in homozygous deletion of *Rb1* and *Tp53* in a subset of lung epithelial cells targeted by the virus, leading to development of multiple tumor lesions within four to six months. These neoplasia recapitulate all essential features of human SCLC, including the histopathological and immunological phenotype as well as metastatic sites and invasion in surrounding lung parenchyma. Therefore, the RP mouse model is an excellent tool to dissect SCLC progression and development *in vivo*²¹¹ (Figure 6).

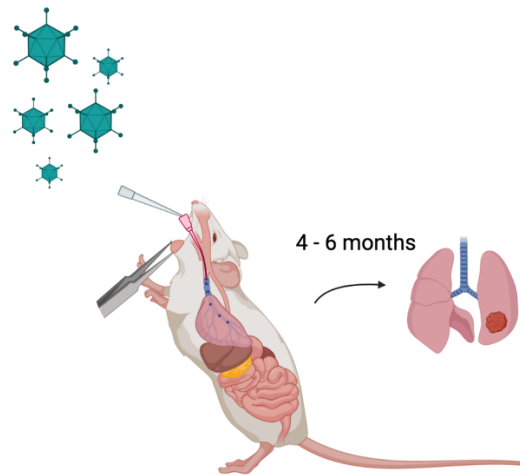


Figure 6. Scheme depicting intratracheal Ad-Cre inhalation for the generation of a mouse model of SCLC. Intratracheal application of adenovirus carrying Cre-recombinase into mice harboring $Rb1^{FL/FL}$ $Tp53^{FL/FL}$ alleles results in development of a SCLC-like phenotype after four to six months. Created with BioRender.com.

1.7 Aims of the study

Here, we aimed to elucidate the mechanisms regulating the *in vivo* downstream signaling of ZBP1. Despite robust evidence that ZBP1 acts as a driver of cell death and inflammation, the downstream pathways of ZBP1 *in vivo* remain incompletely understood.

Since ZBP1 has been identified as a key player of skin homeostasis, we used the skin as a well-established and easy-accessible model system to study ZBP1 signaling.

Furthermore, recent studies have raised hope for the induction of inflammatory cell death as a new therapeutic target in tumor therapy. As ZBP1 is a promising candidate to induce inflammatory cell death, we investigated the potential role of ZBP1 in triggering anti-tumor immunity in SCLC, a tumor entity which urgently needs improved therapeutic options. As a complementary approach, we studied the role of preventing necroptotic signaling in SCLC development and progression.

Lastly, we aimed to shed light on the mechanisms regulating cell death and immune responses in SCLC development, especially dissecting the role of pro-inflammatory NF- κ B and TNFR1 pathways using relevant mouse models.

2. Publications, Manuscripts and Results

2.1 ZBP1 causes skin inflammation by inducing RIPK3-dependent necroptosis and RIPK1-mediated apoptosis in keratinocytes

Manuscript declaration

Here, we identify ZBP1 as a mediator of skin inflammation in FADD^{E-KO} mice and aimed to unravel the role of ZBP1 downstream signaling in the skin by using genetically modified mouse models.

Specific contributions:

- Generation of all *in vitro* and *in vivo* data shown in this study besides Figure 1 F, G; Figure 4A, Figure S2 & S4
- Analysis of all data generated in this study
- Manuscript drafting and editing

ZBP1 causes skin inflammation by inducing RIPK3-dependent necroptosis and RIPK1-mediated apoptosis in keratinocytes

Lioba Koerner^{1,2}, Laurens Wachsmuth^{1,2}, Snehlata Kumari^{1,2}, Robin Schwarzer^{1,2}, Huipeng Jiao^{1,2}, Manolis Pasparakis^{1,2,3,4*}

¹Institute for Genetics, University of Cologne, 50674 Cologne, Germany

²Cologne Excellence Cluster on Cellular Stress Responses in Aging-Associated Diseases (CECAD), University of Cologne, 50931 Cologne, Germany

³Center for Molecular Medicine (CMMC), Medical Faculty and University Hospital Cologne, University of Cologne, 50931 Cologne, Germany

⁴Lead contact

*Correspondence: pasparakis@uni-koeln.de

Abstract

Z-DNA binding protein 1 (ZBP1) has emerged as a potent inducer of necroptosis with important functions in anti-viral immunity and in the regulation of inflammatory responses. Studies in genetic mouse models suggested that ZBP1 primarily signals by interacting with and activating RIPK3 to induce necroptosis and inflammation. However, the mechanisms by which ZBP1 induces inflammation and in particular the role of RIPK1 and the contribution of cell death-independent signaling remain unclear. Here we show that ZBP1 cooperates with TNFR1 to induce skin inflammation in mice with epidermis-specific ablation of FADD by triggering keratinocyte necroptosis. In addition, we show that expression of a C-terminally truncated

version of ZBP1 in mouse epidermal keratinocytes induces severe skin inflammation by triggering RIPK3-mediated necroptosis and caspase-8 mediated apoptosis. Our *in vivo* studies provide genetic evidence that ZBP1 interacts with and activates RIPK1, which induces caspase-8-mediated keratinocyte apoptosis independently of its kinase activity. Collectively, these results showed that ZBP1 induces skin inflammation in mice by triggering RIPK3-mediated necroptosis and RIPK1-caspase-8-mediated apoptosis of keratinocytes.

Introduction

Z-DNA binding protein 1 (ZBP1, also known as DLM1 and DAI) has emerged as a potent mediator of cell death, inflammation and immunity. ZBP1 contains two N-terminal Z α domains that specifically bind to Z-form nucleic acids, DNA and double stranded (ds)RNA with an alternative left-handed double helix structure¹⁻⁴. In addition, ZBP1 contains three C-terminal receptor interacting protein (RIP) homotypic interaction motifs (RHIMs) that facilitate its interaction with other RHIM-containing proteins. RIPK1, RIPK3 and TIR-domain-containing adapter-inducing interferon- β (TRIF) are the only proteins in addition to ZBP1 that harbor RHIMs. ZBP1 has been shown to bind and activate RIPK3, resulting in RIPK3 auto-phosphorylation and the subsequent phosphorylation of mixed lineage kinase-like (MLKL), which translocates to the plasma membrane causing necroptosis^{5,6}. Moreover, ZBP1 was reported to activate inflammatory signaling by interacting with RIPK1 and with RIPK3 to induce activation of nuclear factor kappa B (NF- κ B)-dependent gene transcription^{7,8}. ZBP1 plays an important role in response to infection with certain viruses, including influenza, vaccinia, herpes simplex and murine cytomegalovirus, where it senses viral Z-RNA and induces RIPK3-mediated necroptosis to restrict viral replication⁹⁻¹³.

Studies in genetic mouse models identified ZBP1 as a potent inducer of inflammation in the absence of viral infection. Mice with epidermal keratinocyte-specific ablation of RIPK1 (RIPK1^{E-KO}) develop severe skin inflammation mediated by RIPK3-MLKL-dependent keratinocyte necroptosis, which is strongly suppressed by ZBP1 deficiency but only partially ameliorated by TNFR1 knockout^{5,14}. In addition, mutation of the RIPK1 RHIM in mice (*Ripk1*^{mR/mR}) causes perinatal lethality that is dependent on ZBP1-RIPK3-MLKL-mediated necroptosis^{5,6}. These studies showed that RIPK1 acts via its RHIM to suppress activation of ZBP1 and the induction of necroptosis, which is important for preventing the development of inflammatory skin lesions and early postnatal lethality. ZBP1 also plays an important role in the pathogenesis of intestinal inflammation in mice with intestinal epithelial cell (IEC)-specific ablation of Fas associated with death domain (FADD), an adapter that is essential for activation of caspase-8 downstream of death receptors. FADD^{IEC-KO} mice develop colitis mediated by RIPK3-MLKL-dependent necroptosis, as well as ileitis that is largely dependent on necroptosis and to a lesser extent

on gasdermin D-mediated cell death¹⁵. Ablation of ZBP1 or TNFR1 alone could not inhibit ileitis in FADD^{IEC-KO} mice, however, combined ablation of both ZBP1 and TNFR1 strongly suppressed the pathology revealing a functional redundancy between these two proteins¹⁵. In contrast, loss of ZBP1 or TNFR1 alone could strongly suppress colitis development in FADD^{IEC-KO} mice, showing that in this tissue both proteins are required to induce the disease¹⁵. These findings revealed an interplay between ZBP1 and TNFR1 signaling in triggering epithelial cell necroptosis and intestinal inflammation. Importantly, mutation of the ZBP1 Z α domains prevented skin inflammation in RIPK1^{E-KO} mice and perinatal lethality in *Ripk1*^{mR/mR} mice, as well as intestinal inflammation in FADD^{E-KO} mice^{4,16}, arguing that ZBP1 is activated by sensing endogenous Z-nucleic acids via its Z α domains and induces necroptosis and inflammation. Together, RIPK1 and caspase-8 play a critical role in restricting ZBP1 activation by endogenous Z-nucleic acids and preventing necroptosis and inflammation. ZBP1 was also shown to play an important role in driving intestinal inflammation in mice with IEC-specific knockout of SETDB1, a histone methyltransferase mediating the trimethylation of histone H3 at lysine 9¹⁷. This intestinal pathology was fully prevented by either ZBP1 deficiency or IEC-specific caspase-8 ablation combined with RIPK3 knockout, whereas RIPK3 or MLKL deficiencies alone could only partially prevent the disease, suggesting necroptosis-independent functions of ZBP1. Moreover, ZBP1 was recently reported to mediate heatstroke-induced pathology in a RIPK3-dependent manner¹⁸. Collectively, ZBP1 causes inflammation and disease *in vivo* by activating RIPK3, whereas the possible function of RIPK1 in mediating ZBP1-induced pathology remains unclear.

Here, we investigated the mechanisms by which ZBP1 induces inflammatory pathologies *in vivo*. We show that ZBP1 mediates TNFR1-independent inflammation in FADD^{E-KO} mice by inducing RIPK3-MLKL-dependent necroptosis. In addition, using a newly developed mouse model, we show that ZBP1 acts via its first RHIM to activate RIPK3-MLKL-mediated necroptosis and, importantly, to directly engage RIPK1 inducing caspase-8-mediated apoptosis in keratinocytes. Our results provide experimental evidence that ZBP1 induces skin inflammation exclusively by triggering cell death arguing against a role of ZBP1 in inducing cell death-independent inflammatory signaling.

Results

MLKL-mediated necroptosis drives skin inflammation in FADD^{E-KO} mice

We showed previously that mice lacking FADD specifically in epidermal keratinocytes (*Fadd*^{fl/fl} *K14-Cre*, hereafter referred to as FADD^{E-KO} mice) developed severe inflammatory skin lesions that were prevented by RIPK3 deficiency, suggesting that necroptosis of FADD-deficient

keratinocytes drives skin inflammation¹⁹. Since RIPK3 has been shown to induce also necroptosis-independent inflammatory responses^{15,20}, to unequivocally prove that necroptosis drives the pathology in FADD^{E-KO} mice we crossed them with mice lacking MLKL. All FADD^{E-KO} mice developed inflammatory skin lesions starting at postnatal day 6 (P6), which progressed rapidly to a severe dermatitis requiring their sacrifice by P7 (Figure 1A, B). Histologically, the skin of FADD^{E-KO} mice at P7 was characterized by epidermal thickening, increased expression of the basal keratinocyte marker keratin 14 (K14), loss of the suprabasal keratinocyte marker keratin 10 (K10), as well as by aberrant expression of keratin 6 (K6), which serves as a marker for an inflamed and hyperplastic epidermis (Figure 1C, D). Moreover, FADD^{E-KO} mice at P7 displayed increased expression of the inflammatory cytokines *Tnf* and *Il6* as well as of the chemokines *Ccl4* and *Cxcl9* and of certain interferon stimulated genes including *Oas1* and *Zbp1* (Figure 1E). MLKL deficiency prevented the development of severe skin lesions in FADD^{E-KO} mice early after birth with FADD^{E-KO} *Mlkl*^{-/-} mice reaching adulthood without showing skin lesions (Figure 1B, F). When followed up to the age of 1 year, only 2 out of 8 FADD^{E-KO} *Mlkl*^{-/-} mice showing minor skin lesions at the age of 11 – 12 months (Figure 1B). Histological analysis of skin sections from FADD^{E-KO} *Mlkl*^{-/-} mice at the age of 48-50 weeks revealed a normal tissue structure without signs of hyperplasia and abnormal differentiation or inflammation (Figure 1G). Together, these results demonstrated that MLKL-mediated keratinocyte necroptosis causes severe inflammatory skin pathology in FADD^{E-KO} mice.

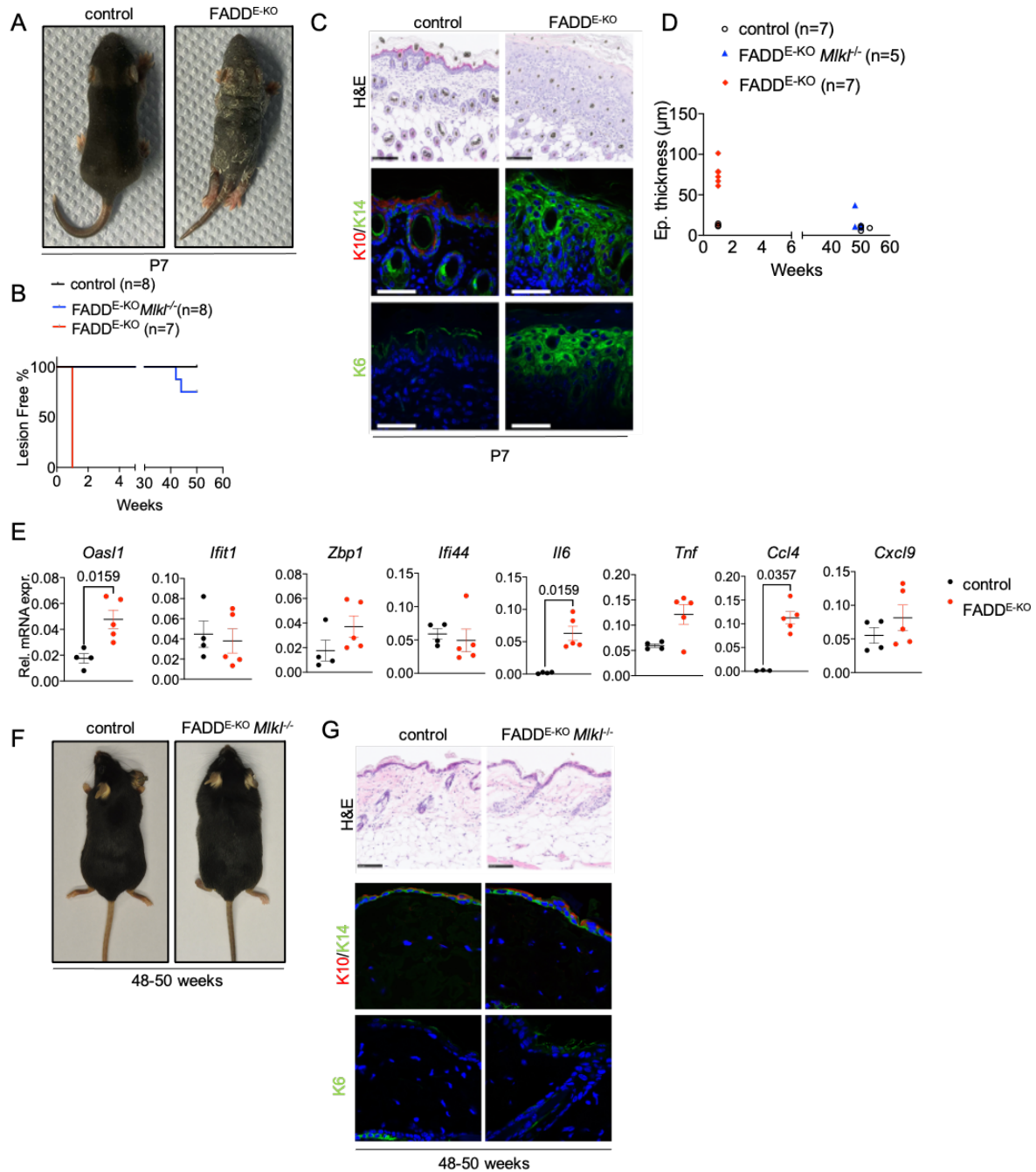


Figure 1. MLKL drives FADD^{E-KO} dependent skin inflammation (A) Representative photographs of FADD^{E-KO} (n=7) mouse with unaffected littermate (n=4) at P7. (B) Graph depicting lesion onset of mice with indicated genotypes (C) Representative images from skin sections of FADD^{E-KO} and littermates stained with H&E (Scale bars = 100 μm, n=7 for FADD^{E-KO}, n=4 for control) or immunostained with K10, K14 and K6 (Scale bars = 50 μm, n=4 for FADD^{E-KO}, n=3 for control). (D) Graph depicting epidermal thickness of mice with indicated genotypes (E) Graphs depicting relative mRNA expression of the indicated cytokines and ISGs in RNA from whole-skin tissue of mice at P7 of the indicated genotypes measured by qRT-PCR. Each dot represents one mouse. Mean ± SEM are shown (n=4 for control, n=5 for FADD^{E-KO} for all genes besides *Ccl4* control n=3) (F) Representative photographs of FADD^{E-KO} *Mik1*^{-/-} mouse and healthy littermate at 48-50 weeks of age (n=8 for FADD^{E-KO} *Mik1*^{-/-}, n=8 for control) (G) Representative images from skin sections of FADD^{E-KO} *Mik1*^{-/-} and healthy control stained with H&E (Scale bars=100 μm n=5 for FADD^{E-KO} *Mik1*^{-/-}, n=4 for control) or immunostained with K10, K14 and K6.

ZBP1 promotes TNFR1-independent skin inflammation in FADD^{E-KO} mice

We showed previously that TNFR1 deficiency delayed but could not prevent the development of inflammatory skin lesions in FADD^{E-KO} mice, suggesting that additional, TNFR1-independent, mechanisms drive keratinocyte necroptosis and skin inflammation in these animals¹⁹. Our previous studies identified ZBP1 as a potent driver of keratinocyte necroptosis and skin inflammation in mice lacking RIPK1 in keratinocytes or expressing RIPK1 with mutated RHIM^{4,5}, suggesting that ZBP1 could be implicated in inducing keratinocyte necroptosis in FADD^{E-KO} mice. Yet, ZBP1 deficiency could not ameliorate the skin pathology in FADD^{E-KO} mice⁵, indicating that ZBP1 does not play an essential role in this model. However, our previous work in mice lacking FADD in intestinal epithelial cells (IECs) showed that TNFR1 cooperates with ZBP1 to induce necroptosis-mediated gut inflammation, revealing an intricate interplay between TNFR1 and ZBP1 in causing IEC necroptosis¹⁵. We therefore hypothesized that ZBP1 might drive TNFR1-independent skin inflammation in FADD^{E-KO} mice. To address this hypothesis, we generated and analyzed *Fadd^{fl/fl} Tnfr1^{fl/fl} K14-Cre Zbp1^{-/-}* (hereafter referred to as FADD^{E-KO} TNFR1^{E-KO} Zbp1^{-/-}) mice, which lack FADD and TNFR1 in keratinocytes in a ZBP1-deficient genetic background. Consistent with our earlier findings that ubiquitous TNFR1 deficiency delayed but could not prevent skin inflammation in FADD^{E-KO} mice, *Fadd^{fl/fl} Tnfr1^{fl/fl} K14-Cre Zbp1^{-WT}* mice (hereafter referred to as FADD^{E-KO} TNFR1^{E-KO} Zbp1^{-WT}), which lack FADD and TNFR1 specifically in epidermal keratinocytes and are heterozygous for the *Zbp1* knockout allele, developed progressive skin lesions between 3-10 weeks of life that reached pre-determined termination criteria requiring the humane sacrifice of the animals by the age of 11 weeks (Figure 2A, B). In contrast, we did not observe any skin lesions in FADD^{E-KO} TNFR1^{E-KO} Zbp1^{-/-} mice up to at least 30 weeks of age (Figure 2A, B). Histopathological analysis revealed that combined loss of TNFR1 and ZBP1 fully prevented the development of inflammatory skin lesions in FADD^{E-KO} mice (Figure 2C, D). Whereas skin sections from FADD^{E-KO} TNFR1^{E-KO} Zbp1^{-WT} littermates showed the characteristic epidermal hyperplasia and altered keratin expression, the skin of FADD^{E-KO} TNFR1^{E-KO} Zbp1^{-/-} mice showed normal epidermal thickness and differentiation with no signs of skin pathology (Figure 2C, D). Collectively, these results showed that ZBP1 and TNFR1 cooperate to induce keratinocyte necroptosis and skin inflammation in FADD^{E-KO} mice.

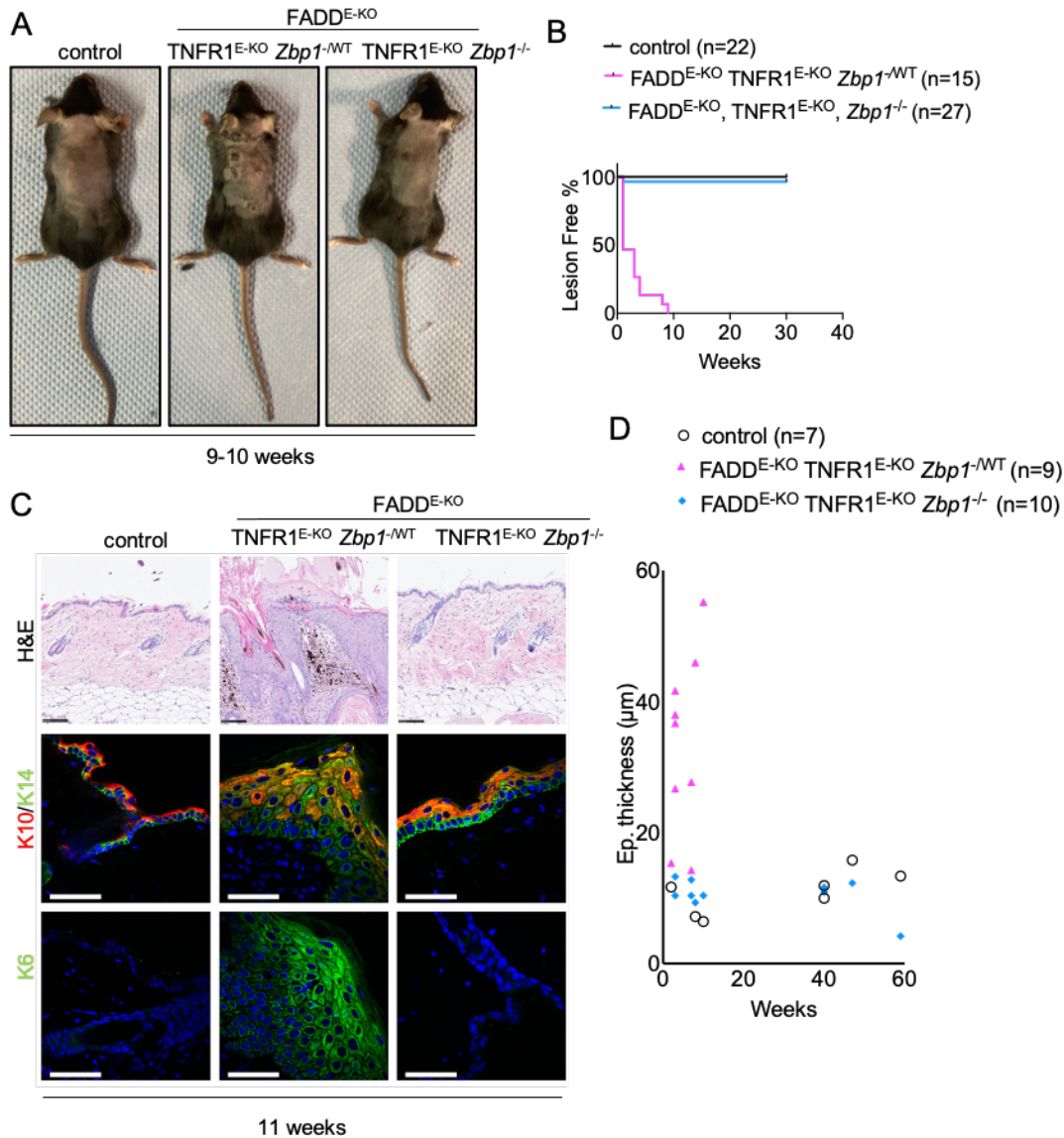


Figure 2. TNFR1 and ZBP1 synergize to drive inflammatory skin disease in FADD^{E-KO} mice. (A) Representative photographs of FADD^{E-KO} TNFR1^{E-KO} Zbp1^{-WT} (n=15), FADD^{E-KO} TNFR1^{E-KO} Zbp1^{-/-} (n=27) mouse with healthy littermate (n=22). (B) Graph depicting lesion onset of mice with indicated genotypes. (C) Representative images from skin sections stained with H&E (Scale bars = 100 μ m, n=9 for FADD^{E-KO} TNFR1^{E-KO} Zbp1^{-WT}, n=10 for FADD^{E-KO} TNFR1^{E-KO} Zbp1^{-/-}, n=7 for control) or immunostained with K10, K14 and K6 (Scale bars= 50 μ m, n=3 for FADD^{E-KO} TNFR1^{E-KO} Zbp1^{-WT} n=5 for FADD^{E-KO} TNFR1^{E-KO} Zbp1^{-/-}, n=6 for control). (D) Graph depicting epidermal thickness of mice with indicated genotypes.

C-terminally truncated ZBP1 induces cell death in the absence of caspase inhibitors

Our results described above, together with our previous findings that ZBP1 causes MLKL-mediated skin inflammation in mice lacking FADD, RIPK1 or expressing RIPK1 with mutated RHIM, showed that ZBP1 is a potent driver of keratinocyte necroptosis^{4,5}. However, in these models the absence of FADD or RIPK1 sensitizes cells to ZBP1-induced necroptosis, therefore it remains unclear whether ZBP1 also causes necroptosis in cells with intact FADD-Caspase-8 and RIPK1 signaling. To this end, we sought to develop an experimental system allowing to

induce ZBP1-mediated death in cells with normal expression of other cell death regulators including FADD, caspase-8 and RIPK1. As shown previously⁴ doxycycline-induced overexpression of wild type full length mouse ZBP1 (FL-ZBP1) could induce cell death in immortalized mouse embryonic fibroblasts (iMEFs) in the presence, but not in the absence, of the caspase inhibitor emricasan (Figure 3A - C). In order to identify a form of ZBP1 that can induce cell death also in the absence of caspase inhibitors, we generated and tested different versions of C-terminally truncated ZBP1 proteins. We found that deletion of the last 203 amino acids resulting in the expression of a C-terminally truncated mouse ZBP1 containing the two Z α domains and the first RHIM was capable of inducing cell death in iMEFs in the absence of emricasan (Figure 3A – C). Hereafter, we refer to this C-terminally truncated ZBP1 version as constitutively active ZBP1, abbreviated as “ZBP1ca”. ZBP1ca-mediated cell death could be enhanced by additional emricasan treatment but could not be blocked by the RIPK3 kinase inhibitor GSK872 (Figure 3C). Importantly, combined treatment with emricasan and GSK872 fully prevented ZBP1ca-induced cell death (Figure 3C), showing that ZBP1ca triggers RIPK3 kinase dependent necroptosis as well as caspase-8-mediated apoptosis. Interestingly, inhibition of RIPK1 kinase activity with Necrostatin-1s (Nec1s) could partially ameliorate ZBP1ca-induced cell death (Figure 3C), suggesting that ZBP1ca could also interact with and activate RIPK1. This finding was unexpected, as we found in our previous studies that, in the absence of caspase inhibitors, ZBP1 could interact with RIPK3 but not with RIPK1^{4,5}. However, caspase inhibition promoted the interaction of ZBP1 with RIPK1, suggesting that caspase-8 inhibits the formation of a ZBP1-nucleated complex containing RIPK1, likely by cleaving RIPK1⁴. In order to investigate whether the truncated ZBP1ca could interact with RIPK1 in the absence of caspase inhibitors, we immunoprecipitated FL-ZBP1 and ZBP1ca using anti-FLAG antibodies followed by immunoblotting for RIPK3 and RIPK1. As described previously^{4,5} we found that overexpressed FL-ZBP1 interacted with RIPK3 but not with RIPK1 (Figure 3D). ZBP1ca also interacted with RIPK3, however, in contrast to the full-length protein, it additionally interacted with RIPK1 (Figure 3D). This finding, together with the results that Nec1s treatment partially prevented ZBP1ca-induced cell death, suggested that ZBP1ca interacts with and activates RIPK1 to induce cell death. Collectively, ZBP1ca triggered cell death in cells with intact caspase-8 and RIPK1 signaling by inducing both apoptosis and necroptosis.

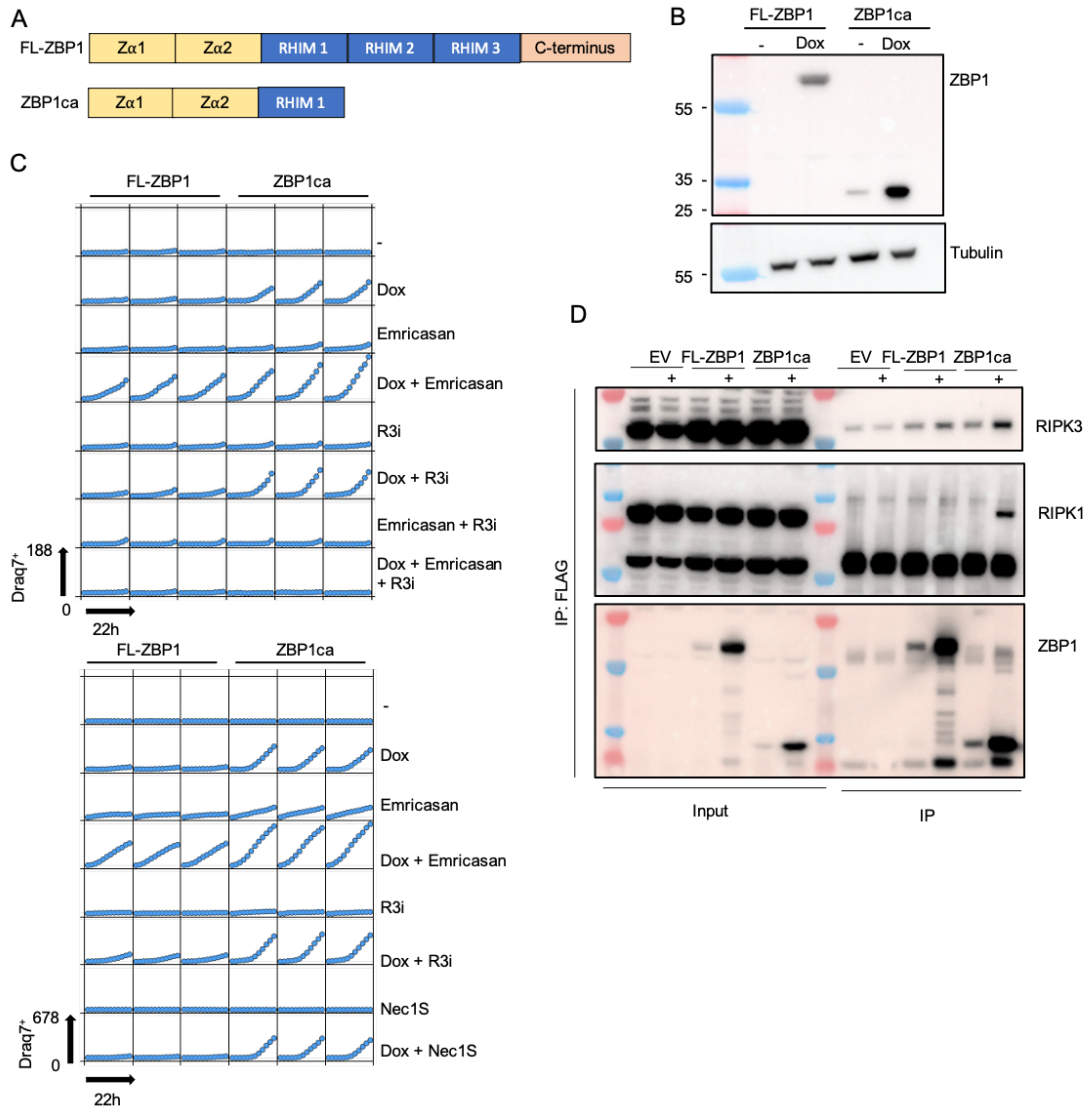


Figure 3. Constitutively active ZBP1 drives cell death *in vitro* (A) Scheme depicting structure of FL-ZBP1 and ZBP1ca (B) Immunoblot analysis of protein extracts from iMEFs transduced with doxycycline (Dox)-inducible FL-ZBP1- or ZBP1ca-expressing vectors. (C) Cell death measured by DraQ7 uptake in iMEFs stimulated with combinations of doxycycline (dox), emricasan, Nec1S and RIPK3 inhibitor GSK827 (R3i) (D) anti-Flag immunoprecipitates in iMEFs expressing dox-induced Flag-tagged FL-ZBP1 or Flag-tagged ZBP1ca stimulated with dox.

ZBP1ca expression in keratinocytes causes skin inflammation

Our results showing that ZBP1ca expression caused cell death in iMEFs without any additional treatment prompted us to employ ZBP1ca expression as a tool to study ZBP1-mediated signaling *in vivo*. To this end, we generated knock-in mice that express ZBP1ca under the control of the ubiquitously expressed *Rosa26* locus after Cre-mediated excision of a loxP-flanked stop cassette ($R26^{LSL.ZBP1ca}$) (Figure 4A). To study the effect of ZBP1ca expression in epidermal keratinocytes, we crossed $R26^{LSL.ZBP1ca}$ animals with *K14-Cre* transgenics²¹ to generate $R26^{LSL.ZBP1ca/WT}$ *K14-Cre* mice (hereafter referred to as ZBP1ca^{E-het}). ZBP1ca^{E-het} mice were born at the expected Mendelian ratio and were macroscopically indistinguishable from their $R26^{LSL.ZBP1ca/WT}$ littermates until P7, when they started to develop skin lesions mainly

affecting the abdominal and tail skin. The phenotype progressed rapidly to severe lesions, characterized by skin thickening and scaling gradually increasing in size and distribution (Figure 4B-C). All ZBP1ca^{E-het} animals had to be culled between P9 and P14 because of reaching pre-determined ethical severity criteria, especially due to severe inflammation affecting the entire tail. ZBP1ca^{E-het} whole skin lysates displayed strong expression of ZBP1ca (Figure 4D). In order to characterize the skin pathology, we examined ZBP1ca^{E-het} mice at different time points after birth. At P2, ZBP1ca^{E-het} mice were macroscopically indistinguishable from their *R26^{LSL.ZBP1ca/WT}* littermates (Figure S1A). Immunohistological analysis of sections from abdominal and tail skin revealed an overall normal epidermal thickness and differentiation as judged by expression of keratin 14 (K14) in basal and K10 in suprabasal keratinocytes (Figure S1B). However, ZBP1ca^{E-het} mice showed upregulation of K6, a marker of skin inflammation, in interfollicular epidermis in both the abdominal and tail skin indicating the initiation of an inflammatory skin reaction already at P2 (Figure S1B). Histopathological analysis of abdominal and tail skin sections of mice sacrificed at P10-P12 revealed pronounced epidermal thickening in ZBP1ca^{E-het} mice compared to their littermate controls (Figure 4E, F). Moreover, the epidermis of ZBP1ca^{E-het} mice showed a nearly complete loss of K10 concomitant with a strong upregulation of K14 and K6 in all epidermal layers, consistent with strong epidermal hyperplasia and loss of differentiation (Figure 4E). To assess whether ZBP1ca expression induced keratinocyte death, we immunostained skin sections for cleaved caspase-3 (CC3) and found increased numbers of CC3⁺ keratinocytes in the skin of ZBP1ca^{E-het} mice (Figure 4E, G). To assess inflammatory gene expression, we performed qRT-PCR analysis on RNA isolated from abdominal skin of ZBP1ca^{E-het} and littermate control mice. These experiments revealed upregulation of inflammatory cytokines and chemokines such as *Tnf*, *IL-1 β* , *Il6*, *Cxcl9* and *Ccl4*, as well as of interferon stimulated genes (ISGs) including *Oas1*, *Ifi44*, and *Ifit1* in the skin of ZBP1ca^{E-het} mice compared to *R26^{LSL.ZBP1ca/WT}* controls (Figure 4H). Taken together, these results showed that expression of ZBP1ca induced keratinocyte death and skin inflammation *in vivo*.

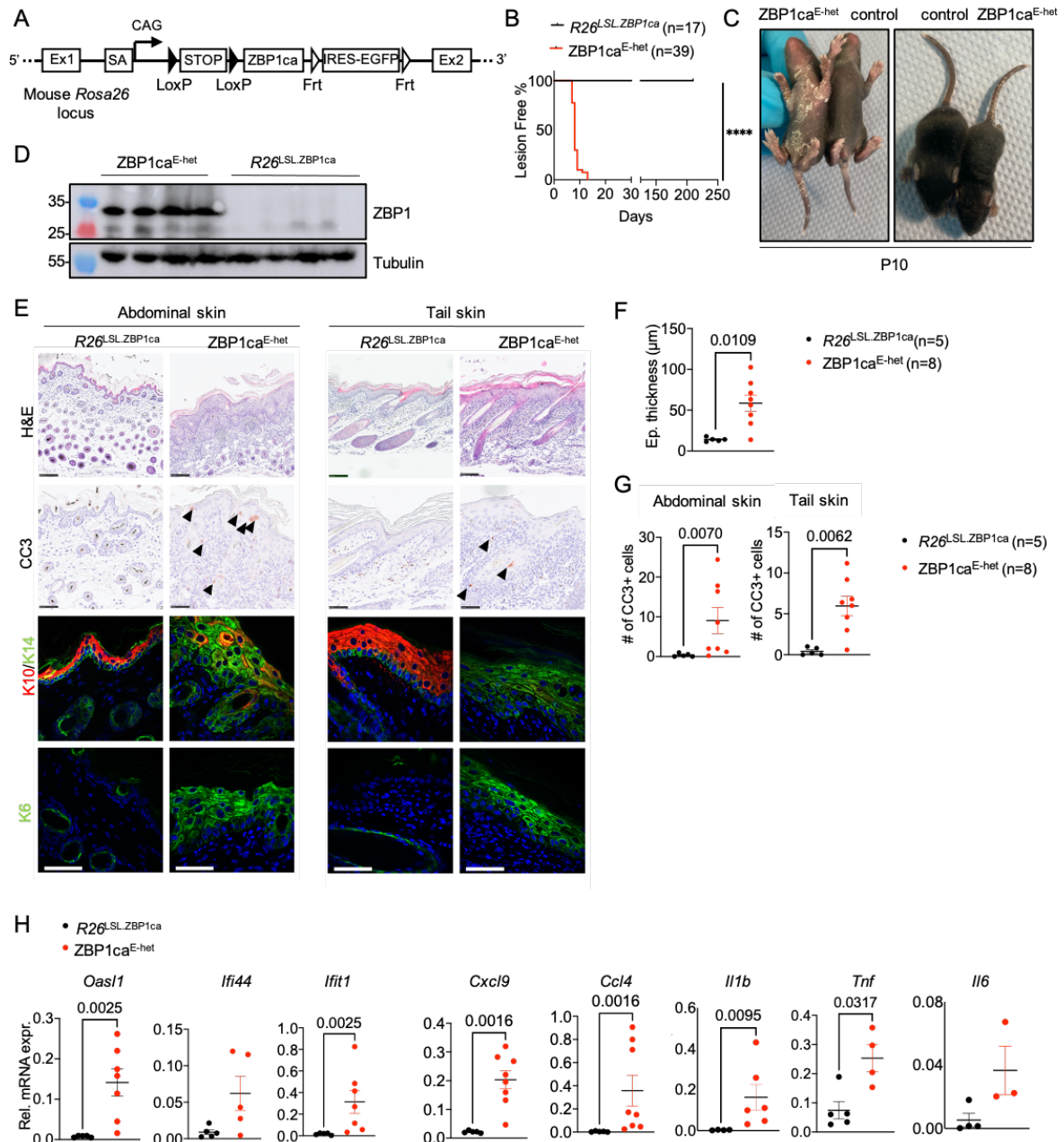


Figure 4. ZBP1ca expression in keratinocytes leads to severe skin inflammation (A) Targeting scheme for generation of *R26^{LSL}.ZBP1ca* mouse strain using CRISPR Cas9. **(B)** Graph depicting lesion onset of mice with indicated genotypes **(C)** Representative photographs of *ZBP1ca^{E-het}* mouse (n=39) and WT littermate (n=17) at P10. **(D)** Immunoblot analysis of whole skin protein lysates from *ZBP1ca^{E-het}* (n=4) and littermate controls (n=4). Mice were analyzed at P10-12. **(E)** Representative images from abdominal and tail skin sections of *ZBP1ca^{E-het}* mice and littermates at P10-12 stained with H&E (Scale bars=100 μ m, n=11 for *ZBP1ca^{E-het}*, n=5 for control), CC3⁺ (n=5 for *ZBP1ca^{E-het}*, n=2 for *R26^{LSL}.ZBP1ca*) or immunostained with K10, K14 and K6 (Scale bars=50 μ m, n=9 for *ZBP1ca^{E-het}*, n=11 for control) **(F)** Graph depicting epidermal thickness of mice with indicated genotypes at P10-12. Mean \pm SEM are shown. Each dot represents one mouse. **(G)** Graph showing the amount of CC3⁺ cells in abdominal and tail skin of mice with indicated genotypes. Mean \pm SEM are shown. Each dot represents one mouse. **(H)** Graphs depicting relative mRNA expression of the indicated cytokines and ISGs in RNA from whole-skin tissue of P10-12 mice of the indicated genotypes measured by qRT-PCR. Each dot represents one mouse. Mean \pm SEM are shown. All qRT-PCRs display data from mouse numbers indicated in table S1.

RHIM-dependent RIPK3 signaling contributes to skin inflammation in ZBP1ca^{E-het} mice

ZBP1 was previously shown to mediate both apoptosis and necroptosis by interacting with and activating RIPK3^{4,5,11,15,22}. We therefore hypothesized, that ZBP1ca induces keratinocyte death and skin inflammation by interacting with RIPK3 via its RHIM. In order to study the role of RHIM-dependent RIPK3 signaling we generated knock-in mice expressing RIPK3 with mutated RHIM by substituting the four conserved amino acids (VQIG) at position 448-451 with alanines (hereafter referred to as *Ripk3^{mR/mR}*) (Figure S2A, B). Primary lung fibroblasts (LFs) from *Ripk3^{mR/mR}* mice expressed normal levels of RIPK3 protein and were fully protected from necroptosis induced by treatment with TNF together with the SMAC mimetic birinapant and emricasan (TSE), confirming that the introduced mutation disrupted RIPK3-dependent signaling (Figure S2C,D). To assess the role of RHIM-dependent RIPK3 signalling in ZBP1ca-mediated cell death and inflammation, we generated and analyzed *R26^{LSL}.ZBP1ca^{WT} x K14-Cre x Ripk3^{mR/mR}* (ZBP1ca^{E-het} *Ripk3^{mR/mR}*) mice. Surprisingly, RIPK3 RHIM mutation strongly ameliorated but could not fully prevent skin lesion development in ZBP1ca^{E-het} mice. Out of 24 animals observed, 14 animals developed inflammatory skin lesions, affecting mainly the tail skin (Figure 5A and S3C). The lesions particularly in tail skin reached the level of severity requiring the humane sacrifice of 6 mice before the age of 4 weeks. In the remaining 18 mice, the lesions appeared to be transient and disappeared after a few weeks, with these animals remaining healthy at least up to the age of 30 weeks (Figure 5B, S3). Consistent with the macroscopic appearance, histopathological analysis revealed an overall milder phenotype in the affected ZBP1ca^{E-het} *Ripk3^{mR/mR}* mice compared to ZBP1ca^{E-het} animals at the age of 10-12 days. Most skin areas showed normal epidermal thickness and differentiation, with only small affected areas showing upregulation of K6 (Figure 5C, D). Immunostaining for cleaved caspase-3 revealed the presence of apoptotic cells in the skin of ZBP1ca^{E-het} *Ripk3^{mR/mR}* mice. Interestingly, whereas the number of CC3⁺ cells was decreased in the abdominal skin of ZBP1ca^{E-het} *Ripk3^{mR/mR}* mice, we found similar if not slightly increased numbers of apoptotic cells in tail skin from ZBP1ca^{E-het} *Ripk3^{mR/mR}* compared to ZBP1ca^{E-het} mice (Figure 5D, E). Consistent with the histological picture, mutation of the RHIM of RIPK3 suppressed the expression of inflammatory cytokines and chemokines as well as of ISGs in the skin of ZBP1ca^{E-het} *Ripk3^{mR/mR}* compared to ZBP1ca^{E-het} mice (Figure 5F). However, ZBP1ca^{E-het} *Ripk3^{mR/mR}* mice showed elevated expression of *Cxcl9*, *Ifi44* and *Ifit1* and a trend towards increased expression of *Tnf* in their skin compared to *K14-Cre* negative control mice, further supporting that blocking RHIM-dependent RIPK3 signaling did not fully prevent skin inflammation. Therefore, mutation of the RIPK3 RHIM strongly ameliorated but could not fully prevent keratinocyte death and skin inflammation in ZBP1ca^{E-het} *Ripk3^{mR/mR}* mice, showing that ZBP1ca drives cell death and inflammation by both RIPK3-dependent and RIPK3-independent mechanisms.

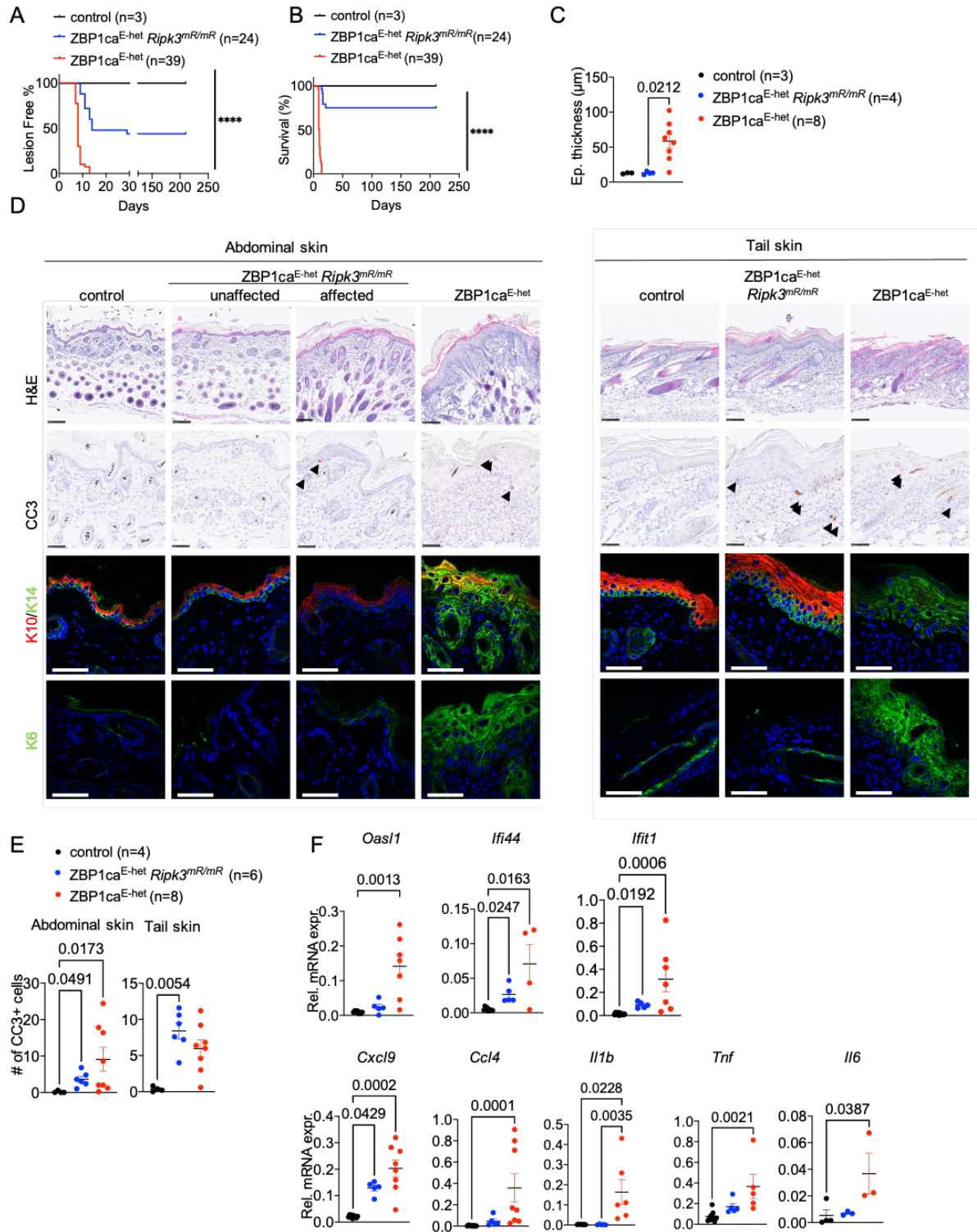


Figure 5. ZBP1ca driven skin inflammation is partially RIPK3-RHIM mediated (A) Graph depicting lesion-free survival of ZBP1ca^{E-het}, ZBP1ca^{E-het} *Ripk3*^{mR/mR} mice and healthy littermates. **(B)** Graph depicting survival curve of ZBP1ca^{E-het}, ZBP1ca^{E-het} *Ripk3*^{mR/mR} mice and healthy littermates **(C)** Graph depicting epidermal thickness of mice with indicated genotypes at P10-12. Mean + SEM are shown. One dot represents one mouse. **(D)** Representative images from abdominal and tail skin sections of ZBP1ca^{E-het} *Ripk3*^{mR/mR}, ZBP1ca^{E-het} and control mice stained with H&E (Scale bars=100 µm, n=5 for ZBP1ca^{E-het} *Ripk3*^{mR/mR}, n= 11 for ZBP1ca^{E-het}, n=3 for control), CC3⁺ (n=5 for ZBP1ca^{E-het}, n=5 for ZBP1ca^{E-het} *Ripk3*^{mR/mR}, n=3 for control) or immunostained with K10, K14 and K6 (Scale bars=50 µm, n=5 for ZBP1ca^{E-het} *Ripk3*^{mR/mR}, n= 11 for ZBP1ca^{E-het}, n=3 for control) at P10-12 **€** Graph showing the amount of CC3⁺ cells in belly and tail skin of mice with indicated genotypes. Mean ± SEM are shown.

Each dot represents one mouse. **(F)** Graphs depicting relative mRNA expression of the indicated cytokines and ISGs in RNA from whole-skin tissue of P10-12 mice of the indicated genotypes measured by qRT-PCR. Each dot represents one mouse. Mean \pm SEM are shown. All qRT-PCRs display data from mouse numbers indicated in table S1.

Combined ablation of caspase-8 and MLKL fully prevents ZBP1ca-driven skin lesion development

Given the surprising finding that mutation of the RIPK3 RHIM domain did not fully prevent skin lesion development in ZBP1ca^{E-KO} mice, we set out to dissect the contribution of caspase-8-dependent apoptosis and MLKL-driven necroptosis in this setting. To study the role of MLKL-dependent necroptosis, we generated knock-in mice expressing MLKL with substitution of the two serine residues at positions 345 and 347, which are essential for RIPK3-mediated phosphorylation and activation of MLKL^{23,24} by alanines (hereafter referred to as *Mikl*^{AA/AA}) (Figure S4A, B). To confirm that mutation of the RIPK3 phosphorylation sites on MLKL fully prevented necroptosis, we analysed side by side primary BMDMs from *Mikl*^{AA/AA} and from *Mikl*^{-/-} mice generated by CRISPR/Cas9-mediated targeting of the *Mikl* gene (Figure S4E). BMDMs from *Mikl*^{AA/AA} mice expressed normal levels of MLKL, but did not show MLKL phosphorylation and were fully protected from necroptosis induced by treatment with TNF together with birinapant and emricasan or Z-VAD, similarly to *Mikl*^{-/-} BMDMs (Figure S4C, D), demonstrating that mutation of the RIPK3 phosphorylation sites fully prevented MLKL-mediated necroptosis. To assess the role of MLKL-induced necroptosis in the pathogenesis of the skin lesions in ZBP1ca^{E-het} mice, we crossed them with *Mikl*^{AA/AA} mice to generate ZBP1ca^{E-het} *Mikl*^{AA/AA} animals. Macroscopic assessment of ZBP1ca^{E-het} *Mikl*^{AA/AA} revealed that inhibition of necroptosis strongly ameliorated but could not prevent skin lesion development. Specifically, 16 out of 29 ZBP1ca^{E-het} *Mikl*^{AA/AA} mice observed developed inflammatory skin lesions, with the remaining mice staying lesion-free at least up to the age of 30 weeks (Figure 6A and S5). In 8 out of the 16 affected mice, skin lesions progressed in severity particularly in the tail reaching the pre-determined termination criteria requiring the sacrifice of the animals (Figure 6B). In line with the macroscopic assessment, histopathological analysis revealed only focal areas displaying epidermal thickening and upregulation of K14 and K6 in abdominal skin sections from ZBP1ca^{E-het} *Mikl*^{AA/AA} mice, with most skin remaining unaffected (Figure 6C, D). On the other hand, the affected ZBP1ca^{E-het} *Mikl*^{AA/AA} mice developed more pronounced skin lesions in the tail, characterized by hyperplasia and upregulation of K14 expression (Figure 6E). Interestingly, the amount of CC3⁺ cells was decreased in the abdominal skin but increased in tail skin of ZBP1ca^{E-het} *Mikl*^{AA/AA} compared to ZBP1ca^{E-het} mice (Figure 6C, E, F), a trend also visible in ZBP1ca^{E-het} *Ripk3*^{mR/mR} mice (Figure 5D, E), indicating that in the absence of MLKL-dependent necroptosis more cells shift to apoptosis. Furthermore, the expression of inflammatory cytokines and chemokines and ISGs was strongly suppressed in the skin of ZBP1ca^{E-het} *Mikl*^{AA/AA} compared to ZBP1ca^{E-het} mice, however, ZBP1ca^{E-het} *Mikl*^{AA/AA} animals

showed a trend towards higher expression of *Oas1*, *Cxcl9*, *Tnf* and *Il-6* compared to K14-Cre negative control mice (Figure 6G). Collectively, these results showed that inhibition of MLKL-mediated necroptosis strongly ameliorated but could not fully prevent skin lesion development in ZBP1ca^{E-het} *Mkl*^{AA/AA} mice, similarly to the inhibition of RHIM-dependent RIPK3 signaling, arguing that necroptosis-independent mechanisms also contribute to the pathology.

We reasoned that caspase-8-mediated apoptosis could mediate the necroptosis-independent pathology in ZBP1ca^{E-het} mice. However, because inhibition of FADD/Caspase-8 signaling in keratinocytes triggers TNFR1- and ZBP1-mediated necroptosis and skin inflammation (Figures 1 and 2), it is not possible to use conditional ablation of FADD or caspase-8 alone to assess the role of FADD/Caspase-8-induced signaling in ZBP1ca^{E-het} mice. For this reason, we generated and analyzed *R26^{LSL}:ZBP1ca/WT* *K14-Cre* *Mkl*^{AA/AA} *Casp8^{FL/FL}* mice (hereafter referred to as ZBP1ca^{E-het} *Mkl*^{AA/AA} *Casp8^{E-KO}*), which express ZBP1ca and lack caspase-8 specifically in keratinocytes in the *Mkl*^{AA/AA} background. Notably, *Casp8^{E-KO}* *Mkl*^{AA/AA} mice generated as controls from these crosses were also fully protected from skin lesion development, demonstrating that mutation of the RIPK3 phosphorylation sites in MLKL prevented necroptosis-induced skin inflammation *in vivo* (data not shown). Macroscopic and histological analysis revealed that ZBP1ca^{E-het} *Mkl*^{AA/AA} *Casp8^{E-KO}* mice had a normal skin and did not develop any signs of pathology at least until the age of 30 weeks (Figure 6 A-F and S5), demonstrating that combined ablation of caspase-8-mediated apoptosis and MLKL-dependent necroptosis fully prevented skin lesion development induced by ZBP1ca expression in keratinocytes. qRT-PCR analysis showed that the expression of inflammatory cytokines and chemokines was suppressed in the skin of ZBP1ca^{E-het} *Mkl*^{AA/AA} *Casp8^{E-KO}* mice, consistent with the absence of inflammatory lesions (Figure 6G). However, the expression of ISGs including *Oas1*, *Ifi44* and *Ifit1* as well as *Cxcl9*, which is also induced by interferons, was not inhibited in ZBP1ca^{E-het} *Mkl*^{AA/AA} *Casp8^{E-KO}* mice. On the contrary, the expression of these genes was further increased in the skin of ZBP1ca^{E-het} *Mkl*^{AA/AA} *Casp8^{E-KO}* compared to ZBP1ca^{E-het} mice, suggesting that caspase-8 deficiency in keratinocytes caused upregulation of ISG expression. Collectively, these results showed that ZBP1ca expression in the epidermis causes skin inflammation by inducing RIPK3-MLKL-dependent necroptosis and to a lesser extent caspase-8-dependent cell death in keratinocytes.

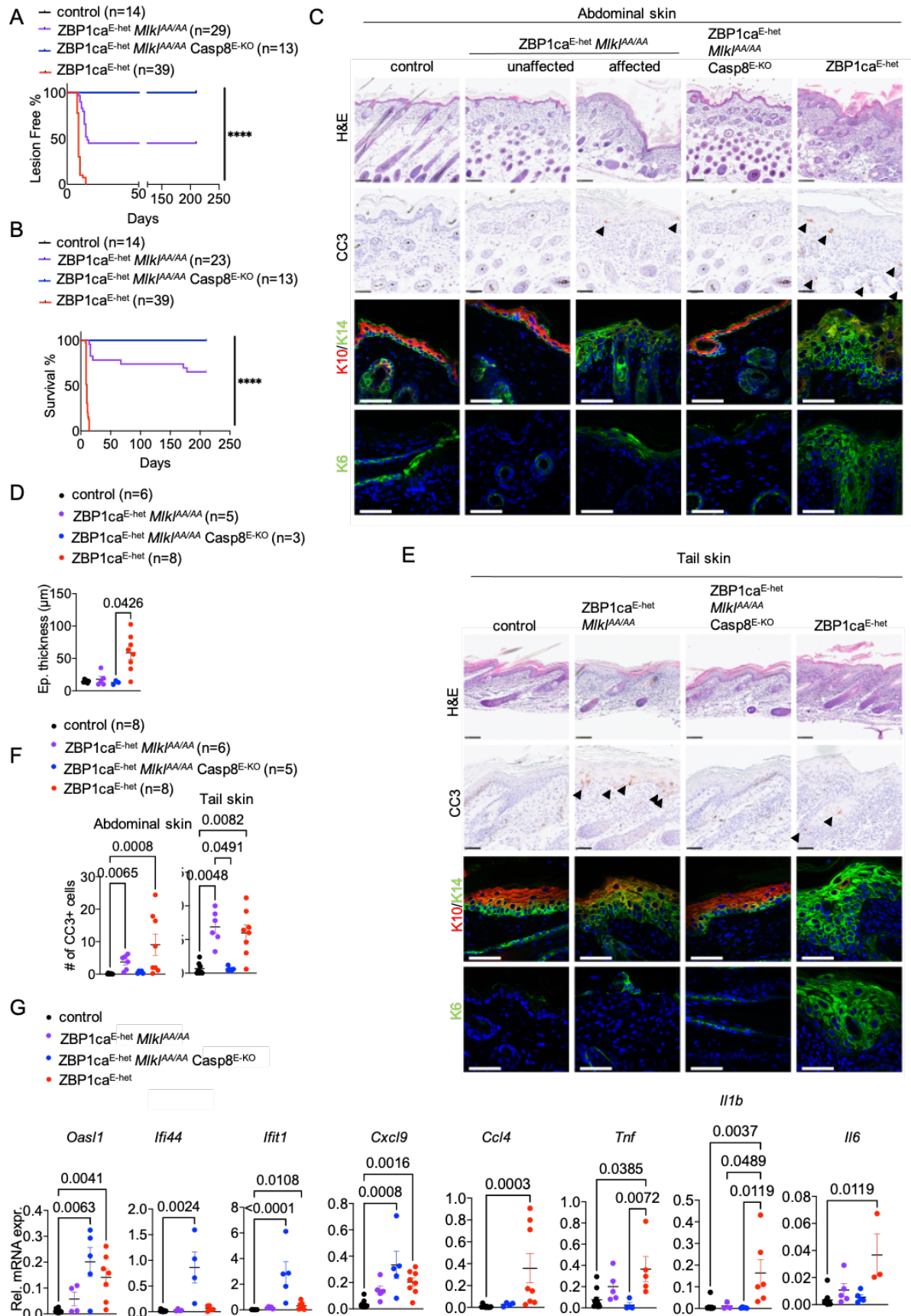


Figure 6. ZBP1ca drives necroptotic and apoptotic cell death in keratinocytes (A) Graph depicting lesion-free survival of ZBP1ca^{E-het}, ZBP1ca^{E-het} *Mik1^{AA/AA}*, ZBP1ca^{E-het} *Mik1^{AA/AA}* Casp8^{E-KO} and control mice. (B) Graph depicting survival curve of ZBP1ca^{E-het}, ZBP1ca^{E-het} *Mik1^{AA/AA}* and ZBP1ca^{E-het} *Mik1^{AA/AA}* Casp8^{E-KO} mice with non-affected littermates. (C) Representative images from skin sections of ZBP1ca^{E-het}

^{het}, ZBP1ca^{E-het} *Mikl*^{AA/AA} and ZBP1ca^{E-het} *Mikl*^{AA/AA} Casp8^{E-KO} mice and control mice stained with H&E (Scale bars=100 μ M, n=5 for ZBP1ca^{E-het} *Mikl*^{AA/AA}, n= 5 for ZBP1ca^{E-het} *Mikl*^{AA/AA} Casp8^{E-KO}, n= 11 for ZBP1ca^{E-het}, n=8 for control), CC3⁺ (n=5 for ZBP1ca^{E-het}, n=4 for ZBP1ca^{E-het} *Mikl*^{AA/AA}, n= 5 for ZBP1ca^{E-het} *Mikl*^{AA/AA} Casp8^{E-KO}, n= 5 for control) or immunostained with K10, K14 and K6 (Scale bars=50 μ M, n=4 for ZBP1ca^{E-het} *Mikl*^{AA/AA}, n= 5 for ZBP1ca^{E-het} *Mikl*^{AA/AA} Casp8^{E-KO}, n= 11 for ZBP1ca^{E-het}, n=5 for control) at P10-12 **(D)** Graph depicting epidermal thickness of mice with indicated genotypes at P10-12. Mean + SEM are shown. Each dot represents one mouse. **(E)** Representative images from tail skin sections of ZBP1ca^{E-het}, ZBP1ca^{E-het} *Mikl*^{AA/AA} and ZBP1ca^{E-het} *Mikl*^{AA/AA} Casp8^{E-KO} mice and control mice stained with H&E (Scale bars=100 μ M, n=5 for ZBP1ca^{E-het} *Mikl*^{AA/AA}, n= 5 for ZBP1ca^{E-het} *Mikl*^{AA/AA} Casp8^{E-KO}, n= 11 for ZBP1ca^{E-het}, n=8 for control), CC3⁺ (n=5 for ZBP1ca^{E-het}, n=4 for ZBP1ca^{E-het} *Mikl*^{AA/AA}, n= 5 for ZBP1ca^{E-het} *Mikl*^{AA/AA} Casp8^{E-KO}, n= 5 for control) or immunostained with K10, K14 and K6 (Scale bars=50 μ M, n=4 for ZBP1ca^{E-het} *Mikl*^{AA/AA}, n= 5 for ZBP1ca^{E-het} *Mikl*^{AA/AA} Casp8^{E-KO}, n= 11 for ZBP1ca^{E-het}, n=5 for control) at P10-12 **(F)** Graph showing the amount of CC3⁺ cells in abdominal and tail skin of mice with indicated genotypes. Mean \pm SEM are shown. Each dot represents one mouse. **(G)** Graphs depicting relative mRNA expression of the indicated ISGs and cytokines in RNA from whole-skin tissue of P10-12 mice of the indicated genotypes measured by qRT-PCR. Each dot represents one mouse. Mean \pm SEM are shown. All qRT-PCRs display data from mouse numbers indicated in table S1.

RHIM-dependent RIPK1 signaling causes necroptosis-independent skin inflammation in ZBP1ca^{E-het} mice

Our findings that inhibition of RHIM-dependent RIPK3 signaling did not fully prevent skin inflammation in ZBP1ca^{E-het} mice suggested that ZBP1ca could induce keratinocyte cell death by activating RIPK1. Moreover, whereas full length ZBP1 did not interact with RIPK3 unless caspases were inhibited^{4,5}, ZBP1ca efficiently interacted with RIPK1 (Figure 3D), further supporting that ZBP1ca could trigger RIPK1-mediated cell death and inflammation in the skin. Therefore, to address the role of RIPK1 we employed *Ripk1*^{mR/mR} mice, which express RIPK1 with mutated RHIM⁵. Because *Ripk1*^{mR/mR} mice die perinatally due to ZBP1-mediated RIPK3-MLKL-dependent necroptosis⁵, it is not possible to study the role of RHIM-dependent RIPK1 signaling in ZBP1ca^{E-het} mice unless if necroptosis is inhibited. We therefore generated and analyzed *R26^{LSL}:ZBP1ca* \times *K14-Cre* \times *Mikl*^{AA/AA} *Ripk1*^{mR/mR} mice (hereafter referred to as ZBP1ca^{E-het} *Mikl*^{AA/AA} *Ripk1*^{mR/mR}), which express RIPK1 with mutated RHIM in the *Mikl*^{AA/AA} background. ZBP1ca^{E-het} *Mikl*^{AA/AA} *Ripk1*^{mR/mR} mice did not develop macroscopically visible skin lesions up to at least 14 weeks of age (Figure 7A, B). Moreover, histological analysis of abdominal and tail skin from mice at P10-12 showed a healthy skin with normal epidermal thickness and differentiation without signs of inflammation and cell death (Figure 8C-E). Additionally, qRT-PCR analysis of inflammatory cytokines and chemokines showed that the RIPK1 RHIM mutation also fully suppressed the upregulation of inflammatory cytokines and chemokines as well as ISGs in the skin of ZBP1ca^{E-het} *Mikl*^{AA/AA} *Ripk1*^{mR/mR} mice. Therefore, inhibition of RHIM-dependent RIPK1 signaling prevented MLKL-independent skin inflammation induced by ZBP1ca expression in keratinocytes. Together with our findings that combined inhibition of MLKL-dependent necroptosis and caspase-8-dependent apoptosis fully prevented skin lesion development in ZBP1ca^{E-het} mice, these results show that ZBP1ca causes skin inflammation

by inducing RIPK3-MLKL-dependent necroptosis and to a lesser extent RIPK1-mediated caspase-8-dependent cell death in keratinocytes.

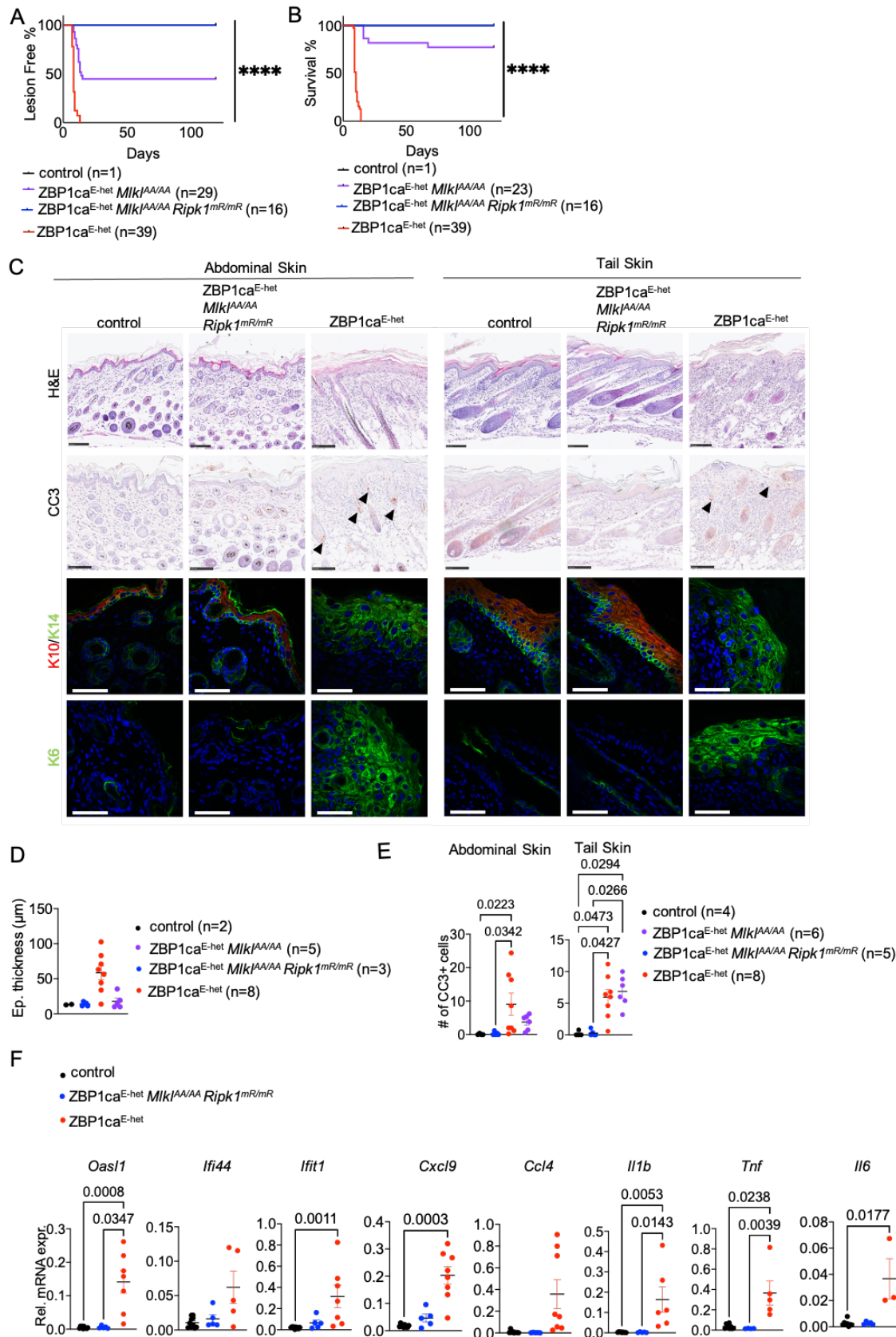


Figure 7. RIPK1 RHIM dependent interaction drives ZBP1ca-mediated skin inflammation (A) Graph depicting lesion-free survival of ZBP1ca^{E-het}, ZBP1ca^{E-het} *Mikl*^{AA/AA} and ZBP1ca^{E-het} *Mikl*^{AA/AA} *Ripk1*^{mR/mR} mice and non-affected littermates. **(B)** Graph depicting survival curve of ZBP1ca^{E-het}, ZBP1ca^{E-het} *Mikl*^{AA/AA} and ZBP1ca^{E-het} *Mikl*^{AA/AA} *Ripk1*^{mR/mR} mice with littermate controls. **(C)** Representative images from skin sections of ZBP1ca^{E-het} and ZBP1ca^{E-het} *Mikl*^{AA/AA} *Ripk1*^{mR/mR} mice and control mice stained with H&E (Scale bars=100 μ M, n=5 for ZBP1ca^{E-het} *Mikl*^{AA/AA} *Ripk1*^{mR/mR}, n= 11 for ZBP1ca^{E-het}, n=5 for control), CC3⁺ (Scale bars=100 μ M, n=5 for ZBP1ca^{E-het} *Mikl*^{AA/AA} *Ripk1*^{mR/mR}, n= 5 for ZBP1ca^{E-het}, n=5 for control), or immunostained with K10, K14 and K6 (Scale bars=50 μ M, n=5 for ZBP1ca^{E-het} *Mikl*^{AA/AA} *Ripk1*^{mR/mR}, n= 8 for ZBP1ca^{E-het}, n=5 for control) at P10-12 **(D)** Graph depicting epidermal thickness of mice with indicated genotypes at P10-12. Mean + SEM are shown. Each dot represents one mouse. **(E)** Graph showing the amount of CC3⁺ cells in abdominal and tail skin of mice with indicated genotypes. Mean \pm SEM are shown. Each dot represents on mouse. **(G)** Graphs depicting relative mRNA expression of the indicated cytokines in RNA from whole-skin tissue of P10-12 mice of the indicated genotypes measured by qRT-PCR. Each dot represents one mouse. Mean \pm SEM are shown. All qRT-PCRs display data from mouse numbers indicated in table S1.

ZBP1ca induces kinase-independent RIPK1-mediated apoptosis and skin inflammation in ZBP1ca^{E-het} mice.

Our results above showed that ZBP1ca activates RIPK1 in a RHIM-dependent manner to induce caspase-8-mediated apoptosis in keratinocytes. RIPK1 kinase activity is required for the induction of apoptosis downstream of TNFR1. We therefore postulated that ZBP1ca may drive keratinocyte apoptosis by triggering RIPK1-kinase dependent activation of caspase-8 in keratinocytes. To address the role of RIPK1 kinase activity we employed *Ripk1*^{D138N/D138N} mice, which express kinase inactive RIPK1²⁵, to generate ZBP1ca^{E-het} *Mikl*^{AA/AA} *Ripk1*^{D138N/D138N} mice. Surprisingly, we found that ZBP1ca^{E-het} *Mikl*^{AA/AA} *Ripk1*^{D138N/D138N} mice developed inflammatory skin lesions, in contrast to ZBP1ca^{E-het} *Mikl*^{AA/AA} *Ripk1*^{mR/mR} mice that did not show skin inflammation. Macroscopic examination revealed that 16 out of 23 ZBP1ca^{E-het} *Mikl*^{AA/AA} *Ripk1*^{D138N/D138N} mice developed skin lesions during the first three weeks of life. Most of these lesions appeared to be transient, with 9 out of 12 mice appearing lesion-free up to at least 14 weeks of age (Figure 8A, B). Histological analysis showed that most areas of abdominal skin in ZBP1ca^{E-het} *Mikl*^{AA/AA} *Ripk1*^{D138N/D138N} mice were unaffected, with only focal areas exhibiting epidermal thickening and upregulation of K14 and K6 expression (Figure 8C, D). Abdominal skin areas exhibiting epidermal thickening showed increased numbers of CC3⁺ cells, which however were significantly reduced compared to ZBP1ca^{E-het} mice (Figure 8E). Similar to ZBP1ca^{E-het} *Mikl*^{AA/AA} mice, CC3⁺ cells were increased in all tail skin sections of the ZBP1ca^{E-het} *Mikl*^{AA/AA} *Ripk1*^{D138N/D138N} mice observed (Figure 8C, E). Moreover, the expression of inflammatory cytokines, chemokines and ISGs was ameliorated in ZBP1ca^{E-het} *Mikl*^{AA/AA} *Ripk1*^{D138N/D138N} mice compared to ZBP1ca^{E-het} mice. Collectively, these results showed that RIPK1 kinase activity is not required for ZBP1ca-induced caspase-8 dependent keratinocyte apoptosis.

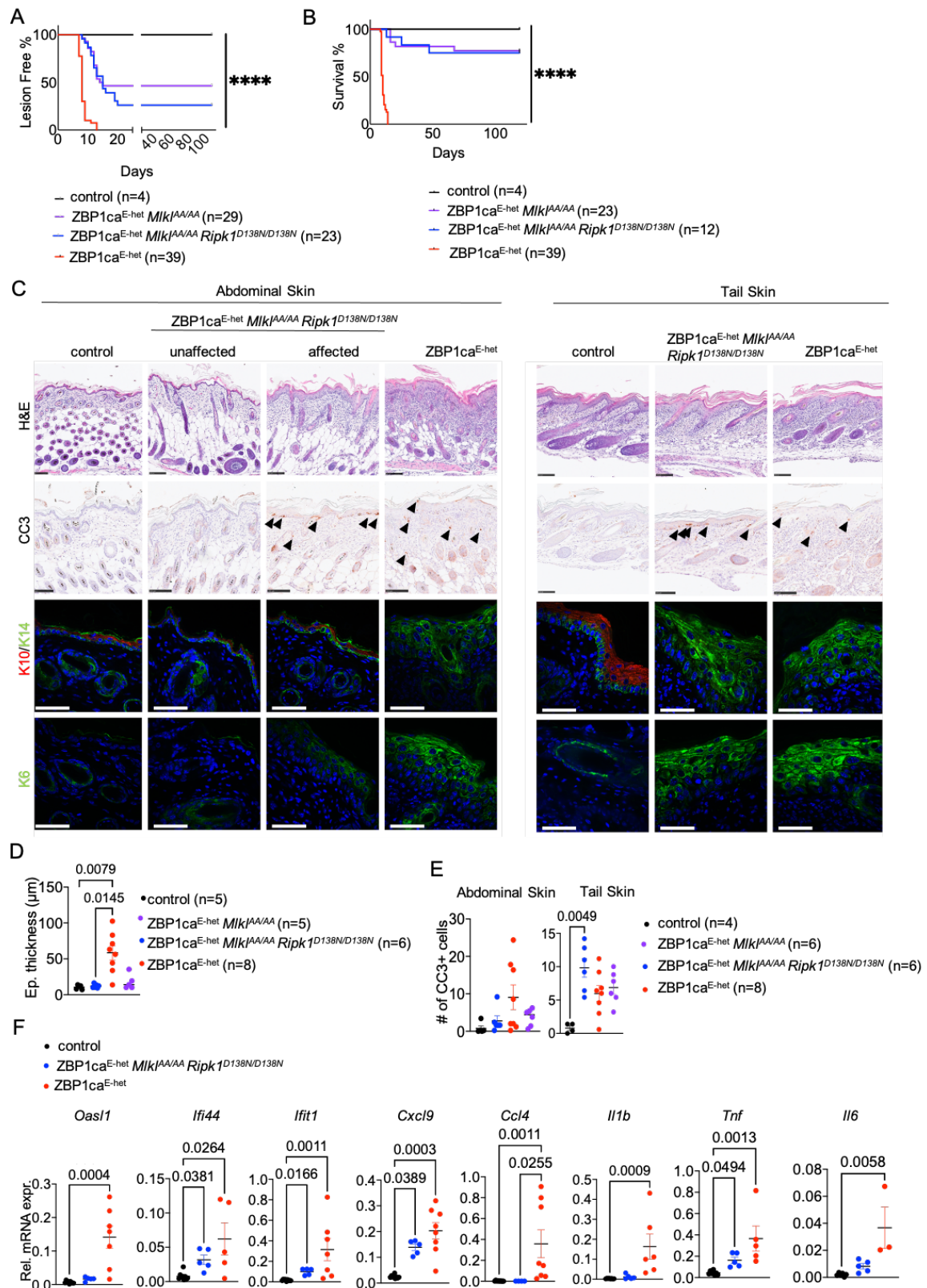


Figure 8. RIPK1 kinase activity does not regulate ZBP1ca^{E-het} driven inflammation (A) Graph depicting lesion-free survival of ZBP1ca^{E-het}, ZBP1ca *Mikl*^{AA/AA}, ZBP1ca^{E-het} *Mikl*^{AA/AA} *Ripk1*^{D138N/D138N} mice and non-affected littermates. **(B)** Graph depicting survival curve of ZBP1ca^{E-het}, ZBP1ca *Mikl*^{AA/AA}, ZBP1ca^{E-het} *Mikl*^{AA/AA} *Ripk1*^{D138N/D138N} mice and non-affected littermates. **(C)** Representative images from skin sections of ZBP1ca^{E-het} and ZBP1ca^{E-het} *Mikl*^{AA/AA} *Ripk1*^{D138N/D138N} mice and control mice stained with H&E (Scale bars=100 μm, n=5 for ZBP1ca^{E-het} *Mikl*^{AA/AA} *Ripk1*^{D138N/D138N}, n= 11 for ZBP1ca^{E-het}, n=5 for control), CC3⁺ (n=5 for ZBP1ca^{E-het} *Mikl*^{AA/AA} *Ripk1*^{D138N/D138N}, n= 5 for ZBP1ca^{E-het}, n=5 for control), or

immunostained with K10, K14 and K6 (Scale bars=50 μ M, n=5 for ZBP1ca^{E-het} *MLKL*^{AA/AA} *Ripk1*^{D138N/D138N}, n= 8 for ZBP1ca^{E-het}, n=5 for control) at P10-12 **(D)** Graph depicting epidermal thickness of mice with indicated genotypes at P10-12. Mean + SEM are shown. Each dot represents one mouse **(E)** Graph showing the amount of CC3⁺ cells in abdominal and tail skin of mice with indicated genotypes. Mean \pm SEM are shown. Each dot represents one mouse **(F)** Graphs depicting relative mRNA expression of the indicated ISGs and cytokines in RNA from whole-skin tissue of P10-12 mice of the indicated genotypes measured by qRT-PCR. Each dot represents one mouse. Mean \pm SEM are shown. All qRT-PCRs display data from mouse numbers indicated in table S1.

Discussion

Earlier studies revealed a critical role of FADD/caspase-8-dependent signaling in epidermal keratinocytes in suppressing skin inflammation, however, the underlying mechanisms have remained controversial¹⁹. We showed previously that FADD^{E-KO} mice develop severe inflammatory skin disease that depends on RIPK3 and suggested that keratinocyte necroptosis drives skin inflammation upon inhibition of FADD/caspase-8 signaling¹⁹. Here we report that ablation of MLKL fully prevents skin lesion development in FADD^{E-KO} mice, demonstrating that MLKL-dependent necroptosis drives the pathology. Our previous experiments revealed that TNFR1 deficiency delayed and ameliorated but did not fully prevent skin lesion development in FADD^{E-KO} mice¹⁹ suggesting that TNFR1-independent mechanism cause keratinocyte necroptosis and inflammation in these mice. Here we show that ZBP1 causes TNFR1-independent skin inflammation in FADD^{E-KO} mice by inducing MLKL-dependent keratinocyte necroptosis. Notably, ZBP1 ablation on its own was not sufficient to prevent or ameliorate skin inflammation in FADD^{E-KO} mice⁵ demonstrating that TNFR1 plays a critical role in initiating early lesions while ZBP1 is activated later to induce the TNFR1-independent keratinocyte necroptosis and inflammation in FADD^{E-KO} mice. This interplay is reminiscent of the role of TNFR1 and ZBP1 in FADD^{IEC-KO} mice, where they cooperate to induce intestinal inflammation in a functionally redundant or synergistic fashion depending on the anatomic location. In the colon, ablation of either TNFR1 or ZBP1 strongly suppressed colitis, whereas in the small intestine only combined ablation of both TNFR1 and ZBP1 could strongly ameliorate ileitis whilst single knockouts did not have any effect¹⁵. Together, these studies identify ZBP1 as a potent inducer of TNFR1-independent inflammation in barrier epithelial tissues, suggesting that ZBP1 may be implicated in the pathogenesis of inflammatory diseases of the skin and the gut, particularly in patients that do not respond to TNF blockers.

Our results reported here as well as earlier studies showed that ZBP1 induces inflammation by triggering RIPK3-MLKL-dependent necroptosis^{4-6,15}. However, in these mouse models cells were sensitized to necroptosis by the loss of FADD, caspase-8 or RIPK1 and were unable to undergo RIPK1-mediated apoptosis. Therefore, it remained unclear whether ZBP1 could also directly engage and activate RIPK1 to induce caspase-8-mediated apoptosis and associated pathology *in vivo*. Addressing this question was hampered by the fact that expression of ZBP1

does not kill cells unless if caspase-8 is inhibited or RIPK1 is absent or RIPK1 lacks its RHIM^{4-6,15}. Here we report the identification of a truncated version of ZBP1, which we termed ZBP1ca, that is capable of inducing death in cells with intact RIPK1 and caspase-8 signaling. Doxycycline-inducible expression of ZBP1ca killed iMEFs through induction of both, necroptosis and apoptosis. Moreover, ZBP1ca interacted with both RIPK3 and RIPK1, in contrast to full length ZBP1 that co-immunoprecipitated with RIPK3 but not with RIPK1 in vitro. These findings suggested that ZBP1ca induces both RIPK3-MLKL-mediated necroptosis and RIPK1-caspase-8-mediated apoptosis. Moreover, our study indicated that the C-terminal part of ZBP1 containing the second and third RHIMs exerts a negative regulatory function that prevents ZBP1 from inducing cell death.

Our *in vivo* experiments showed that ZBP1ca expression specifically in K14-expressing epithelial cells induced keratinocyte death and caused skin inflammation. Inhibition of necroptosis by mutation of the RIPK3 RHIM strongly suppressed but could not fully prevent skin lesion development in ZBP1ca^{E-het} mice, showing that ZBP1 induces inflammation by activating RIPK3 via its RHIM. Mutation of the RIPK3 phosphorylation sites on MLKL had a similar effect in strongly suppressing but not fully preventing skin inflammation in ZBP1ca^{E-het} mice. These results showed that ZBP1ca induces skin inflammation primarily by triggering RIPK3-MLKL-mediated keratinocyte necroptosis and, to a lesser extent, by necroptosis-independent mechanisms. We reasoned that caspase-8-dependent cell death could trigger necroptosis-independent inflammation in ZBP1ca^{E-het} mice. Indeed, keratinocyte-specific caspase-8 ablation combined with mutation of the MLKL phosphorylation sites completely prevented skin lesion development in ZBP1ca^{E-het} mice, demonstrating that ZBP1ca induces skin inflammation by triggering necroptosis and apoptosis. To assess whether ZBP1ca triggers caspase-8-mediated apoptosis by engaging RIPK1, we generated ZBP1ca^{E-het} *Ripk1*^{mR/mR} *Mlkl*^{AA/AA} mice and found that mutation of the RIPK1 RHIM combined with mutation of the MLKL phosphorylation sites fully prevented skin lesion development. These findings revealed that ZBP1ca induced keratinocyte apoptosis by engaging RIPK1. The kinase activity of RIPK1 is required for inducing caspase-8-dependent apoptosis downstream of TNFR1, therefore we assessed whether RIPK1 kinase activity is also required for ZBP1ca-induced apoptosis by generating and analyzing ZBP1ca^{E-het} *Ripk1*^{D138N/D138N} *Mlkl*^{AA/AA} mice. Surprisingly, we found that, in contrast to mutation of its RHIM, inhibition of the kinase activity of RIPK1 did not prevent the caspase-8-mediated inflammation in ZBP1ca^{E-het} mice, arguing that ZBP1ca induces caspase-8-mediated apoptosis in a RIPK1 kinase activity-independent manner. These results are reminiscent of the RIPK1 kinase activity-independent apoptosis induced after inhibition of RIPK3 kinase activity, either genetically by mutation of aspartic acid in position 161 to asparagine (D161N) or in response to high concentration of RIPK3 inhibitors^{26,27}. Therefore,

whereas its kinase activity is required for inducing apoptosis downstream of TNFR1, RIPK1 mediated caspase-8 activation in a kinase-independent manner downstream of RIPK3 and ZBP1. Whereas the underlying molecular mechanism remains to be fully elucidated, these results suggest that when RIPK1 is engaged via its death domain its kinase activation and autophosphorylation is required for the formation and activation of the death-inducing signaling complex resulting in activation of caspase-8. In contrast, when RIPK1 is engaged via its RHIM downstream of ZBP1 or RIPK3, then it induces caspase-8 activation in a kinase-independent manner.

ZBP1 has been suggested to induce inflammatory gene expression independently from cell death^{7,8}. ZBP1ca^{E-het} mice do show upregulation of inflammatory cytokines in the skin, however, these are strongly suppressed by inhibition of necroptosis and fully normalized by combined ablation of necroptosis and apoptosis. Therefore, in this *in vivo* experimental system ZBP1ca drives cytokine production indirectly by inducing RIPK3-MLKL-dependent necroptosis and to a lesser extent by RIPK1-caspase-8-mediated apoptosis. Our interpretation of these results is that cytokine production is induced by the release of DAMPs from the dying cells. Interestingly, ZBP1ca additionally induced the expression of ISGs, which also depended largely on necroptosis as they were strongly suppressed by mutation of the RIPK3 RHIM or the MLKL phosphorylation sites. Combined mutation of the RIPK1 RHIM and the MLKL phosphorylation sites fully normalized ISG expression in ZBP1ca^{E-het} mice. However, ZBP1ca^{E-het} Casp8^{E-KO} Mlkl^{AA/AA} mice showed strongly enhanced ISG expression compared to ZBP1ca^{E-het} mice, although cytokine expression levels were fully normalized in these animals. While the underlying mechanism remains elusive at present, these results suggest that caspase-8 has an important role in suppressing ISG expression in the skin of ZBP1ca^{E-het} mice.

Taken together, we identified ZBP1 as a critical mediator that cooperates with TNFR1 to induce cell death and inflammation. Our results revealed that ZBP1 utilizes its first RHIM to interact with RIPK3 and RIPK1 inducing necroptosis and apoptosis respectively, whereas its C-terminal part encompassing the second and third RHIMs exerts inhibitory functions that prevent ZBP1-mediated cell death. Importantly, our findings provide experimental *in vivo* evidence that ZBP1 causes inflammation exclusively by triggering necroptosis and, to a lesser extent, apoptosis, arguing against a role of ZBP1 in inducing cell death-independent inflammatory signaling. These findings suggest that ZBP1 could be implicated in the pathogenesis of inflammatory diseases.

Acknowledgements

We thank J. Kuth, C. Uthoff-Hachenberg, E. Stade, E. Gareus and J. vR. for excellent technical assistance, S. Hedrick for *Casp8^{fl/fl}* mice and the CECAD Transgenic Core Facility for CRISPR/Cas9-assisted generation of *R26^{LSL.ZBP1ca}*, *Mik1^{AA/AA}* and *Ripk3^{mR/mR}* mice. Research reported in this publication was supported by funding from the European Research Council (grant agreement no. 787826) and the Deutsche Forschungsgemeinschaft (DFG, German Research Foundation; project SFB1403).

Author contributions

L.K designed and performed all experiments, analyzed the data and drafted and revised the manuscript. L.W generated *R26^{LSL.ZBP1ca}* (Figure 4A), *Ripk3^{mR/mR}* (Figure S2) and *Mik1^{AA/AA}* (Figure S4) mouse strains using CRISPR Cas9. S.K bred and analyzed *FADD^{E-KO} Mik1^{-/-}* mice (Figure 1F, G). L.W. and R.S. generated the ZBP1ca construct. H.J. carried out the cell death assay and western blot in Figure S2. M.P. designed and supervised the study and wrote the manuscript together with L.K.

Declaration of Interests

The authors declare no competing interests.

Methods

Mice

K14-Cre²¹ Caspase-8^{fl/fl} 28 Ripk1^{D138N/D138N 25} and Ripk1^{mR/mR 5} mice were described previously. *R26^{LSL.ZBP1ca}*, *Ripk3^{mR/mR}* and *Mik1^{AA/AA}* mice were generated in this study. All mice were maintained on a C57BL/6N background and mouse studies and immunohistochemical analysis were performed in a blinded fashion. For all experiments, littermates carrying the loxP-flanked alleles but not *K14-Cre* recombinase were used as controls. Female and male animals of the indicated genotypes were randomly assigned to groups. For comparability, the same *ZBP1ca^{E-het}* mice were used in all graphs.

Animals were maintained at the SPF animal facility of the CECAD Research Center, University of Cologne, at 22°C (±2°C), a relative humidity of 55% (±5%) in individually ventilated cages under a 12-h light cycle. Mice were given access to a sterilized commercial diet (Ssniff Spezialdiäten GmbH) and given water ad libitum. All animal experiments were approved by local government authorities (Landesamt für Natur, Umwelt und Verbraucherschutz Nordrhein Westfalen) and conducted in accordance with European, national and institutional guidelines. Animals requiring medical attention were provided with appropriate care and sacrificed when reaching pre-determined criteria of disease severity. No other exclusion criteria existed.

Cell culture

Cell lines were cultured in DMEM-Dulbecco's Modified Eagle Medium (ThermoFisher, #41965-039) supplemented with 10%FCS, 1%P/S, 1% L-Glutamate and 1mM Sodium Pyruvate (ThermoFisher Scientific, #11360).

Generation of stable cell lines via lentiviral transduction

For lentiviral production, HEK293T cells were transfected with pCW-sFLAG-mZBP1 (10µg) or pCW-sFLAG-ZBP1ca (10µg) and psPAX2 (5µg) (Addgene, #12260) and pMD2.G (5µg) (Addgene #12259). Plasmids were mixed with 500µl 0.25M CaCl₂ and 500µl 2xHBS and incubated for 5 min at RT. The solution was added to HEK293T cells, which were fed with new medium prior to transfection. After 1 day, medium was replaced with fresh medium and after 2 and 3 days the supernatant containing the virus was collected. For transduction of immortalized mouse embryonic fibroblasts (iMEFs), 300.000 cells were incubated with 1.5 ml fresh medium, 1.5 ml viral supernatant and 8µg/ml Polybrene (Sigma Aldrich, #H9268) for 24 h. After 1 day, the virus-containing medium was replaced with new medium containing 2 µg/ml puromycin. After 2 days, puromycin-containing medium was removed and cell pools were used for experiments.

Cell death assay

iMEFs were plated 24h before stimulation in a 96 well plate (Sigma-Aldrich, CLS3340-50EA, 1x10⁴ cells/well). Cells were stimulated with combinations out of Doxycycline (Sigma-Aldrich D9891), Emricasan (5µM, Selleckchem, #S7775), Necrostatin 1s (20µM, BioCat, 2263-5-BV) or GSK872 (3µM). Cell death was measured by YOYO -1 Iodide (491/509, ThermoScientific, Cat#3601) incorporation and analyzed using the IncuCyte bioimaging platform (Essen).

Immunohistochemical analysis

Haematoxylin & Eosin staining

Abdominal skin and tail skin samples were fixed in 4% paraformaldehyde for 24 h, embedded in paraffin and cut in 3-5 µm sections. Paraffin sections were de-paraffinized using xylene and re-hydrated with ethanol. Sections were stained for 2 minutes in hematoxylin, 15 min differentiated in tap water and 1 min incubated in eosin. Stained sections were de-hydrated with ethanol and fixed in xylene. Epidermal thickness was analyzed by measuring epidermal thickness in four optical fields per sections with four measurements per field.

CC3⁺ staining

Paraffin-embedded sections were re-hydrated with xylene and ethanol. Heat induced antigen retrieval was performed and endogenous peroxidase was blocked in peroxidase buffer. Endogenous avidin was blocked with biotin (Vector, no. SP-2001) and sections were incubated

with primary a-cleaved Caspase-3 antibody (Cell Signaling, 9661) and avidin (Vector, no. SP-2001) overnight at 4°C. For visualization, the ABC Kit Vectastain Elite (Vector Laboratories) and DAB substrate (DAKO and Vector Laboratories) were utilized. Sections were counterstained with hematoxylin. CC3 positive cells were counted manually in five optical fields per section (20x magnification).

Immunofluorescence staining

Paraffin sections were re-hydrated and heat-induced epitope retrieval was performed. NGS was used for blocking. Sections were stained with a-K6 (905701, Biolegend) a-K10 (905401, Biolegend) and a-K14(MA5-11599, Invitrogen) overnight at 4°C. Stainings were visualized using Alexa-488 (A11008/A11001, Molecular Probes) and Alexa-549 (A11012, Molecular probes) fluorescent-conjugated secondary antibodies and all sections were counterstained with DAPI.

Immunoblotting

Skin tissue samples were homogenized in protein lysis buffer supplemented with protease and phosphatase inhibitors using Precellys tissue homogenizer. Cells were lysed in protein lysis buffer supplemented with protease and phosphatase inhibitors for 20 min on ice. Cell suspension was centrifuged at 13.000 rpm and the protein concentration in the supernatant was measured using PIERCE 600nm Protein Assay Reagent. Lysates were adjusted to 2 µg/µl. SDS Laemmli loading buffer (1 mM DTT) was added and samples were boiled at 95°C for 8 min. Protein lysates were separated using SDS-Gelelectrophoresis and transferred to PDVF-membranes (IPVH00010). Membranes were blocked for 1 h in 5% milk/0.1% PBS-T and incubated overnight at 4° in primary antibodies against a-Tubulin (T6074, Sigma), a-ZBP1 (Adipogen AG-20B-0010), a-RIPK3 (Enzo Life Sciences, ADI-095-242-100) and a-RIPK1 (3492 Cell signaling technology). Membranes were washed 3x for 10 min in 0.1% PBS-T and probed with secondary HRP-coupled antibody (anti-mouse or anti-rabbit, GE Healthcare, Jackson ImmunoResearch) for 1 h. Proteins were detected using ECL Western Blotting Detection Reagent (RPN2106, GE Healthcare) and SuperSignal West Pico PLUS Chemiluminescent substrate (34580, ThermoScientific).

Immunoprecipitation

iMEFs were plated 24h before stimulation in a 10 cm plate (3×10^6 cells/well). Cells were stimulated with doxycycline (Sigma-Aldrich D9891) for 12 h, washed 3x with ice-cold PBS and lysed for 20 min on ice using ALB lysis buffer (30 mM Tris HCl pH 7,5, 40 mM NaCl, 2 mM EDTA, 2 mM KCL, 10% Glycerin, 1% Triton x 100). The lysates were centrifuged for 30 min at 13.000 (4°C) and protein concentration was calculated using PIERCE 600nm Protein Assay

Reagent. M2 Flag beads were washed 3x in lysis buffer, resuspend in an appropriate volume and 100 µl of beads (20 µl beads for 2×10^7 cells) were added to protein lysates. Lysates were incubated moving ON, washed 3x with lysis buffer on the next day and boiled at 95°C for 8 min in 50 µl Laemmli + 1 mM DTT. Samples were immunoblotted as described above.

qRT-PCR

Total RNA was extracted from abdominal and tail skin tissue using Trizol (Life Technologies) and Rneasy Columns (Qiagen) or the Direct-zol RNA isolation kit (Biozol). cDNA was prepared with the LUNA RT SuperMix Kit (E3010L, NEC). qRT-PCR was performed with TaqMan probes (ThermoScientific, *Il1b* Mm00434228_m1, *Il6* Mm00446190_m1, *Tnf* Mm00443258_m1, *Ifi44* Mm00505670_m1, *Oas1* Mm00455081_m1, *Ifit1* Mm00515153_m1, *Zbp1* Mm00457979_m1, *Ccl4* Mm00443111_m1, *Cxcl9* Mm00434946_m1) in duplicates for each sample, using *Tbp* (Mm00446973_m1) as a reference gene. Relative expression of gene transcript was analyzed by $2^{-\Delta\Delta CT}$. In all graphs healthy littermate controls as well as the original *R26^{LSL.ZBP2ca}* controls were used.

Statistical analysis

Data shown in graphs display mean \pm SEM. In order to compare two groups, Mann-Whitney *U* test was performed, to compare more than 2 groups, Kruskal-Wallis test was chosen. The Log-Rank (Mantel-Cox) test was used in order to compare survival curves and lesion onset of mice. * $p \leq 0.05$; ** $p \leq 0.01$; *** $p \leq 0.005$, **** $p \leq 0.001$. All statistical analysis was performed using GraphPad Prism.

References

- 1 Schwartz, T., Behlke, J., Lowenhaupt, K., Heinemann, U. & Rich, A. Structure of the DLM-1-Z-DNA complex reveals a conserved family of Z-DNA-binding proteins. *Nat Struct Biol* **8**, 761-765, doi:10.1038/nsb0901-761 (2001).
- 2 Ha, S. C. *et al.* The crystal structure of the second Z-DNA binding domain of human DAI (ZBP1) in complex with Z-DNA reveals an unusual binding mode to Z-DNA. *Proc Natl Acad Sci U S A* **105**, 20671-20676, doi:10.1073/pnas.0810463106 (2008).
- 3 Placido, D., Brown, B. A., 2nd, Lowenhaupt, K., Rich, A. & Athanasiadis, A. A left-handed RNA double helix bound by the Z alpha domain of the RNA-editing enzyme ADAR1. *Structure* **15**, 395-404, doi:10.1016/j.str.2007.03.001 (2007).
- 4 Jiao, H. *et al.* Z-nucleic-acid sensing triggers ZBP1-dependent necroptosis and inflammation. *Nature* **580**, 391-395, doi:10.1038/s41586-020-2129-8 (2020).
- 5 Lin, J. *et al.* RIPK1 counteracts ZBP1-mediated necroptosis to inhibit inflammation. *Nature* **540**, 124-128, doi:10.1038/nature20558 (2016).
- 6 Newton, K. *et al.* RIPK1 inhibits ZBP1-driven necroptosis during development. *Nature* **540**, 129-133, doi:10.1038/nature20559 (2016).
- 7 Rebsamen, M. *et al.* DAI/ZBP1 recruits RIP1 and RIP3 through RIP homotypic interaction motifs to activate NF-kappaB. *EMBO Rep* **10**, 916-922, doi:10.1038/embor.2009.109 (2009).

- 8 Kaiser, W. J., Upton, J. W. & Mocarski, E. S. Receptor-interacting protein homotypic interaction motif-dependent control of NF-kappa B activation via the DNA-dependent activator of IFN regulatory factors. *J Immunol* **181**, 6427-6434, doi:10.4049/jimmunol.181.9.6427 (2008).
- 9 Balachandran, S. & Mocarski, E. S. Viral Z-RNA triggers ZBP1-dependent cell death. *Curr Opin Virol* **51**, 134-140, doi:10.1016/j.coviro.2021.10.004 (2021).
- 10 Guo, H. *et al.* Species-independent contribution of ZBP1/DAI/DLM-1-triggered necroptosis in host defense against HSV1. *Cell Death Dis* **9**, 816, doi:10.1038/s41419-018-0868-3 (2018).
- 11 Thapa, R. J. *et al.* DAI Senses Influenza A Virus Genomic RNA and Activates RIPK3-Dependent Cell Death. *Cell Host Microbe* **20**, 674-681, doi:10.1016/j.chom.2016.09.014 (2016).
- 12 Sridharan, H. *et al.* Murine cytomegalovirus IE3-dependent transcription is required for DAI/ZBP1-mediated necroptosis. *EMBO Rep* **18**, 1429-1441, doi:10.15252/embr.201743947 (2017).
- 13 Koehler, H. *et al.* Vaccinia virus E3 prevents sensing of Z-RNA to block ZBP1-dependent necroptosis. *Cell Host Microbe* **29**, 1266-1276 e1265, doi:10.1016/j.chom.2021.05.009 (2021).
- 14 Dannappel, M. *et al.* RIPK1 maintains epithelial homeostasis by inhibiting apoptosis and necroptosis. *Nature* **513**, 90-94, doi:10.1038/nature13608 (2014).
- 15 Schwarzer, R., Jiao, H., Wachsmuth, L., Tresch, A. & Pasparakis, M. FADD and Caspase-8 Regulate Gut Homeostasis and Inflammation by Controlling MLKL- and GSDMD-Mediated Death of Intestinal Epithelial Cells. *Immunity* **52**, 978-993 e976, doi:10.1016/j.immuni.2020.04.002 (2020).
- 16 Devos, M. *et al.* Sensing of endogenous nucleic acids by ZBP1 induces keratinocyte necroptosis and skin inflammation. *J Exp Med* **217**, doi:10.1084/jem.20191913 (2020).
- 17 Wang, R. *et al.* Gut stem cell necroptosis by genome instability triggers bowel inflammation. *Nature* **580**, 386-390, doi:10.1038/s41586-020-2127-x (2020).
- 18 Yuan, F. *et al.* Z-DNA binding protein 1 promotes heatstroke-induced cell death. *Science* **376**, 609-615, doi:10.1126/science.abg5251 (2022).
- 19 Bonnet, M. C. *et al.* The adaptor protein FADD protects epidermal keratinocytes from necroptosis in vivo and prevents skin inflammation. *Immunity* **35**, 572-582, doi:10.1016/j.immuni.2011.08.014 (2011).
- 20 Moriwaki, K. *et al.* The necroptosis adaptor RIPK3 promotes injury-induced cytokine expression and tissue repair. *Immunity* **41**, 567-578, doi:10.1016/j.immuni.2014.09.016 (2014).
- 21 Hafner, M. *et al.* Keratin 14 Cre transgenic mice authenticate keratin 14 as an oocyte-expressed protein. *Genesis* **38**, 176-181, doi:10.1002/gene.20016 (2004).
- 22 Zhang, T. *et al.* Influenza Virus Z-RNAs Induce ZBP1-Mediated Necroptosis. *Cell* **180**, 1115-1129 e1113, doi:10.1016/j.cell.2020.02.050 (2020).
- 23 Sun, L. *et al.* Mixed lineage kinase domain-like protein mediates necrosis signaling downstream of RIP3 kinase. *Cell* **148**, 213-227, doi:10.1016/j.cell.2011.11.031 (2012).
- 24 Rodriguez, D. A. *et al.* Characterization of RIPK3-mediated phosphorylation of the activation loop of MLKL during necroptosis. *Cell Death Differ* **23**, 76-88, doi:10.1038/cdd.2015.70 (2016).
- 25 Polykratis, A. *et al.* Cutting edge: RIPK1 Kinase inactive mice are viable and protected from TNF-induced necroptosis in vivo. *J Immunol* **193**, 1539-1543, doi:10.4049/jimmunol.1400590 (2014).
- 26 Newton, K. *et al.* Activity of protein kinase RIPK3 determines whether cells die by necroptosis or apoptosis. *Science* **343**, 1357-1360, doi:10.1126/science.1249361 (2014).
- 27 Mandal, P. *et al.* RIP3 induces apoptosis independent of pronecrotic kinase activity. *Mol Cell* **56**, 481-495, doi:10.1016/j.molcel.2014.10.021 (2014).
- 28 Beisner, D. R., Ch'en, I. L., Kolla, R. V., Hoffmann, A. & Hedrick, S. M. Cutting edge: innate immunity conferred by B cells is regulated by caspase-8. *J Immunol* **175**, 3469-3473, doi:10.4049/jimmunol.175.6.3469 (2005).

Supplementary Material

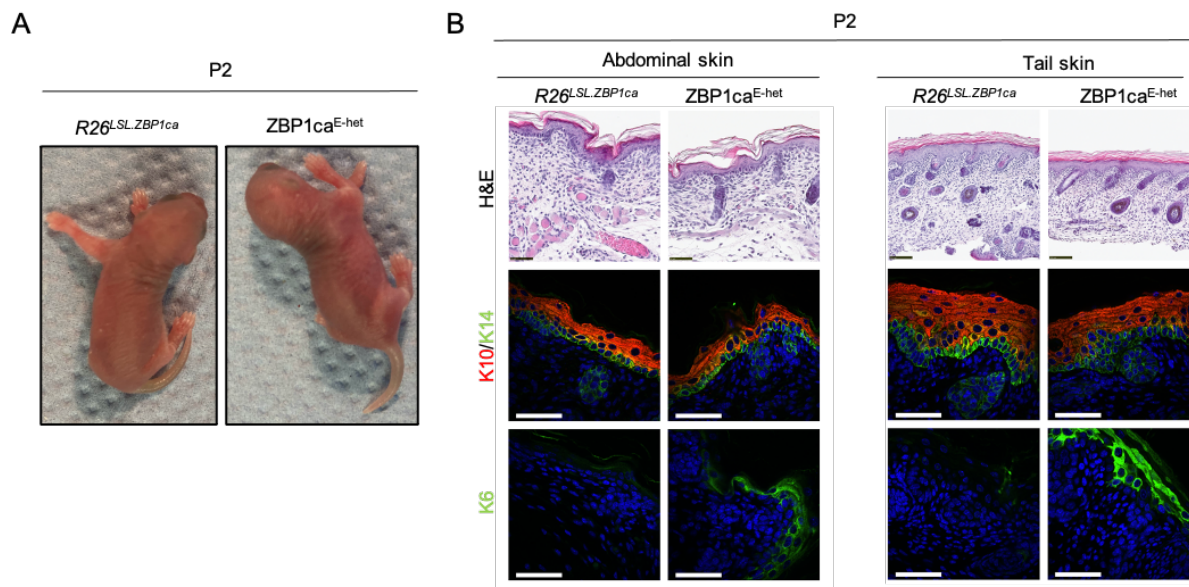


Figure S1. ZBP1ca-driven tail skin inflammation starts at postnatal day 2 (A) Representative photographs of *ZBP1ca^{E-het}* mouse (n=7) and control littermate (n=12) at P2. **(B)** Representative images from skin sections of *ZBP1ca^{E-het}* mice and littermate at P2 stained with H&E (Scale bars=50 μ M, n=6 for *ZBP1ca^{E-het}*, n=5 for control) or immunostained with K10, K14 and K6 (Scale bars=50 μ M, n=4 for *ZBP1ca^{E-het}*, n=4 for *R26^{LSL.ZBP1ca}*).

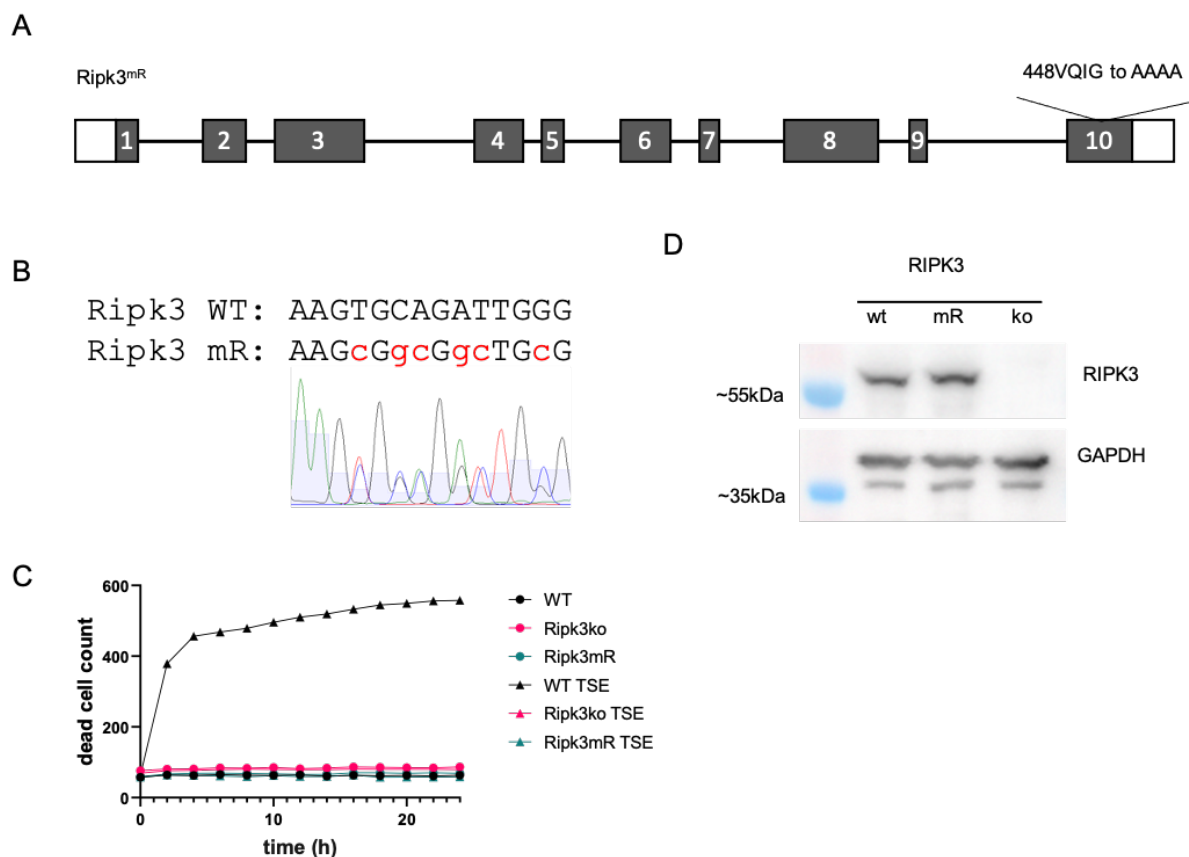


Figure S2. Generation of *Ripk3^{mR}* mice. (A) The core RHIM motif in exon 10 of the *Ripk3* gene was altered from the amino acid sequence VQIG to AAAA using CRISPR/Cas9 technology with the gRNA target sequence 5'ACTGTTCTGAAGTGCAGATT3' and the repair ssODN

5'CACCATCACCTCCTCCTTTCTCTTAAAGGGCCACCGGCTCTCGTCTTCAACAACCTGTTCTGAA
GCGGCGGCTGCGAACTACAACCTCCTTGGTAGCACCACCAAGAACTACTGCCTCAAGTTCGGCCA
AGTATGACCAAG3' **(B)** Sanger sequencing indicates the desired mutations in heterozygous *Ripk3^{mR/WT}* mice with the mutated nucleotides indicated in red **(C)** Nucleotide substitutions did not abrogate protein expression, as demonstrated by western blotting of primary lung fibroblasts (LFs) with *Ripk3^{ko/ko}* cells as a control **(D)** Necroptosis induction by combined treatment with TNF (T), smac mimetic (S) and emricasan € in primary LFs revealed, that *Ripk3^{mR/mR}* cells are resistant to this form of cell death, as assessed by Incucyte-based life cell imaging.

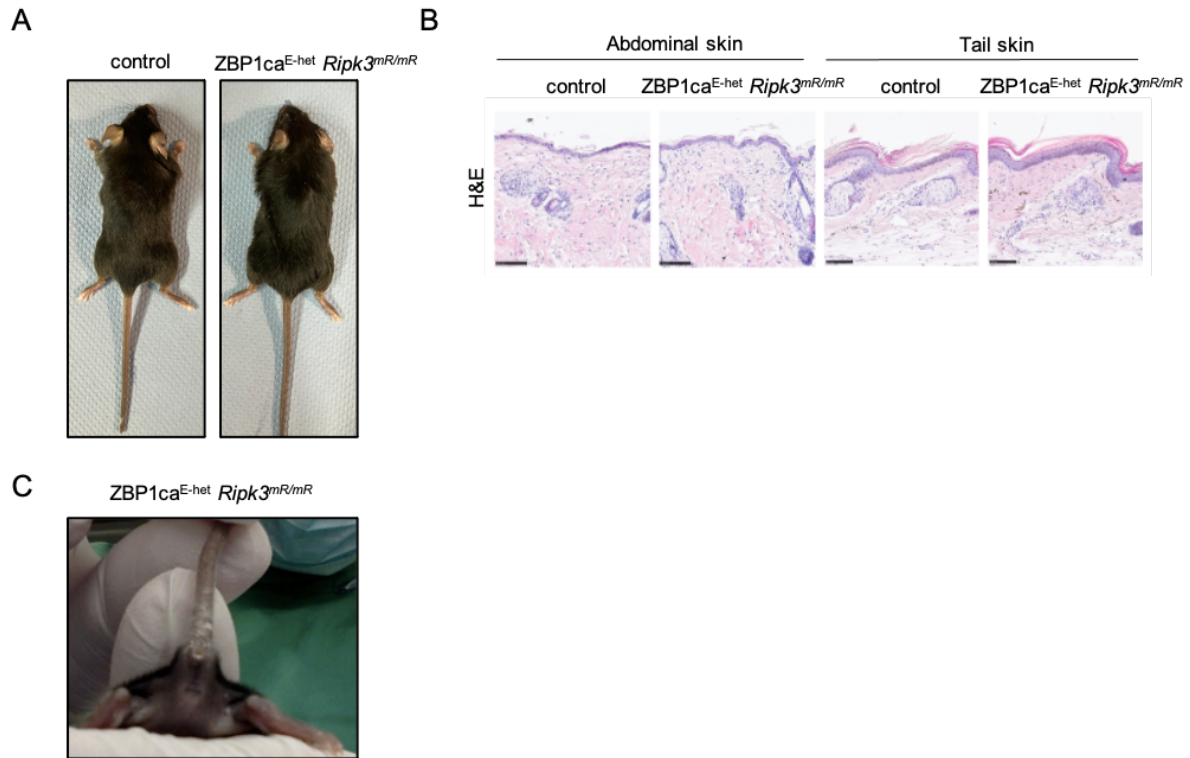


Figure S3. ZBP1ca^{E-het} *Ripk3^{mR/mR}* mice can age at least up to 30 weeks of age. **(A)** Representative photographs of ZBP1ca^{E-het} *Ripk3^{mR/mR}* mouse (n=12) and control (n=3) at 30 weeks of age **(B)** Representative images from skin sections of ZBP1ca^{E-het} *Ripk3^{mR/mR}* mice and littermate at 30 weeks of age stained with H&E (Scale bars=100 μM, n=6 for ZBP1ca^{E-het} *Ripk3^{mR/mR}*, n=3 for control). **(C)** Representative photograph of ZBP1ca^{E-het} *Ripk3^{mR/mR}* mouse at P14.

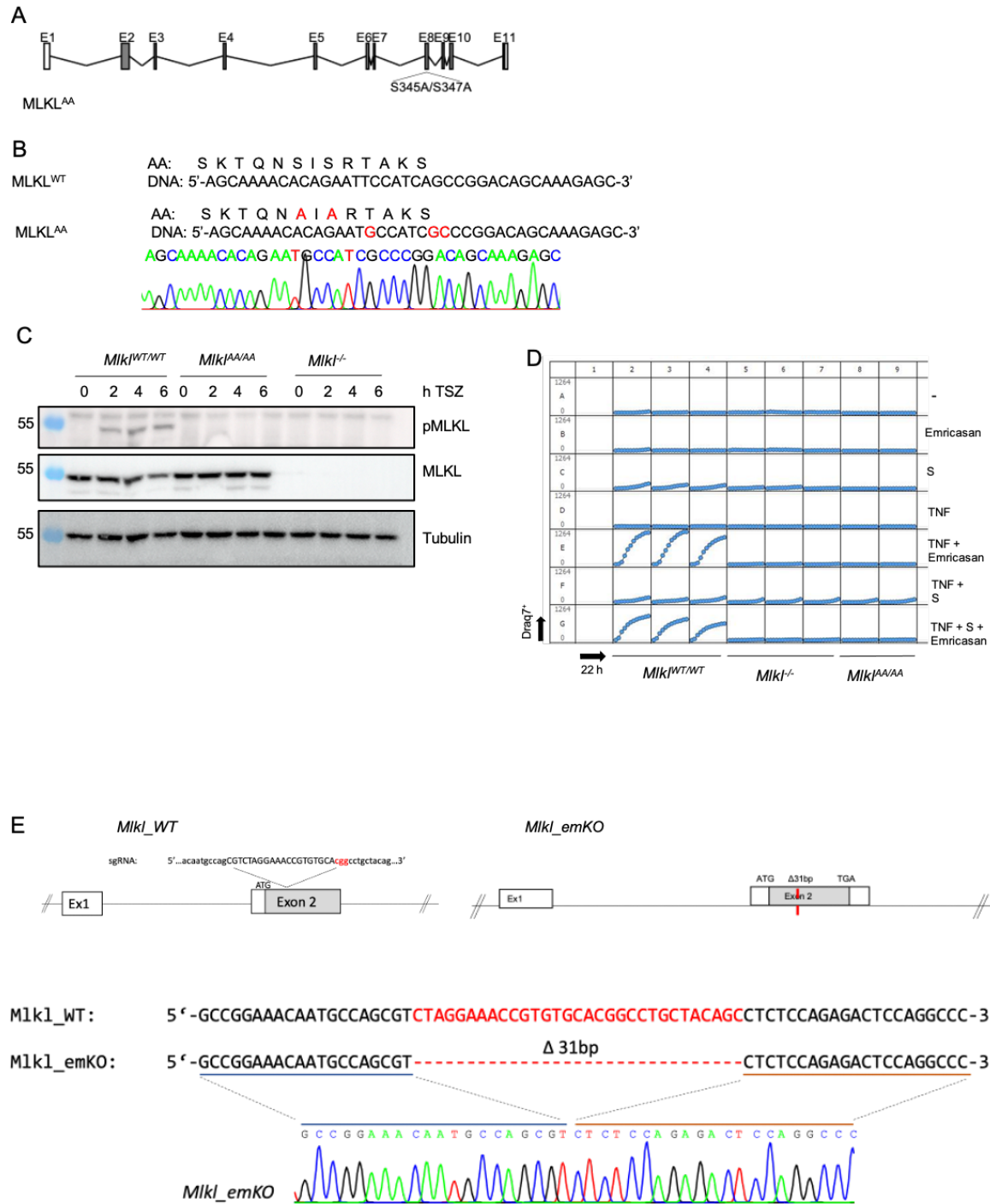


Figure S4. Generation of *Mkl* mutant mice (A) Serines at positions 345 and 347 encoded from exon 8 in the mouse *Mkl* gene were mutated to alanine using CRISPR/Cas9 technology with the gRNA target sequence 5' AAACACAGAATTCCATCAGC3' and the ssODN repair template 5' AACGTCTGCATCTAACACATCTGTCTGTCTAGCTTGCAGGATTTGAGTTAAGCAAAACACAGAATGCCATCGCCCGGACAGCAAAGAGCACTAAAGCAGAGAGATCCAGTTCAACGATATATGTCTCCCTGAGAGAC3' to generate the *Mkl*^{AA} mice **(B)** Successful generation of the *Mkl*^{AA} allele was assessed by sanger sequencing; red nucleotides (DNA) and amino acids (Prot.) indicate the desired mutations that are visible on the sequencing trace from a homozygous *Mkl*^{AA/AA} mouse **(C)** Expression of total MLKL and p-MLKL protein was assessed by western blot after TNF (T), Smac mimetic (S) and Z-VAD-FMK (Z) stimulation with tubulin as a loading control **(D)** Incucyte based life cell microscopy analysis of cell death in *Mkl*^{WT/WT}, *Mkl*^{emKO/emKO} and *Mkl*^{AA/AA} cells upon stimulation with TNF (T), Smac mimetic (S) and Emricasan, with total count of dead cells (Draq7+) displayed over time **(E)** The *Mkl*^{emKO} allele was generated using CRISPR/Cas9 technology and a single sgRNA binding in Exon 2 of the mouse *Mkl*

gene. The resulting *Mikl*^{emKO} allele resulted from a 31 bp deletion (visible in the sanger sequencing trace of a homozygous mouse) that caused a frameshift and premature stop codon (TGA) in exon 2.

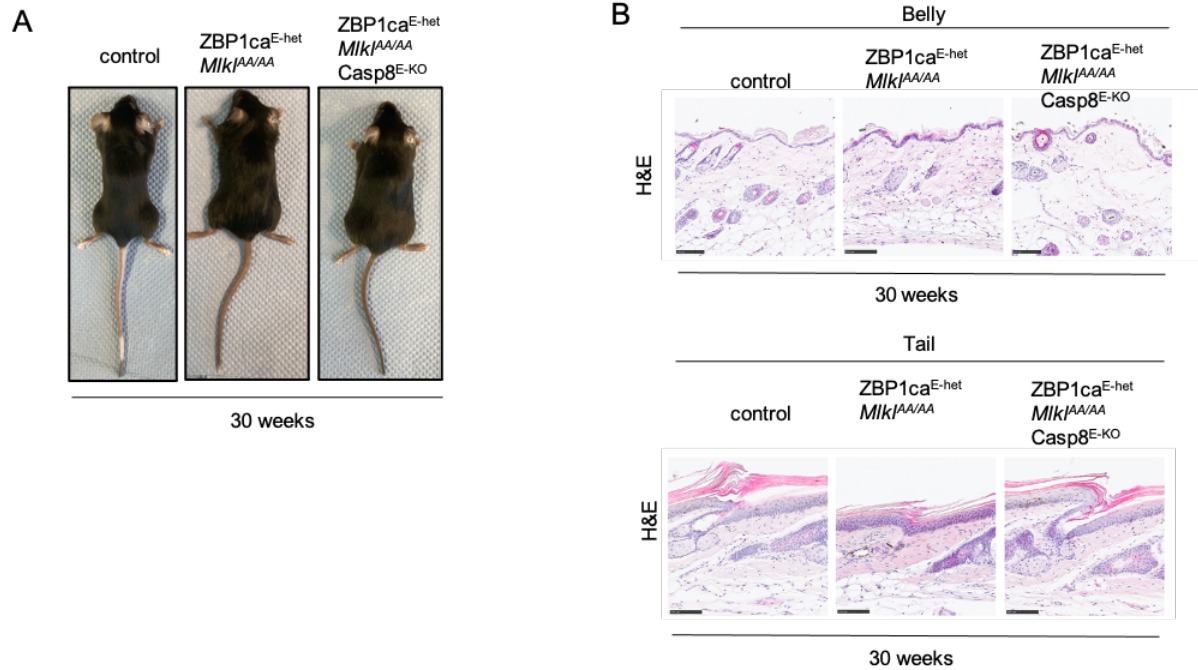


Figure S5. ZBP1ca^{E-het} *Mikl*^{AA/AA} and ZBP1ca *Mikl*^{AA/AA} *Casp8*^{E-KO} mice can age at least up to 30 weeks of age. (A) Representative photographs of ZBP1ca^{E-het} *Mikl*^{SA/SA} (n=12), ZBP1ca^{E-het} *Mikl*^{AA/AA} *Casp8*^{E-KO} (n=13) and control (n=13) at 30 weeks of age. (B) Representative images from abdominal and tail skin sections of ZBP1ca^{E-het} *Mikl*^{AA/AA}, ZBP1ca^{E-het} *Mikl*^{AA/AA} *Casp8*^{E-KO} mice and control at 30 weeks of age stained with H&E (Scale bars=100 μM, n=5 for ZBP1ca^{E-het} *Mikl*^{AA/AA}, n=3 for ZBP1ca^{E-het} *Mikl*^{AA/AA} *Casp8*^{E-KO}, n=4 for control).

Table S1. Number of mice for which qRT-PCR analysis was carried out for ZBP1ca^{E-het} mouse lines.

Genotype	<i>Oasl1</i>	<i>Ifi44</i>	<i>Ifit1</i>	<i>Cxcl9</i>	<i>Ccl4</i>	<i>Il1b</i>	<i>Tnf</i>	<i>Il6</i>
ZBP1ca ^{E-het}	7	5	7	8	8	6	4	3
<i>R26</i> ^{LSL} ZBP1ca	5	5	5	5	6	4	5	4
ZBP1ca ^{E-het} <i>Ripk3</i> ^{mR/mR}	5	5	5	5	5	5	5	3
control	7	10	10	10	8	6	9	4
ZBP1ca ^{E-het} <i>Mikl</i> ^{AA/AA}	4	4	5	5		3	5	5
ZBP1ca ^{E-het} <i>Mikl</i> ^{AA/AA} <i>Casp8</i> ^{E-KO}	5	4	5	5	4	5	4	5
control	14	14	12	15	10	10	11	11
ZBP1ca ^{E-het} <i>Mikl</i> ^{AA/AA} <i>Ripk1</i> ^{mR/mR}	5	5	5	5	5	5	5	5
control	10	10	10	10	9	9	10	8
ZBP1ca ^{E-het} <i>Mikl</i> ^{AA/AA} <i>Ripk1</i> ^{D138N/D138N}	5	5	5	5	4	5	5	5
control	9	9	9	9	9	8	8	6

2.2 Small Cell Lung Cancer development is independent of necroptotic signaling

Necroptotic cell death is ultimately executed by the protein MLKL, which consecutive to phosphorylation by RIPK3 leads to membrane permeabilization and release of intracellular components. Inhibition as well as induction of necroptosis was demonstrated to exert tumor-promoting as well as tumor-suppressing functions, however the functional role of necroptosis in SCLC remains unclear. In order to disentangle the role of necroptotic signaling in SCLC we aimed to dissect the effect of inhibiting or activating necroptosis in the RP mouse model. As we had previously identified a constitutively active version of ZBP1 as a potent driver of apoptotic as well as necroptotic cell death in the skin (section 2.1), we aimed to investigate a potential therapeutic role for ZBP1ca in SCLC. Since additionally to necroptosis, also pyroptosis has been shown to trigger anti-tumor immunity we compared these different lytic cell death modalities side by side^{153,154}.

2.2.1 Expression of ZBP1ca kills murine SCLC cell lines *in vitro*

Inflammatory cell death has been reported to trigger potent anti-tumor immunity due to release of intracellular components and thereby activation of bystander cells. We aimed to address, whether induction of lytic cell death can result in tumor regression of SCLC. To this end, we generated mouse SCLC cell lines, isolated from the RP mouse model (section 1.6.2), which can potentially undergo necroptosis and pyroptosis due to expression of drivers of the respective type of cell death. We created SCLC cell lines expressing doxycycline-inducible active MLKL₁₋₁₈₀ (these residues contain the N-terminal HELO domain which induces necroptosis upon overexpression)⁹². Since it has been suggested that immunogenic properties of necroptosis are due to RIPK3-dependent inflammatory cytokine production^{150,151}, we also expressed the aforementioned ZBP1ca construct in SCLC cell lines to trigger RIPK3 and MLKL activation. Lastly, we included overexpression of the N-terminal gasdermin D protein (here annotated as GSDMDN) lacking the C-terminal inhibitory domain, which leads to membrane permeabilization during pyroptosis²¹² (Figure 7).

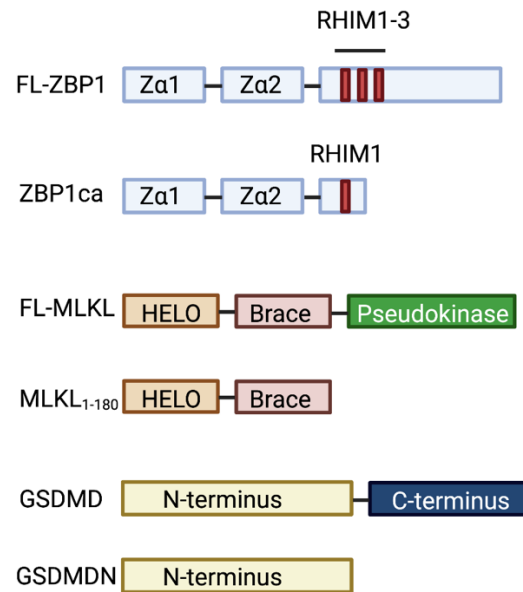


Figure 7. Schematic representation of constitutively active cell death-inducing constructs and the respective full-length protein. Active MLKL contains the N-terminal helical bundle and the brace region, ZBP1ca is composed out of the first 4 exons spanning from Zα1 to RHIM1 and active gasdermin D stops at AA 276. Created with BioRender.com.

Interestingly, we observed induction of cell death in only one out of two SCLC cell lines upon MLKL₁₋₁₈₀ expression, indicating a resistance of a subset of SCLC cells for plasma membrane permeabilization by MLKL, suggesting that different SCLC tumors may be resistant to lytic cell death downstream of MLKL. We could potentially trigger GSDMDN- and ZBP1ca-dependent cell death in both SCLC cell lines, suggesting a potential therapeutic effect for ZBP1ca or GSDMDN in SCLC (Figure 8).

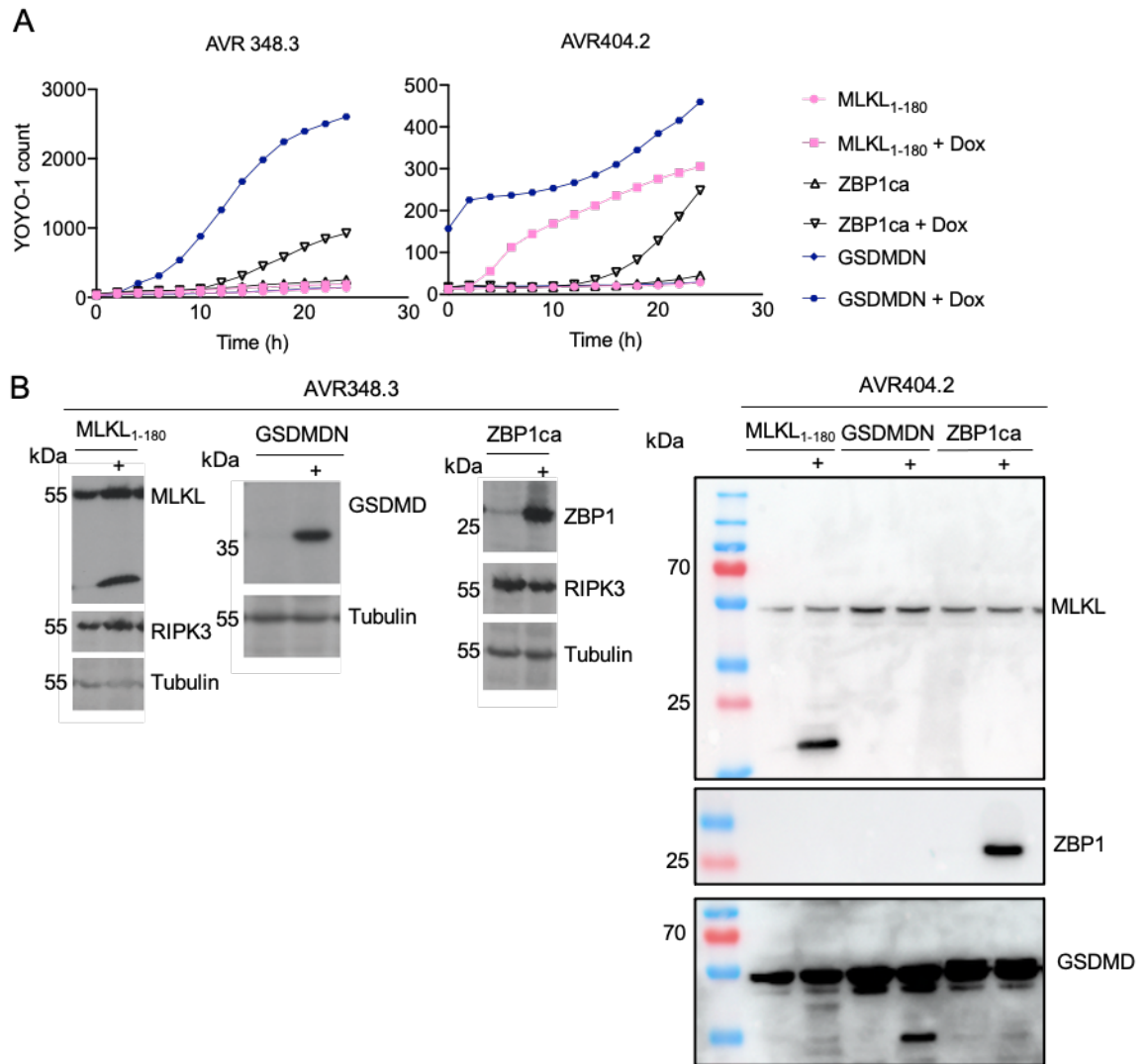


Figure 8. ZBP1ca and GSDMDN but not MLKL₁₋₁₈₀ efficiently kill SCLC cell lines. (A) Cell death measured by YOYO-1 uptake in 404.2 and 348.3 SCLC cell lines transduced with doxycycline (Dox)-inducible ZBP1ca-, MLKL₁₋₁₈₀- or GSDMDN-expressing vectors **(B)** Respective immunoblot analysis of cell death assays shown in (A). AVR404.2 cell lines are single cell clones.

Our data suggested that SCLC cell lines can become resistant to plasma membrane permeabilization downstream of MLKL. As ZBP1ca can induce apoptosis and necroptosis, we further analyzed signaling events downstream of ZBP1ca.

Indeed, we observed strong cleavage of caspase-8 upon ZBP1ca overexpression but could not detect phosphorylated MLKL although the ZBP1ca construct is generally capable of necroptosis induction (section 2.1, data not shown). Additionally, ZBP1ca-induced cell death could be fully blocked by addition of the pan-caspase inhibitor emricasan but not by inhibition of RIPK3, indicating apoptosis but not necroptosis. Conclusively, ZBP1ca potently triggered caspase-dependent cell death in SCLC cell lines and a subset of SCLC cell lines appear to become resistant to plasma membrane permeabilization by MLKL₁₋₁₈₀ (Figure 9).

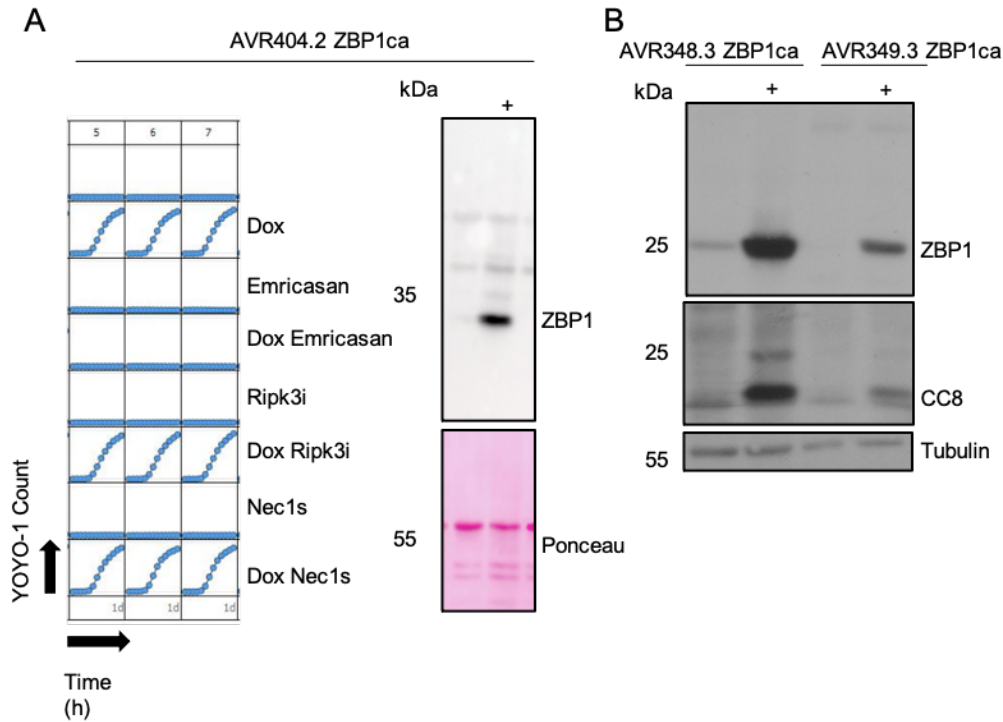


Figure 9. ZBP1ca expression in SCLC cell lines leads to apoptotic cell death. (A) Cell death measured by YOYO-1 uptake in the SCLC cell line 404.2 transduced with dox-inducible ZBP1ca after treatment with combinations of dox, emricasan or RIPK3 inhibitor GSK872 (R3i). Data from single cell clone are shown. **(B)** Respective immunoblot analysis of protein lysates from SCLC 404.2 after Dox stimulation (A). **(C)** Immunoblot analysis of the SCLC cell lines AVR348.3 and AVR349.3 transduced with dox-inducible ZBP1ca after dox stimulation.

2.2.2 ZBP1ca expression *in vivo* does not alter SCLC development

Our results thus far indicated that expression of ZBP1ca could effectively kill SCLC cells. Although, we found that ZBP1ca mediated apoptosis and not necroptosis in SCLC cell lines, we wondered whether ZBP1ca expression led to cell death of tumor cells and depletion of tumor growth *in vivo*. Therefore, we utilized a mouse model, which allows autochthonous Cre-mediated overexpression of ZBP1ca ($R26^{LSL.ZBP1ca}$, section 2.1) and crossed these mice to mice carrying *Rb1* and *Tp53* flanked FRT alleles as well as a $R26^{FSF.CreERT2}$ allele to generate $Rb1^{FRT/FRT} Tp53^{FRT/FRT} R26^{FSF.CreERT2/LSL.ZBP1ca}$ mice. In this genetic background, CreERT2 expression is restricted by a FRT-flanked STOP cassette. Inhalation of mice with an adenovirus expressing Flp recombinase leads to induction of SCLC due to loss of RB1 and TP53 while also removing the STOP cassette upstream of CreERT2. Consequently, CreERT2 is only expressed and can only be activated in viral targeted cells. At the age of 8-12 weeks, $Rb1^{FRT/FRT} Tp53^{FRT/FRT} R26^{FSF.CreERT2/LSL.ZBP1ca}$ and $Rb1^{FRT/FRT} Tp53^{FRT/FRT} R26^{FSF.CreERT2/WT}$ mice were inhaled with adenovirus expressing Flp recombinase (Ad-Flp), leading to loss of *Rb1*, *Tp53* and to expression of CreERT2 in cells targeted by the virus (Figure 10). Starting 6 months after Ad-Flp inhalation, animals were monitored for tumor development by biweekly MRI scans. Upon detection of visible tumor lesions, mice were treated intraperitoneal for five consecutive

days with tamoxifen in order to activate CreERT2 and to thereby induce ZBP1ca expression in tumor cells.

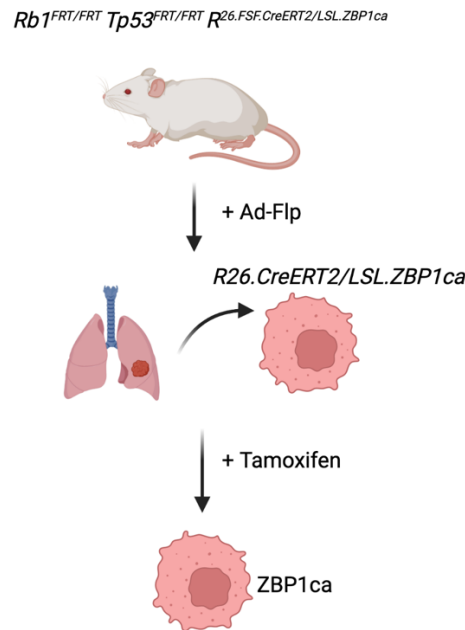


Figure 10. Activation of ZBP1ca in tumor cells of RP mice. Following Ad-Flp inhalation, *Rb1* and *Tp53* are ablated in lung epithelial cells and tumors start to develop. After onset of visible tumor lesions, tamoxifen treatment leads to CreERT2 activation, thus ZBP1ca expression in tumor cells. Created with BioRender.com.

Additionally, we aimed to investigate whether inducing ZBP1ca-dependent cell death can synergize with checkpoint inhibition in order to reach tumor regression. Given that SCLC is generally considered to be an immune cold tumor, induction of cell death may overcome this caveat and potentiate ICI. To achieve this, a subgroup of tamoxifen-treated mice was additionally treated with PD-1 blocking antibody (aPD-1).

All inhaled mice developed tumors; however, we could not detect considerable differences in tumor growth between $Rb1^{FRT/FRT} Tp53^{FRT/FRT} R26^{FSF.CreERT2/LSL.ZBP1ca}$ and $Rb1^{FRT/FRT} Tp53^{FRT/FRT} R26^{FSF.CreERT2/WT}$ mice after tamoxifen treatment. Furthermore, additional treatment with aPD-1 did not lead to any alterations regarding tumor fold change comparing both genotypes (Figure 11).

To learn whether SCLC cells are resistant to ZBP1ca-induced cell death *in vivo*, we performed immunoblotting with protein lysates isolated from lung tumors dissected from $Rb1^{FRT/FRT} Tp53^{FRT/FRT} R26^{FSF.CreERT2/LSL.ZBP1ca}$ and $Rb1^{FRT/FRT} Tp53^{FRT/FRT} R26^{FSF.CreERT2/WT}$ mice at the humane endpoint. Surprisingly, we were unable to find ZBP1ca expression in any of the tumors from $Rb1^{FRT/FRT} Tp53^{FRT/FRT} R26^{FSF.CreERT2/LSL.ZBP1ca}$ mice after tamoxifen treatment. Absence of detectable ZBP1ca suggests induction of cell death in a subset of SCLC cells, thus counterselection of the cells expressing the protein (Figure 12). As there was no effect on

tumor growth *in vivo* we would need to ensure proper functionality of CreERT2-mediated induction of ZBP1ca in order to make a clear statement, however these data suggest that ZBP1ca induction did not alter SCLC progression in RP mice.

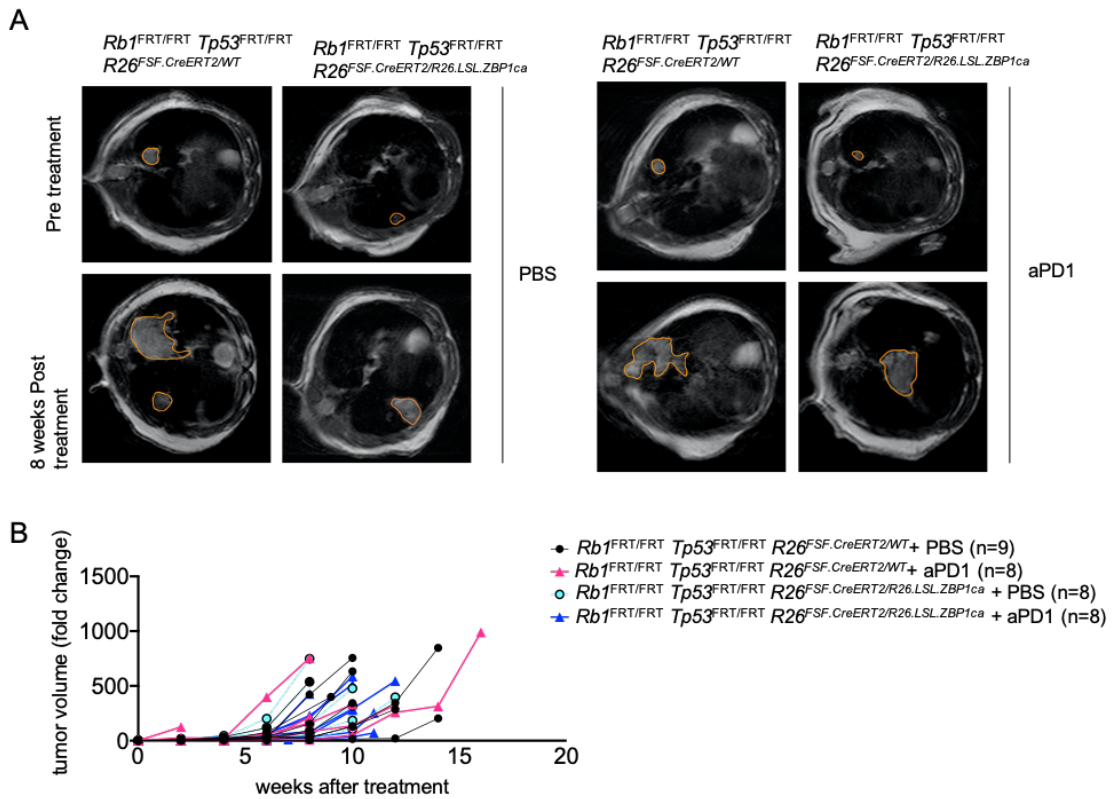


Figure 11. Induction of ZBP1ca expression \pm aPD1 treatment does not affect SCLC tumor growth in RP mice. (A) Representative images of MRI scans of mice with indicated genotypes pre-treatment and 8 weeks post-treatment with either aPD-1 (aPD1) or PBS. All mice received tamoxifen. Tumor areas were marked using Horos software **(B)** Graph depicting tumor growth indicated by fold change of mice with the indicated genotypes.

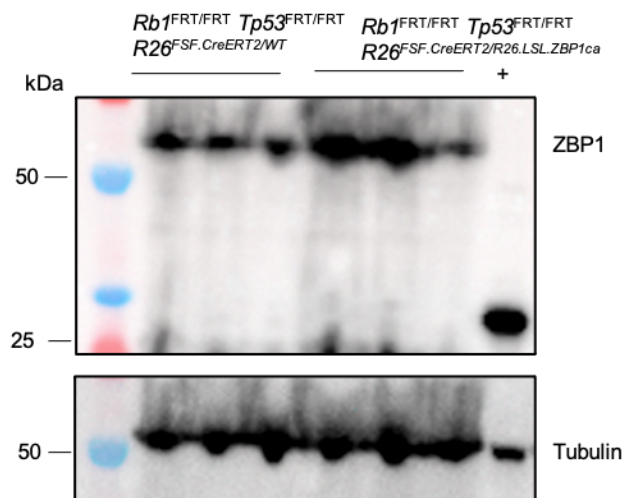


Figure 12. ZBP1ca expression could not be detected in tumor tissue at the humane endpoint. Immunoblot analysis of tumor tissue isolated from *Rb1^{FRT/FRT} Tp53^{FRT/FRT} R26^{FSF,CreERT2/WT}* and from *Rb1^{FRT/FRT} Tp53^{FRT/FRT} R26^{FSF,CreERT2/LSL.ZBP1ca}* mice after Ad-Flp inhalation and tamoxifen treatment at the humane endpoint.

2.2.3 Impairment of necroptosis does not affect SCLC progression

Our studies described above suggested that induction of cell death using ZBP1ca may not alter the SCLC phenotype in RP mice in the experimental setting we used. As a complementary approach, we aimed to assess how inhibition of necroptotic cell death might affect SCLC progression and development.

In response to phosphorylation at Serine 345/7 (T357/S358 in humans), MLKL is recruited to the plasma membrane, where it triggers necroptosis. In order to determine whether necroptosis plays an essential role in SCLC development, we crossed mice which harbor ubiquitously a non-phosphorylatable and therefore inactive version of MLKL (*Mkl^{AA/AA}* section 2.1) to mice carrying *Rb1^{FL/FL}* and *Tp53^{FL/FL}* alleles, generating *Rb1^{FL/FL} Tp53^{FL/FL} Mkl^{AA/AA}* mice. *Rb1^{FL/FL} Tp53^{FL/FL}* as well as *Rb1^{FL/FL} Tp53^{FL/FL} Mkl^{AA/AA}* mice were inhaled with Ad-Cre, leading to Cre-mediated deletion of the respective loxP-flanked alleles in cells targeted by the virus. We assessed tumor development via biweekly MRI scans, starting 20 weeks after Ad-Cre inhalation (Figure 13). All *Rb1^{FL/FL} Tp53^{FL/FL}* mice inhaled developed tumor lesions with a median tumor onset of 26 weeks. 9 out of 10 *Rb1^{FL/FL} Tp53^{FL/FL} Mkl^{AA/AA}* mice eventually developed neoplasia, with a similar median onset of 26 weeks. Thus, we observed no differences between necroptosis-competent animals and mice that were impaired of necroptotic signaling. In line with a similar tumor onset, we did not observe considerable differences in the survival curves between *Rb1^{FL/FL} Tp53^{FL/FL}* and *Rb1^{FL/FL} Tp53^{FL/FL} Mkl^{AA/AA}* mice with a median survival of 258 and 267 days, respectively (Figure 13).

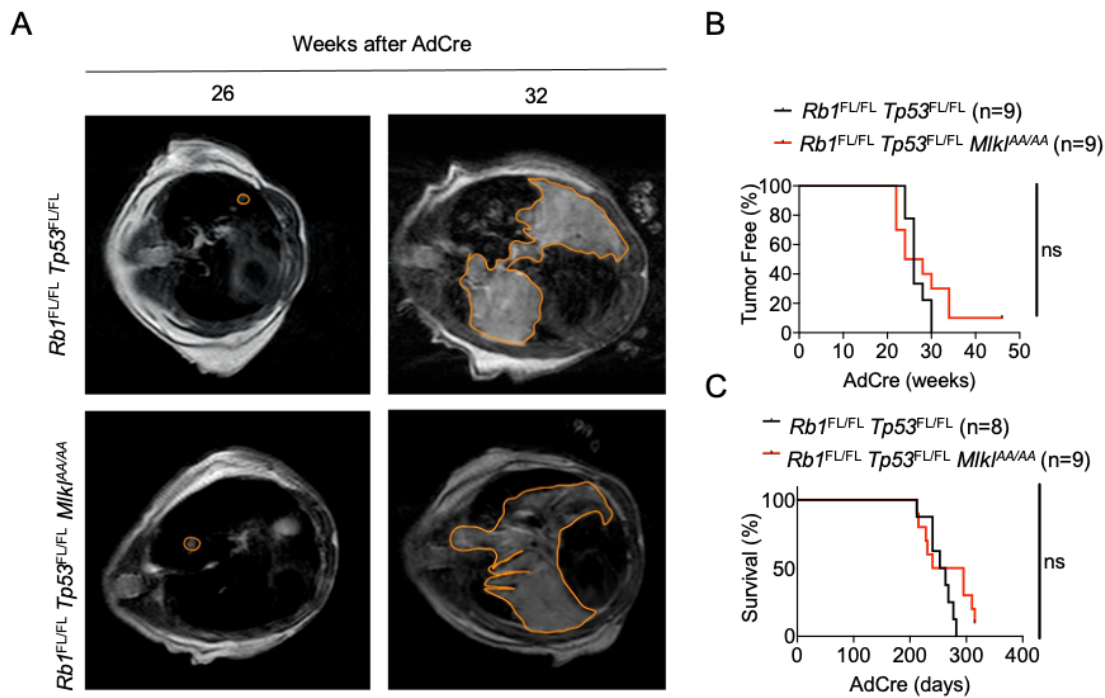


Figure 13. Impairment of necroptosis does not alter SCLC development in RP mice. (A) Representative images of MRI scans of *Rb1^{FL/FL} Tp53^{FL/FL}* (n=9) and *Rb1^{FL/FL} Tp53^{FL/FL} Mkl^{AA/AA}* (n=10) mice 26 and 32 weeks after Ad-Cre instillation. Tumor areas were marked using Horos Software. **(B)**

Graph depicting tumor onset assessed via MR imaging of mice with indicated genotypes. **(C)** Graph showing survival of mice with indicated genotypes.

Examination of lungs from mice sacrificed due to termination criteria of the experimental protocol revealed similar tumor burden and immunohistochemical analysis of lung tissues showed similar tumor load and morphology in both genotypes (Figure 14).

Immunostaining for Ki67 revealed a similar amount of proliferating tumor cells comparing $Rb1^{FL/FL} Tp53^{FL/FL}$ and $Rb1^{FL/FL} Tp53^{FL/FL} Mkl^{AA/AA}$ mice. Additionally, we could not observe differences in CD45 positive cells, indicating that inhibition of necroptotic signaling did not change immune cell infiltration. In line with these results, RNAseq analysis of tumor tissue isolated at the endpoint of the experimental protocol did not show any changes between $Rb1^{FL/FL} Tp53^{FL/FL}$ and $Rb1^{FL/FL} Tp53^{FL/FL} Mkl^{AA/AA}$ mice. Conclusively, inhibition of necroptosis due to impaired MLKL phosphorylation did not modify SCLC development, arguing that necroptosis does not play an essential role in the RP mouse model of SCLC.

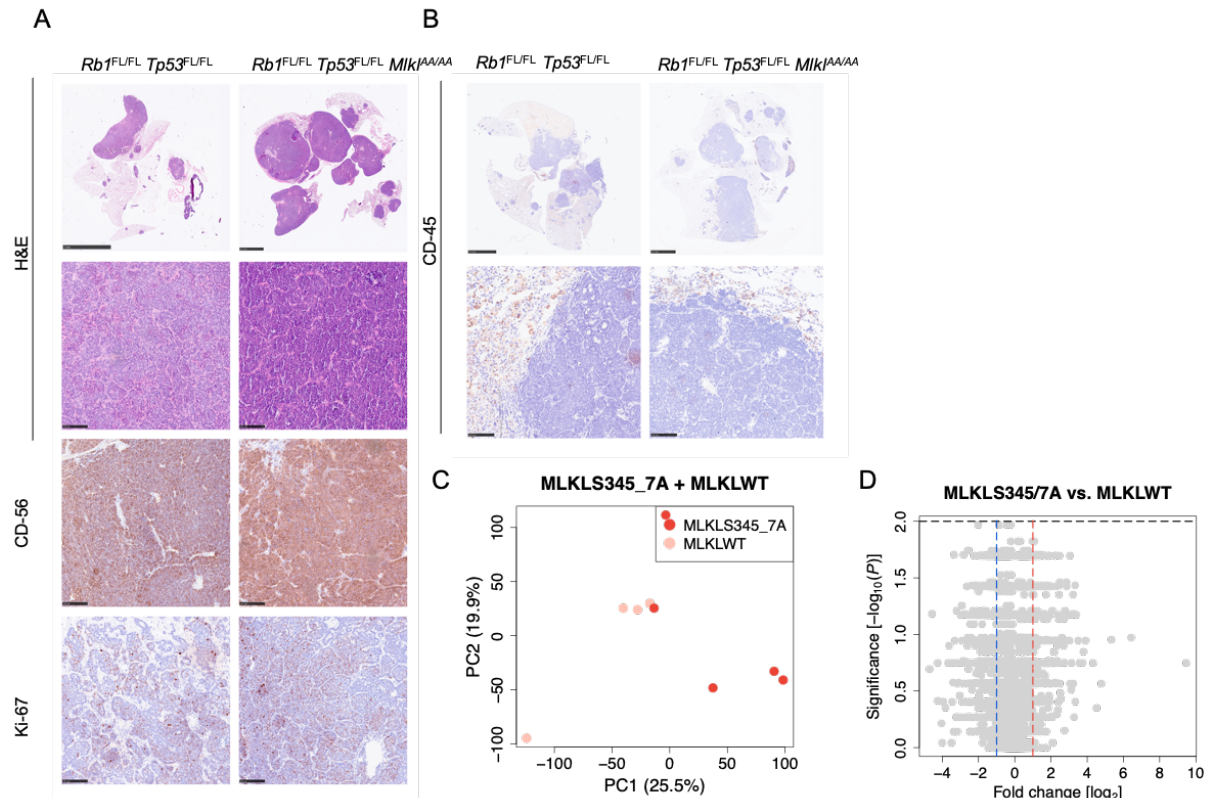


Figure 14. Histological and molecular analysis of lung tumors in $Rb1^{FL/FL} Tp53^{FL/FL} Mkl^{AA/AA}$ mice. **(A)** Representative images of lung sections from mice with indicated genotypes stained with H&E or immunostained for CD56 and for Ki67. Scale bars = 5 mm & 100 μ m. **(B)** Representative images of lung sections immunostained for CD45. Scale bars = 5mm & 100 μ m. **(C-D)** Principal component analysis (PCA) **(C)** and Volcano plot **(D)** of RNAseq data from tumor tissues of $Rb1^{FL/FL} Tp53^{FL/FL}$ (annotated as MLKLWT) compared to $Rb1^{FL/FL} Tp53^{FL/FL} Mkl^{AA/AA}$ mice (annotated as MLKLS345/7A).

2.3 NEMO- and RelA-dependent NF- κ B Signaling Promotes Small Cell Lung Cancer

Manuscript Declaration

After investigating cell death in SCLC in the aforementioned study, we next unraveled the mechanistic role of inflammatory signaling, specifically NF- κ B and TNFR1, in SCLC

Specific contributions:

- Generation of all *in vitro* and *in vivo* data in this study
- Analysis of all data generated in this study besides the RNAseq data in Figure 2FE, 4FE, 8FE
- Histologic analysis was performed together with M.S. and R.B.
- Manuscript drafting and editing

NEMO- and RelA-dependent NF- κ B Signaling Promotes Small Cell Lung Cancer

Lioba Koerner^{1,2}, Marcel Schmiel^{3,4}, Tsun-Po Yang³, Martin Peifer^{3,4,5}, Reinhard Buettner^{4,5}, Manolis Pasparakis^{1,2,5,6, *}

¹Institute for Genetics, University of Cologne, 50674 Cologne, Germany

²Cologne Excellence Cluster on Cellular Stress Responses in Aging-Associated Diseases (CECAD), University of Cologne, 50931 Cologne, Germany

³Department of Translational Genomics, Faculty of Medicine and University Hospital Cologne, University of Cologne, 50931 Cologne, Germany

⁴Institute of Pathology, Faculty of Medicine and University Hospital Cologne, University of Cologne, 50931 Cologne, Germany

⁵Center for Molecular Medicine (CMMC), Medical Faculty and University Hospital Cologne, University of Cologne, 50931 Cologne, Germany

⁶Lead contact

*Correspondence: pasparakis@uni-koeln.de

Running Title

NF- κ B signaling promotes small cell lung cancer

Abstract

Small cell lung cancer (SCLC) is an aggressive type of lung cancer driven by combined loss of the tumor suppressors *RB1* and *TP53*. SCLC is highly metastatic and despite good initial response to chemotherapy patients usually relapse, resulting in poor survival. Therefore, better understanding of the mechanisms driving SCLC pathogenesis is required to identify

new therapeutic targets. Here we identified a critical role of the IKK/NF- κ B signaling pathway in SCLC development. Using a relevant mouse model of SCLC, we found that ablation of NEMO/IKK γ , the regulatory subunit of the IKK complex that is essential for activation of canonical NF- κ B signaling, strongly delayed the onset and growth of SCLC resulting in considerably prolonged survival. In addition, ablation of the main NF- κ B family member p65/RelA also delayed the onset and growth of SCLC and prolonged survival, albeit to a lesser extent than NEMO. Interestingly, constitutive activation of IKK/NF- κ B signaling within the tumor cells did not exacerbate the pathogenesis of SCLC, suggesting that endogenous NF- κ B levels are sufficient to fully support tumor development. Moreover, TNFR1 deficiency did not affect the development of SCLC, showing that TNF signaling does not play an important role in this tumor type. Taken together, our results revealed that IKK/NF- κ B signaling plays an important role in promoting SCLC, identifying the IKK/NF- κ B pathway as a promising therapeutic target.

Introduction

Small cell lung cancer (SCLC) is a very aggressive lung cancer subtype with a median survival of ~1 year for patients with metastatic disease¹. SCLC is characterized by early metastatic spread, neuroendocrine differentiation and small tumor cells^{1, 2, 3, 4}. Patients often initially respond to chemotherapy but in most cases the tumors subsequently relapse and become resistant to cytotoxic treatments^{1, 5}. Comprehensive genomic profiling of SCLC revealed a bi-allelic loss of *RB1* and *TP53* in all patients, showing that loss of these two tumor suppressors is obligatory in SCLC^{6, 7, 8, 9, 10}. However, the mechanisms determining the aggressive nature of SCLC and its increased metastatic potential remain poorly understood¹. Therefore, a better understanding of the molecular pathways that determine SCLC initiation, progression and metastasis will be critical to develop new therapeutic approaches.

The interplay between tumor and immune cells plays an essential role in cancer progression and critically determines tumor development. Indeed, inflammation has been recognized as one of the hallmarks of cancer¹¹. While chronic inflammation can fuel tumor growth, an adaptive immune response against tumor-specific antigens can also trigger anti-cancer immunity, resulting in elimination of transformed cells¹¹. SCLC ranks among the tumor entities with the highest tumor mutational burden, likely due to its cigarette smoke-induced nature, which is expected to result in large number of neoantigens. However, immunotherapies based on checkpoint inhibitors had limited success with only a small percentage of patients responding¹. Tumor necrosis factor (TNF) is a potent pro-inflammatory cytokine exerting both tumor-promoting and anti-cancer effects¹². TNF was discovered as a factor inducing the death of tumor cells but was subsequently shown to promote tumor development in different models,

such as DMBA/TPA induced skin carcinogenesis and obesity-associated liver cancer^{13, 14}. TNF signaling via TNFR1 regulates inflammation, cell survival and death by inducing distinct intracellular signaling cascades¹⁵. TNFR1 stimulation induces the activation of the inhibitor of NF- κ B (I κ B) kinase (IKK) complex, resulting in the nuclear accumulation of NF- κ B promoting the transcription of genes regulating inflammation and cell survival^{15, 16}. The IKK complex consists of the regulatory subunit NEMO (also termed IKK γ) and the catalytic subunits IKK1 and IKK2 (also termed IKK α and IKK β , respectively)^{16, 17, 18}. NEMO is essential for activation of canonical NF- κ B signaling, which primarily depends on IKK2 kinase activity and the RelA NF- κ B subunit^{16, 17, 18}. IKK/NF- κ B signaling has emerged as a crucial driver of tumor growth and progression^{17, 19}. Multiple studies in mouse models demonstrated that NF- κ B signaling promotes tumorigenesis in several cancer entities, including colitis-associated colon cancer²⁰, mammary tumors^{21, 22, 23}, DMBA/TPA-induced skin carcinogenesis²⁴, as well as *Kras* mutation-driven lung adenocarcinoma^{25, 26, 27}. However, NF- κ B signaling has also been shown to exhibit tumor suppressing functions in different tissues and models of carcinogenesis. Inhibition of NF- κ B signaling in human keratinocytes promoted Ras-mediated oncogenic transformation in a xenograft model²⁸ and NF- κ B inhibition via expression of a dominant-negative mutant I κ B α super-repressor (I κ B α SR) in murine skin triggered the development of squamous cell carcinoma^{29, 30}. Additionally, liver parenchymal cell-specific knockout of NEMO caused the spontaneous development of chronic hepatitis and hepatocellular carcinoma (HCC) in mice^{31, 32}, whereas ablation of IKK2 in hepatocytes led to increased diethylnitrosamine (DEN)-induced liver tumorigenesis³³. Interestingly, NF- κ B activation has been proposed to induce T-cell mediated immune surveillance and therefore tumor rejection in lung adenocarcinoma³⁴. Thus, the role of NF- κ B signaling has been extensively studied in various tumor entities, amongst them *Kras*-driven lung adenocarcinoma, however, its function in SCLC remains elusive.

Here we aimed to study the role of TNFR1 and NF- κ B signaling in SCLC using an autochthonous mouse model of SCLC induced by the simultaneous ablation of *Rb1* and *Tp53* in mouse lung epithelial cells, which has been shown previously to recapitulate the morphological and molecular features of SCLC^{1, 35}. We show that inhibition of NF- κ B signaling by depletion of NEMO or RelA considerably delayed tumor onset, slowed tumor growth and significantly prolonged mouse survival. Surprisingly, neither constitutive activation of NF- κ B signaling, nor ablation of TNFR1 resulted in changes in SCLC development or progression. Together, these results show that NEMO and RelA-dependent NF- κ B signaling plays a critical role in SCLC.

Materials and Methods

Mice

Rb^{FL/FL 36}, *Tp53*^{FL/FL 37}, *Nemo*^{FL/FL38}, *Rela*^{FL/FL 39}, *R26*^{LSL.IKK2ca 40}, *Tnfr1*^{FL/FL 41} and *Tnfr1*^{-/- 42} mice have been described before. Mice used in these experiments were kept on a mixed C57Bl6/J/N background. Before MR imaging, mice were maintained at the specific pathogen-free animal facility of the CECAD Research Center, University of Cologne, under a 12-hour dark/12-hour light cycle in individually ventilated cages (Greenline GM500; Tecniplast) at 22 (±2) °C and a relative humidity of 55 (±5) %. They were given a sterilized commercial pelleted diet (Ssniff Spezialdiäten GmbH) as well as water ad libitum. All animal procedures were conducted in accordance with European, national and institutional guidelines and experimental protocols were approved by local government authorities (Landesamt für Natur, Umwelt und Verbraucherschutz Nordrhein-Westfalen). Animals requiring medical attention were provided with appropriate care and excluded from the studies described when reaching pre-determined criteria of disease severity. No other exclusion criteria existed. Mouse studies as well as immunohistochemical assessment of pathology and evaluation of MR imaging were performed in a blinded fashion.

RP mouse model & MRI scans

For induction of lung tumor formation, 8–12-week-old mice were anesthetized with Ketavet (100mg/kg)/Rompun (20mg/kg) by intraperitoneal injection, followed by intratracheal application of replication-deficient Cre-expressing adenovirus (Ad5-CMV-Cre, 2.5 x 10⁷ PFU, University of Iowa). Mice were inhaled in three different cohorts, every cohort including all genotypes used in this study. Only cohort 1 did not include *Rb1*^{FL/FL}*Tp53*^{FL/FL}*Nemo*^{FL/FL} mice. One *Rb1*^{FL/FL}*Tp53*^{FL/FL}*Tnfr1*^{-/-} mouse was inhaled at a later timepoint. All experiments carried out were pooled. Starting 20 weeks after AdenoCre inhalation, tumor development was monitored bi-weekly by magnetic resonance imaging by using the MRI (A 3.0 T Philips Achieva clinical MRI) in combination with a specific mouse solenoid coil (Philips Hamburg, Germany). MR images were acquired using turbo-spin echo (TSE) sequence (repetition time = 3819ms, echo time = 60ms, field of view = 40 x 40 x 20 mm³, reconstructed voxel size = 0.13 x 0.13 x 1.0 mm³) under 2,5% isoflurane anesthesia. Resulting MR images were analyzed blindly by marking regions of interests employing Horos software. For MRI analysis, mice were maintained in the animal facility of the nuclear medicine, University Hospital Cologne, in individually ventilated cages at 12h/12h light/dark cycle, 55 (±10%) humidity and 22 (±2) °C. All animal experiments were approved by local government authorities (Landesamt für Natur, Umwelt und Verbraucherschutz, Nordrhein-Westfalen, Germany). All animal experiments were conducted in compliance with 64isualiz, national and institutional guidelines on animal welfare. Animals requiring medical attention were provided with appropriate care and excluded from

the studies described when reaching pre-determined criteria of disease severity. No other exclusion criteria existed.

Tissue preparation

Mice were sacrificed using cervical dislocation. For histopathological analysis the trachea was injected with 4% PFA to inflate and the lung. Lung tissue was fixed in 4% PFA O/N at 4°C. Small pieces of tumor tissues were snap frozen on dry ice for RNA and protein expression analysis and stored at -80°C until further processing. Tumors were cut from the lungs, in order to isolate cell lines as described below.

Cell culture

Tumors were isolated from RP-mice at the humane endpoint. The tumors were incubated in 10X TrypLE™ (ThermoFisher Scientific #A1217701) at 37°C and 5% CO₂ for 20 minutes. Roswell Park Memorial Institute (RPMI) 1640 medium containing 10% FCS and 1% P/S was added and the tissue was incubated at 37°C, 5% CO₂ overnight. After incubation, remaining tumor tissue was removed from the culture and cells were grown at 37°C, 5% CO₂, washed with PBS every third day and supplied with new RPMI medium + 1%P/S + 10% FCS until they grew confluent. Cell lines were then maintained at 37°C and 5% CO₂.

Histologic analysis

Formalin-fixed paraffin embedded (FFPE) 4 μm-thick lung tissue sections were de-paraffinized using xylene and re-hydrated with decreasing ethanol concentrations (100%, 96%, 75%, 0%). The tissue sections were stained in haematoxylin for 2 minutes, 15 minutes differentiated in tap water and stained for 1 minute with eosin. Then, sections were de-hydrated using increasing ethanol concentrations and fixed in xylene. The slides were mounted in Entellan. In addition, FFPE lungs were stained for Ki-67 (Cell Marque 275-R10), CD45 (BD 550539) and CD56 (Zytomed RBK050). The amount of tumor-infiltrating Ki67⁺ and CD45⁺ cells was assessed by a board-certified pathologist.

Immunoblotting

For immunoblot analyses, 3 x 10⁵ cells were seeded in 6-well plates and cultured O/N. Cells were lysed in RIPA buffer (HEPES 20 mM, NaCl 350 mM, MgCl₂ 1mM, EDTA 0.5mM, EGTA 0.1mM, Glycerol 20%, Nonident P-40 1%) supplemented with protease and phosphatase inhibitor tablets (Roche) for 20 minutes on ice. Proteins from tumor tissue were isolated using precellys 24 tissue homogenizer (bertin instruments). Protein concentration was measured using PIERCE 660nm Protein Assay Reagent (Thermo Scientific, #22660) and BSA standard.

Lysate concentration was adjusted to 5 µg/µl and 2x Laemmli sample buffer (Bio-Rad 1610737) was added. Samples were boiled at 95°C for 8 minutes.

Cell lysates were separated using Sodium dodecyl-sulfate polyacrylamide gel electrophoresis and transferred to polyvinylidene difluoride membranes (IPVH00010, Millipore) at 80V for 3h at 4°C. Membranes were blocked using 5% milk in 0.1% PBST for 1 h, washed three times with 0.1% PBST and probed with following primary antibodies: α -NEMO (homemade 1:1000), α -p65 (Cell Signaling 3179 1:1000), α -IKK2 (Cell Signaling 2684S 1:1000) and α -Tubulin (Sigma T6074 1:1000) O/N at 4°C. Membranes were washed three times with 0.1% PBS-T and were incubated with secondary horseradish peroxidase-coupled antibodies for 1h at RT (GE Healthcare, Jackson ImmunoResearch, 1:10000). ECL Western Blotting Detection Reagent (RPN2106, GE Healthcare) was used to detect the proteins. Membranes were stripped if necessary, using stripping buffer (ThermoScientific, 21059) for 15 minutes at RT.

3' mRNA sequencing analysis

RNA isolation from tumor tissue was performed using a NucleoSpin RNA isolation kit (Macherey Nagel Ref. 740955.250). RNA quality was evaluated based on OD260/280 and OD260/230 ratios as well as on RNA integrity number (RIN). For determination of gene expression, the Quant 3'mRNAseq Library Prep Kit FWD for Illumina (Lexogen). Samples with RIN < 4, OD260/260 < 1.8 or OD 260/230 < 1.5 were excluded from the analysis. Five mice per genotype were used. Single-end sequencing reads were aligned to Ensembl GRCm38 (mm10) cDNA sequences using kallisto 0.43.1⁴³ with default average fragment length parameters. Transcript-level transcripts per million (TPM) 66isualized66on were estimated, and gene-level aggregated TPMs were calculated using sleuth 0.29.0⁴⁴ resulting in 35,930 genes with a Ensembl BioMart annotation. Only 18,383 of those were considered expressed (median TPM > 0) across 41 transcriptomes and subsequently used for further analysis.

Gene set enrichment analysis (GSEA)

All expressed genes were first weighted using the calculation shown below to convert the two-dimension dynamics (i.e., fold changes and p-value significances) derived from differential analysis into a one-dimension gene list. Then this pre-ranked gene list was used to run against the hallmark gene sets downloaded from MsigDB mouse draft database 0.3 to test for enrichment using GSEA tool 4.2.3⁴⁵.

Weight = $\text{Log}_2(\text{Fold change}) \times (-\text{Log}_{10}(\text{p-value}))$.

Data availability statement

The RNA-seq data reported in the manuscript have been deposited in the European Nucleotide Archive (ENA) at EMBL-EBI under accession number PRJEB53995 (<https://www.ebi.ac.uk/ena/browser/view/PRJEB53995>).

Statistical analysis

Data shown in graphs display mean. Wilcoxon rank-sum/ Mann-Whitney *U* test was used to test for differential gene expression between two non-parametric groups, and the results were visualized via volcano plots using purpose-written R scripts. For comparison of more than two groups, Kruskal-Wallis Test was used. The Log-Rank (Mantel-Cox) test was used in order to compare survival curves and tumor onset of mice. * $p \leq 0.05$; ** $p \leq 0.01$; *** $p \leq 0.005$, **** $p \leq 0.001$ for all figures. All statistical analysis was performed with Prism6, GraphPad. No data were excluded.

Results

Critical role of NEMO in SCLC development

To study the role of NF- κ B signaling in SCLC, we employed a well-characterized genetically engineered mouse model of the disease based on combined ablation of *Rb1* and *Tp53* in mouse lung epithelial cells via adenovirus-mediated delivery of Cre recombinase, which causes the development of SCLC within 9 months³⁵ (Figure 1A). This mouse model recapitulates the key features of human SCLC, including the histopathological, molecular and immunological phenotype³⁵. To inhibit canonical NF- κ B signaling, we chose to target NEMO, the regulatory subunit of the IKK complex that is essential for canonical NF- κ B activation, and p65/RelA, which is the NF- κ B subunit primarily responsible for the transcriptional activation of canonical NF- κ B target genes^{16, 18}. To address the role of NEMO in SCLC we crossed mice carrying loxP-flanked *Nemo* alleles to mice carrying loxP-flanked *Rb1* and *Tp53* alleles. At the age of 8-12 weeks, *Rb1*^{FL/FL} *Tp53*^{FL/FL} as well as *Rb1*^{FL/FL} *Tp53*^{FL/FL} *Nemo*^{FL/FL} mice were inhaled with adenovirus expressing Cre recombinase (Ad-Cre), which results in Cre-mediated deletion of the respective loxP-flanked alleles in lung epithelial cells. Starting at 20 weeks after Ad-Cre inhalation, mice were monitored for tumor development by magnetic resonance imaging (MRI) scanning biweekly (Figure 1A, B). Ad-Cre-inhaled *Rb1*^{FL/FL} *Tp53*^{FL/FL} mice developed tumor lesions with a median tumor onset of 24 weeks after inhalation (Figure 1B, C). In contrast, *Rb1*^{FL/FL} *Tp53*^{FL/FL} *Nemo*^{FL/FL} mice showed a strong delay in tumor development with a median tumor onset of 37 weeks after Ad-Cre inhalation (Figure 1B, C). Overall, 10 out of 11 *Rb1*^{FL/FL} *Tp53*^{FL/FL} *Nemo*^{FL/FL} mice eventually developed tumors, whereas one mouse did not show signs of tumor development as late as 400 days after Ad-Cre inhalation (Figure 1B, C). At 26 weeks

after Ad-Cre inhalation, we detected the presence of several lung tumors in 8 out of 17 *Rb1^{FL/FL} Tp53^{FL/FL}* mice, whereas none of the *Rb1^{FL/FL} Tp53^{FL/FL} Nemo^{FL/FL}* mice showed lung tumor development at this stage (Figure 1D). Longitudinal measurements of tumor volume by MRI showed that, in addition to the delayed onset, lung tumors in *Rb1^{FL/FL} Tp53^{FL/FL} Nemo^{FL/FL}* mice displayed considerably reduced growth compared to *Rb1^{FL/FL} Tp53^{FL/FL}* mice during the first six weeks after tumor detection (Figure 1E). In addition to biweekly MRI scans, all mice were screened regularly for distress symptoms and were sacrificed humanely when reaching pre-determined termination criteria. In line with delayed tumor onset and reduced tumor growth, *Rb1^{FL/FL} Tp53^{FL/FL} Nemo^{FL/FL}* mice showed a significantly increased overall survival with a median survival of 358 days, compared to *Rb1^{FL/FL} Tp53^{FL/FL}* mice that had a median survival of 247 days (Figure 1F). Collectively, ablation of NEMO strongly delayed tumor onset, reduced tumor growth and significantly prolonged survival in a relevant mouse model of SCLC induced by combined inactivation of RB1 and TP53.

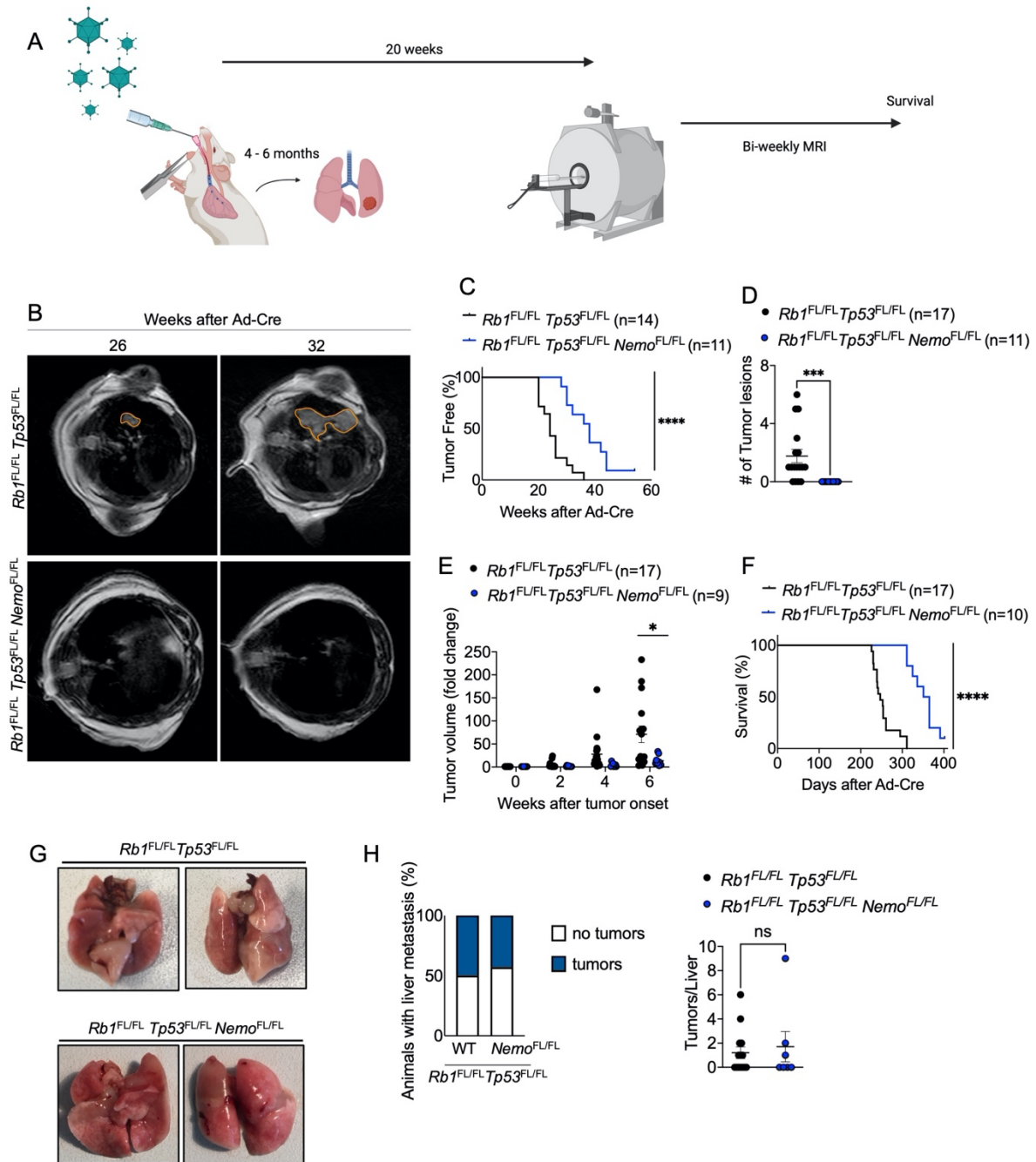


Figure 1. Epithelial NEMO ablation delays tumor onset and prolongs survival in a mouse model of SCLC. (A) Schematic showing intratracheal Ad-Cre inhalation and experimental procedure for the generation and analysis of a mouse model of SCLC (created with BioRender.com) (B) Representative images of MRI scans of *Rb1^{FL/FL} Tp53^{FL/FL}* (n=17) and *Rb1^{FL/FL} Tp53^{FL/FL} Nemo^{FL/FL}* (n=9) mice 26 and 32 weeks after Ad-Cre inhalation. Tumor areas were marked using Horos Software. (C) Graph depicting tumor onset assessed via MR imaging of mice with indicated genotypes. ****p < 0.0001, Log-rank test. (D) Graph depicting the number of tumor lesions 6 weeks after Ad-Cre inhalation of the indicated genotypes. ***p = 0.001, Mann-Whitney Test. Mean ± SEM. Each dot represents one mouse. (E) Graph depicting tumor fold change assessed via MR imaging 2-6 weeks after Ad-Cre inhalation for indicated genotypes. Each dot represents one mouse. Bars represent mean ± SEM. *p < 0.05, Mann-Whitney Test. (F) Graph depicting survival of mice with indicated genotypes. ****p < 0.0001, Log-rank test. (G) Representative photographs of lungs of *Rb1^{FL/FL} Tp53^{FL/FL}* (n=17) and *Rb1^{FL/FL} Tp53^{FL/FL} Nemo^{FL/FL}* (n=10) mice sacrificed at the humane endpoint. (H) Graphs depicting the percentage of mice with liver

metastasis and the amount of liver tumor lesions at the humane endpoint. N= 7 for *Rb1^{FL/FL} Tp53^{FL/FL} Nemo^{FL/FL}*, n=14 for *Rb1^{FL/FL} Tp53^{FL/FL}*. Mann-Whitney test. Mean \pm SEM.

Despite the delayed onset and reduced growth of tumors in Ad-Cre-treated *Rb1^{FL/FL} Tp53^{FL/FL} Nemo^{FL/FL}* compared to *Rb1^{FL/FL} Tp53^{FL/FL}* mice, macroscopic examination of lungs dissected from mice sacrificed at the humane endpoint revealed similar tumor burden in both genotypes (Figure 1G). In addition to the lung tumors, SCLC metastasis to the liver was also detected in about half of the mice with no difference in metastatic prevalence between the genotypes (Figure 1H). Histopathological analysis of lung sections showed the presence of tumors displaying classical characteristics of SCLC, such as homogenous tissue composed out of small tumor cells and expression of CD56, a marker frequently used in SCLC diagnosis ⁴⁶ (Figure 2A, B). Immunohistochemical staining with antibodies against Ki-67 revealed similar numbers of proliferating cells in tumors from *Rb1^{FL/FL} Tp53^{FL/FL} Nemo^{FL/FL}* compared to *Rb1^{FL/FL} Tp53^{FL/FL}* mice (Figure 2C). Considering that NF- κ B signaling regulates various aspects of innate and adaptive immunity ⁴⁷, we additionally investigated tumor immune cell infiltration by immunostaining for CD45, a marker expressed in all immune cells. Immunostaining for CD45 revealed the presence of immune cells in lung tissue surrounding the malignant lesions, however, we did not observe prominent immune cell infiltration within the tumor mass in either *Rb1^{FL/FL} Tp53^{FL/FL} Nemo^{FL/FL}* or *Rb1^{FL/FL} Tp53^{FL/FL}* mice (Figure 2D). To obtain insights into possible effects of NEMO deficiency in the transcriptional profile of SCLC, we performed RNA sequencing (RNAseq) analysis in RNA isolated from lung tumors dissected from *Rb1^{FL/FL} Tp53^{FL/FL} Nemo^{FL/FL}* and *Rb1^{FL/FL} Tp53^{FL/FL}* mice. Surprisingly, we did not find considerable differences in the gene transcriptional profile of the tumors between the two genotypes (Figure 2E). Specifically, we only found only 6 genes significantly upregulated and 6 genes significantly downregulated in tumors from *Rb1^{FL/FL} Tp53^{FL/FL} Nemo^{FL/FL}* compared to *Rb1^{FL/FL} Tp53^{FL/FL}* mice (Figure 2F). Therefore, analysis of tumors at the time of humane sacrifice did not reveal differences in tumor size, proliferation or immune cell infiltration between *Rb1^{FL/FL} Tp53^{FL/FL} Nemo^{FL/FL}* and *Rb1^{FL/FL} Tp53^{FL/FL}* mice.

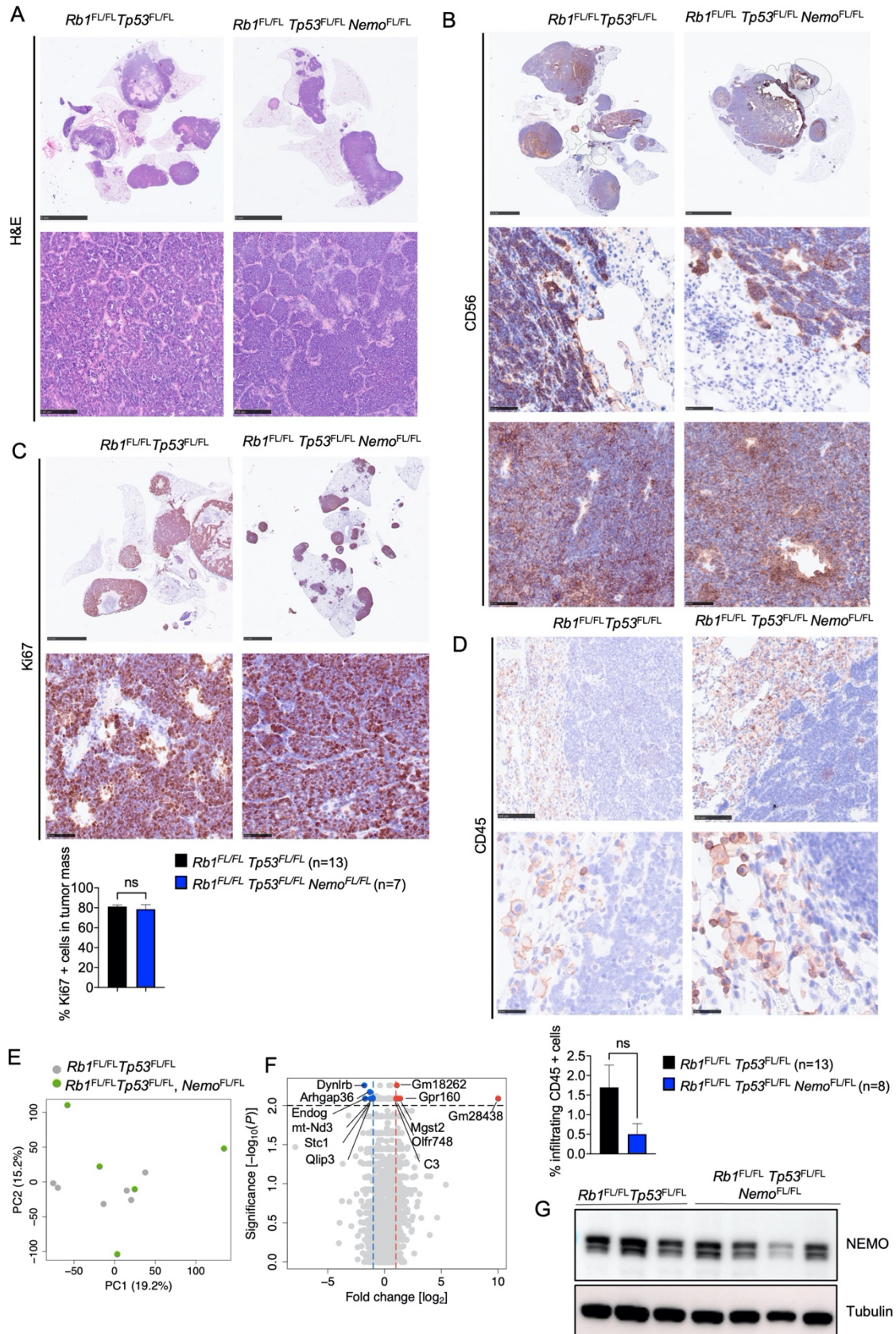


Figure 2. Histological and molecular analysis of lung tumors in *Rb1^{FL/FL} Tp53^{FL/FL} Nemo^{FL/FL}* mice. (A) Representative images of lung sections from mice with indicated genotypes sacrificed at the humane endpoint, stained with H&E (Scale bars = 5mm (top) and 100µm (bottom)) (B) Representative images of lung sections from mice with indicated genotypes immunostained for CD56 (Scale bars = 2.5mm & 5mm (top) and 50µm (bottom), n=8 for *Rb1^{FL/FL} Tp53^{FL/FL} Nemo^{FL/FL}*, n=11 for *Rb1^{FL/FL}*

Tp53^{FL/FL} (C) Representative images of lung sections from mice with indicated genotypes immunostained for Ki67 and graph depicting quantification of Ki67 positive cells (Scale bars 2.5mm (top) and 50µm (bottom) , n=7 for *Rb1^{FL/FL} Tp53^{FL/FL} Nemo^{FL/FL}*, n=13 for *Rb1^{FL/FL} Tp53^{FL/FL}*). (D) Representative images of lung sections from mice at the humane endpoint immunostained for CD45 and graph showing quantification of infiltrating CD45 positive cells (Scale bars = 100µm (top) and 25µm (bottom), n=8 for *Rb1^{FL/FL} Tp53^{FL/FL} Nemo^{FL/FL}*, n=13 for *Rb1^{FL/FL} Tp53^{FL/FL}*). (E-F) Principal component analysis (PCA) I and Volcano plot (F) of RNA seq data from tumor tissues of *Rb1^{FL/FL} Tp53^{FL/FL} Nemo^{FL/FL}* (n=5) compared to *Rb1^{FL/FL} Tp53^{FL/FL}* (n=6) mice. Genes that were found significantly upregulated ($p < 0.01$, $\log_2(|FC|) > 2$) or downregulated ($p < 0.01$, $\log_2(|FC|) < 2$) in tumors from *Rb1^{FL/FL} Tp53^{FL/FL} Nemo^{FL/FL}* compared to *Rb1^{FL/FL} Tp53^{FL/FL}* mice are indicated with red or blue dots, respectively. (G) Representative immunoblot analysis of protein extracts from SCLC cell lines isolated from *Rb1^{FL/FL} Tp53^{FL/FL}* and *Rb1^{FL/FL} Tp53^{FL/FL} Nemo^{FL/FL}* mice at the humane endpoint (n=4).

To assess whether tumors developing in Ad-Cre-inhaled *Rb1^{FL/FL} Tp53^{FL/FL} Nemo^{FL/FL}* mice have lost the expression of NEMO, we isolated SCLC cell lines from the lungs of mice sacrificed at the humane endpoint and analyzed NEMO protein expression by immunoblotting. Surprisingly, we found that NEMO was expressed in all tumor cell lines isolated from *Rb1^{FL/FL} Tp53^{FL/FL} Nemo^{FL/FL}* mice, with only one out of four cell lines showing reduced levels of NEMO protein compared to cell lines from *Rb1^{FL/FL} Tp53^{FL/FL}* mice (Figure 2G). Therefore, tumors developing in *Rb1^{FL/FL} Tp53^{FL/FL} Nemo^{FL/FL}* mice express NEMO, suggesting that they are derived from cells that recombined the *Rb1^{FL/FL}* and *Tp53^{FL/FL}* alleles, thus losing expression of both tumor suppressors, but failed to undergo recombination of the *Nemo^{FL}* alleles. These findings indicate that tumor development in *Rb1^{FL/FL} Tp53^{FL/FL} Nemo^{FL/FL}* mice appears to be driven by the selection of clones that have escaped NEMO deletion, which could also contribute to the kinetics observed with a strong delay in tumor onset and progression. Taken together, these results revealed an essential role of NEMO in SCLC.

Lack of RelA delays tumor onset and prolongs mouse survival in SCLC

NEMO is essential for canonical NF-κB activation but has also important, NF-κB-independent functions in preventing cell death^{31, 48}. Thus, to specifically address the role of NF-κB, we chose to target RelA, the NF-κB subunit that is critical for canonical NF-κB-mediated gene transcription induction^{16, 18}, in addition to NEMO. To this end, we generated *Rb1^{FL/FL} Tp53^{FL/FL} RelA^{FL/FL}* mice and assessed SCLC development induced by inhalation of Ad-Cre. Assessment of lung tumor presence by MRI revealed that *Rb1^{FL/FL} Tp53^{FL/FL} RelA^{FL/FL}* mice showed considerably delayed tumor development with a median tumor onset of 28 weeks compared to 24 weeks in *Rb1^{FL/FL} Tp53^{FL/FL}* mice (Figure 3A, B). Quantification of tumor lesions at 26 weeks after Ad-Cre inhalation revealed that *Rb1^{FL/FL} Tp53^{FL/FL} RelA^{FL/FL}* mice showed a trend towards reduced tumor presence compared to *Rb1^{FL/FL} Tp53^{FL/FL}* mice, which however did not reach statistical significance (Figure 3C). Moreover, longitudinal measurement of tumor volume by MRI did not reveal statistically significant changes between the two groups,

although $Rb1^{FL/FL} Tp53^{FL/FL} Rela^{FL/FL}$ mice showed a trend towards reduced tumor growth compared to $Rb1^{FL/FL} Tp53^{FL/FL}$ mice (Figure 3D). In line with delayed tumor onset and reduced tumor growth, $Rb1^{FL/FL} Tp53^{FL/FL} Rela^{FL/FL}$ mice showed significantly increased overall survival with a median survival of 311 days compared to $Rb1^{FL/FL} Tp53^{FL/FL}$ mice that had a median survival of 247 days (Figure 3E).

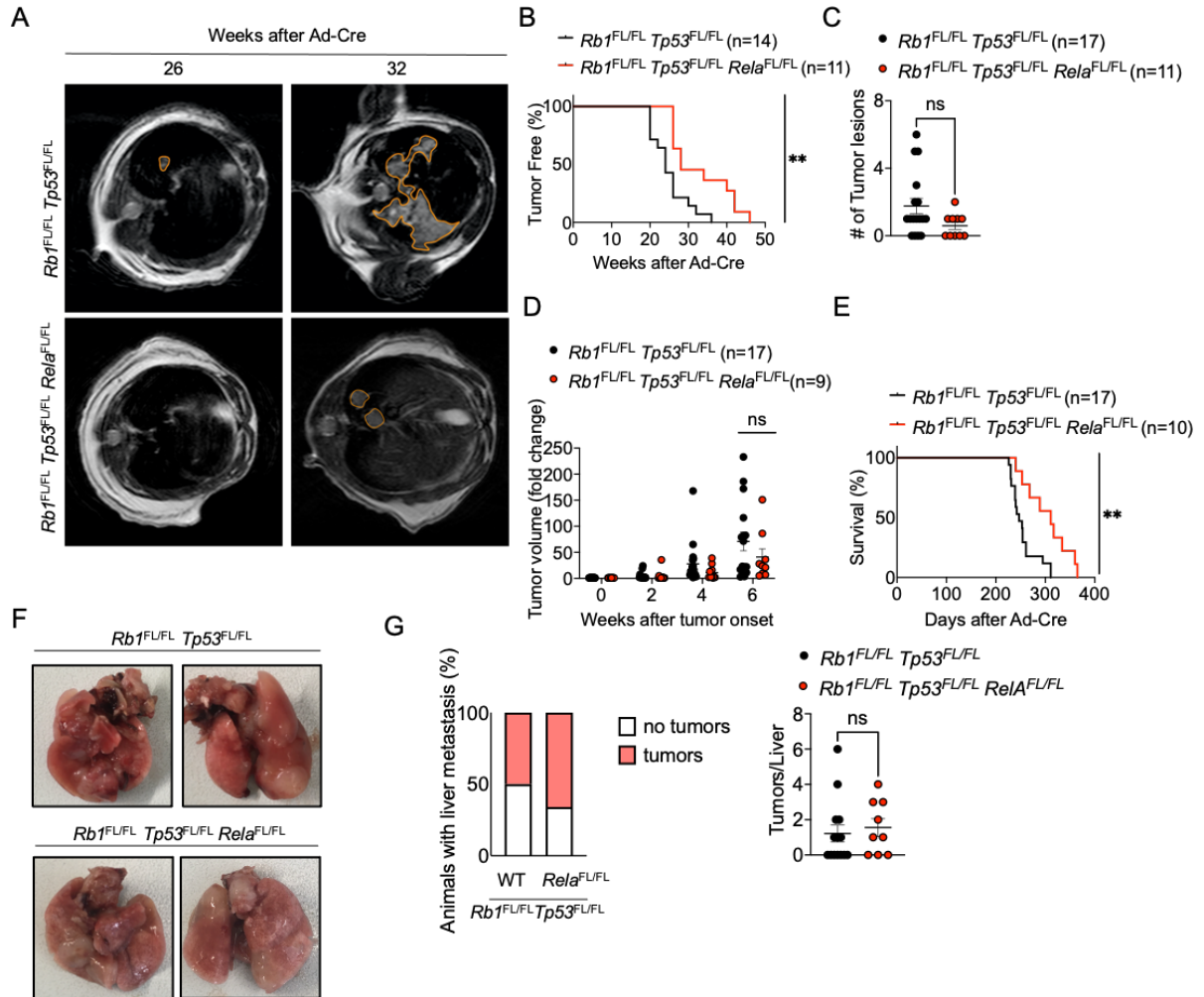


Figure 3. RelA deficiency delays tumor onset and prolongs survival in SCLC. (A) Representative images of MRI scans of $Rb1^{FL/FL} Tp53^{FL/FL}$ (n=17) and $Rb1^{FL/FL} Tp53^{FL/FL} Rela^{FL/FL}$ (n=11) mice 26 and 32 weeks after Ad-Cre inhalation. Tumor areas were marked using Horos Software. (B) Graph depicting tumor onset assessed via MR imaging of $Rb1^{FL/FL} Tp53^{FL/FL}$ and $Rb1^{FL/FL} Tp53^{FL/FL} Rela^{FL/FL}$ mice. **p < 0.005, Log-rank test. (C) Graph depicting the number of lung tumor lesions 6 weeks after Ad-Cre inhalation. Each dot represents one mouse. Mean \pm SEM are shown. Mann-Whitney Test (D) Graph depicting tumor fold change assessed via MR imaging 2-6 weeks after Ad-Cre inhalation for $Rb1^{FL/FL} Tp53^{FL/FL}$ and $Rb1^{FL/FL} Tp53^{FL/FL} Rela^{FL/FL}$ mice. Each dot represents one mouse. Bars represent mean \pm SEM. Mann-Whitney Test. (E) Graph depicting survival of mice with indicated genotypes. **p < 0.005, Log-rank test. Data from the same $Rb1^{FL/FL} Tp53^{FL/FL}$ cohort are included in all figures for comparison. (F) Representative photographs of lungs from $Rb1^{FL/FL} Tp53^{FL/FL}$ (n=17) and $Rb1^{FL/FL} Tp53^{FL/FL} Rela^{FL/FL}$ (n=10) mice sacrificed at the humane endpoint. (G) Graphs depicting the percentage of mice with liver metastasis and the amount of liver tumor lesions at the humane endpoint. N= 9 for $Rb1^{FL/FL} Tp53^{FL/FL}$, n=17 for $Rb1^{FL/FL} Tp53^{FL/FL} Rela^{FL/FL}$. Mann Whitney test, mean \pm SEM.

Macroscopic examination of lung tissues dissected from mice sacrificed at the humane endpoint revealed similar tumor load in *Rb1^{FL/FL} Tp53^{FL/FL} RelA^{FL/FL}* compared to *Rb1^{FL/FL} Tp53^{FL/FL}* mice (Figure 3F). In addition to the lung tumors, SCLC metastasis to the liver was also detected in about half of the mice with no significant difference in metastatic prevalence between the genotypes (Figure 3G). Histopathological analysis of lung sections revealed no difference in tumor morphology, proliferation and immune cell infiltration between *Rb1^{FL/FL} Tp53^{FL/FL} RelA^{FL/FL}* compared to *Rb1^{FL/FL} Tp53^{FL/FL}* mice (Figure 4A-D). RNAseq analysis also failed to reveal considerable gene expression changes, with only 12 genes significantly upregulated and 9 genes significantly downregulated in tumors from *Rb1^{FL/FL} Tp53^{FL/FL} RelA^{FL/FL}* compared to *Rb1^{FL/FL} Tp53^{FL/FL}* mice (Figure 4E, F). Therefore, analysis of tumors at the time of humane sacrifice did not reveal differences in tumor size, proliferation or immune cell infiltration between *Rb1^{FL/FL} Tp53^{FL/FL} RelA^{FL/FL}* and *Rb1^{FL/FL} Tp53^{FL/FL}* mice.

Immunoblot analysis of tumor cell lines isolated from *Rb1^{FL/FL} Tp53^{FL/FL} RelA^{FL/FL}* animals showed lack of RelA expression in all samples analyzed (n=3, Figure 4G), demonstrating that RelA was efficiently deleted in the tumors from these mice. Therefore, in contrast to NEMO that appears to be essential for SCLC, RelA promotes tumor initiation and growth but is not necessary for SCLC development. Collectively, these results showed that inhibition of NF-κB signaling by RelA ablation delayed tumor onset and prolonged mouse survival, revealing a tumor-promoting role of NF-κB in SCLC.

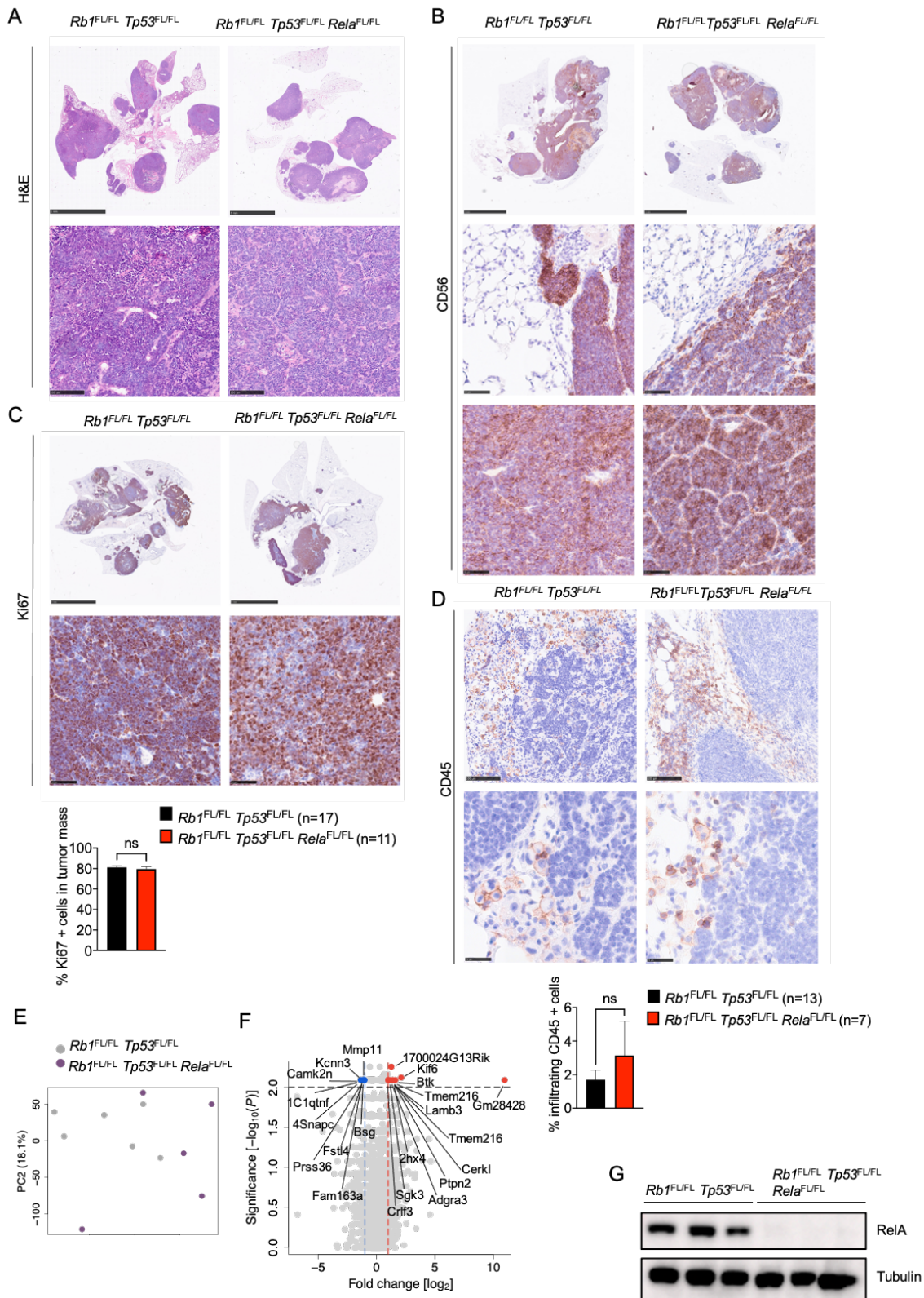


Figure 4. Histological and molecular analysis of lung tumors in *Rb1^{FL/FL} Tp53^{FL/FL} Rela^{FL/FL}* mice. (A) Representative images of lung sections from mice with indicated genotypes at the humane endpoint stained with H&E (Scale bars = 5mm (top) and 100µm (bottom)) (B) Representative images of lung sections from mice with indicated genotypes at the humane endpoint immunostained for CD56 (Scale bars = 5mm (top) and 50µm (bottom) , n=9 for *Rb1^{FL/FL} Tp53^{FL/FL} Rela^{FL/FL}*, n=11 for *Rb1^{FL/FL} Tp53^{FL/FL}*) (C) Representative images of lung sections from mice with indicated genotypes at the humane endpoint immunostained for Ki67 and graph depicting quantification of Ki67 positive cells (Scale bars 5mm(top) & 50µm (bottom, n=7 for *Rb1^{FL/FL} Tp53^{FL/FL} Rela^{FL/FL}*, n=13 for *Rb1^{FL/FL} Tp53^{FL/FL}*). (D) Representative

images of lung sections from mice at the humane endpoint immunostained for CD45. Scale bars = 5mm (top) and 25µm (bottom) and graph showing the amount of CD45 positive cells (n=7 for *Rb1^{FL/FL} Tp53^{FL/FL} RelA^{FL/FL}*, n=13 for *Rb1^{FL/FL} Tp53^{FL/FL}*). **(E-F)** Principal component analysis (PCA) I and Volcano plot **(F)** of RNA seq data from tumor tissues of *Rb1^{FL/FL} Tp53^{FL/FL} RelA^{FL/FL}* (n=5) compared to *Rb1^{FL/FL} Tp53^{FL/FL}* (n=6) mice. Genes that were found significantly upregulated ($p < 0.01$, $\log_2(|FC|) > 2$) or downregulated ($p < 0.01$, $\log_2(|FC|) < 2$) in tumors from *Rb1^{FL/FL} Tp53^{FL/FL} RelA^{FL/FL}* (n=5) compared to *Rb1^{FL/FL} Tp53^{FL/FL}* (n=6) mice are indicated with red or blue dots, respectively. **(G)** Representative immunoblot analysis of protein extracts from SCLC cell lines isolated from *Rb1^{FL/FL} Tp53^{FL/FL}* and *Rb1^{FL/FL} Tp53^{FL/FL} RelA^{FL/FL}* mice at the humane endpoint (n=3). Data from the same *Rb1^{FL/FL} Tp53^{FL/FL}* cohort are included in all figures for comparison.

Constitutive NF-κB signaling does not affect SCLC development

Our studies described above showed that inhibition of IKK/NF-κB signaling considerably delayed the onset and progression of SCLC. As a complementary approach, we aimed to assess how constitutively increased activation of IKK/NF-κB signaling might affect SCLC development. For this reason, we employed a mouse model allowing the Cre-mediated expression of a constitutively active IKK2 (IKK2ca) transgene from the ubiquitously expressed Rosa26 locus (*R26^{LSL.IKK2ca}* mice)⁴⁰. We therefore generated *Rb1^{FL/FL} Tp53^{FL/FL} R26^{LSL.IKK2ca}* mice and induced SCLC development by inhalation of Ad-Cre as described above. Based on our findings that NEMO but also RelA ablation delayed tumor development, we hypothesized that persistently elevated NF-κB activation might accelerate and aggravate SCLC. Surprisingly however, MRI-assisted assessment of lung tumor load did not reveal considerable differences in tumor onset or growth between *Rb1^{FL/FL} Tp53^{FL/FL} R26^{LSL.IKK2ca}* and *Rb1^{FL/FL} Tp53^{FL/FL}* mice (Figure 5A-D). Consistently, *Rb1^{FL/FL} Tp53^{FL/FL} R26^{LSL.IKK2ca}* mice showed similar overall survival compared to *Rb1^{FL/FL} Tp53^{FL/FL}* animals (Figure 5E).

Macroscopic examination of dissected lungs from mice sacrificed at the humane endpoint of the experimental protocol revealed similar tumor load in *Rb1^{FL/FL} Tp53^{FL/FL} R26^{LSL.IKK2ca}* and *Rb1^{FL/FL} Tp53^{FL/FL}* mice (Figure 5F). Examination of livers from these mice revealed metastasis to this tissue in 2 out of 9 *Rb1^{FL/FL} Tp53^{FL/FL} R26^{LSL.IKK2ca}* mice compared to 7 out 14 *Rb1^{FL/FL} Tp53^{FL/FL}* mice, suggesting that expression of IKK2ca could negatively affect the metastatic potential of SCLC (Figure 5G). Moreover, immunohistochemical examination of lung tissues revealed similar tumor burden and morphology in the two genotypes (Figure 6A-B). Immunostaining for Ki-67 showed similar numbers of proliferating tumor cells in *Rb1^{FL/FL} Tp53^{FL/FL} R26^{LSL.IKK2ca}* compared to *Rb1^{FL/FL} Tp53^{FL/FL}* mice (Figure 6C). Furthermore, immunostaining for CD45 revealed no differences in immune cell infiltration in *Rb1^{FL/FL} Tp53^{FL/FL} R26^{LSL.IKK2ca}* compared to *Rb1^{FL/FL} Tp53^{FL/FL}* mice, with immune cells surrounding the lesions but generally not found within the tumor mass (Figure 6D).

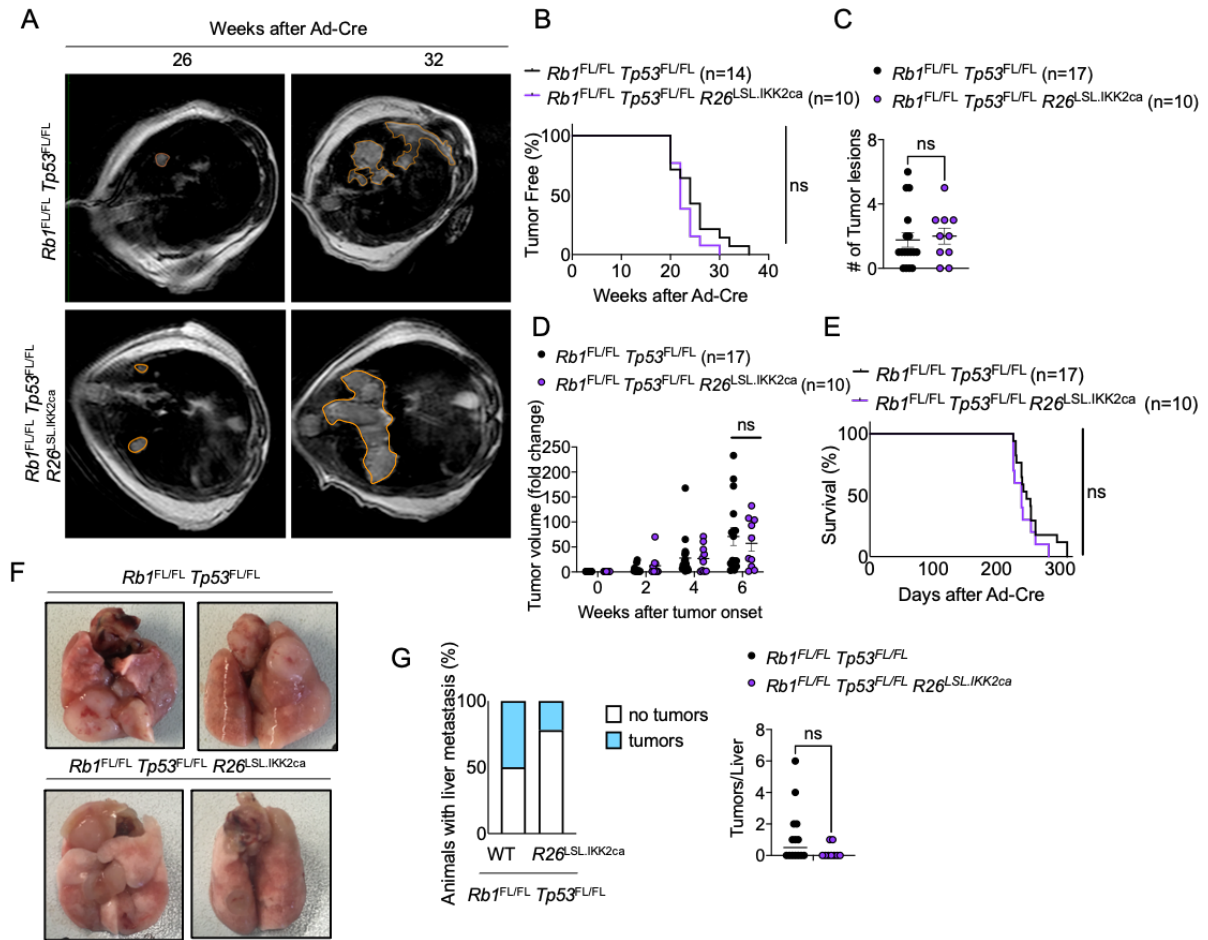


Figure 5. Constitutively increased NF- κ B activation did not affect the onset and progression of SCLC. (A) Representative images of MRI scans of *Rb1^{FL/FL} Tp53^{FL/FL}* (n=17) and *Rb1^{FL/FL} Tp53^{FL/FL} R26^{LSL.IKK2ca}* (n= 10) mice 26 and 32 weeks after Ad-Cre inhalation. Tumor areas are marked. (B) Graph depicting tumor onset assessed via MR imaging of mice with indicated genotypes. (C) Graph depicting the number of lung tumor lesions 6 weeks after Ad-Cre inhalation. Each dot represents one mouse. Mean \pm SEM are shown. Mann-Whitney Test. (D) Graph depicting tumor fold change assessed via MR imaging 2-6 weeks after Ad-Cre inhalation for indicated genotypes. Every dot represents one mouse. Bars represent mean \pm SEM. Mann-Whitney Test. (E) Graph depicting survival of *Rb1^{FL/FL} Tp53^{FL/FL}* and *Rb1^{FL/FL} Tp53^{FL/FL} R26^{LSL.IKK2ca}* mice. Data from the same *Rb1^{FL/FL} Tp53^{FL/FL}* cohort are included in all figures for comparison. (F) Representative photographs of lungs from *Rb1^{FL/FL} Tp53^{FL/FL}* (n=17) and *Rb1^{FL/FL} Tp53^{FL/FL} R26^{LSL.IKK2ca}* (n=10) mice sacrificed at the humane endpoint. (G) Graphs depicting the percentage of mice with liver metastasis and the amount of liver tumor lesions at the humane endpoint n=9 for *Rb1^{FL/FL} Tp53^{FL/FL} R26^{LSL.IKK2ca}*, n=14 for *Rb1^{FL/FL} Tp53^{FL/FL}*. Mann-Whitney test, mean \pm SEM.

RNAseq analysis revealed considerable changes in gene expression in tumors expressing IKK2ca (Figures 6E-G). Specifically, we found that 152 genes were significantly upregulated in tumors from *Rb1^{FL/FL} Tp53^{FL/FL} R26^{LSL.IKK2ca}* mice compared to *Rb1^{FL/FL} Tp53^{FL/FL}* mice, with genes described under the hallmarks “INFLAMMATORY RESPONSE” and “TNFA_SIGNALING_VIA_NFKB” being significantly enriched within the upregulated gene set (Figures 6E-G). Thus, IKK2ca expression induced the transcriptional upregulation of NF- κ B dependent inflammatory genes in SCLC. It is intriguing that the increased expression of inflammatory genes did not enhance immune cell infiltration into the tumors in *Rb1^{FL/FL}*

Tp53^{FL/FL} *R26*^{LSL.IKK2ca} compared to *Rb1*^{FL/FL} *Tp53*^{FL/FL} mice (Figure 6D). Consistent with the elevated expression of NF-κB target genes, immunoblot analysis of IKK2 protein levels revealed strongly increased IKK2ca expression in SCLC tissue isolated from the lungs of *Rb1*^{FL/FL} *Tp53*^{FL/FL} *R26*^{LSL.IKK2ca} mice (Figure 6H). Taken together, these results showed that IKK2ca expression caused persistent activation of NF-κB and the transcriptional upregulation of NF-κB target genes. However, this elevated NF-κB activity did not considerably impact on tumor initiation, growth and progression and did not alter the tumor immune landscape in this mouse model of SCLC.

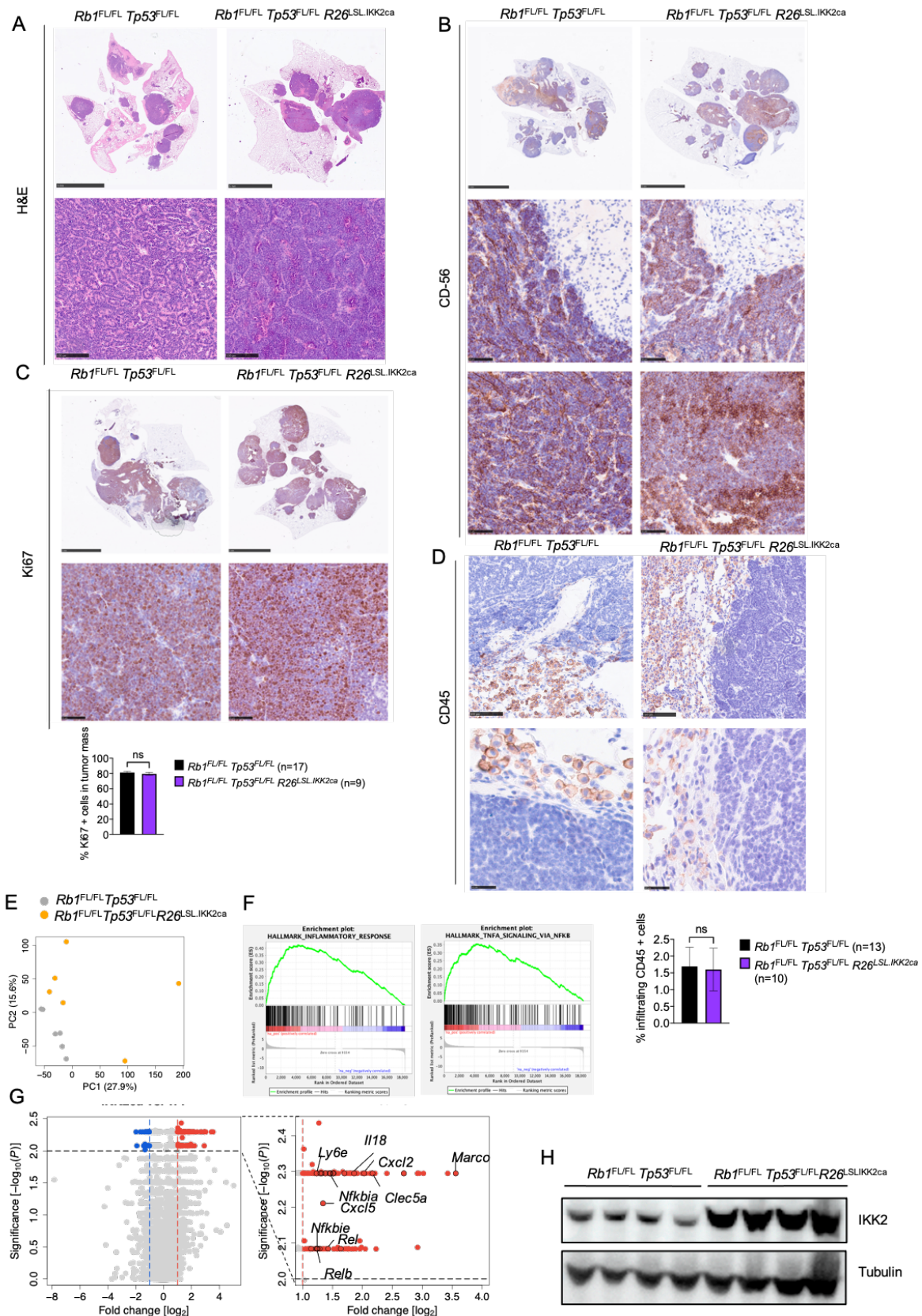


Figure 6. IKK2ca expression increased inflammatory gene transcription but did not alter the morphology or immune cell infiltration of SCLC. (A) Representative images of lung sections from mice stained with H&E. (Scale bars = 5mm (top) and 100µm (bottom)). Samples were taken at the humane endpoint **(B)** Representative images of lung sections from mice of the indicated genotypes at the humane endpoint immunostained for CD56. (Scale bars 5mm (top) and 50µm (bottom), n=8 for *Rb1^{FL/FL} Tp53^{FL/FL} R26^{LSL.IKK2ca}*, n=11 for *Rb1^{FL/FL} Tp53^{FL/FL}*) **(C)** Representative images of lung sections

from mice of the indicated genotypes at the humane endpoint immunostained for Ki67 and graph showing quantifications of Ki67 positive cells. (Scale bars 5mm (top) and 50µm (bottom), n=10 for *Rb1^{FL/FL} Tp53^{FL/FL} R26^{LSL.IKK2ca}*, n=13 for *Rb1^{FL/FL} Tp53^{FL/FL}*). (D) Representative images of lung sections from *Rb1^{FL/FL} Tp53^{FL/FL} R26^{LSL.IKK2ca}* (n=10) and *Rb1^{FL/FL} Tp53^{FL/FL}* (n=13) mice at the humane endpoint immunostained for CD45 and graph depicting the amount of CD45 positive cells. Scale bars = 100µm (top) and 25µm (bottom). (E-G) Graphs depicting PCA I, Gene set enrichment analysis (F) and Volcano plot (G) of RNA seq data from tumor tissues of *Rb1^{FL/FL} Tp53^{FL/FL} R26^{LSL.IKK2ca}* (n=6) compared to *Rb1^{FL/FL} Tp53^{FL/FL}* (n=6) mice. In (G), genes that were found significantly upregulated ($p < 0.01$, $\log_2(|FC|) > 2$) or downregulated ($p < 0.01$, $\log_2(|FC|) < 2$) in tumors from *Rb1^{FL/FL} Tp53^{FL/FL} R26^{LSL.IKK2ca}* compared to *Rb1^{FL/FL} Tp53^{FL/FL}* mice are indicated with red or blue dots, respectively. (H) Representative immunoblot analysis with the indicated antibodies of protein extracts from tumor tissue derived from RP-mice with indicated genotypes at the humane endpoint. Data from the same *Rb1^{FL/FL} Tp53^{FL/FL}* cohort are included in all figures for comparison.

SCLC development is independent of TNFR1 signaling

TNF signaling via TNFR1 has important functions in tumorigenesis^{12, 49}. However, the role of TNFR1 in SCLC has not been studied and remains unknown. Here, we aimed to address whether TNFR1 signaling contributes to SCLC development using two distinct approaches. On the one hand, we employed TNFR1-deficient (*Tnfr1^{-/-}*) mice to assess the role of TNFR1 in both the tumor cells and the cells of the microenvironment. In parallel, we used *Tnfr1^{FL/FL}* mice allowing to assess the tumor cell-intrinsic role of TNFR1. Specifically, we generated *Rb1^{FL/FL} Tp53^{FL/FL} Tnfr1^{-/-}* and *Rb1^{FL/FL} Tp53^{FL/FL} Tnfr1^{FL/FL}* mice and examined SCLC development after inhalation with Ad-Cre. MRI-assisted assessment of lung tumors revealed that neither tumor cell intrinsic nor systemic TNFR1 deficiency considerably affected the onset and growth of SCLC (Figure 7A-D). Moreover, *Rb1^{FL/FL} Tp53^{FL/FL} Tnfr1^{-/-}* and *Rb1^{FL/FL} Tp53^{FL/FL} Tnfr1^{FL/FL}* mice showed similar overall survival compared to *Rb1^{FL/FL} Tp53^{FL/FL}* animals (Figure 7E). Therefore, TNFR1 deficiency did not considerably affect tumor initiation, progression and overall survival in SCLC.

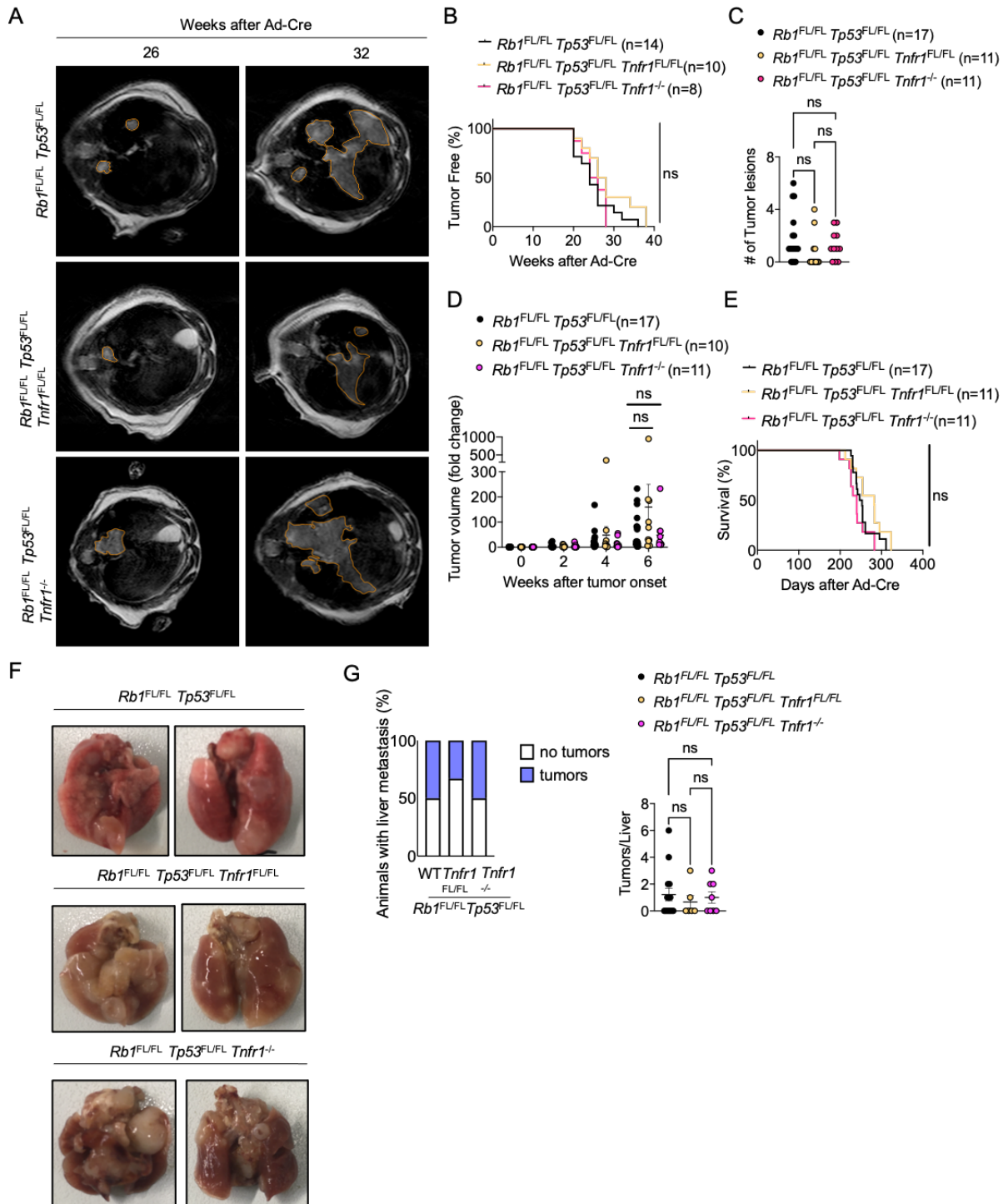


Figure 7. TNFR1 deficiency did not alter SCLC onset or progression. (A) Representative images of MRI scans of *Rb1^{FL/FL} Tp53^{FL/FL}* (n=17), *Rb1^{FL/FL} Tp53^{FL/FL} Tnfr1^{FL/FL}* (n=10) and *Rb1^{FL/FL} Tp53^{FL/FL} Tnfr1^{-/-}* (n=11) mice 26 and 32 weeks after Ad-Cre inhalation. Tumor areas are marked. (B) Graph depicting tumor onset assessed via MR imaging of mice with indicated genotypes. (C) Graph depicting the number of lung tumor lesions 6 weeks after Ad-Cre inhalation. Each dot represents one mouse. Mean \pm SEM are shown. Mann-Whitney Test. (D) Graph depicting tumor fold change assessed via MR imaging 2-6 weeks after AdenoCre inhalation for indicated genotypes. Every dot represents one mouse. Bars represent mean \pm SEM. Mann-Whitney Test. (E) Graph depicting survival of *Rb1^{FL/FL} Tp53^{FL/FL}*, *Rb1^{FL/FL} Tp53^{FL/FL} Tnfr1^{FL/FL}* and *Rb1^{FL/FL} Tp53^{FL/FL} Tnfr1^{-/-}* mice. Data from the same *Rb1^{FL/FL} Tp53^{FL/FL}* cohort are included in all figures for comparison. (F) Photographs of lungs of *Rb1^{FL/FL} Tp53^{FL/FL}* (n=17), *Rb1^{FL/FL} Tp53^{FL/FL} Tnfr1^{FL/FL}* (n=11) and *Rb1^{FL/FL} Tp53^{FL/FL} Tnfr1^{-/-}* (n=11) mice at the humane endpoint. (G) Graphs depicting the percentage of mice with liver metastasis and the amount of liver tumor lesions at

the humane endpoint $n=6$ for $Rb1^{FL/FL} Tp53^{FL/FL} Tnfr1^{FL/FL}$, $n=8$ for $Rb1^{FL/FL} Tp53^{FL/FL} Tnfr1^{-/-}$, $n=14$ for $Rb1^{FL/FL} Tp53^{FL/FL}$. Kruskal-Wallis test.

Macroscopic examination of lungs from mice sacrificed at the humane endpoint revealed a similar tumor burden in $Rb1^{FL/FL} Tp53^{FL/FL} Tnfr1^{-/-}$ and $Rb1^{FL/FL} Tp53^{FL/FL} Tnfr1^{FL/FL}$ mice compared to $Rb1^{FL/FL} Tp53^{FL/FL}$ animals (Figure 7F). In addition to the lung tumors, SCLC metastasis to the liver was also detected in several mice with no difference in metastatic prevalence between the genotypes (Figure 7G). Immunohistochemical analysis of lung sections revealed that neither tumor-intrinsic nor ubiquitous lack of TNFR1 could alter tumor morphology and proliferation (Figure 8A-C). Moreover, immunostaining for CD45 failed to reveal differences in immune cell infiltration between the three genotypes, arguing that inhibition of TNFR1 signaling did not change the immune landscape of SCLC (Figure 8D). Similarly, RNAseq analysis of gene expression in tumors dissected at the humane endpoint did not reveal considerably changed transcription profiles between $Rb1^{FL/FL} Tp53^{FL/FL} Tnfr1^{-/-}$ or $Rb1^{FL/FL} Tp53^{FL/FL} Tnfr1^{FL/FL}$ and $Rb1^{FL/FL} Tp53^{FL/FL}$ mice (Figure 8E, F). Taken together, our results revealed that TNFR1 deficiency, either cell intrinsic or systemic, did not considerably alter SCLC development, arguing that TNFR1 does not play an important role in this type of cancer.

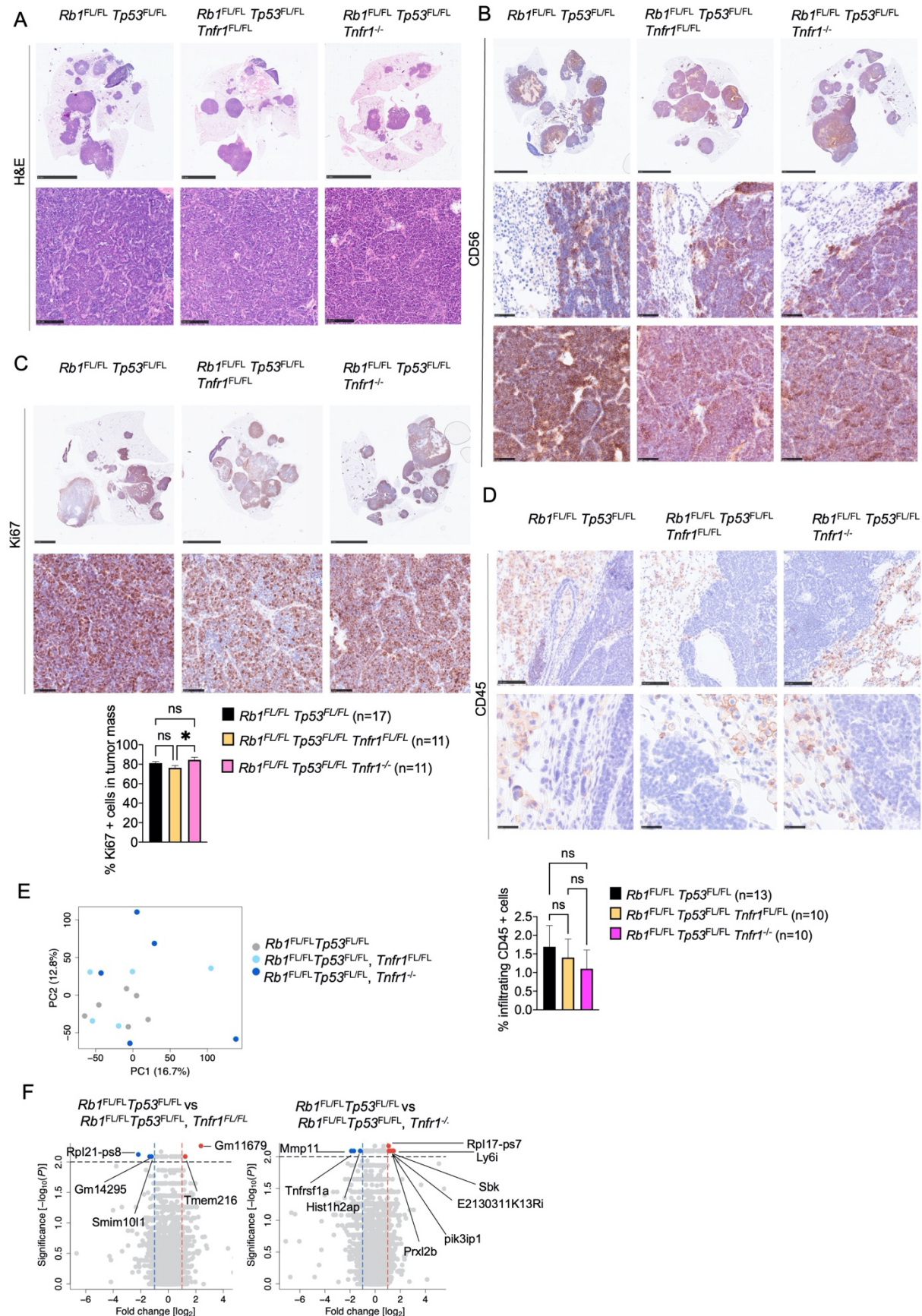


Figure 8. TNFR1 deficiency did not alter SCLC morphology and immune cell infiltration. (A) Representative images of lung sections from mice at the humane endpoint stained with H&E (Scale bars= 5 mm (top) and 100µm (bottom)) (B) or immunostained for CD56 (Scale bars 5mm (top) and 50µm (bottom), n=5 for *Rb1*^{FL/FL} *Tp53*^{FL/FL} *Tnfr1*^{FL/FL}, n=8 for *Rb1*^{FL/FL} *Tp53*^{FL/FL} *Tnfr1*^{-/-}, n=11 for *Rb1*^{FL/FL}

Tp53^{FL/FL} (C) Representative images of lung sections from mice at the humane endpoint immunostained for Ki67 and graph depicting Ki67 positive cells (Scale bars 2.5 & 5mm (top) and 50µm (bottom), n=10 for *Rb1^{FL/FL} Tp53^{FL/FL} Tnfr1^{FL/FL}*, n=10 for *Rb1^{FL/FL} Tp53^{FL/FL} Tnfr1^{-/-}*; n=13 for *Rb1^{FL/FL} Tp53^{FL/FL}*). (D) Representative images of lung sections immunostained for CD45. Scale bars = 100µm (top) and 25µm (bottom). Samples were taken at the humane endpoint (n=10 for *Rb1^{FL/FL} Tp53^{FL/FL} Tnfr1^{FL/FL}*, n=10 for *Rb1^{FL/FL} Tp53^{FL/FL} Tnfr1^{-/-}*, n=13 for *Rb1^{FL/FL} Tp53^{FL/FL}*). (E-F) PCA I and Volcano plot (F) of RNA seq data from tumor tissues of *Rb1^{FL/FL} Tp53^{FL/FL} Tnfr1^{FL/FL}* (n=5) and *Rb1^{FL/FL} Tp53^{FL/FL} Tnfr1^{-/-}* (n=5) mice compared to tumors from *Rb1^{FL/FL} Tp53^{FL/FL}* (n=6) mice. Genes that were found significantly upregulated ($p < 0.01$, $\log_2(|FC|) > 2$) or downregulated ($p < 0.01$, $\log_2(|FC|) < 2$) in these comparisons are indicated with red or blue dots, respectively. Data from the same *Rb1^{FL/FL} Tp53^{FL/FL}* cohort are included in all figures for comparison.

Discussion

Despite the progress made in the treatment of different cancer entities during the last decade, SCLC remains a type of cancer with very limited therapeutic options and exceptionally poor prognosis¹. Whereas the introduction of immunotherapies had some beneficial effects in patients with SCLC, these were limited to a small fraction (about 15%) of the patients¹. Therefore, new therapeutic targets for SCLC are urgently needed. Here, we have addressed the role of TNFR1 and NF-κB signaling in development and progression of SCLC in a well-established and relevant mouse model of the disease. Our results revealed a critical role of IKK/NF-κB signaling in the development of SCLC. Ablation of NEMO or RelA significantly delayed tumor onset, slowed tumor growth and considerably prolonged survival in mice with SCLC induced by combined inactivation of RB1 and TP53. Whereas both *Rb1^{FL/FL} Tp53^{FL/FL} Nemo^{FL/FL}* and *Rb1^{FL/FL} Tp53^{FL/FL} RelA^{FL/FL}* mice eventually developed tumors and succumbed to the disease, they reached the humane endpoint considerably later (about 3 and 2 months respectively) compared to the *Rb1^{FL/FL} Tp53^{FL/FL}* mice. Immunohistological analysis of tumors isolated from mice at the humane endpoint did not reveal differences between control *Rb1^{FL/FL} Tp53^{FL/FL}* and *Rb1^{FL/FL} Tp53^{FL/FL} Nemo^{FL/FL}* or *Rb1^{FL/FL} Tp53^{FL/FL} RelA^{FL/FL}* mice. Interestingly, we found that SCLC cell lines isolated from *Rb1^{FL/FL} Tp53^{FL/FL} Nemo^{FL/FL}* mice sacrificed at the humane endpoint displayed expression of NEMO, showing that these were derived from cells that failed to recombine the NEMO floxed allele. Considering the critical pro-survival function of NEMO, these results suggest that NEMO deficiency causes the death of transformed cells early on resulting in strong counter-selection of these cells, with the tumors eventually developing in these animals arising from rare cells that underwent Cre-mediated recombination of the *Rb1^{FL/FL} Tp53^{FL/FL}* but not of the *Nemo^{FL/FL}* alleles. NEMO exhibits both NF-κB-dependent and NF-κB-independent pro-survival functions^{31, 48}. Our findings that RelA ablation delayed the onset and growth of SCLC resulting in considerably prolonged mouse survival provided experimental evidence that RelA-dependent NF-κB-dependent gene transcription also plays an important role in SCLC. RelA deficiency had a less pronounced effect compared to loss of NEMO, suggesting that NEMO ablation suppresses SCLC development by both NF-κB-

dependent and -independent mechanisms. Importantly, analysis of SCLC cell lines isolated from lungs of Ad-Cre-inhaled *Rb1^{FL/FL} Tp53^{FL/FL} RelA^{FL/FL}* mice sacrificed at the humane endpoint revealed efficient ablation of RelA, showing that RelA-deficient cells can give rise to SCLC, in contrast to loss of NEMO that appears to be incompatible with SCLC development. Together, these studies suggest a dual function of the IKK/NF- κ B signaling pathway in SCLC. Complete inhibition of canonical IKK/NF- κ B signaling by NEMO deficiency prevented the development of SCLC, most likely by sensitizing RB1-TP53 double-deficient cells to death, whereas RelA knockout had a less pronounced effect in delaying tumor development and progression.

Interestingly, expression of constitutively active IKK2ca did not exacerbate SCLC development, showing that persistently elevated IKK/NF- κ B activity by did not provide an advantage to the tumors. Surprisingly, despite the upregulation of inflammatory gene expression, *Rb1^{FL/FL} Tp53^{FL/FL} R26^{LSL.IKK2ca}* mice did not show increased infiltration of immune cells within the tumor mass. Surprisingly, we found that TNFR1 deficiency, either tumor cell-intrinsic or systemic, did not affect SCLC development, in contrast to the important role of TNF signaling in other types of cancer^{12, 49}. This finding suggests that, at least in this specific mouse model driven by acute inactivation of the two important tumor suppressors RB1 and TP53, TNF-mediated inflammatory and cell death signaling is not critically involved. It should be noted however, that these findings do not exclude a role of TNF in human patients with SCLC associated with comorbidities such as chronic obstructive pulmonary disease, where lung inflammation may contribute to tumor progression. In light of our findings that NF- κ B inhibition considerably delayed SCLC development, these results also indicate that TNFR1-independent pathways drive activation of NF- κ B to promote SCLC. Although at this stage the upstream mediators inducing NF- κ B in this context remain elusive, several pathways have been implicated in driving tumor-promoting NF- κ B activity in cancer, such as other members of the TNF receptor superfamily, growth factor receptors, replicative stress and DNA damage⁵⁰. Taken together, our results revealed a tumor-promoting role of IKK/NF- κ B signaling in SCLC, in line with previous studies showing that NF- κ B critically contributes to *Kras* mutation-driven lung adenocarcinoma^{25, 26, 27}. These findings suggest that IKK/NF- κ B signaling could provide a promising therapeutic target in SCLC and warrant further studies experimentally assessing the effect of NF- κ B pathway inhibition on established SCLC.

Acknowledgements

We thank A. Florin, F. Schneider, J. Kuth, C. Uthoff-Hachenberg, E. Stade and E. Gareus for excellent technical assistance, as well as C.M. Bebbber, A. Androulidaki and H. Schuenke for help with the *Rb1^{FL/FL} Tp53^{FL/FL}* mouse model. We also thank H. Gröll for support with MRI imaging, H.C. Reinhardt and R. Thomas for valuable discussions and G. Kollias for providing

Tnfr1^{FL/FL} mice. This work was supported by funding from the Deutsche Forschungsgemeinschaft (DFG, German Research Foundation), project SFB1399 (Project No. 413326622), to M. Pasparakis, M. Peifer and R. Buettner, and from the Federal Ministry of Education and Research (BMBF, e:med project InCa, Grant No. 01ZX1901A) to M.Pasparakis.

Author contributions

L.K. designed and performed all experiments, analyzed the data and drafted and revised the manuscript. T.-P.Y. and M. Peifer analyzed RNA sequencing data sets. M.S. and R.B. contributed to the histologic analysis. M. Pasparakis designed and supervised the study and wrote the manuscript together with L.K.

Conflict of interest

R.B. is an employee of Targos Molecular Pathology. The other authors declare no competing interests.

References

1. Rudin CM, Brambilla E, Faivre-Finn C, Sage J. Small-cell lung cancer. *Nat Rev Dis Primers* 2021, **7**(1): 3.
2. Junker K, Wiethage T, Muller KM. Pathology of small-cell lung cancer. *J Cancer Res Clin Oncol* 2000, **126**(7): 361-368.
3. Rom WN, Hay JG, Lee TC, Jiang Y, Tchou-Wong KM. Molecular and genetic aspects of lung cancer. *Am J Respir Crit Care Med* 2000, **161**(4 Pt 1): 1355-1367.
4. Wistuba II, Gazdar AF, Minna JD. Molecular genetics of small cell lung carcinoma. *Semin Oncol* 2001, **28**(2 Suppl 4): 3-13.
5. Sandler AB. Chemotherapy for small cell lung cancer. *Semin Oncol* 2003, **30**(1): 9-25.
6. Harbour JW, Lai SL, Whang-Peng J, Gazdar AF, Minna JD, Kaye FJ. Abnormalities in structure and expression of the human retinoblastoma gene in SCLC. *Science* 1988, **241**(4863): 353-357.
7. George J, Lim JS, Jang SJ, Cun Y, Ozretic L, Kong G, *et al.* Comprehensive genomic profiles of small cell lung cancer. *Nature* 2015, **524**(7563): 47-53.
8. Peifer M, Fernandez-Cuesta L, Sos ML, George J, Seidel D, Kasper LH, *et al.* Integrative genome analyses identify key somatic driver mutations of small-cell lung cancer. *Nat Genet* 2012, **44**(10): 1104-1110.
9. Sekido Y, Fong KM, Minna JD. Molecular genetics of lung cancer. *Annu Rev Med* 2003, **54**: 73-87.
10. Gouyer V, Gazzeri S, Bolon I, Drevet C, Brambilla C, Brambilla E. Mechanism of retinoblastoma gene inactivation in the spectrum of neuroendocrine lung tumors. *Am J Respir Cell Mol Biol* 1998, **18**(2): 188-196.
11. Hanahan D, Weinberg RA. Hallmarks of cancer: the next generation. *Cell* 2011, **144**(5): 646-674.
12. Montfort A, Colacios C, Levade T, Andrieu-Abadie N, Meyer N, Segui B. The TNF Paradox in Cancer Progression and Immunotherapy. *Front Immunol* 2019, **10**: 1818.
13. Moore RJ, Owens DM, Stamp G, Arnott C, Burke F, East N, *et al.* Mice deficient in tumor necrosis factor-alpha are resistant to skin carcinogenesis. *Nat Med* 1999, **5**(7): 828-831.

14. Park EJ, Lee JH, Yu GY, He G, Ali SR, Holzer RG, *et al.* Dietary and genetic obesity promote liver inflammation and tumorigenesis by enhancing IL-6 and TNF expression. *Cell* 2010, **140**(2): 197-208.
15. Varfolomeev E, Vucic D. Intracellular regulation of TNF activity in health and disease. *Cytokine* 2018, **101**: 26-32.
16. Pasparakis M. Regulation of tissue homeostasis by NF-kappaB signalling: implications for inflammatory diseases. *Nat Rev Immunol* 2009, **9**(11): 778-788.
17. Taniguchi K, Karin M. NF-kappaB, inflammation, immunity and cancer: coming of age. *Nat Rev Immunol* 2018, **18**(5): 309-324.
18. Hayden MS, Ghosh S. NF-kappaB, the first quarter-century: remarkable progress and outstanding questions. *Genes Dev* 2012, **26**(3): 203-234.
19. Karin M. Nuclear factor-kappaB in cancer development and progression. *Nature* 2006, **441**(7092): 431-436.
20. Greten FR, Eckmann L, Greten TF, Park JM, Li ZW, Egan LJ, *et al.* IKKbeta links inflammation and tumorigenesis in a mouse model of colitis-associated cancer. *Cell* 2004, **118**(3): 285-296.
21. Pratt MA, Tibbo E, Robertson SJ, Jansson D, Hurst K, Perez-Iratxeta C, *et al.* The canonical NF-kappaB pathway is required for formation of luminal mammary neoplasias and is activated in the mammary progenitor population. *Oncogene* 2009, **28**(30): 2710-2722.
22. Liu M, Sakamaki T, Casimiro MC, Willmarth NE, Quong AA, Ju X, *et al.* The canonical NF-kappaB pathway governs mammary tumorigenesis in transgenic mice and tumor stem cell expansion. *Cancer Res* 2010, **70**(24): 10464-10473.
23. Connelly L, Barham W, Onishko HM, Sherrill T, Chodosh LA, Blackwell TS, *et al.* Inhibition of NF-kappa B activity in mammary epithelium increases tumor latency and decreases tumor burden. *Oncogene* 2011, **30**(12): 1402-1412.
24. Kim C, Pasparakis M. Epidermal p65/NF-kappaB signalling is essential for skin carcinogenesis. *EMBO Mol Med* 2014, **6**(7): 970-983.
25. Xia Y, Yeddula N, Leblanc M, Ke E, Zhang Y, Oldfield E, *et al.* Reduced cell proliferation by IKK2 depletion in a mouse lung-cancer model. *Nat Cell Biol* 2012, **14**(3): 257-265.
26. Basseres DS, Ebbs A, Levantini E, Baldwin AS. Requirement of the NF-kappaB subunit p65/RelA for K-Ras-induced lung tumorigenesis. *Cancer Res* 2010, **70**(9): 3537-3546.
27. Meylan E, Dooley AL, Feldser DM, Shen L, Turk E, Ouyang C, *et al.* Requirement for NF-kappaB signalling in a mouse model of lung adenocarcinoma. *Nature* 2009, **462**(7269): 104-107.
28. Dajee M, Lazarov M, Zhang JY, Cai T, Green CL, Russell AJ, *et al.* NF-kappaB blockade and oncogenic Ras trigger invasive human epidermal neoplasia. *Nature* 2003, **421**(6923): 639-643.
29. van Hogerlinden M, Rozell BL, Ahrlund-Richter L, Toftgard R. Squamous cell carcinomas and increased apoptosis in skin with inhibited Rel/nuclear factor-kappaB signaling. *Cancer Res* 1999, **59**(14): 3299-3303.
30. Lind MH, Rozell B, Wallin RP, van Hogerlinden M, Ljunggren HG, Toftgard R, *et al.* Tumor necrosis factor receptor 1-mediated signaling is required for skin cancer development induced by NF-kappaB inhibition. *Proc Natl Acad Sci U S A* 2004, **101**(14): 4972-4977.
31. Kondylis V, Polykratis A, Ehlken H, Ochoa-Callejero L, Straub BK, Krishna-Subramanian S, *et al.* NEMO Prevents Steatohepatitis and Hepatocellular Carcinoma by Inhibiting RIPK1 Kinase Activity-Mediated Hepatocyte Apoptosis. *Cancer Cell* 2015, **28**(5): 582-598.
32. Luedde T, Beraza N, Kotsikoris V, van Loo G, Nenci A, De Vos R, *et al.* Deletion of NEMO/IKKgamma in liver parenchymal cells causes steatohepatitis and hepatocellular carcinoma. *Cancer Cell* 2007, **11**(2): 119-132.

33. Maeda S, Kamata H, Luo JL, Leffert H, Karin M. IKKbeta couples hepatocyte death to cytokine-driven compensatory proliferation that promotes chemical hepatocarcinogenesis. *Cell* 2005, **121**(7): 977-990.
34. Hopewell EL, Zhao W, Fulp WJ, Bronk CC, Lopez AS, Massengill M, *et al.* Lung tumor NF-kappaB signaling promotes T cell-mediated immune surveillance. *J Clin Invest* 2013, **123**(6): 2509-2522.
35. Meuwissen R, Linn SC, Linnoila RI, Zevenhoven J, Mooi WJ, Berns A. Induction of small cell lung cancer by somatic inactivation of both Trp53 and Rb1 in a conditional mouse model. *Cancer Cell* 2003, **4**(3): 181-189.
36. Vooijs M, van der Valk M, te Riele H, Berns A. Flp-mediated tissue-specific inactivation of the retinoblastoma tumor suppressor gene in the mouse. *Oncogene* 1998, **17**(1): 1-12.
37. Jonkers J, Meuwissen R, van der Gulden H, Peterse H, van der Valk M, Berns A. Synergistic tumor suppressor activity of BRCA2 and p53 in a conditional mouse model for breast cancer. *Nat Genet* 2001, **29**(4): 418-425.
38. Schmidt-Supprian M, Bloch W, Courtois G, Addicks K, Israel A, Rajewsky K, *et al.* NEMO/IKK gamma-deficient mice model incontinentia pigmenti. *Mol Cell* 2000, **5**(6): 981-992.
39. Luedde T, Heinrichsdorff J, de Lorenzi R, De Vos R, Roskams T, Pasparakis M. IKK1 and IKK2 cooperate to maintain bile duct integrity in the liver. *Proc Natl Acad Sci U S A* 2008, **105**(28): 9733-9738.
40. Sasaki Y, Derudder E, Hobeika E, Pelanda R, Reth M, Rajewsky K, *et al.* Canonical NF-kappaB activity, dispensable for B cell development, replaces BAFF-receptor signals and promotes B cell proliferation upon activation. *Immunity* 2006, **24**(6): 729-739.
41. Van Hauwermeiren F, Armaka M, Karagianni N, Kranidioti K, Vandenbroucke RE, Loges S, *et al.* Safe TNF-based antitumor therapy following p55TNFR reduction in intestinal epithelium. *J Clin Invest* 2013, **123**(6): 2590-2603.
42. Pfeffer K, Matsuyama T, Kundig TM, Wakeham A, Kishihara K, Shahinian A, *et al.* Mice deficient for the 55 kd tumor necrosis factor receptor are resistant to endotoxic shock, yet succumb to L. monocytogenes infection. *Cell* 1993, **73**(3): 457-467.
43. Bray NL, Pimentel H, Melsted P, Pachter L. Near-optimal probabilistic RNA-seq quantification. *Nat Biotechnol* 2016, **34**(5): 525-527.
44. Pimentel H, Bray NL, Puente S, Melsted P, Pachter L. Differential analysis of RNA-seq incorporating quantification uncertainty. *Nat Methods* 2017, **14**(7): 687-690.
45. Subramanian A, Tamayo P, Mootha VK, Mukherjee S, Ebert BL, Gillette MA, *et al.* Gene set enrichment analysis: a knowledge-based approach for interpreting genome-wide expression profiles. *Proc Natl Acad Sci U S A* 2005, **102**(43): 15545-15550.
46. Kontogianni K, Nicholson AG, Butcher D, Sheppard MN. CD56: a useful tool for the diagnosis of small cell lung carcinomas on biopsies with extensive crush artefact. *J Clin Pathol* 2005, **58**(9): 978-980.
47. Hayden MS, West AP, Ghosh S. NF-kappaB and the immune response. *Oncogene* 2006, **25**(51): 6758-6780.
48. Vlantis K, Wullaert A, Polykratis A, Kondylis V, Dannappel M, Schwarzer R, *et al.* NEMO Prevents RIP Kinase 1-Mediated Epithelial Cell Death and Chronic Intestinal Inflammation by NF-kappaB-Dependent and -Independent Functions. *Immunity* 2016, **44**(3): 553-567.
49. Balkwill F. Tumour necrosis factor and cancer. *Nat Rev Cancer* 2009, **9**(5): 361-371.
50. Godwin P, Baird AM, Heavey S, Barr MP, O'Byrne KJ, Gately K. Targeting nuclear factor-kappa B to overcome resistance to chemotherapy. *Front Oncol* 2013, **3**: 120.

3. Discussion

3.1 ZBP1 causes skin inflammation by inducing RIPK3-dependent apoptosis and RIPK1-mediated apoptosis in keratinocytes

ZBP1 has previously been identified as a potent inducer of RIPK3-mediated cell death and inflammation in response to viral infections *in vivo*. While the mechanisms by which ZBP1 activity drives cell death in the absence of RIPK1 are well characterized, ZBP1 activation in the presence of WT RIPK1 remains elusive to a large extent^{100,101,120}. A recent study identified ZBP1 as an essential contributor to intestinal inflammation in mice lacking FADD in intestinal epithelial cells but the mechanistic importance of ZBP1 signaling in other tissues remains unclear¹⁰². Here, we investigated the role of ZBP1 in mice with keratinocyte-specific FADD deletion and untangled the mechanistic importance of ZBP1 downstream signaling in the skin in the presence of FADD and RIPK1.

In line with previously published results, FADD deletion led to severe skin inflammation that was ameliorated but not fully blocked by additional loss of TNFR1¹³⁶. Interestingly, ZBP1 deletion did not have any effect on the inflammatory phenotype of FADD^{E-KO} mice¹⁰⁰, but combined ablation of ZBP1 and TNFR1 fully prevented FADD^{E-KO}-driven skin inflammation. This result indicates a synergistic function for ZBP1 and TNFR1 in driving necroptotic cell death upon keratinocyte-specific deletion of FADD. It is currently unclear why TNFR1 signaling prevents ZBP1 driven skin inflammation in FADD^{E-KO} mice in the presence of RIPK1. RIPK1 has been suggested to be an inhibitor of ZBP1 signaling and its presence in FADD^{E-KO} mice might prevent sufficient activation of ZBP1 in the skin. This inhibitory role of RIPK1 on ZBP1 might be TNFR1 dependent given the prominent role of RIPK1 in TNFR1 signaling. Deletion of TNFR1 may consequently impair RIPK1 and its inhibitory function on ZBP1 signaling. Another possible explanation could be an increased ZBP1 ligand expression after TNFR1 deletion, reaching a threshold for potent ZBP1 activation only after loss of TNFR1. Last but not least, FADD deficient keratinocytes may die due to TNFR1 signaling ahead of sufficient ZBP1 ligand accumulation and activation. Therefore, our results further establish an important connection between TNFR1 and ZBP1 signaling and broaden our knowledge on this relationship to skin homeostasis and inflammation.

ZBP1 activation upon IAV infection has been shown to drive RIPK3-mediated necroptosis as well as RIPK1/RIPK3-mediated apoptosis, suggesting that RIPK3 is required for ZBP1 signaling¹⁰⁴. Our data indicate that C-terminally truncated ZBP1 (ZBP1ca) can directly activate RIPK1 in order to drive caspase-8-dependent cell death. Overexpression of ZBP1ca could trigger cell death *in vitro* and could not be inhibited by either caspase-8 or RIPK3 inhibitors, but required a combination of both.

We could mimic these results *in vivo*, as ZBP1ca expression in keratinocytes resulted in severe skin inflammation and only combined ablation of caspase-8 and mutation of MLKL phosphorylation sites protected from the inflammatory phenotype, while neither MLKL AA nor RIPK3 RHIM mutation alone could fully prevent the development of inflammatory skin lesions. Interestingly, RIPK1 RHIM mutation in combination with MLKL AA mutation protected ZBP1ca^{E-het} mice from skin inflammation, indicating a direct RHIM-RHIM interaction between ZBP1ca and RIPK1 to trigger apoptotic cell death (Figure 15). However, we cannot exclude a role for RIPK3 in this setting which may connect ZBP1 and RIPK1. In order to make a clear statement regarding a ZBP1-RIPK1 RHIM-RHIM mediated interaction, additional mutation of the RIPK1 RHIM in the *Ripk3*^{mR/mR} background would be required to dissect the exact complex formation. Nevertheless, the fact that ZBP1ca^{E-het} *Ripk3*^{mR/mR} mice develop inflammatory skin lesions strongly hints at a direct ZBP1-RIPK1 interaction.

Surprisingly, the kinase activity of RIPK1 was not required for its apoptosis inducing role in the absence of MLKL signaling, suggesting a sole scaffolding RHIM-dependent function for RIPK1 in mediating ZBP1ca-triggered apoptosis. Our data propose that a RHIM-RHIM dependent interaction between ZBP1ca and RIPK1 might be sufficient to drive a conformational change of RIPK1 in order to activate caspase-8. However, as before, we cannot not exclude, that RIPK3 acts upstream of RIPK1 in this setting which may be best addressed by additional mutation of the RHIM of RIPK3 in ZBP1ca^{E-het} *MLKL*^{AA/AA} *Ripk1*^{D138N/D138N} animals.

Given that ZBP1ca only harbors the first RHIM, our data demonstrate that the first RHIM of ZBP1 is sufficient to drive cell death and skin inflammation *in vivo* in a RIPK3-dependent and -independent manner. While mutation of the RHIM of the RIPK1 protein results in ZBP1-driven necroptosis and premature lethality¹⁰⁰, we observe the opposite function upon ZBP1ca expression, namely RIPK1 RHIM-driven cell death.

This raises the question, on how the RIPK1 RHIM can inhibit as well as promote ZBP1-dependent death. A possible explanation is a different affinity for the RHIM1 and the RHIM2 of ZBP1 to bind to RIPK1 and RIPK3 respectively. ZBP1ca only harbors the first RHIM, so the order of recruitment of RIPK1 or RIPK3 to ZBP1 could potentially determine whether a cell is destined to die or to live. Furthermore, the RHIM2 could be required for RIPK1 to inhibit ZBP1, whereas absence of RHIM2 and/or the C-terminus of ZBP1 turns RIPK1 into a pro-death molecule in ZBP1 signaling. Step-by-step shortening of full length ZBP1 may unravel the exact mechanism that determines a pro-death or pro-survival function of RIPK1 in ZBP1 signaling.

Interestingly, we detected an increased production of interferon-stimulated genes following ZBP1ca expression that appeared to be dependent on necroptosis, as RIPK3 RHIM as well as MLKL AA mutations strongly suppressed this effect. However, combined deletion of caspase-8 and MLKL AA mutation did not prevent but exaggerated the ISG signature indicating that

caspase-8 plays an important role in inhibiting ISG production. Indeed, it was recently shown, that ZBP1 can drive fatal type I interferon induction in mice harboring a hemizygous mutation of ADAR1.

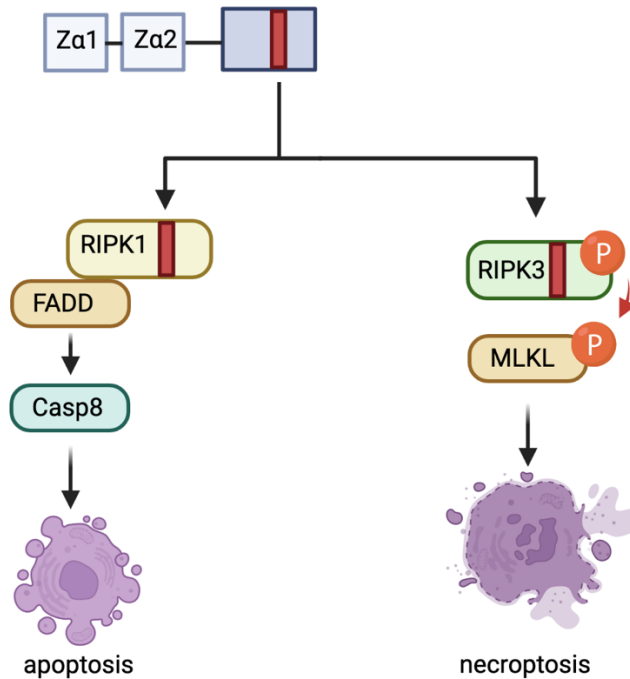


Figure 15. Model of ZBP1ca-mediated signaling in keratinocytes. ZBP1ca undergoes a RHIM-homotypic interaction with RIPK3 to drive MLKL-mediated necroptosis. If the ZBP1ca-RIPK3 interaction is inhibited, ZBP1ca undergoes a RHIM-homotypic interaction with RIPK1 to drive caspase-8-dependent apoptosis. RHIM motifs are depicted in red. Created with BioRender.com.

The exact mechanism of how ZBP1 can drive ISG production remains elusive¹²⁹⁻¹³¹. Noteworthy, whilst our data propose a vital role for RIPK1 as well as RIPK3 in ZBP1ca-mediated ISG production, the aforementioned studies showed a ZBP1-driven interferon induction independent of RIPK1 and RIPK3 signaling and independent of cell death, indicating that the C-terminus of ZBP1 might play a so far-unknown role in mediating RIPK1/RIPK3 independent signaling. Further investigation of these pathways and different ZBP1 constructs might lead to new insights on the under-investigated RHIM2/3 domains of ZBP1.

A recent publication suggested that caspase-8 prevents ISG production via RIPK1 cleavage²¹³. As our results suggest that RIPK1, as well as RIPK3, play a role in ZBP1ca-driven ISG upregulation, it is possible that loss of RIPK1 cleavage by caspase-8 hyperactivates a ZBP1ca-driven ISG response. In this context, Wang et al. proposed that ISG production by RIPK1 relies on a complex formation of RIPK1-TBK1 and subsequent activation of the interferon inducing transcription factor 3 (IRF3) recruitment. However, it should be noted that Liu et al. identified the molecular mechanisms leading to TBK1-dependent IFN production downstream of PRRs such as cGAS, RIG-I and TLR3²¹⁴. The adaptor proteins TRIF (TLR3/4), STING (cGAS) and MAVS (RIG-I) contain a conserved pLxIS motif that is required for IRF3 recruitment.

Recruitment of IRF3 is essential for TBK1-dependent IRF3-phosphorylation and subsequent IFN production. The pLxIS motif is absent in RIPK1 and in other TNFR1-complex-I-components that may be involved in IFN production downstream of ZBP1. Therefore, it seems rather unlikely that RIPK1/TBK1 recruits and activates IRF3 directly. Instead RIPK1/TBK1-dependent IFN production would most likely require one of the aforementioned adaptors. Interestingly, Muendlein et al. have recently suggested that ZBP1 promotes RIPK1 binding to TRIF downstream of TLR3/4^{121,215}. The reported effect has yet to be validated by independent laboratories but may hint at the exact mechanisms for ISG production downstream of ZBP1ca. Combined, based on the functionality of ZBP1ca identified in this study, it will be important to explore mechanisms of ZBP1-autoinhibition, the roles of the different RHIM domains *in vivo* as well as ZBP1-driven ISG upregulation.

3.2 Small Cell Lung Cancer development is independent of necroptotic signaling

Based on previous studies, necroptotic signaling can promote tumor development but can also exert anti-tumorigenic functions, which highly depends on each tumor entity¹⁴⁷⁻¹⁵¹.

Our data show that inhibition of necroptotic signaling does not have a functional role in altering SCLC development or progression in a relevant mouse model of the disease.

In the context of cell death in SCLC, we aimed to induce different types of cell death to trigger a potential anti-tumor response as it has been suggested that necroptotic as well as pyroptotic cell death can potentially trigger anti-tumor immunity¹⁵⁰⁻¹⁵⁴. Surprisingly, we found that SCLC cell lines isolated from RP mice were partly resistant to expression of an active version of the necroptotic executioner protein MLKL. The ESCRTIII complex is a membrane repair complex that has recently been reported to prevent and/or delay cell death induction downstream of MLKL and GSDMD. It is tempting to speculate that SCLC may upregulate ESCRTIII activity to prevent lytic, inflammatory cell death^{94,216}. Another possible explanation would be defects in localization of MLKL to the plasma membrane or expression of different, so far unknown, inhibitory downstream targets. However, expression of the ZBP1ca construct as well as expression of GSDMDN could induce death in both murine SCLC lines tested. Contrary to the skin, where we observed a combination of apoptotic and necroptotic cell death upon ZBP1ca expression, ZBP1ca was able to drive apoptosis but not necroptosis in SCLC cell lines. Our data suggest that resistance to necroptosis may be a feature of a subset of SCLC cells and that the induction of apoptosis may be a more potent therapeutic strategy, which is in line with initial sensitivity of human patients to chemotherapy (section 1.6). Whether susceptibility of ZBP1-induced cell death is equally true in human SCLC and if that is a feature of lung epithelial cells, specific to SCLC tumors or a cell line effect, remains to be investigated.

By providing evidence that ZBP1ca can kill murine SCLC cell lines *in vitro*, we show that murine SCLC cell lines retain the ability to undergo apoptosis. However, induction of ZBP1ca expression *in vivo* could not reduce tumor growth. It remains to be investigated whether this is due to a very limited number of cells that expressed the construct and underwent cell death or whether ZBP1ca was not expressed due to lack of CreERT2 induction. It seems likely that ZBP1ca expression leads to an immune-tolerant type of cell death, as we solely observed apoptotic death *in vitro*. Furthermore, low targeting efficiency could result in minor cell death, but have no effect on tumor development. Lack of expression of ZBP1ca at the humane endpoint hints at negative selection due to ZBP1ca expression and suggests that apoptosis induced by ZBP1ca does not alter SCLC development. However, since we cannot exclude that ZBP1ca was not induced, we cannot clearly state whether activation of ZBP1 might be a therapeutic option for SCLC. Of note, a recent study showed that components of necroptotic and apoptotic cell death were downregulated in SCLC patients, suggesting lack of the cell death machinery and indicating counter-selection of regulated cell death pathways in SCLC development. Interestingly, this study reported sensitivity of neuroendocrine SCLC to ferroptosis, pointing out a new therapeutic route for SCLC²¹⁷.

Collectively, our data suggest that necroptotic signaling is dispensable for SCLC development and that induction of necroptosis of cancer cells by using active executioner proteins does not provide a platform for development of new therapeutic options in SCLC.

3.3. NEMO- and RelA-dependent NF- κ B Signaling Promotes Small Cell Lung Cancer

Inflammatory signaling has previously been established as being tumor-suppressive as well as tumor-promotive. SCLC is a highly aggressive lung cancer subtype and its underlying molecular mechanisms, specifically in light of inflammatory signaling, are poorly understood. Here, we investigated the role of inflammation in SCLC *in vivo* by using a well-established genetic mouse model recapitulating the disease. We specifically addressed the role of TNFR1 and NF- κ B signaling in the development and progression of SCLC. Our findings underscore a crucial role for NEMO/RelA mediated NF- κ B signaling in tumor onset and development. We found that ablation of NEMO in RP mice significantly delayed tumor onset by depleting tumor growth. Interestingly, this is in contrast to liver-parenchymal cell (LPC)-specific NEMO-deficient mice which develop hepatocellular carcinoma and chronic steatohepatitis due to chronic cell death and inflammation^{15,174}.

Whereas NEMO works as a tumor suppressor in the liver by preventing cell death and inflammation, our experiments reveal NEMO as a tumor promotor in lung epithelial cells (LECs). We hypothesized that NEMO deletion led to cell death and impaired NF- κ B signaling in LECs. In contrast to LPC-specific NEMO ablation, this cell death did not result in increased

inflammation and tumor development, but likely in loss of cells which were prone to become tumors upon RB1 and TP53 deletion.

We postulate that the significantly delayed tumor onset and prolonged survival in *Rb1^{FL/FL} Tp53^{FL/FL} Nemo^{FL/FL}* mice is due to a strongly decreased number of tumorigenic cells compared to *Rb1^{FL/FL} Tp53^{FL/FL}* mice. Surprisingly, deletion of the essential cell death regulator NEMO in LECs did not lead to a spontaneous inflammatory phenotype macroscopically affecting the mice, whereas deletion of NEMO in LPCs, in intestinal epithelial cells (IECs) and in keratinocytes results in a strong cell-death dependent inflammatory response^{15,16,71,72}. In line with this, deletion of Fas-associated protein with death domain (FADD), another essential cell death regulator, in LECs does not lead to a spontaneous phenotype in lung tissue, contrary to FADD deletion in IECs or keratinocytes (section 2.1)^{136,218,219}. Therefore, our data suggest that negative regulators of cell death are potential targets during SCLC development without the severe side effects observed in other tissues. Together, non-inflammatory cell death is likely the main pathway driving delayed tumor onset upon NEMO deletion in RP mice.

Our results suggest a tumor-promoting role of LEC-specific NF-κB signaling, which is in line with previous reports on reduced cell proliferation upon NF-κB depletion in Kras-driven mouse lung cancer models¹⁶³⁻¹⁶⁵. The significantly delayed tumor onset upon ablation of RelA extends NF-κB as an essential driver of RB1/TP53 driven lung carcinogenesis. The stronger effect of *Nemo^{FL/FL}* compared to *Rela^{FL/FL}* on animal survival is consistent with a total loss of NF-κB activation and induction of cell death upon NEMO depletion, whereas RelA ablation diminishes but does not fully block NF-κB signaling (Figure 16). These results are in line with the findings that inhibition of NF-κB signaling compromises or inhibits tumor development in mouse models of lung adenocarcinoma, colon cancer or skin carcinogenesis¹⁶³⁻¹⁶⁷. Collectively, our study demonstrates that NF-κB signaling significantly contributes to carcinogenesis in a RB1/TP53 driven lung cancer mouse model and reinforces a promoting role for NF-κB in human cancer development. Of note, a recent study suggested that NLRP6/NF-κB mediated signaling led to SCLC-derived exosome secretion and thereby promoted SCLC metastasis *in vitro* and *in vivo*. Although we did not observe a difference in metastatic prevalence in SCLC mice upon loss of NF-κB signaling, this study confirms a crucial role for NF-κB in promoting SCLC progression²²⁰. While the presence of NF-κB signaling is critical for tumor progression, persistent activation of NF-κB signaling using the expression of an IKK2ca construct did not lead to faster tumor growth. This is especially surprising in the context of previously published data by our group which showed that constitutive NF-κB signaling is sufficient to induce spontaneous intestinal tumorigenesis without an additional tumor-inducing stimulus²²¹.

At first glance, these results contradict our finding that depletion of NF-κB signaling considerably inhibited tumorigenesis. However, RB1 as well as TP53 can serve as efficient inhibitors of NF-κB signaling²²²⁻²²⁴. One possible explanation of these results is that NF-κB is

already strongly activated due to RB1 and TP53 loss in the *Rb1^{FL/FL} Tp53^{FL/FL}* mouse model and additional IKK2ca expression does not significantly change the NF-κB-dependent gene expression landscape.

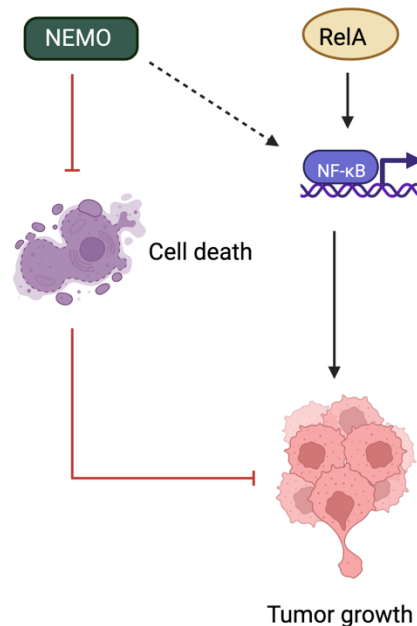


Figure 16. Model of NF-κB signaling in SCLC initiation. NEMO expression prevents from cell death and ensures proper NF-κB signaling. Thus, loss of NEMO results in cell death and in loss of NF-κB which prevents tumor growth. Loss of RelA delays tumor onset due to strong suppression of NF-κB signaling. Created with BioRender.com

Therefore, although NF-κB signaling is essential for lung carcinogenesis, constitutively activated NF-κB signaling cannot further increase tumor progression in RP mice.

Our experiments using TNFR1 mice showed that TNFR1 signaling is not required for tumor development or progression, suggesting that TNFR1 is not the sole upstream stimulus for NF-κB signaling in this tumor entity. These findings are interesting in view of previous studies, which reported TNF as an essential regulator of skin and obesity-dependent liver carcinogenesis^{157,158} and that TNFR1 is a potential prognostic molecule for ovarian cancer¹⁵⁹. Our findings demonstrate that TNFR1 is not crucially involved in the development of RB1/TP53 driven cancer, and that TNFR1 inhibition may not result in drastic overall changes in SCLC patients.

Our *in vivo* experiments highlight the functions of TNFR1 and NF-κB signaling in RB1/TP53 driven lung tumorigenesis. Most importantly, NF-κB serves as a substantial tumor driver upon combined ablation of RB1 and TP53 where NF-κB signaling appears to be especially important at the time of tumor initiation. While we did not address inhibition of NF-κB in established SCLC tumors, it is intriguing to speculate that this may lead to reduced tumor growth or shrinkage as a potential therapeutic treatment. In contrast, persistent activation of NF-κB signaling does not

increase tumor development, indicating that the presence of NF- κ B is crucial but can reach a signaling threshold after which there is no additive effect. In contrast to NF- κ B signaling, TNFR1 signaling is not crucially involved in SCLC development although TNFR1 is a well-known NF- κ B inducer. In summary, our results identify the NF- κ B signaling pathway as a critical driver of lung carcinogenesis and a potential drug target in SCLC.

3.4. Concluding Remarks and Future Prospects

In this study, we unravel new mechanisms of ZBP1 signaling as a potent driver of skin inflammation. Our findings reinforce ZBP1 as a crucial player in skin homeostasis not only upon ablation of RIPK1 but also upon deletion of FADD, identifying FADD as an inhibitor of ZBP1-induced necroptosis in the skin. Additionally, we show that the first RHIM of ZBP1 can potentially induce apoptotic and necroptotic cell death driven by RIPK1 and RIPK3, respectively. Generation and analysis of mice harboring different ZBP1 constructs will be key to fully unravel the mechanisms of ZBP1-autoinhibition and ZBP1-driven cell death induction.

Having generated and characterized the ZBP1ca construct as a driver of apoptosis, necroptosis and ISG production we aimed to make use of this construct in a therapeutic setting.

The introduction of inflammatory and non-inflammatory cell death has substantially improved cancer therapy. However, the outcome of inflammation and cell death induction strongly depends on each cancer entity so that development of treatment options remains challenging. While induction of ZBP1ca-dependent cell death could not lead to reduction of SCLC development in a mouse model of SCLC, activation of ZBP1 should be tested in different cancer entities, especially in light of two recent studies providing evidence that ZBP1-mediated necroptosis of stromal fibroblasts could trigger a potent anti-tumor immunity^{143,144}.

Additionally, we provide important insights into the role of NF- κ B signaling as a driver of SCLC at tumor initiation. Inhibition of NF- κ B signaling in established tumors will be crucial to investigate the therapeutic potential of targeting this pathway. Considering a potentially non-immunogenic cell death of lung epithelial cells upon loss of NEMO, SCLC might not have been the proper model in order to test induction of immunogenic cell death as a potential therapeutic approach. This is further emphasized by the lack of an inflammatory response upon loss of FADD in lung epithelial cells. Tumor entities arising in tissues potentially more sensitized to inflammatory cell death, such as melanoma might be more susceptible to induction of tumor cell death, demonstrating the necessity of a concerted effort in understanding each cancer entity and the underlying molecular mechanisms in order to identify tumor-specific vulnerabilities.

4. General Material & Methods

4.1 Chemical and biological materials

Chemicals and kits used in this study were purchased from indicated companies. All solutions were prepared using double-distilled water (ddH₂O).

Table 1: Reagents and chemicals used in this study

Reagent/Chemical	Supplier
Acrylamid/Bis solution	Serva (10688.01)
Agarose ultra-pure	Biozym (840004)
Albumine bovine fraction (BSA)	Biorad (500-0006)
Ammonium persulphate (APS)	Sigma (A3678-100G)
Chloroform	VWR (22711290)
cOmplete Tablets Mini (Protease EDTA-free Inhibitor Cocktail)	Roche (11836145001)
Corn oil	Sigma (C8267)
Dimethyl sulfoxide (DMSO)	AppliChem (A3672, 0050)
dNTPs	Invitrogen (10297-117)
Doxycycline	Sigma Aldrich (D9891-1G)
Draq7	Cell Signaling Technology (7406)
Dulbecco's Modified Eagle Medium (DMEM)	Gibco (41965-062)
ECL Western Blotting Detection Reagent	GE Healthcare
Emricasan (IDN6556)	Selleckchem (S7775)
Entellan	Merck Millipore (107960)
Ethanol absolute	AnalR Normapur (20821-321)
Fetal Bovine Serum	PAN Biotech
Flag M2 affinity gel	Sigma-Aldrich (A4596)
Fluoromount-G	Southern Biotech (0100-01)
Glutamine	Invitrogen (25030123)
Glycerol	VWR (24386-298)
Glycine	VWR (101196X)
GSK'872	Millipore (530389)
Isopropanol (2-Propanol)	AppliChem (A2427-2500)
2x Laemmli sample buffer	Bio-Rad (1610737)
4x Laemmli sample buffer	Bio-Rad (1610747)
Methanol	AppliChem (A3928)
NaCl	VWR (7647-14-5)
Nec-1s	BioVision (2263)

Paraformaldehyde (PFA)	AppliChem (A3813)
Penicillin (10000U/ml)/Streptomycin (10000ug/ml)	Invitrogen (15140163)
Phosphate buffered saline (PBS)	Gibco (14190-094)
Phosphatase inhibitor cocktail tablets, PhosSTOP	Roche (04906837 001)
Pierce™ 660 nm Protein Assay	ThermoScientific (22660)
Ponceau	Sigma (09276)
Proteinase K	Roche (3115852)
Proteinmarker PeqGold	Peqlab (27-2210)
Random hexamer primers	Invitrogen (48190-011)
Red-Taq DNA Polymerase 2X MasterMix	VWR (733-2131)
RNAse OUT	Invitrogen (10777-019)
RNAzol	Sigma-Aldrich (R4533)
Sodium Azide (NaN ₃)	Merck (S2002)
Sodium dodecyl sulfate (SDS)	Millipore (817034.1000)
Sodium pyruvate (100mM)	Gibco (11360-039)
Stripping buffer	ThermoScientific (21059)
SuperScript III Reverse Transcriptase	Invitrogen (18080-044)
SuperScript™ III First Strand Synthesis System	Thermo Fisher Scientific (18080-051)
Tamoxifen	Sigma (T5648-1G)
TaqMan Gene Expression Master Mix RTqPCR Mastermix	Thermo Fisher Scientific (4369542)
TEMED	Serva (35925)
Tissue-Tek O.C.T™ Compound	Sakura (4583)
Tris(hydroxymethyl)aminomethane (TRIS)	VWR (103156X)
Triton X-100	AppliChem (A4975-0500)
Trypsin EDTA (TrypLE)	Gibco (12603-010)
10x Trypsin EDTA	Gibco (A12177-01)
Tween-20	Sigma (P1379-500)
Z-VAD-FMK	Enzo (ALX-260-020-M005)

Table 2: Buffers and solutions used in this study

Buffer/solution/medium	Composition
Antigen retrieval buffer	10 mM NaCitrate 0.05% Tween-20, pH 6
Blocking buffer	PBS, nonfat dry milk, 0.1% Tween-20
Fibroblast medium	DMEM, 10% Fetal Bovine Serum, 1% Penicillin-Streptomycin, 1% glutamine, 1% sodium pyruvate, 1% HEPES buffer

Freezing medium	Fetal Bovine Serum (Superior), 10% DMSO
IHC blocking buffer	PBS, 1% BSA 0.003% NaN ₃ , 0.2% fish skin gelatine, 0.05% Tween-20
Immunoprecipitation (IP) buffer	30 mM Tris HCl pH7,5 40mM NaCl 2mM EDTA 2mM KCl 10% Glycerin 1% Triton X
PCR reaction mix (per reaction)	12.5 µl Taq 2x Mastermix, 2µl Primer mix (forward & reverse 1:1, 19 µM), 10.5 µl H ₂ O, 2µl genomic DNA
Peroxidase blocking buffer	0.04 M NaCitrate, 0.121 M Na ₂ HPO ₄ 0.03 M NaN ₃ , 3% H ₂ O ₂
Primary antibody dilution buffer	PBS, 0.1% Tween-20, (1% BSA), NaN ₃
Retrieval buffer	NaCitrate (10mM), Tween-20 (pH6, 0.05%), Tri-sodium citrate 2,94 g
RIPA lysis buffer	Supplemented with PhosStop and cComplete Tablets
SDS polyacrylamide gel	10% resolving gel (for 20 ml) H ₂ O (7.9 ml), 30% Acrylamide mix (6.7 ml), 1.5 M Tris (pH 8.8, 5 ml), 10% (w/v) SDS (0.2 ml) 10% (w/v) APS (0.2 ml) TEMED (0.008 ml) 5% stacking gel (for 10 ml) H ₂ O (6.8 ml), 30% Acrylamide mix (1.7 ml), 1 M Tris (pH 6.8), 10% (w/v) SDS (0.1 ml) 10% (w/v) APS (0.1 ml) TEMED (0.01 ml)
Secondary antibody dilution buffer	PBS, 0.1% Tween-20
Tail lysis buffer	100 mM Tris/HCl, 5 mM EDTA, 0.2% SDS, 200 mM NaCl
TE-buffer	10 mM Tris-base, 192 mM Glycine, 20% MetOH
Western blot running buffer	Tris 25 mM, Glycine 92 mM, SDS 0.1%
Western blot transfer buffer	Tris-Base 25 mM, Glycine 192 mM, Methanol 20%

Table 3: Kits used in this study

Kit	Supplier (Catalogue Number)
ABC Kit Vectastain Elite	Vector (PK 6100)
Avidin/Biotin Blocking Kit	Vector (SP-2001)
Liquid DAB Substrate Chromogen System	DakoCytomation (Code K3466)
NucleoSpin™ Gel- and PCR Cleanup Kit	Macherey-Nagel (740955.50)
NucleoSpin™ RNA kit	Macherey-Nagel (740955.50)
SuperScriptIII cDNA synthesis Kit	Invitrogen (18080-044)
TaqMan Gene Expression Master Mix	Applied Biosystems (4369542)
Direct-zol RNA MiniPrep	Biozol (ZYM-R2052)

4.2 Mouse experiments

4.2.1 Animal care

Mice used in this study were maintained at the specific-pathogen free (SPF) animal facilities of the CECAD Research Center (University of Cologne) and of the nuclear medicine (University Hospital of Cologne) under a 12-hour dark/light cycle in individually ventilated cages at 22 (±2) °C and a relative humidity of 55 (±5) %. Mice were given a sterilized commercial diet (Harlan, diet no.2918) as well as water ad libitum. All animal procedures were conducted in accordance with European, national and institutional guidelines and protocols were approved by the Landesamt für Natur, Umwelt und Verbraucherschutz Nordrhein-Westfalen (LANUV). In case of need for medical attention, animals were provided with appropriate care. No other exclusion criteria existed. *Rb1^{fl/fl}*, *Tp53^{fl/fl}* ²²⁵ and *Rb1^{frt/frt}*, *Tp53^{frt/frt}*, *R26^{FSF-CreERT2}* ¹⁰⁰ mice were described previously. *Mkl^{AA/AA}* mice and *R26^{LSL-ZBP1ca}* mice were generated using CrispR/Cas9 mediated gene disruption in fertilized oocytes (section 2.1). All mouse studies were performed in a blinded fashion.

4.2.2 Adenovirus Inhalation

Animals with an age of 8–12-weeks- were anesthetized with Ketavet (100mg/kg)/Rompun (20mg/kg) by intraperitoneal (i.p.) injection, followed by intratracheal application of replication-deficient Cre-expressing adenovirus (Ad5-CMV-Cre, 2.5 x 10⁷ PFU, University of Iowa) or intratracheal application of replication-deficient Flp-expressing adenovirus (Ad5-CMV-Flp, 2.5 x 10⁷ PFU, University of Iowa) in order to induce lung tumor formation. All experiments carried out were pooled for the indicated genotypes.

4.2.3 MRI scans

Tumor development was monitored via bi-weekly MR imaging starting 20 weeks after Ad-Cre instillation (A 3.0 T Philips Achieva clinical MRI in combination with a specific mouse solenoid coil (Philips Hamburg, Germany) was used). MR images were acquired using turbo-spin echo (TSE) sequence (repetition time = 3819ms, echo time = 60ms, field of view = 40 x 40 x 20

mm³, reconstructed voxel size = 0.13 x 0.13 x 1.0 mm³). Mice were anesthetized with 2,5% isoflurane prior to MRI scans. MR images were analyzed blindly by marking regions of interests using Horos software.

4.2.4 Tamoxifen & anti-PD1 Injections

Tamoxifen (Sigma, T5648-1G, 100mg) was dissolved in 200 µl sterile DMSO and added to preheated (65°C) corn oil (Sigma, C8267). The solution was kept at 65°C until completely dissolved and stored at -20°C. After tumor detection a group of mice received 100 µl of the tamoxifen/corn oil solution for 5 consecutive days i.p. Additionally, mice were either treated with 250 µg aPD1 antibody (InVivoMAb anti mouse PD-1 (CD279) #BE0273 BioXcell) twice a week (i.p., 200 µl) or with PBS (i.p., 200 µl).

4.2.5 Lung tissue preparation

Mice were sacrificed using cervical dislocation. For histopathological analysis the trachea was injected with 4% PFA to inflate and fix the lung. Lung tissue was fixed overnight in 4% PFA at 4°C. Pieces of tumor tissues were cut from the lungs and snap frozen on dry ice for RNA and Protein expression analysis. These tissue pieces were stored at -80°C until further processing.

4.3 Histological analysis

4.3.1 Haematoxylin & Eosin staining

Paraffin sections were de-paraffinized using xylene and re-hydrated with increasing concentrations of ethanol. Sections were stained for 2 minutes in haematoxylin, 15 min differentiated in tap water and 1 min incubated in eosin. Stained sections were de-hydrated with decreasing concentrations of ethanol and fixed in xylene.

4.3.2 DAB stainings

Paraffin-embedded sections were re-hydrated with xylene and ethanol. Heat induced antigen retrieval was performed and endogenous peroxidase was blocked in peroxidase buffer. Sections were stained for a-Ki67 antibody, (Cell Marque 275-R10), a-CD45 antibody (BD 550539) and a-CD56 antibody (Zytomed RBK050).

4.4 Molecular Biology

4.4.1 Isolation of genomic DNA from tail biopsies

Tail biopsies were used for identifying the genotypes of mice. For genomic DNA isolation, tail biopsies were incubated in tail lysis buffer (table 2) at 56°C overnight at 600 rpm. Then 200 µl isopropanol were added. Samples were centrifuged at 11.000 x g for 1 min, the supernatant was discarded and the pellet was washed with 70% ethanol. After a second centrifugation at

11.000 x g for 1 min, the supernatant was removed and the remaining pellet was air-dried for 20 min at RT. Finally, the pellet was re-suspended in 100 µl TE-buffer (table 2).

4.4.2 Genotyping PCRs

Polymerase-chain-reaction (PCR) was used to amplify allele specific regions. Allele specific primers (2µl) (table 4), PCR master mix (12.5 µl) (VWR, 733-1316), H₂O (8,5µl) and genomic DNA (2µl) were mixed and specific PCR protocols were used to amplify allele specific regions (table 4). PCR products were separated with 2% low melting agarose gels containing 0.5 mg/ml ethidiumbromid in 1X TAE buffer at 120V and visualized with UV-light. To determine size of PCR products a DNA marker (ThermoFisher, 10787018) was used.

Table 4. Genotyping primers

Allele	Primer sequence (5' – 3')	Expected band size	Program (step 1-5)	Cycles (step2-4)
<i>R26</i> ^{LSL.ZBP1ca}	GCACTTGCTCTCCCAAAGTC GCGAAGAGTTTGTCTCAACC GCCTTTAAGCCTGCCAGAA	wt: 254 bp knock-in: 316 bp	94°C 3 min 94°C 30 sec 60°C 45 sec 72°C 1 min 72°C 3 min	34
<i>Ripk3</i> ^{mRhim}	WT: TCTCCCATCACCTTCCTCCTCA GAGTTGTAGTTCCCAATCTGCA Mut: TCTCCCATCACCTTCCTCCTCA AGTTGTAGTTTCGAGCCGCCG	wt: 528 bp mut: 528 bp	94°C 3 min 94°C 30 sec 60°C 45 sec 72°C 1 min 72°C 3 min	35
<i>Mik</i> ^{AA/AA}	WT: GTGGAAGGAGAGAAATGGCCCT GCAAAACACAGAATTCCATCAG Mut: GTGGAAGGAGAGAAATGGCCCT AAAACACAGAATGCCATCGC	wt: 850 bp mut: 850 bp	94°C 3 min 94°C 30 sec 60°C 45 sec 72°C 1 min 72°C 3 min	35
<i>Ripk1</i> ^{D138N}	TACCTTCTAACAAGCTTTCC AATGGAACCACAGCATTGGC CCCTCGAAGAGGTTCACTAG	Wt: 220 bp D138N: 180 bp	94°C 3 min 94°C 30 sec 60°C 30 sec 72°C 1 min 72°C 3 min	40
<i>Ripk1</i> ^{mRhim}	WT: GTTCTGGTATTCAGATTGGAA GCACTTGTTCTTGCTTGGGTCA	wt: 518 bp	94°C 3 min 94°C 30 sec 60°C 45 sec	34

	Mut: TCTCTCTTTAGGCCCCAGTCCT TAATTGTGGTTAGCTGCTGC	Mut: 760 bp	72°C 1 min 72°C 3 min	
<i>K14-Cre</i>	AGC ACC TTC TCT TCA CTC AGC CGC ATA ACC AGT GAA ACA GCA T	Cre: 400 bp	94°C 3 min 94°C 20 sec 58°C 20 sec 72°C 20 sec 72°C 2 min	30
<i>Caspase-8^{FL}</i>	ATA ATT CCC CCA AAT CCT CGC ATC GGC TCA CTC CCA GGG CTT CCT	wt: 200 bp floxed: 300 bp	95°C 3 min 94°C 30 sec 62°C 30 sec 72°C 30 sec 72°C 5 min	30
<i>Rb1^{FL} & Rb1^{FRT}</i>	CTC ATG GAC TAG GTT AAG TTG TGG GCA TTT AAT TGT CCC CTA ATC C	wt: 163 bp Floxed: 201 bp	94°C 3 min 94°C 20 sec 65°C 15 sec 72°C 15 sec 94°C 15 sec 60°C 15 sec 72°C 15 sec 72°C 2 min	2-4: 10 5-7: 28
<i>Tp53^{FL} & Tp53^{FRT}</i>	CAC AAA AAC AGG TTA AAC CCA AGC ACA TAG GAG GCA GAG AC	wt: 288 bp Floxed: 370 bp	94°C 3 min 94°C 30 sec 60°C 30 sec 72°C 30 sec 72°C 3 min	35
<i>Nemo^{FL}</i>	CGT GGA CCT GCT AAA TTG TCT ATC ACC TCT GCA AAT CAC CAG ATG TGC CCA AGA ACC ATC CAG	wt: 301 bp floxed: 446 bp	94°C 3 min 94°C 30 sec 60°C 30 sec 72°C 30 sec 72°C 3 min	35
<i>RelA^{FL}</i>	TACCAGTTGGTAAAACCAGGC TAACGAGTTCAAGGCCAGCTT CGCCTTGACTCAGTGTCCC	wt: 151 bp Floxed: 219 bp	94°C 2 min 94°C 30 sec 60°C 30 sec 72°C 30 sec	35
<i>R26^{LSL.IKK2ca}</i>	AAA GTC GCT CTG AGT TGT TAT C GAT ATG AAG TAC TGG GCT CTT GCA TCG CCT TCT ATC GCC T	wt: 570 bp Floxed: 450 bp	94°C 3 min 94°C 30 sec 60°C 30 sec 72°C 45 sec 72°C 5 min	35

<i>Tnfr1^{FL}</i>	CAA GTG CTT GGG GTT CAG GG CGT CCT GGA GAA AGG GAA AG	wt: 134 bp Floxed: 195 bp	94°C 3 min 94°C 30 sec 60°C 1 min 72°C 2 min 72°C 5 min	29
<i>Tnfr1^{Ko}</i>	AGA AAT GTC CCA GGT GGA GAT CTC GGC TGC AGT CCA CGC ACT GG ATT CGC CAA TGA CAA GAC GCT GG	wt: 120 bp ko: 300 bp	94°C 3 min 94°C 1 min 61°C 30 sec 72°C 30 sec 72°C 2 min	30
<i>R26^{FSFcreERT2/LSLZBP1ca}</i>	AAA GTC GCT CTG AGT TGT TAT GGA GCG GGA GAA ATG GAT ATG TCA ATG GGC GGG GGT CGT T	Wt: 600 bp Cre: 461 bp ZBP1ca: 1800 bp	94°C 3 min 94°C 30 sec 62°C 30 sec 72°C 1 min 72°C 3 min	34

4.4.3 3' mRNA sequencing analysis

RNA was isolated from tumor tissue with a NucleoSpin RNA isolation kit (Macherey Nagel Ref. 740955.250). Based on OD260/280 and OD260/230 and on RNA integrity number (RIN) RNA quality was measured. Gene expression was determined using the Quant 3' mRNAseq Library Prep Kit FWD for Illumina (Lexogen). All samples showing RIN <4, OD260/280 < 1.8 or OD260/230 <1.5 were not used for analysis. Single-end sequencing reads were aligned to Ensembl GRCm38 (mm10). Gene-level aggregated TPMs were calculated using sleuth 0.29.0⁴⁴ with Ensembl BioMart annotation. 18,383 genes out of 35,930 calculated TPMs were considered expressed (median TPM > 0) across 41 transcriptomes. Thus, these were used for analysis (also, see section 2.3, Material & Methods. *Rb1^{FL/FL} Tp53^{FL/FL} Mkl^{AA/AA}* and respective *Rb1^{FL/FL} Tp53^{FL/FL}* RNA samples were run and analyzed together with tumor tissue samples from section 2.3).

4.4.4 Ligase-independent cloning

Doxycycline-inducible MLKL₁₋₁₈₀, GSDMDN and ZBP1ca lentiviral expression plasmids were generated using the pCW_Cas9 plasmid (Addgene #50661). The pCW_Cas9 plasmid was digested using NheI and BamHI. MLKL₁₋₁₈₀, GSDMDN and ZBP1ca coding sequences were amplified from mouse cDNA using primers listed in table 5. Ligase-independent cloning was used to generate pCW-ZBP1ca, pCW-GSDMDN and pCW-MLKL₁₋₁₈₀.

Table 5. Primers used for ligase independent cloning.

Construct	Primer Sequence (5' – 3')
ZBP1ca	cagatcgctggagaattgggcagaagctcctgttgactt cgcaacccaaccccgatcctggctcaccacaggcttc
MLKL ₁₋₁₈₀	cagatcgctggagaattggatggataaattgggacagat cgcaacccaaccccgatctcatgagcattgcttcaggg
GSDMDN	cgctggagaattggctagcatgccatcggccttgagaa atacgatatcttgatcgatatctgacaggagactgagct

4.5 Cell culture

Cell lines were maintained at 5% CO₂ and 37°C and cultured in RPMI Medium supplemented with 10% FCS and 1%P/S. Cells were passed by washing with Ca²⁺ free PBS (Gibco, 14190-094), followed by trypsinizing with 1x TrypLE Express Enzyme (ThermoScientific, #12605-010) for 5 minutes. The reaction was stopped by addition of culture medium, and cells were harvested and centrifuged at 1200 rpm for 5 minutes. Supernatant was removed, cells were resuspended in culture medium and 10% of the cells were re-seeded.

4.5.1 Generation of stable cell lines via lentiviral transduction

HEK293T cells were seeded on a 10cm culture dish and fed with fresh medium 1 h prior to transfection. The HEK293T cells were then transfected with pCW-MLKL₁₋₁₈₀, pCW-ZBP1ca or pCW-GSDMDN (10µg) in combination with psPAX (5 µg, Addgene #12260) and pMD2.G (Addgene, #12259) plasmids by mixing plasmids with 500 µl 0.25M CaCl₂. Following, 500 µl 2xHBS was added and after 5 min of incubation time the solution was dropped onto HEK293T cells. After 24h medium was replaced with fresh culture medium and after 2 and 3 days the supernatant containing the virus was collected. Prior to transduction, 300.000 SCLC cells/well were plated in a 6-well plate (Sigma Aldrich, #CLS3335). Cells were fed with 1.5 ml Virus supernatant, 1.5 ml fresh medium and 8µg/ml Polybrene (Sigma Aldrich, #H9268). After 24h, the medium was replaced with fresh medium containing 2µg/ml puromycin. After 48h, puromycin-containing medium was removed and cells were splitted at least 3 times before being transferred to a S1 area and used for experiments.

Single cell clones were generated by seeding 1 cell/well on a 96-well plate in duplicates. Cells were grown and after being confluent one duplicate was treated with doxycycline. In case of death of all cells, the second duplicate was cultured and used for experiments.

4.5.2 Cell death assay

SCLC cell lines were seeded 24 h prior to stimulation (96 well plate, Sigma-Aldrich, CLS3340-50EA, 1x10⁴ cells/well). Cells were stimulated overnight with combinations of doxycycline (1

µg/ml), emricasan (5 µM) and GSK872 (2,5µM). Cell viability was measured using the Incucyte (Sartorius) and evaluated by Draq7 or YOYO-1 uptake.

4.6 Biochemistry

4.6.1 Preparation of protein extracts from tissue

Proteins from tumor tissues were isolated using precellys 24 tissue homogenizer (bertin instruments). Protein concentration was measured using PIERCE 660nm Protein Assay Reagent (Thermo Scientific, #22660) and BSA standard. Lysate concentration was adjusted to 5 µg/µl and 2x Laemmli sample buffer (Bio-Rad 1610737) was added. Samples were boiled at 95°C for 8 minutes.

4.6.2 Protein lysate preparation from cells

For immunoblot analyses, 3×10^5 cells were seeded in 6-well plates and cultured O/N. Cells were lysed 2x in Laemmli sample buffer (Bio-Rad 1610737) supplemented with DTT. Samples were boiled at 95°C for 8 minutes.

4.6.3 Western blot analysis

Cell lysates were separated using Sodium dodecyl-sulfate polyacrylamide gel electrophoresis and transferred to polyvinylidene difluoride membranes (IPVH00010, Millipore) at 80V for 3h at 4°C. Membranes were blocked using 5% milk in 0.1% PBST for 1 h, washed three times with 0.1% PBST and probed with following primary antibodies: a-ZBP1 (1:1000, Adipogen AG-20B-0010), a-MLKL (1:1000, Millipore MABC604), a-GSDMD (1:1000 abcam, ab219800), a-RIPK3 (1:1000, Enzo Life Sciences ADI-905-242-100) and a-Tubulin (Sigma T6074 1:1000) O/N at 4°C. Membranes were washed three times with 0.1% PBS-T and were incubated with secondary horseradish peroxidase-coupled antibodies for 1h at RT (GE Healthcare, Jackson ImmunoResearch, 1:10000). ECL Western Blotting Detection Reagent (RPN2106, GE Healthcare) was used to detect the proteins. Membranes were stripped if necessary, using stripping buffer (ThermoScientific, 21059) for 15 minutes at RT.

4.7 Statistical analysis

In case of gaussian distribution, student's t test was used. Mann-Whitney *U* test was used for statistical analysis of comparisons between 2 groups of nonparametric data. The Log-Rank (Mantel-Cox) test was used in order to compare survival curves and tumor onset of mice. **p* ≤ 0.05; ***p* ≤ 0.01; ****p* ≤ 0.005, *****p* ≤ 0.001 for all figures. All statistical analysis was performed with Prism9, GraphPad. No data were excluded.

5. General References

- 1 Wallach, D., Kang, T. B. & Kovalenko, A. Concepts of tissue injury and cell death in inflammation: a historical perspective. *Nat Rev Immunol* **14**, 51-59, doi:10.1038/nri3561 (2014).
- 2 Zhang, Q., Lenardo, M. J. & Baltimore, D. 30 Years of NF-kappaB: A Blossoming of Relevance to Human Pathobiology. *Cell* **168**, 37-57, doi:10.1016/j.cell.2016.12.012 (2017).
- 3 Kumar, H., Kawai, T. & Akira, S. Pathogen recognition by the innate immune system. *Int Rev Immunol* **30**, 16-34, doi:10.3109/08830185.2010.529976 (2011).
- 4 Pasparakis, M. & Vandenabeele, P. Necroptosis and its role in inflammation. *Nature* **517**, 311-320, doi:10.1038/nature14191 (2015).
- 5 Green, D. R. The Coming Decade of Cell Death Research: Five Riddles. *Cell* **177**, 1094-1107, doi:10.1016/j.cell.2019.04.024 (2019).
- 6 Kerr, J. F., Wyllie, A. H. & Currie, A. R. Apoptosis: a basic biological phenomenon with wide-ranging implications in tissue kinetics. *Br J Cancer* **26**, 239-257, doi:10.1038/bjc.1972.33 (1972).
- 7 Elmore, S. Apoptosis: a review of programmed cell death. *Toxicol Pathol* **35**, 495-516, doi:10.1080/01926230701320337 (2007).
- 8 Poon, I. K., Lucas, C. D., Rossi, A. G. & Ravichandran, K. S. Apoptotic cell clearance: basic biology and therapeutic potential. *Nat Rev Immunol* **14**, 166-180, doi:10.1038/nri3607 (2014).
- 9 Segawa, K. & Nagata, S. An Apoptotic 'Eat Me' Signal: Phosphatidylserine Exposure. *Trends Cell Biol* **25**, 639-650, doi:10.1016/j.tcb.2015.08.003 (2015).
- 10 Suzuki, J., Denning, D. P., Imanishi, E., Horvitz, H. R. & Nagata, S. Xk-related protein 8 and CED-8 promote phosphatidylserine exposure in apoptotic cells. *Science* **341**, 403-406, doi:10.1126/science.1236758 (2013).
- 11 Suzuki, J., Imanishi, E. & Nagata, S. Exposure of phosphatidylserine by Xk-related protein family members during apoptosis. *J Biol Chem* **289**, 30257-30267, doi:10.1074/jbc.M114.583419 (2014).
- 12 Nagata, S., Hanayama, R. & Kawane, K. Autoimmunity and the clearance of dead cells. *Cell* **140**, 619-630, doi:10.1016/j.cell.2010.02.014 (2010).
- 13 Montico, B., Nigro, A., Casolaro, V. & Dal Col, J. Immunogenic Apoptosis as a Novel Tool for Anticancer Vaccine Development. *Int J Mol Sci* **19**, doi:10.3390/ijms19020594 (2018).
- 14 Kumari, S. *et al.* Sharpin prevents skin inflammation by inhibiting TNFR1-induced keratinocyte apoptosis. *Elife* **3**, doi:10.7554/eLife.03422 (2014).
- 15 Kondylis, V. *et al.* NEMO Prevents Steatohepatitis and Hepatocellular Carcinoma by Inhibiting RIPK1 Kinase Activity-Mediated Hepatocyte Apoptosis. *Cancer Cell* **28**, 582-598, doi:10.1016/j.ccell.2015.10.001 (2015).
- 16 Vlantis, K. *et al.* NEMO Prevents RIP Kinase 1-Mediated Epithelial Cell Death and Chronic Intestinal Inflammation by NF-kappaB-Dependent and -Independent Functions. *Immunity* **44**, 553-567, doi:10.1016/j.immuni.2016.02.020 (2016).
- 17 Vanden Berghe, T. *et al.* Determination of apoptotic and necrotic cell death in vitro and in vivo. *Methods* **61**, 117-129, doi:10.1016/j.ymeth.2013.02.011 (2013).
- 18 Vanden Berghe, T., Linkermann, A., Jouan-Lanhuet, S., Walczak, H. & Vandenabeele, P. Regulated necrosis: the expanding network of non-apoptotic cell death pathways. *Nat Rev Mol Cell Biol* **15**, 135-147, doi:10.1038/nrm3737 (2014).
- 19 Messmer, M. N., Snyder, A. G. & Oberst, A. Comparing the effects of different cell death programs in tumor progression and immunotherapy. *Cell Death Differ* **26**, 115-129, doi:10.1038/s41418-018-0214-4 (2019).

- 20 Tan, Y. *et al.* Correction to: Pyroptosis: a new paradigm of cell death for fighting against cancer. *J Exp Clin Cancer Res* **40**, 296, doi:10.1186/s13046-021-02101-7 (2021).
- 21 Carswell, E. A. *et al.* An endotoxin-induced serum factor that causes necrosis of tumors. *Proc Natl Acad Sci U S A* **72**, 3666-3670, doi:10.1073/pnas.72.9.3666 (1975).
- 22 Varfolomeev, E. & Vucic, D. Intracellular regulation of TNF activity in health and disease. *Cytokine* **101**, 26-32, doi:10.1016/j.cyto.2016.08.035 (2018).
- 23 Legler, D. F., Micheau, O., Doucey, M. A., Tschopp, J. & Bron, C. Recruitment of TNF receptor 1 to lipid rafts is essential for TNF α -mediated NF-kappaB activation. *Immunity* **18**, 655-664, doi:10.1016/s1074-7613(03)00092-x (2003).
- 24 Hayden, M. S. & Ghosh, S. Regulation of NF-kappaB by TNF family cytokines. *Semin Immunol* **26**, 253-266, doi:10.1016/j.smim.2014.05.004 (2014).
- 25 Hsu, H., Huang, J., Shu, H. B., Baichwal, V. & Goeddel, D. V. TNF-dependent recruitment of the protein kinase RIP to the TNF receptor-1 signaling complex. *Immunity* **4**, 387-396, doi:10.1016/s1074-7613(00)80252-6 (1996).
- 26 Shu, H. B., Takeuchi, M. & Goeddel, D. V. The tumor necrosis factor receptor 2 signal transducers TRAF2 and c-IAP1 are components of the tumor necrosis factor receptor 1 signaling complex. *Proc Natl Acad Sci U S A* **93**, 13973-13978, doi:10.1073/pnas.93.24.13973 (1996).
- 27 Vince, J. E. *et al.* TRAF2 must bind to cellular inhibitors of apoptosis for tumor necrosis factor (tnf) to efficiently activate nf- κ b and to prevent tnf-induced apoptosis. *J Biol Chem* **284**, 35906-35915, doi:10.1074/jbc.M109.072256 (2009).
- 28 Ikeda, F. *et al.* SHARPIN forms a linear ubiquitin ligase complex regulating NF-kappaB activity and apoptosis. *Nature* **471**, 637-641, doi:10.1038/nature09814 (2011).
- 29 Tokunaga, F. *et al.* SHARPIN is a component of the NF-kappaB-activating linear ubiquitin chain assembly complex. *Nature* **471**, 633-636, doi:10.1038/nature09815 (2011).
- 30 Haas, T. L. *et al.* Recruitment of the linear ubiquitin chain assembly complex stabilizes the TNF-R1 signaling complex and is required for TNF-mediated gene induction. *Mol Cell* **36**, 831-844, doi:10.1016/j.molcel.2009.10.013 (2009).
- 31 Gerlach, B. *et al.* Linear ubiquitination prevents inflammation and regulates immune signalling. *Nature* **471**, 591-596, doi:10.1038/nature09816 (2011).
- 32 Kanayama, A. *et al.* TAB2 and TAB3 activate the NF-kappaB pathway through binding to polyubiquitin chains. *Mol Cell* **15**, 535-548, doi:10.1016/j.molcel.2004.08.008 (2004).
- 33 Dynek, J. N. *et al.* c-IAP1 and Ubch5 promote K11-linked polyubiquitination of RIP1 in TNF signalling. *EMBO J* **29**, 4198-4209, doi:10.1038/emboj.2010.300 (2010).
- 34 Rahighi, S. *et al.* Specific recognition of linear ubiquitin chains by NEMO is important for NF-kappaB activation. *Cell* **136**, 1098-1109, doi:10.1016/j.cell.2009.03.007 (2009).
- 35 Wu, C. J., Conze, D. B., Li, T., Srinivasula, S. M. & Ashwell, J. D. Sensing of Lys 63-linked polyubiquitination by NEMO is a key event in NF-kappaB activation [corrected]. *Nat Cell Biol* **8**, 398-406, doi:10.1038/ncb1384 (2006).
- 36 Wang, C. *et al.* TAK1 is a ubiquitin-dependent kinase of MKK and IKK. *Nature* **412**, 346-351, doi:10.1038/35085597 (2001).
- 37 Woronicz, J. D., Gao, X., Cao, Z., Rothe, M. & Goeddel, D. V. IkappaB kinase-beta: NF-kappaB activation and complex formation with IkappaB kinase-alpha and NIK. *Science* **278**, 866-869, doi:10.1126/science.278.5339.866 (1997).
- 38 Mercurio, F. *et al.* IKK-1 and IKK-2: cytokine-activated IkappaB kinases essential for NF-kappaB activation. *Science* **278**, 860-866, doi:10.1126/science.278.5339.860 (1997).
- 39 Dondelinger, Y. *et al.* MK2 phosphorylation of RIPK1 regulates TNF-mediated cell death. *Nat Cell Biol* **19**, 1237-1247, doi:10.1038/ncb3608 (2017).

- 40 Xu, D. *et al.* TBK1 Suppresses RIPK1-Driven Apoptosis and Inflammation during Development and in Aging. *Cell* **174**, 1477-1491 e1419, doi:10.1016/j.cell.2018.07.041 (2018).
- 41 Feltham, R. *et al.* Mind Bomb Regulates Cell Death during TNF Signaling by Suppressing RIPK1's Cytotoxic Potential. *Cell Rep* **23**, 470-484, doi:10.1016/j.celrep.2018.03.054 (2018).
- 42 Lafont, E. *et al.* TBK1 and IKKepsilon prevent TNF-induced cell death by RIPK1 phosphorylation. *Nat Cell Biol* **20**, 1389-1399, doi:10.1038/s41556-018-0229-6 (2018).
- 43 Mevissen, T. E. *et al.* OTU deubiquitinases reveal mechanisms of linkage specificity and enable ubiquitin chain restriction analysis. *Cell* **154**, 169-184, doi:10.1016/j.cell.2013.05.046 (2013).
- 44 Ritorto, M. S. *et al.* Screening of DUB activity and specificity by MALDI-TOF mass spectrometry. *Nat Commun* **5**, 4763, doi:10.1038/ncomms5763 (2014).
- 45 Wertz, I. E. *et al.* De-ubiquitination and ubiquitin ligase domains of A20 downregulate NF-kappaB signalling. *Nature* **430**, 694-699, doi:10.1038/nature02794 (2004).
- 46 Draber, P. *et al.* LUBAC-Recruited CYLD and A20 Regulate Gene Activation and Cell Death by Exerting Opposing Effects on Linear Ubiquitin in Signaling Complexes. *Cell Rep* **13**, 2258-2272, doi:10.1016/j.celrep.2015.11.009 (2015).
- 47 Takiuchi, T. *et al.* Suppression of LUBAC-mediated linear ubiquitination by a specific interaction between LUBAC and the deubiquitinases CYLD and OTULIN. *Genes Cells* **19**, 254-272, doi:10.1111/gtc.12128 (2014).
- 48 Keusekotten, K. *et al.* OTULIN antagonizes LUBAC signaling by specifically hydrolyzing Met1-linked polyubiquitin. *Cell* **153**, 1312-1326, doi:10.1016/j.cell.2013.05.014 (2013).
- 49 Heger, K. *et al.* OTULIN limits cell death and inflammation by deubiquitinating LUBAC. *Nature* **559**, 120-124, doi:10.1038/s41586-018-0256-2 (2018).
- 50 Bosanac, I. *et al.* Ubiquitin binding to A20 ZnF4 is required for modulation of NF-kappaB signaling. *Mol Cell* **40**, 548-557, doi:10.1016/j.molcel.2010.10.009 (2010).
- 51 Tokunaga, F. *et al.* Specific recognition of linear polyubiquitin by A20 zinc finger 7 is involved in NF-kappaB regulation. *EMBO J* **31**, 3856-3870, doi:10.1038/emboj.2012.241 (2012).
- 52 Verhelst, K. *et al.* A20 inhibits LUBAC-mediated NF-kappaB activation by binding linear polyubiquitin chains via its zinc finger 7. *EMBO J* **31**, 3845-3855, doi:10.1038/emboj.2012.240 (2012).
- 53 Zilberman-Rudenko, J. *et al.* Recruitment of A20 by the C-terminal domain of NEMO suppresses NF-kappaB activation and autoinflammatory disease. *Proc Natl Acad Sci U S A* **113**, 1612-1617, doi:10.1073/pnas.1518163113 (2016).
- 54 Trompouki, E. *et al.* CYLD is a deubiquitinating enzyme that negatively regulates NF-kappaB activation by TNFR family members. *Nature* **424**, 793-796, doi:10.1038/nature01803 (2003).
- 55 Wright, A. *et al.* Regulation of early wave of germ cell apoptosis and spermatogenesis by deubiquitinating enzyme CYLD. *Dev Cell* **13**, 705-716, doi:10.1016/j.devcel.2007.09.007 (2007).
- 56 Sato, Y. *et al.* Structures of CYLD USP with Met1- or Lys63-linked diubiquitin reveal mechanisms for dual specificity. *Nat Struct Mol Biol* **22**, 222-229, doi:10.1038/nsmb.2970 (2015).
- 57 Sabio, G. & Davis, R. J. TNF and MAP kinase signalling pathways. *Semin Immunol* **26**, 237-245, doi:10.1016/j.smim.2014.02.009 (2014).
- 58 Sakurai, H., Miyoshi, H., Mizukami, J. & Sugita, T. Phosphorylation-dependent activation of TAK1 mitogen-activated protein kinase kinase kinase by TAB1. *FEBS Lett* **474**, 141-145, doi:10.1016/s0014-5793(00)01588-x (2000).
- 59 Micheau, O. & Tschopp, J. Induction of TNF receptor I-mediated apoptosis via two sequential signaling complexes. *Cell* **114**, 181-190, doi:10.1016/s0092-8674(03)00521-x (2003).

- 60 Polykratis, A. *et al.* Cutting edge: RIPK1 Kinase inactive mice are viable and protected from TNF-induced necroptosis in vivo. *J Immunol* **193**, 1539-1543, doi:10.4049/jimmunol.1400590 (2014).
- 61 Wang, L., Du, F. & Wang, X. TNF-alpha induces two distinct caspase-8 activation pathways. *Cell* **133**, 693-703, doi:10.1016/j.cell.2008.03.036 (2008).
- 62 Salvesen, G. S. & Dixit, V. M. Caspase activation: the induced-proximity model. *Proc Natl Acad Sci U S A* **96**, 10964-10967, doi:10.1073/pnas.96.20.10964 (1999).
- 63 Hughes, M. A. *et al.* Reconstitution of the death-inducing signaling complex reveals a substrate switch that determines CD95-mediated death or survival. *Mol Cell* **35**, 265-279, doi:10.1016/j.molcel.2009.06.012 (2009).
- 64 Chang, D. W., Xing, Z., Capacio, V. L., Peter, M. E. & Yang, X. Interdimer processing mechanism of procaspase-8 activation. *EMBO J* **22**, 4132-4142, doi:10.1093/emboj/cdg414 (2003).
- 65 Hughes, M. A. *et al.* Co-operative and Hierarchical Binding of c-FLIP and Caspase-8: A Unified Model Defines How c-FLIP Isoforms Differentially Control Cell Fate. *Mol Cell* **61**, 834-849, doi:10.1016/j.molcel.2016.02.023 (2016).
- 66 Oberst, A. *et al.* Catalytic activity of the caspase-8-FLIP(L) complex inhibits RIPK3-dependent necrosis. *Nature* **471**, 363-367, doi:10.1038/nature09852 (2011).
- 67 Dillon, C. P. *et al.* Survival function of the FADD-CASPASE-8-cFLIP(L) complex. *Cell Rep* **1**, 401-407, doi:10.1016/j.celrep.2012.03.010 (2012).
- 68 Dondelinger, Y. *et al.* RIPK3 contributes to TNFR1-mediated RIPK1 kinase-dependent apoptosis in conditions of cIAP1/2 depletion or TAK1 kinase inhibition. *Cell Death Differ* **20**, 1381-1392, doi:10.1038/cdd.2013.94 (2013).
- 69 Legarda-Addison, D., Hase, H., O'Donnell, M. A. & Ting, A. T. NEMO/IKKgamma regulates an early NF-kappaB-independent cell-death checkpoint during TNF signaling. *Cell Death Differ* **16**, 1279-1288, doi:10.1038/cdd.2009.41 (2009).
- 70 Schmidt-Suppran, M. *et al.* NEMO/IKK gamma-deficient mice model incontinentia pigmenti. *Mol Cell* **5**, 981-992, doi:10.1016/s1097-2765(00)80263-4 (2000).
- 71 Nenci, A. *et al.* Skin lesion development in a mouse model of incontinentia pigmenti is triggered by NEMO deficiency in epidermal keratinocytes and requires TNF signaling. *Hum Mol Genet* **15**, 531-542, doi:10.1093/hmg/ddi470 (2006).
- 72 Nenci, A. *et al.* Epithelial NEMO links innate immunity to chronic intestinal inflammation. *Nature* **446**, 557-561, doi:10.1038/nature05698 (2007).
- 73 Kumari, S. *et al.* NF-kappaB inhibition in keratinocytes causes RIPK1-mediated necroptosis and skin inflammation. *Life Sci Alliance* **4**, doi:10.26508/lsa.202000956 (2021).
- 74 Steinbrecher, K. A., Harmel-Laws, E., Sitcheran, R. & Baldwin, A. S. Loss of epithelial RelA results in deregulated intestinal proliferative/apoptotic homeostasis and susceptibility to inflammation. *J Immunol* **180**, 2588-2599, doi:10.4049/jimmunol.180.4.2588 (2008).
- 75 Luo, X., Budihardjo, I., Zou, H., Slaughter, C. & Wang, X. Bid, a Bcl2 interacting protein, mediates cytochrome c release from mitochondria in response to activation of cell surface death receptors. *Cell* **94**, 481-490, doi:10.1016/s0092-8674(00)81589-5 (1998).
- 76 Tait, S. W. & Green, D. R. Mitochondria and cell death: outer membrane permeabilization and beyond. *Nat Rev Mol Cell Biol* **11**, 621-632, doi:10.1038/nrm2952 (2010).
- 77 Czabotar, P. E., Lessene, G., Strasser, A. & Adams, J. M. Control of apoptosis by the BCL-2 protein family: implications for physiology and therapy. *Nat Rev Mol Cell Biol* **15**, 49-63, doi:10.1038/nrm3722 (2014).
- 78 Du, C., Fang, M., Li, Y., Li, L. & Wang, X. Smac, a mitochondrial protein that promotes cytochrome c-dependent caspase activation by eliminating IAP inhibition. *Cell* **102**, 33-42, doi:10.1016/s0092-8674(00)00008-8 (2000).
- 79 Zou, H., Henzel, W. J., Liu, X., Lutschg, A. & Wang, X. Apaf-1, a human protein homologous to *C. elegans* CED-4, participates in cytochrome c-dependent activation of caspase-3. *Cell* **90**, 405-413, doi:10.1016/s0092-8674(00)80501-2 (1997).

- 80 Zou, H., Li, Y., Liu, X. & Wang, X. An APAF-1.cytochrome c multimeric complex is a functional apoptosome that activates procaspase-9. *J Biol Chem* **274**, 11549-11556, doi:10.1074/jbc.274.17.11549 (1999).
- 81 Acehan, D. *et al.* Three-dimensional structure of the apoptosome: implications for assembly, procaspase-9 binding, and activation. *Mol Cell* **9**, 423-432, doi:10.1016/s1097-2765(02)00442-2 (2002).
- 82 Yoshida, H. *et al.* Apaf1 is required for mitochondrial pathways of apoptosis and brain development. *Cell* **94**, 739-750, doi:10.1016/s0092-8674(00)81733-x (1998).
- 83 Srinivasula, S. M., Ahmad, M., Fernandes-Alnemri, T. & Alnemri, E. S. Autoactivation of procaspase-9 by Apaf-1-mediated oligomerization. *Mol Cell* **1**, 949-957, doi:10.1016/s1097-2765(00)80095-7 (1998).
- 84 Eskes, R., Desagher, S., Antonsson, B. & Martinou, J. C. Bid induces the oligomerization and insertion of Bax into the outer mitochondrial membrane. *Mol Cell Biol* **20**, 929-935, doi:10.1128/MCB.20.3.929-935.2000 (2000).
- 85 Wei, M. C. *et al.* tBID, a membrane-targeted death ligand, oligomerizes BAK to release cytochrome c. *Genes Dev* **14**, 2060-2071 (2000).
- 86 Thomas, A. F., Kelly, G. L. & Strasser, A. Of the many cellular responses activated by TP53, which ones are critical for tumour suppression? *Cell Death Differ* **29**, 961-971, doi:10.1038/s41418-022-00996-z (2022).
- 87 Galluzzi, L. *et al.* Molecular mechanisms of cell death: recommendations of the Nomenclature Committee on Cell Death 2018. *Cell Death Differ* **25**, 486-541, doi:10.1038/s41418-017-0012-4 (2018).
- 88 Sun, L. *et al.* Mixed lineage kinase domain-like protein mediates necrosis signaling downstream of RIP3 kinase. *Cell* **148**, 213-227, doi:10.1016/j.cell.2011.11.031 (2012).
- 89 Murphy, J. M. *et al.* The pseudokinase MLKL mediates necroptosis via a molecular switch mechanism. *Immunity* **39**, 443-453, doi:10.1016/j.immuni.2013.06.018 (2013).
- 90 Rodriguez, D. A. *et al.* Characterization of RIPK3-mediated phosphorylation of the activation loop of MLKL during necroptosis. *Cell Death Differ* **23**, 76-88, doi:10.1038/cdd.2015.70 (2016).
- 91 Dovey, C. M. *et al.* MLKL Requires the Inositol Phosphate Code to Execute Necroptosis. *Mol Cell* **70**, 936-948 e937, doi:10.1016/j.molcel.2018.05.010 (2018).
- 92 Dondelinger, Y. *et al.* MLKL compromises plasma membrane integrity by binding to phosphatidylinositol phosphates. *Cell Rep* **7**, 971-981, doi:10.1016/j.celrep.2014.04.026 (2014).
- 93 Cai, Z. *et al.* Plasma membrane translocation of trimerized MLKL protein is required for TNF-induced necroptosis. *Nat Cell Biol* **16**, 55-65, doi:10.1038/ncb2883 (2014).
- 94 Gong, Y. N. *et al.* ESCRT-III Acts Downstream of MLKL to Regulate Necroptotic Cell Death and Its Consequences. *Cell* **169**, 286-300 e216, doi:10.1016/j.cell.2017.03.020 (2017).
- 95 Ablasser, A. & Chen, Z. J. cGAS in action: Expanding roles in immunity and inflammation. *Science* **363**, doi:10.1126/science.aat8657 (2019).
- 96 Rehwinkel, J. & Gack, M. U. RIG-I-like receptors: their regulation and roles in RNA sensing. *Nat Rev Immunol* **20**, 537-551, doi:10.1038/s41577-020-0288-3 (2020).
- 97 Blasius, A. L. & Beutler, B. Intracellular toll-like receptors. *Immunity* **32**, 305-315, doi:10.1016/j.immuni.2010.03.012 (2010).
- 98 Franchi, L., Warner, N., Viani, K. & Nunez, G. Function of Nod-like receptors in microbial recognition and host defense. *Immunol Rev* **227**, 106-128, doi:10.1111/j.1600-065X.2008.00734.x (2009).
- 99 Fu, Y. *et al.* Cloning of DLM-1, a novel gene that is up-regulated in activated macrophages, using RNA differential display. *Gene* **240**, 157-163, doi:10.1016/s0378-1119(99)00419-9 (1999).
- 100 Lin, J. *et al.* RIPK1 counteracts ZBP1-mediated necroptosis to inhibit inflammation. *Nature* **540**, 124-128, doi:10.1038/nature20558 (2016).
- 101 Newton, K. *et al.* RIPK1 inhibits ZBP1-driven necroptosis during development. *Nature* **540**, 129-133, doi:10.1038/nature20559 (2016).

- 102 Schwarzer, R., Jiao, H., Wachsmuth, L., Tresch, A. & Pasparakis, M. FADD and Caspase-8 Regulate Gut Homeostasis and Inflammation by Controlling MLKL- and GSDMD-Mediated Death of Intestinal Epithelial Cells. *Immunity* **52**, 978-993 e976, doi:10.1016/j.immuni.2020.04.002 (2020).
- 103 Maelfait, J. *et al.* Sensing of viral and endogenous RNA by ZBP1/DAI induces necroptosis. *EMBO J* **36**, 2529-2543, doi:10.15252/embj.201796476 (2017).
- 104 Thapa, R. J. *et al.* DAI Senses Influenza A Virus Genomic RNA and Activates RIPK3-Dependent Cell Death. *Cell Host Microbe* **20**, 674-681, doi:10.1016/j.chom.2016.09.014 (2016).
- 105 Guo, H. *et al.* Species-independent contribution of ZBP1/DAI/DLM-1-triggered necroptosis in host defense against HSV1. *Cell Death Dis* **9**, 816, doi:10.1038/s41419-018-0868-3 (2018).
- 106 Sridharan, H. *et al.* Murine cytomegalovirus IE3-dependent transcription is required for DAI/ZBP1-mediated necroptosis. *EMBO Rep* **18**, 1429-1441, doi:10.15252/embr.201743947 (2017).
- 107 Koehler, H. *et al.* Inhibition of DAI-dependent necroptosis by the Z-DNA binding domain of the vaccinia virus innate immune evasion protein, E3. *Proc Natl Acad Sci U S A* **114**, 11506-11511, doi:10.1073/pnas.1700999114 (2017).
- 108 Kuriakose, T. *et al.* ZBP1/DAI is an innate sensor of influenza virus triggering the NLRP3 inflammasome and programmed cell death pathways. *Sci Immunol* **1**, doi:10.1126/sciimmunol.aag2045 (2016).
- 109 Upton, J. W., Kaiser, W. J. & Mocarski, E. S. DAI/ZBP1/DLM-1 complexes with RIP3 to mediate virus-induced programmed necrosis that is targeted by murine cytomegalovirus vIRA. *Cell Host Microbe* **11**, 290-297, doi:10.1016/j.chom.2012.01.016 (2012).
- 110 Herbert, A. *et al.* A Z-DNA binding domain present in the human editing enzyme, double-stranded RNA adenosine deaminase. *Proc Natl Acad Sci U S A* **94**, 8421-8426, doi:10.1073/pnas.94.16.8421 (1997).
- 111 Kim, Y. G. *et al.* The zab domain of the human RNA editing enzyme ADAR1 recognizes Z-DNA when surrounded by B-DNA. *J Biol Chem* **275**, 26828-26833, doi:10.1074/jbc.M003477200 (2000).
- 112 Schwartz, T., Behlke, J., Lowenhaupt, K., Heinemann, U. & Rich, A. Structure of the DLM-1-Z-DNA complex reveals a conserved family of Z-DNA-binding proteins. *Nat Struct Biol* **8**, 761-765, doi:10.1038/nsb0901-761 (2001).
- 113 Tome, A. R. *et al.* Crystal structure of a poxvirus-like zalpha domain from cyprinid herpesvirus 3. *J Virol* **87**, 3998-4004, doi:10.1128/JVI.03116-12 (2013).
- 114 Quyen, D. V. *et al.* Characterization of DNA-binding activity of Z alpha domains from poxviruses and the importance of the beta-wing regions in converting B-DNA to Z-DNA. *Nucleic Acids Res* **35**, 7714-7720, doi:10.1093/nar/gkm748 (2007).
- 115 Sun, X., Yin, J., Starovasnik, M. A., Fairbrother, W. J. & Dixit, V. M. Identification of a novel homotypic interaction motif required for the phosphorylation of receptor-interacting protein (RIP) by RIP3. *J Biol Chem* **277**, 9505-9511, doi:10.1074/jbc.M109488200 (2002).
- 116 Kaiser, W. J., Upton, J. W. & Mocarski, E. S. Receptor-interacting protein homotypic interaction motif-dependent control of NF-kappa B activation via the DNA-dependent activator of IFN regulatory factors. *J Immunol* **181**, 6427-6434, doi:10.4049/jimmunol.181.9.6427 (2008).
- 117 Ha, S. C. *et al.* The crystal structure of the second Z-DNA binding domain of human DAI (ZBP1) in complex with Z-DNA reveals an unusual binding mode to Z-DNA. *Proc Natl Acad Sci U S A* **105**, 20671-20676, doi:10.1073/pnas.0810463106 (2008).
- 118 Placido, D., Brown, B. A., 2nd, Lowenhaupt, K., Rich, A. & Athanasiadis, A. A left-handed RNA double helix bound by the Z alpha domain of the RNA-editing enzyme ADAR1. *Structure* **15**, 395-404, doi:10.1016/j.str.2007.03.001 (2007).
- 119 Rebsamen, M. *et al.* DAI/ZBP1 recruits RIP1 and RIP3 through RIP homotypic interaction motifs to activate NF-kappaB. *EMBO Rep* **10**, 916-922, doi:10.1038/embo.2009.109 (2009).

- 120 Jiao, H. *et al.* Z-nucleic-acid sensing triggers ZBP1-dependent necroptosis and inflammation. *Nature* **580**, 391-395, doi:10.1038/s41586-020-2129-8 (2020).
- 121 Muendlein, H. I. *et al.* ZBP1 promotes LPS-induced cell death and IL-1 β release via RHIM-mediated interactions with RIPK1. *Nat Commun* **12**, 86, doi:10.1038/s41467-020-20357-z (2021).
- 122 Li, J. *et al.* The RIP1/RIP3 necrosome forms a functional amyloid signaling complex required for programmed necrosis. *Cell* **150**, 339-350, doi:10.1016/j.cell.2012.06.019 (2012).
- 123 Takaoka, A. *et al.* DAI (DLM-1/ZBP1) is a cytosolic DNA sensor and an activator of innate immune response. *Nature* **448**, 501-505, doi:10.1038/nature06013 (2007).
- 124 Wang, Z. *et al.* Regulation of innate immune responses by DAI (DLM-1/ZBP1) and other DNA-sensing molecules. *Proc Natl Acad Sci U S A* **105**, 5477-5482, doi:10.1073/pnas.0801295105 (2008).
- 125 Kesavardhana, S. *et al.* ZBP1/DAI ubiquitination and sensing of influenza vRNPs activate programmed cell death. *J Exp Med* **214**, 2217-2229, doi:10.1084/jem.20170550 (2017).
- 126 Zhang, T. *et al.* Influenza Virus Z-RNAs Induce ZBP1-Mediated Necroptosis. *Cell* **180**, 1115-1129 e1113, doi:10.1016/j.cell.2020.02.050 (2020).
- 127 Nogusa, S. *et al.* RIPK3 Activates Parallel Pathways of MLKL-Driven Necroptosis and FADD-Mediated Apoptosis to Protect against Influenza A Virus. *Cell Host Microbe* **20**, 13-24, doi:10.1016/j.chom.2016.05.011 (2016).
- 128 Rodriguez, D. A. *et al.* Caspase-8 and FADD prevent spontaneous ZBP1 expression and necroptosis. *Proc Natl Acad Sci U S A* **119**, e2207240119, doi:10.1073/pnas.2207240119 (2022).
- 129 Jiao, H. *et al.* ADAR1 averts fatal type I interferon induction by ZBP1. *Nature* **607**, 776-783, doi:10.1038/s41586-022-04878-9 (2022).
- 130 Hubbard, N. W. *et al.* ADAR1 mutation causes ZBP1-dependent immunopathology. *Nature* **607**, 769-775, doi:10.1038/s41586-022-04896-7 (2022).
- 131 de Reuver, R. *et al.* ADAR1 prevents autoinflammation by suppressing spontaneous ZBP1 activation. *Nature* **607**, 784-789, doi:10.1038/s41586-022-04974-w (2022).
- 132 Schunke, H., Gobel, U., Dikic, I. & Pasparakis, M. OTULIN inhibits RIPK1-mediated keratinocyte necroptosis to prevent skin inflammation in mice. *Nat Commun* **12**, 5912, doi:10.1038/s41467-021-25945-1 (2021).
- 133 Belokhvostova, D. *et al.* Homeostasis, regeneration and tumour formation in the mammalian epidermis. *Int J Dev Biol* **62**, 571-582, doi:10.1387/ijdb.170341fw (2018).
- 134 Rognoni, E. & Watt, F. M. Skin Cell Heterogeneity in Development, Wound Healing, and Cancer. *Trends Cell Biol* **28**, 709-722, doi:10.1016/j.tcb.2018.05.002 (2018).
- 135 Devos, M. *et al.* Sensing of endogenous nucleic acids by ZBP1 induces keratinocyte necroptosis and skin inflammation. *J Exp Med* **217**, doi:10.1084/jem.20191913 (2020).
- 136 Bonnet, M. C. *et al.* The adaptor protein FADD protects epidermal keratinocytes from necroptosis in vivo and prevents skin inflammation. *Immunity* **35**, 572-582, doi:10.1016/j.immuni.2011.08.014 (2011).
- 137 Rothenburg, S., Schwartz, T., Koch-Nolte, F. & Haag, F. Complex regulation of the human gene for the Z-DNA binding protein DLM-1. *Nucleic Acids Res* **30**, 993-1000, doi:10.1093/nar/30.4.993 (2002).
- 138 Szczesny, B. *et al.* Mitochondrial DNA damage and subsequent activation of Z-DNA binding protein 1 links oxidative stress to inflammation in epithelial cells. *Sci Rep* **8**, 914, doi:10.1038/s41598-018-19216-1 (2018).
- 139 Chen, D. *et al.* PUMA amplifies necroptosis signaling by activating cytosolic DNA sensors. *Proc Natl Acad Sci U S A* **115**, 3930-3935, doi:10.1073/pnas.1717190115 (2018).
- 140 Lladser, A. *et al.* DAI (DLM-1/ZBP1) as a genetic adjuvant for DNA vaccines that promotes effective antitumor CTL immunity. *Mol Ther* **19**, 594-601, doi:10.1038/mt.2010.268 (2011).

- 141 Ishii, K. J. *et al.* TANK-binding kinase-1 delineates innate and adaptive immune responses to DNA vaccines. *Nature* **451**, 725-729, doi:10.1038/nature06537 (2008).
- 142 Yang, Y. *et al.* ZBP1-MLKL necroptotic signaling potentiates radiation-induced antitumor immunity via intratumoral STING pathway activation. *Sci Adv* **7**, eabf6290, doi:10.1126/sciadv.abf6290 (2021).
- 143 Zhang, T. *et al.* ADAR1 masks the cancer immunotherapeutic promise of ZBP1-driven necroptosis. *Nature* **606**, 594-602, doi:10.1038/s41586-022-04753-7 (2022).
- 144 Karki, R. *et al.* ADAR1 restricts ZBP1-mediated immune response and PANoptosis to promote tumorigenesis. *Cell Rep* **37**, 109858, doi:10.1016/j.celrep.2021.109858 (2021).
- 145 Baik, J. Y. *et al.* ZBP1 not RIPK1 mediates tumor necroptosis in breast cancer. *Nat Commun* **12**, 2666, doi:10.1038/s41467-021-23004-3 (2021).
- 146 Ponnusamy, K. *et al.* The innate sensor ZBP1-IRF3 axis regulates cell proliferation in multiple myeloma. *Haematologica*, doi:10.3324/haematol.2020.274480 (2021).
- 147 Seifert, L. *et al.* The necrosome promotes pancreatic oncogenesis via CXCL1 and Mincle-induced immune suppression. *Nature* **532**, 245-249, doi:10.1038/nature17403 (2016).
- 148 Seehawer, M. *et al.* Necroptosis microenvironment directs lineage commitment in liver cancer. *Nature* **562**, 69-75, doi:10.1038/s41586-018-0519-y (2018).
- 149 Van Hoecke, L. *et al.* Treatment with mRNA coding for the necroptosis mediator MLKL induces antitumor immunity directed against neo-epitopes. *Nat Commun* **9**, 3417, doi:10.1038/s41467-018-05979-8 (2018).
- 150 Yatim, N. *et al.* RIPK1 and NF-kappaB signaling in dying cells determines cross-priming of CD8(+) T cells. *Science* **350**, 328-334, doi:10.1126/science.aad0395 (2015).
- 151 Snyder, A. G. *et al.* Intratumoral activation of the necroptotic pathway components RIPK1 and RIPK3 potentiates antitumor immunity. *Sci Immunol* **4**, doi:10.1126/sciimmunol.aaw2004 (2019).
- 152 Aaes, T. L. *et al.* Vaccination with Necroptotic Cancer Cells Induces Efficient Anti-tumor Immunity. *Cell Rep* **15**, 274-287, doi:10.1016/j.celrep.2016.03.037 (2016).
- 153 Zhang, Z. *et al.* Gasdermin E suppresses tumour growth by activating anti-tumour immunity. *Nature* **579**, 415-420, doi:10.1038/s41586-020-2071-9 (2020).
- 154 Wang, Q. *et al.* A bioorthogonal system reveals antitumour immune function of pyroptosis. *Nature* **579**, 421-426, doi:10.1038/s41586-020-2079-1 (2020).
- 155 Casares, N. *et al.* Caspase-dependent immunogenicity of doxorubicin-induced tumor cell death. *J Exp Med* **202**, 1691-1701, doi:10.1084/jem.20050915 (2005).
- 156 Hanahan, D. & Weinberg, R. A. Hallmarks of cancer: the next generation. *Cell* **144**, 646-674, doi:10.1016/j.cell.2011.02.013 (2011).
- 157 Moore, R. J. *et al.* Mice deficient in tumor necrosis factor-alpha are resistant to skin carcinogenesis. *Nat Med* **5**, 828-831, doi:10.1038/10552 (1999).
- 158 Park, E. J. *et al.* Dietary and genetic obesity promote liver inflammation and tumorigenesis by enhancing IL-6 and TNF expression. *Cell* **140**, 197-208, doi:10.1016/j.cell.2009.12.052 (2010).
- 159 Peng, C., Su, J., Zeng, W., Zhang, X. & Chen, X. TNFR1 Regulates Ovarian Cancer Cell Tumorigenicity Through PIK3CB-p110Beta. *Curr Mol Med* **15**, 487-496, doi:10.2174/1566524015666150630125734 (2015).
- 160 Pasparakis, M. Regulation of tissue homeostasis by NF-kappaB signalling: implications for inflammatory diseases. *Nat Rev Immunol* **9**, 778-788, doi:10.1038/nri2655 (2009).
- 161 Taniguchi, K. & Karin, M. NF-kappaB, inflammation, immunity and cancer: coming of age. *Nat Rev Immunol* **18**, 309-324, doi:10.1038/nri.2017.142 (2018).
- 162 Karin, M. Nuclear factor-kappaB in cancer development and progression. *Nature* **441**, 431-436, doi:10.1038/nature04870 (2006).
- 163 Xia, Y. *et al.* Reduced cell proliferation by IKK2 depletion in a mouse lung-cancer model. *Nat Cell Biol* **14**, 257-265, doi:10.1038/ncb2428 (2012).

- 164 Basseres, D. S., Ebbs, A., Levantini, E. & Baldwin, A. S. Requirement of the NF-kappaB subunit p65/RelA for K-Ras-induced lung tumorigenesis. *Cancer Res* **70**, 3537-3546, doi:10.1158/0008-5472.CAN-09-4290 (2010).
- 165 Meylan, E. *et al.* Requirement for NF-kappaB signalling in a mouse model of lung adenocarcinoma. *Nature* **462**, 104-107, doi:10.1038/nature08462 (2009).
- 166 Greten, F. R. *et al.* IKKbeta links inflammation and tumorigenesis in a mouse model of colitis-associated cancer. *Cell* **118**, 285-296, doi:10.1016/j.cell.2004.07.013 (2004).
- 167 Kim, C. & Pasparakis, M. Epidermal p65/NF-kappaB signalling is essential for skin carcinogenesis. *EMBO Mol Med* **6**, 970-983, doi:10.15252/emmm.201303541 (2014).
- 168 Pratt, M. A. *et al.* The canonical NF-kappaB pathway is required for formation of luminal mammary neoplasias and is activated in the mammary progenitor population. *Oncogene* **28**, 2710-2722, doi:10.1038/onc.2009.131 (2009).
- 169 Liu, M. *et al.* The canonical NF-kappaB pathway governs mammary tumorigenesis in transgenic mice and tumor stem cell expansion. *Cancer Res* **70**, 10464-10473, doi:10.1158/0008-5472.CAN-10-0732 (2010).
- 170 Connelly, L. *et al.* Inhibition of NF-kappa B activity in mammary epithelium increases tumor latency and decreases tumor burden. *Oncogene* **30**, 1402-1412, doi:10.1038/onc.2010.521 (2011).
- 171 Dajee, M. *et al.* NF-kappaB blockade and oncogenic Ras trigger invasive human epidermal neoplasia. *Nature* **421**, 639-643, doi:10.1038/nature01283 (2003).
- 172 van Hogerlinden, M., Rozell, B. L., Ahrlund-Richter, L. & Toftgard, R. Squamous cell carcinomas and increased apoptosis in skin with inhibited Rel/nuclear factor-kappaB signaling. *Cancer Res* **59**, 3299-3303 (1999).
- 173 Lind, M. H. *et al.* Tumor necrosis factor receptor 1-mediated signaling is required for skin cancer development induced by NF-kappaB inhibition. *Proc Natl Acad Sci U S A* **101**, 4972-4977, doi:10.1073/pnas.0307106101 (2004).
- 174 Luedde, T. *et al.* Deletion of NEMO/IKKgamma in liver parenchymal cells causes steatohepatitis and hepatocellular carcinoma. *Cancer Cell* **11**, 119-132, doi:10.1016/j.ccr.2006.12.016 (2007).
- 175 Maeda, S., Kamata, H., Luo, J. L., Leffert, H. & Karin, M. IKKbeta couples hepatocyte death to cytokine-driven compensatory proliferation that promotes chemical hepatocarcinogenesis. *Cell* **121**, 977-990, doi:10.1016/j.cell.2005.04.014 (2005).
- 176 Hopewell, E. L. *et al.* Lung tumor NF-kappaB signaling promotes T cell-mediated immune surveillance. *J Clin Invest* **123**, 2509-2522, doi:10.1172/JCI67250 (2013).
- 177 Jemal, A. *et al.* Cancer statistics, 2007. *CA Cancer J Clin* **57**, 43-66, doi:10.3322/canjclin.57.1.43 (2007).
- 178 Torre, L. A. *et al.* Global cancer statistics, 2012. *CA Cancer J Clin* **65**, 87-108, doi:10.3322/caac.21262 (2015).
- 179 Sung, H. *et al.* Global Cancer Statistics 2020: GLOBOCAN Estimates of Incidence and Mortality Worldwide for 36 Cancers in 185 Countries. *CA Cancer J Clin* **71**, 209-249, doi:10.3322/caac.21660 (2021).
- 180 Schabath, M. B. & Cote, M. L. Cancer Progress and Priorities: Lung Cancer. *Cancer Epidemiol Biomarkers Prev* **28**, 1563-1579, doi:10.1158/1055-9965.EPI-19-0221 (2019).
- 181 Noguchi, M. *et al.* Small adenocarcinoma of the lung. Histologic characteristics and prognosis. *Cancer* **75**, 2844-2852, doi:10.1002/1097-0142(19950615)75:12<2844::aid-cnrc2820751209>3.0.co;2-# (1995).
- 182 Chan, B. A. & Hughes, B. G. Targeted therapy for non-small cell lung cancer: current standards and the promise of the future. *Transl Lung Cancer Res* **4**, 36-54, doi:10.3978/j.issn.2218-6751.2014.05.01 (2015).
- 183 Zappa, C. & Mousa, S. A. Non-small cell lung cancer: current treatment and future advances. *Transl Lung Cancer Res* **5**, 288-300, doi:10.21037/tlcr.2016.06.07 (2016).
- 184 Rudin, C. M. *et al.* Author Correction: Molecular subtypes of small cell lung cancer: a synthesis of human and mouse model data. *Nat Rev Cancer* **19**, 415, doi:10.1038/s41568-019-0164-2 (2019).

- 185 Gazdar, A. F., Bunn, P. A. & Minna, J. D. Small-cell lung cancer: what we know, what we need to know and the path forward. *Nat Rev Cancer* **17**, 765, doi:10.1038/nrc.2017.106 (2017).
- 186 Pietanza, M. C., Byers, L. A., Minna, J. D. & Rudin, C. M. Small cell lung cancer: will recent progress lead to improved outcomes? *Clin Cancer Res* **21**, 2244-2255, doi:10.1158/1078-0432.CCR-14-2958 (2015).
- 187 Peifer, M. *et al.* Integrative genome analyses identify key somatic driver mutations of small-cell lung cancer. *Nat Genet* **44**, 1104-1110, doi:10.1038/ng.2396 (2012).
- 188 Yang, D. *et al.* Intertumoral Heterogeneity in SCLC Is Influenced by the Cell Type of Origin. *Cancer Discov* **8**, 1316-1331, doi:10.1158/2159-8290.CD-17-0987 (2018).
- 189 Sutherland, K. D. *et al.* Cell of origin of small cell lung cancer: inactivation of Trp53 and Rb1 in distinct cell types of adult mouse lung. *Cancer Cell* **19**, 754-764, doi:10.1016/j.ccr.2011.04.019 (2011).
- 190 Minna, J. D., Kurie, J. M. & Jacks, T. A big step in the study of small cell lung cancer. *Cancer Cell* **4**, 163-166, doi:10.1016/s1535-6108(03)00221-6 (2003).
- 191 Simon, G. R., Wagner, H. & American College of Chest, P. Small cell lung cancer. *Chest* **123**, 259S-271S, doi:10.1378/chest.123.1_suppl.259s (2003).
- 192 Junker, K., Wiethage, T. & Muller, K. M. Pathology of small-cell lung cancer. *J Cancer Res Clin Oncol* **126**, 361-368, doi:10.1007/pl00008483 (2000).
- 193 Rom, W. N., Hay, J. G., Lee, T. C., Jiang, Y. & Tchou-Wong, K. M. Molecular and genetic aspects of lung cancer. *Am J Respir Crit Care Med* **161**, 1355-1367, doi:10.1164/ajrccm.161.4.9908012 (2000).
- 194 Wistuba, II, Gazdar, A. F. & Minna, J. D. Molecular genetics of small cell lung carcinoma. *Semin Oncol* **28**, 3-13 (2001).
- 195 Jackman, D. M. & Johnson, B. E. Small-cell lung cancer. *Lancet* **366**, 1385-1396, doi:10.1016/S0140-6736(05)67569-1 (2005).
- 196 Sandler, A. B. Chemotherapy for small cell lung cancer. *Semin Oncol* **30**, 9-25, doi:10.1053/sonc.2003.50012 (2003).
- 197 Horn, L. & Liu, S. V. Atezolizumab plus Chemotherapy in Small-Cell Lung Cancer. Reply. *N Engl J Med* **380**, 889-890, doi:10.1056/NEJMc1900123 (2019).
- 198 Gouyer, V. *et al.* Mechanism of retinoblastoma gene inactivation in the spectrum of neuroendocrine lung tumors. *Am J Respir Cell Mol Biol* **18**, 188-196, doi:10.1165/ajrcmb.18.2.3008 (1998).
- 199 Sekido, Y., Fong, K. M. & Minna, J. D. Molecular genetics of lung cancer. *Annu Rev Med* **54**, 73-87, doi:10.1146/annurev.med.54.101601.152202 (2003).
- 200 Harbour, J. W. *et al.* Abnormalities in structure and expression of the human retinoblastoma gene in SCLC. *Science* **241**, 353-357, doi:10.1126/science.2838909 (1988).
- 201 George, J. *et al.* Comprehensive genomic profiles of small cell lung cancer. *Nature* **524**, 47-53, doi:10.1038/nature14664 (2015).
- 202 Aubrey, B. J., Strasser, A. & Kelly, G. L. Tumor-Suppressor Functions of the TP53 Pathway. *Cold Spring Harb Perspect Med* **6**, doi:10.1101/cshperspect.a026062 (2016).
- 203 Dyson, N. J. RB1: a prototype tumor suppressor and an enigma. *Genes Dev* **30**, 1492-1502, doi:10.1101/gad.282145.116 (2016).
- 204 Linn, P. *et al.* Targeting RB1 Loss in Cancers. *Cancers (Basel)* **13**, doi:10.3390/cancers13153737 (2021).
- 205 Lochmann, T. L., Bouck, Y. M. & Faber, A. C. BCL-2 inhibition is a promising therapeutic strategy for small cell lung cancer. *Oncoscience* **5**, 218-219, doi:10.18632/oncoscience.455 (2018).
- 206 Ben-Ezra, J. M., Kornstein, M. J., Grimes, M. M. & Krystal, G. Small cell carcinomas of the lung express the Bcl-2 protein. *Am J Pathol* **145**, 1036-1040 (1994).
- 207 Ikegaki, N., Katsumata, M., Minna, J. & Tsujimoto, Y. Expression of bcl-2 in small cell lung carcinoma cells. *Cancer Res* **54**, 6-8 (1994).

- 208 Belyanskaya, L. L. *et al.* TRAIL-induced survival and proliferation of SCLC cells is mediated by ERK and dependent on TRAIL-R2/DR5 expression in the absence of caspase-8. *Lung Cancer* **60**, 355-365, doi:10.1016/j.lungcan.2007.11.005 (2008).
- 209 Shivapurkar, N. *et al.* Differential inactivation of caspase-8 in lung cancers. *Cancer Biol Ther* **1**, 65-69, doi:10.4161/cbt.1.1.45 (2002).
- 210 Rudin, C. M., Brambilla, E., Faivre-Finn, C. & Sage, J. Small-cell lung cancer. *Nat Rev Dis Primers* **7**, 3, doi:10.1038/s41572-020-00235-0 (2021).
- 211 Meuwissen, R. *et al.* Induction of small cell lung cancer by somatic inactivation of both Trp53 and Rb1 in a conditional mouse model. *Cancer Cell* **4**, 181-189, doi:10.1016/s1535-6108(03)00220-4 (2003).
- 212 Kayagaki, N. *et al.* Caspase-11 cleaves gasdermin D for non-canonical inflammasome signalling. *Nature* **526**, 666-671, doi:10.1038/nature15541 (2015).
- 213 Wang, Y. *et al.* Molecular mechanism of RIPK1 and caspase-8 in homeostatic type I interferon production and regulation. *Cell Rep* **41**, 111434, doi:10.1016/j.celrep.2022.111434 (2022).
- 214 Liu, S. *et al.* Phosphorylation of innate immune adaptor proteins MAVS, STING, and TRIF induces IRF3 activation. *Science* **347**, aaa2630, doi:10.1126/science.aaa2630 (2015).
- 215 Muendlein, H. I. *et al.* ZBP1 promotes inflammatory responses downstream of TLR3/TLR4 via timely delivery of RIPK1 to TRIF. *Proc Natl Acad Sci U S A* **119**, e2113872119, doi:10.1073/pnas.2113872119 (2022).
- 216 Ruhl, S. *et al.* ESCRT-dependent membrane repair negatively regulates pyroptosis downstream of GSDMD activation. *Science* **362**, 956-960, doi:10.1126/science.aar7607 (2018).
- 217 Bebbber, C. M. *et al.* Ferroptosis response segregates small cell lung cancer (SCLC) neuroendocrine subtypes. *Nat Commun* **12**, 2048, doi:10.1038/s41467-021-22336-4 (2021).
- 218 Oikonomou, N. *et al.* Airway epithelial cell necroptosis contributes to asthma exacerbation in a mouse model of house dust mite-induced allergic inflammation. *Mucosal Immunol* **14**, 1160-1171, doi:10.1038/s41385-021-00415-5 (2021).
- 219 Welz, P. S. *et al.* FADD prevents RIP3-mediated epithelial cell necrosis and chronic intestinal inflammation. *Nature* **477**, 330-334, doi:10.1038/nature10273 (2011).
- 220 Rao, X. *et al.* NLRP6 is required for cancer-derived exosome-modified macrophage M2 polarization and promotes metastasis in small cell lung cancer. *Cell Death Dis* **13**, 891, doi:10.1038/s41419-022-05336-0 (2022).
- 221 Vlantis, K. *et al.* Constitutive IKK2 activation in intestinal epithelial cells induces intestinal tumors in mice. *J Clin Invest* **121**, 2781-2793, doi:10.1172/JCI45349 (2011).
- 222 Jin, X. *et al.* Phosphorylated RB Promotes Cancer Immunity by Inhibiting NF-kappaB Activation and PD-L1 Expression. *Mol Cell* **73**, 22-35 e26, doi:10.1016/j.molcel.2018.10.034 (2019).
- 223 Webster, G. A. & Perkins, N. D. Transcriptional cross talk between NF-kappaB and p53. *Mol Cell Biol* **19**, 3485-3495, doi:10.1128/MCB.19.5.3485 (1999).
- 224 Schwitalla, S. *et al.* Loss of p53 in enterocytes generates an inflammatory microenvironment enabling invasion and lymph node metastasis of carcinogen-induced colorectal tumors. *Cancer Cell* **23**, 93-106, doi:10.1016/j.ccr.2012.11.014 (2013).
- 225 Jonkers, J. *et al.* Synergistic tumor suppressor activity of BRCA2 and p53 in a conditional mouse model for breast cancer. *Nat Genet* **29**, 418-425, doi:10.1038/ng747 (2001).

6. Acknowledgements

First of all, I would like to thank **Prof. Dr. Manolis Pasparakis** for providing me with the opportunity to work on several exciting projects in his lab. I am thankful for his scientific guidance and encouragement during the past years. I highly appreciate his major contributions to deepen my scientific understanding, his help to further develop my abilities to think critically and his mentoring throughout this time. Thank you!

Second, I want to thank **Laurens Wachsmuth** and **Huipeng Jiao** for solving any kind of occurring problem and for consistent scientific input as well as Laurens for his help with this manuscript. Also, thanks to all **collaborators** for their contributions to this work. Thanks to **Neil Stair** for proof-reading this thesis.

Furthermore, I am very grateful to **Jennifer Kuth, Claudia Uthoff-Hachenberg, Elza Gareus, Edeltraud Stade, Paul Roggan and Julia von Rhein** for endless genotyping PCRs and histology sections.


Thanks to **all former and present lab members of the Pasparakis lab** for providing a great working atmosphere, for fruitful scientific discussions and great friendships in and outside of the lab. This time would not have been the same without you guys.

I also would like to express my deep gratitude to all my **friends** and **family**, especially to my **parents and my sister**, for their endless support, for cheering me up and distracting me when I needed it. Thank you for being there, no matter what. I cannot express how much this means to me.

Very special thanks go to **Robin Schwarzer**. This work would not have been possible without his support, trust and understanding as well as his scientific input. Thanks for putting up with me, trusting in me and cheering me up in all frustrating situations in and outside of the lab. Danke – das kann ich gar nicht oft genug sagen.

7. Erklärung zur Dissertation

„Hiermit versichere ich an Eides statt, dass ich die vorliegende Dissertation selbstständig und ohne die Benutzung anderer als der angegebenen Hilfsmittel und Literatur angefertigt habe. Alle Stellen, die wörtlich oder sinngemäß aus veröffentlichten und nicht veröffentlichten Werken dem Wortlaut oder dem Sinn nach entnommen wurden, sind als solche kenntlich gemacht. Ich versichere an Eides statt, dass diese Dissertation noch keiner anderen Fakultät oder Universität zur Prüfung vorgelegen hat; dass sie - abgesehen von unten angegebenen Teilpublikationen und eingebundenen Artikeln und Manuskripten - noch nicht veröffentlicht worden ist sowie, dass ich eine Veröffentlichung der Dissertation vor Abschluss der Promotion nicht ohne Genehmigung des Promotionsausschusses vornehmen werde. Die Bestimmungen dieser Ordnung sind mir bekannt. Darüber hinaus erkläre ich hiermit, dass ich die Ordnung zur Sicherung guter wissenschaftlicher Praxis und zum Umgang mit wissenschaftlichem Fehlverhalten der Universität zu Köln gelesen und sie bei der Durchführung der Dissertation zugrundeliegenden Arbeiten und der schriftlich verfassten Dissertation beachtet habe und verpflichte mich hiermit, die dort genannten Vorgaben bei allen wissenschaftlichen Tätigkeiten zu beachten und umzusetzen. Ich versichere, dass die eingereichte elektronische Fassung der eingereichten Druckfassung vollständig entspricht.“

19.12.22, Lioba Körner 

Datum, Name und Unterschrift

Teilpublikationen:

Koerner, L., Schmiel, M., Yang, T.-P., Peifer, M., Buettner, R., and Pasparakis, M. (2023). NEMO- and RelA-dependent NF- κ B Signaling Promotes Small Cell Lung Cancer. *Cell Death & Differentiation*, (2023) 30:938-951

Koerner, L., Wachsmuth L., Kumari S., Schwarzer R., Jiao H. and Pasparakis M., (2023). ZBP1 causes inflammation by inducing RIPK3-mediated necroptosis and RIPK1 kinase activity-independent apoptosis. *Research Square*, (2023) <https://doi.org/10.21203/rs.3.rs-2511750/v1>

www.nature.com/cdd

CDDpress

ARTICLE OPEN

 Check for updates

NEMO- and RelA-dependent NF- κ B signaling promotes small cell lung cancer

Lioba Koerner^{1,2}, Marcel Schmiel^{3,4}, Tsun-Po Yang³, Martin Peifer^{3,4,5}, Reinhard Buettner^{4,5}  and Manolis Pasparakis^{1,2,5} 

© The Author(s) 2023

Small cell lung cancer (SCLC) is an aggressive type of lung cancer driven by combined loss of the tumor suppressors *RB1* and *TP53*. SCLC is highly metastatic and despite good initial response to chemotherapy patients usually relapse, resulting in poor survival. Therefore, better understanding of the mechanisms driving SCLC pathogenesis is required to identify new therapeutic targets. Here we identified a critical role of the IKK/NF- κ B signaling pathway in SCLC development. Using a relevant mouse model of SCLC, we found that ablation of NEMO/IKK γ , the regulatory subunit of the IKK complex that is essential for activation of canonical NF- κ B signaling, strongly delayed the onset and growth of SCLC resulting in considerably prolonged survival. In addition, ablation of the main NF- κ B family member p65/RelA also delayed the onset and growth of SCLC and prolonged survival, albeit to a lesser extent than NEMO. Interestingly, constitutive activation of IKK/NF- κ B signaling within the tumor cells did not exacerbate the pathogenesis of SCLC, suggesting that endogenous NF- κ B levels are sufficient to fully support tumor development. Moreover, TNFR1 deficiency did not affect the development of SCLC, showing that TNF signaling does not play an important role in this tumor type. Taken together, our results revealed that IKK/NF- κ B signaling plays an important role in promoting SCLC, identifying the IKK/NF- κ B pathway as a promising therapeutic target.

Cell Death & Differentiation (2023) 30:938–951; <https://doi.org/10.1038/s41418-023-01112-5>